An International Journal of Optimization and Control:

Theories & Applications

www.ijocta.com

An International Journal of Optimization and Control:
Theories & Applications
Volume: 10   Number: 2
July 2020

CONTENTS

RESEARCH ARTICLE

A mathematical model for personnel task assignment problem and an application for banking sector

Kenan Cetin [a,b], Gulfem Tuzkaya [b*], Ozalp Vayvay [c]

[a] R&D Center, Vakıfbank, Turkey
[b] Department of Industrial Engineering, Marmara University, Turkey
c Department of Business Administration, Marmara University, Turkey
kenan.cetin@vakifbank.com.tr, gulfem.tuzkaya@marmara.edu.tr, ozalp@marmara.edu.tr

ARTICLE INFO	ABSTRACT
	Efficient planning and management of the workforce resources is one of the most essential requirements for the companies operating in the service sector. For banks, a large number of transactions comes to Central Operations Department from the branches or directly from the customers and their aim is to provide the best operational service with the highest efficiency with the limited workforce resources in the departments. In this study, a real assignment problem was discussed and the problem was considered as Generalized Assignment Problem. For the solution of the problem, related algorithms were listed and examined in the literature survey section. Then, a two-step method is proposed. First step prioritizes the task coming to the system by considering the customer types, service level agreement (SLA) times, cut-off times, task type. In the second step, a multi-objective mathematical model was developed to assign task to employee groups. A preference based optimization method called Linear Physical Programming (LPP) is used to solve the model. Afterward, proposed model was tested on real banking data. For all the tests, GAMS was used as a solver. Results show that proposed model gave better results compared with current situation. With the proposed solution method, the workloads of the profile groups working above their capacity were transferred to other profile groups with idle capacity. Thus, the capacity utilization rates of the profile groups were more balanced and the minimum capacity utilization rate was calculated as 41%.

1. Introduction

It is a well-known fact that workforce is the most important resource for the companies operating in the service sector. A company's success or failure depends mainly on the skill level of the people working for it. Without positive and creative employee contributions, organizations are unable to advance and thrive. Thus, they need to recruit employees with the necessary abilities, experience and capabilities to accomplish a company's objectives or events. In this way, both the present and the company's future requirements should also be kept in mind. Therefore; effective and efficient utilization, planning and directing of the workforce resource are the most essential requirements. To enable companies to respond quickly to its clients by managing their available workforce resource effectively, some major challenges related to business

and marketing constraints are needed to be considered such as; number of available workforce, customer segmentation, SLA times and cut-off times, operation type and their processing time, workforce competence, number of operations executed by customers and priority score.

This study's main goal is to develop a task assignment methodology that based on optimization techniques which assigns a set of jobs to a set of employees with different levels of expertise to meet the due dates and satisfy SLAs. As a result, the proposed model aims to assign the proper number of workforce to the appropriate jobs by considering competence, experience and other capabilities of employees, and also prioritize the incoming jobs considering some criteria such as; customer types, amount of money, SLAs, cut-off times and operation type.

---

*Corresponding author

In this study, a two-step method is proposed to solve a real life assignment problem. First step prioritizes the jobs coming to the system based on a multi-criteria evaluation. In the second step, a mathematical model is developed to assign jobs to employee groups. The methodology has been proposed in order to make the best assignment in the best way considering different objectives. Our mathematical model has three different objectives. The first objective function seeks to assign tasks to the most appropriately qualified employee. The second objective tries to maximize assignment level of higher priority tasks. Although all tasks are required to be completed, the workload of the employees also wanted to be more balanced. Therefore; the third objective function tries to balance the workloads of the profile groups. After that, the jobs assigned to the related employee groups are pushed to the employees according to the priority score calculated in the first step.

The rest of this paper is organized as follows: A definition of the GAP and an overview of related works is given in Section 2. Solution methodology is explained in Section 3. Section 4 describes the methodology and algorithm proposed to solve the problem. The computational results and conclusions are given in Section 5.

2. Literature review

The assignment problem which is the subject of our study is called The Generalized Assignment Problem (GAP) in the literature. In a simple definition, the Generalized Assignment Problem (GAP) is the problem of assigning a set of tasks to a set of agents with a minimum total cost. In each agent, there is a single resource and the resources in the agents have limited capacity. Each tasks that are assigned to an agent, needs a certain number of resource. The generalized assignment problem (GAP) is a well-known, NP-complete combinatorial optimization problem [1]. The first study for GAP in literature is proposed by Kuhn [2]. GAP has been applied in many real world problems ranging from job assignment from computer networks to machine loading in flexible manufacturing systems [3-6].

Several optimization and the approximation algorithms are proposed in order to solve the GAP effectively in the literature. Osman [7] has presented λ-generation mechanism. In this paper, different kind of parameter settings and search methods were examined for hybrid Simulated Annealing (SA) and Tabu Search (TS) algorithms. The results of this technique is compared with SA, branch and bound algorithm and set partitioning heuristics. A genetic algorithm (GA) which tries to improve feasibility and optimality simultaneously was presented by Chu and Beasley [8]. This algorithm was applied on a set of relatively large 84 test problems with 20 agents and 200 jobs. The 60 of these problems were accepted as small-size and optimal solutions can be found. Racer and Amini [9]

presented a hybrid heuristic (HH) method which consists of Variable-Depth-Search Heuristic (VDSH) and Heuristic GAP (HGAP). The HH was tested on 450 test problems and after all, it is found that VDSH gives better solutions, HGAP gives results quickly. Laguna et al. [10] proposed a new heuristic approach to solve the multi-level generalized assignment problem (MGAP). MGAP is different from the classical GAP. Lot sizing problem can be formulated as MGAP. An optimum solution cannot be found by using commercial solvers. Therefore, a new heuristic approach is presented to overcome this problem and also, this approach involves TS applications with neighbourhood search mechanism defined by ejection chains. A Tabu Search Heuristic presented by Diaz and Fernandez [11]. This method uses short term and long term computer memories in order to find feasible solutions and to fix up the penalty weights. In this paper, a relaxed formulation of GAP which is called Relaxed GAP (RGAP) is considered. In this way, the capacity constraints are eliminated and a penalty parameter is added to objective function of the GAP model. Yagiura and Ibaraki [12] proposed a methodology by using the ejection chain algorithms and a neighbourhood construction method. Variable Depth Search (VDS), Tabu Search with Ejection Chains (TSEC) and Path Relinking with Ejection Chains (PREC) were compared on benchmark cases. Randall [13] studied the solution components and the local search heuristics from the literature. And also, two different probabilistic component selection heuristics were proposed with the adaptive and static schemes. As a result, performance of Ant Colony Optimization based methods gives better results against SA and TS. Lourenco and Serra [14] proposed a hybrid approach which combines a Greedy Randomized Adaptive Search Procedure (GRASP) and a Max-Min Ant System (MMAS). MMAS is a generation of the Ant Colony Optimization Algorithm to improve ant system. GRASP is a two-phase iterative randomized sampling method. Alfandari et al. [15] presented a Path-Relinking (PR) heuristics which is a kind of generalized scatter search for the GAP. This algorithm has two phases. The first phase contains LP and local search. In the second phase, paths are created between the feasible solution pairs picked from the first phase. It can be seen in the paper, TS might be very effective compared with PR. Yagiura et al. [16] proposed an algorithm which features ejection chains and a path relinking approach for the GAP. A neighbourhood construction is used to provide more complex and strong moves. And also, this algorithm has a mechanism for fitting parameters to keep the balance among feasible and infeasible regions. Haddai and Ouzia [17] presented an algorithm for generating and improving feasible assignments. This algorithm is applied at each iteration of a subgradient method for the weak Lagrangian relaxation of the GAP. Qu et al. [18] proposed an algorithm for multi-agent assignment problem where there is a need for a group of agents to select assignments from their eligible assignments. The objective is to find an assignment

profile that maximizes the global utility. Jacyna et al. [19] presented a mathematical model to solve task assignment problem of vehicles for a production company. They defined two stages for this problem. The first stage is to identify the tasks, the other is to determine the amount of vehicles required to fulfill these tasks. The algorithm was applied for real data. Demir and Canpolat [20] addressed due date assignment problem. In this study; genetic algorithms, evolutionary strategies and random search techniques are used and compared.

In addition, Cattrysse et al. [21] discussed some extensions of the generalized assignment problem. According to Mozzola [22], the GAP is a well known model for allocation, production planning and scheduling. In their paper, generalization of the GAP called the 0-1 generalized assignment problem with nonlinear capacity constraints (NLGAP) was presented. They aimed to consider capacity interactions among the tasks which are assigned to same employees. The multi-constraint generalized assignment problem (MCGAP) is a generalization of the GAP with multiple resources. LeBlanc et al. [23] proposed a methodology to solve the MCGAP with the considiration of the effects of setup times and costs to permit partitioning the inputs among the different machines. Genetic Algorithm (GA), Simulated Annealing (SA) and Lagrangian Relaxation (LR) are used to obtain results with systematic evaluations. The bottleneck GAP (BGAP) is defined by Mazzola et al. [24] and there are two types of this problem. First one is task based which minimizes the maximum cost of the assignments (TBGAP) and second one is employee based which minimizes the maximum of the total costs assigned to each employee (ABGAP). Martello and Toth [25] introduced approximation algorithms and an exact branch and bound approach to solve BGAP.

In the literature, many studies have been carried out on the service sector. Thomas and Terry [26] presented mixed-integer stochastic programming approach which has two stages for call centers. First stage compounds the staff scheduling and server sizing steps. And the second stage considers the uncertainty in arrival rates from period to period. According to them, the stochastic model generally gives a substantial reduction in the expected operation costs. Rodney and Ward [27] developed an algorithm for staffing and routing problems to minimize the overall workforce. They focused on the necessary agents with limited cross-training. Christian and Rainer [28] proposed a mixed-integer linear programming (MIP) model to minimize labor costs. They considered assigning multi-skilled employees to IT-projects. Krishnamoorthy et al. [29] presented a model to the Personnel Task Scheduling Problem (PTSP). They focused on minimising overall cost of employee with different skills required to perform the given set of tasks. Cordeau et al. [30] proposed an adaptive large neighborhood search heuristic and a construction heuristic for a telecommunication company to overcome technician

and task scheduling problem. Hojati and Patil [31] proposed an integer linear programming model and a heuristic to solve assingment and scheduling problem in service sector for part-time service employee with different availability and skills. The proposed model contains two steps. First step is determining shifts and second step is assigning the proper shifts to employees. Lin et al. [32] presented a problem-specific approach with three stages for crew rostering problem. Fuzzy sets are used to deal with job characteristics and the personal attributes. A linear goal programming model is proposed for effective assingment. Borenstein et al. [33] proposed a stochastic model to solve workforce scheduling problem for the British Telecom, in which technicians with different abilities are assigned to tasks which require different competences.

As can seen from the literature review, several methods are presented in the literature to address to GAP and a large number studies have examined to deal with this problem.

3. Linear physical programming

As Messac et al. [34] stated, optimization problems can be classified into two categories: blind optimization and physical optimization. The decision maker does not really know the nature of the problem or the nature of the solution expected in blind optimization. In physical optimization, the decision maker has information and clearly defined objectives which can be expressed as physically meaningful terms related to the problem. Almost all operational research and engineering problems fall into the second category. In this chapter, linear physical programming (LPP) is described. Physical programming is a technique that requires the retrieval of physically meaningful information from the designer and produces a problem structure that is appropriate to the structure of the designer's preferences [35]. Within the Physical Programming procedure, DM explains their preferences using 4 different classes for each criterion (each criterion is described as belonging to one of 4 different classes). The lower value of the class function is better than the higher value. The ideal value of the class function is zero. Each class, depending on the sharpness of the choice, includes two states: hard and soft. All soft class functions will be a part of the integrated objective function (to be minimized). A class criterion is defined in one of 8 sub-classes: 4 soft (S), 4 hard (H). Physical programming avoids the limits of such a problem structure. In the flexible case, it characterizes the degree of desirability up to 11 intervals. The 6 intervals of the degree of desirability is defined in the 1S and 2S class criteria. 10 of the intervals is defined in class 3S, 11 of the intervals is defined in class 4S.

There are many studies using LPP in the literature. Onut et al. [36] presented a model to allocate the current energy resources to the Turkish manufacturing industry sub-groups by using LPP. Gulsun et al. [37] proposed a multi-objective model for aggregate production

planning and solved by using LPP. A production planning model developed by Maria et al. [38] and multi-objective model is solved by using LPP. Kucukbay and Araz [39] focused on the portfolio selection problem. In this study, fuzzy goal programming and linear physical programming are used and compared.

3.1. Linear physical programming problem model

This section will describe the procedure that will shape the problem of physical programming. Physical programming application procedure requires 4 short steps [35]:

1. For each criterion, class function type will be determined by decision maker (DM) among from 4 hard and 4 soft classes.
2. For each criterion, DM will determine the target values.
3. The LPP weight algorithm (LPPWA) is used to obtain weights with the DM inputs specified in the range limits.
4. Then problem is converted to LPP model.

4. Problem definition

The Central Operations Department (MOB), which aims to provide the best operational service with the highest efficiency, has a large number of transactions from the branches and directly from the customers during the day, such as loan application, guarantee letters preparation, money order based on written instructions, etc. After the transactions coming to the MOB, they are directed to the related departments. They try to complete the transactions with the limited employee resources in the departments. Transactions occur in multiple steps. As an example of the steps of the process, welcome (reading the customer order and specifying what they want), data entry, document control, approval steps can be provided. There are certain cut-off times for some operations. For example, the final closing time for EFT transactions should not exceed 17:30 as it is linked to the central bank system and the central bank system is being closed at 17:30. In addition, the SLA durations are calculated for the steps (steps of the operations) and the steps are intended to be completed within the calculated SLA period from the moment each step arrives at the MOB.

Depending on the workload intensity, other departments can support the related departments. Employees are empowered to perform certain operations according to their experience and training they have received, and the probabilities of making mistakes with the duration of operations can vary from employee to employee. The competencies of the employees gain importance at the point of giving support to other departments in a busy situation. The competencies of the employees are improved with the help of training programs organized by the bank.

In the current situation; in the MOB departments,

certain employees are selected to determine which transactions are related to their departments from the common pool, and they assign to transactions to the employees in their own departments. Prioritization of transactions and assignment of employees are based on the responsible employee's preferences and general rules could not be defined. Thus, while transactions with less priority levels can be completed, transactions that have already exceeded the SLA durations in other departments can be pretermited. In the departments where the transactions are directly selected by the employees, relatively easy and short transactions can be selected and priority of the transactions are not considered.

In this study, a two-step solution procedure is proposed to solve problems such as administrative difficulties, inefficient use of employees and inadequate management of priorities (Figure 1).
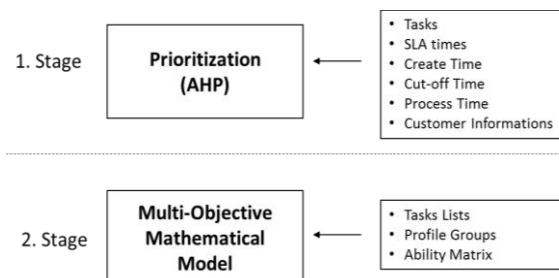
Figure 1. Problem solution procedure

Stage 1 is about the prioritization of tasks coming to the system. Tasks can be prioritized based on customer type, transaction type, urgency status and SLA times. The outputs of this stage are used in the second stage as inputs of mathematical model. Stage 2 is the assignment of tasks to profile groups created by considering specific experience and competencies. The second stage of the problem is the solution of the integer programming model by using the Linear Physical Programming (LPP). In the second stage, the transactions assigned to profile groups are directed to the relevant professionals. Each profile group has more than one employee, and each profile group is competent to conduct the transactions directed to them. Then first stage's results (prioritization stage) are used to push the tasks, assigned to the related profile groups, to the employees.

To summarize briefly, the following problems are observed in the current system:

- Inproper assignments of tasks to the profile groups,
- Non-effective use of resources,
- Unbalanced workloads of profile groups,
- Tendency of employees on easy tasks during task selection phase
- Waiting transactions in the pool

In response to these problems; solutions have been

produced with two-step methododology. Since, by applying this approach, task prioritazion phase becomes more standardized, their acceptance by the related employees and managers becomes easier. With the new system, the selection of tasks is entirely independent from the initiative of the employees. Hence, the tendency of employees on selecting easier tasks firstly is eliminated and the tasks with higher priority levels are assigned and finalized initially.

Also, the proposed methodology increases the communication level among profile groups. Employees have the flexibility of carrying out tasks of other profile groups when needed. It is possible for an employee to perform urgent and higher priority tasks of another profile group instead of performing a task with less priority score of his/her own profile group. In the current situation, employees wouldn't know the tasks in the queues of other profile groups and may remain idle when the other profile groups are overloaded. By applying the new methodology, capacity utilization balanced can be accuired among profile groups, and this would have a positive effect on the employees' moral. And finally, the proposed methodology would have a positive effect on customer satisfaction level.

In this study, below assumptions are made:

- Each incoming job consists of different tasks.
- Similar tasks are grouped into specific task pools.
- Different types of tasks in the same group require similar competences.
- Each employee in the same profile groups has similar competences.
- Each employee must be part of a profile group.
- Each employee can only be included in one profile group.
- Each task type may be carried out by different profile groups.
- All employees work hours are restricted to their shift start and end times.
- Each employee's completion time is different. However, it was assumed to be equal and average processing times were taken into account.
- Preparation and setup times for the works are neglected.
- Lunch times, break times etc. are neglected.

4.1. Prioritization stage

The prioritization stage constitutes the first step of the proposed method. During the working hours, many transactions are coming to the bank. These tasks have different importance levels. The order of importance in the current structure is determined by SLA time, cut-off time, customer information, and type of tasks. Generally, importance level of the tasks are determined by the employees. With our proposed method, the

prioritization structure is unbounded from the employees' initiative and a new structure is introduced. With the new structure, the priority score of each tasks is calculated. Employees will receive the most prioritized task among all tasks assigned to their group according to the calculated priority score. The priority score is calculated according to following rules:

1. Step: Calculation of Tolerance.
2. Step: Calculation of Significance Coefficient.
3. Step: Calculation of Final Score.

Firstly, the tolerance value is calculated. The tolerance value refers to the difference between the SLA time and average process time. The tasks can be kept up to tolerance value in the queue. However, only the tolerance value is not sufficient. Because; although the duration of the SLA is taken into account, there may be different types of tasks with the same duration and there may be different importance ratings among them. There may be a difference in the importance level between two similar transactions according to the customer type or the urgency of the transaction. Therefore; tolerance value is multiplied by the significance coefficient. Significance (Final) scores are calculated by using Analytic Hierarchy Process (AHP) method in second step. Then, final score value is calculated from second step's value for tasks with cut off time.
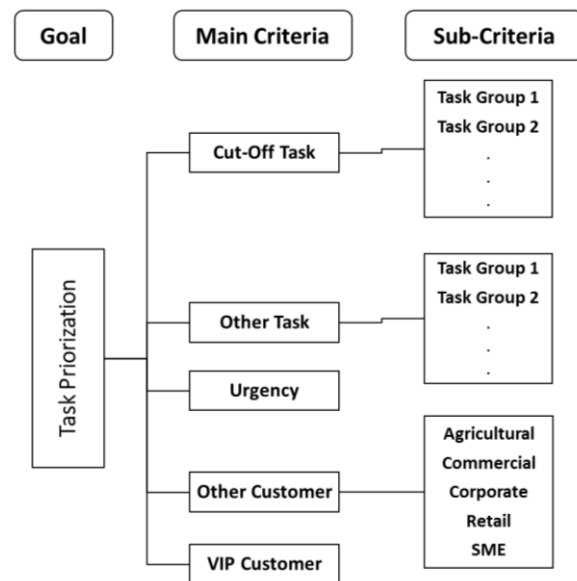
Figure 2. Structure of hierarchy

By using AHP technique, our aim is to standardize the tasks selection logic of employees. With this technique, the criteria are compared with each other. Thus, the importance of the criteria can be expressed numerically. The Analytic Hierarchy Process (AHP) is a multi-criteria decision-making technique and was developed by Saaty [40] to deal with complex decision problems. AHP Scores are calculated as follows and structure of hierarchy can be seen in Figure 2. A questionnaire is prepared to obtain the evaluations and

a 1 to 9 scale is used. According to Saaty's [40] pairwise comparison scale, 9 is extremely important and 1 is equally important. After the surveys were completed, inconsistency rates were performed and final scores were obtained.

And final score is calculated by using each criterion's score as shown in Figure 3.
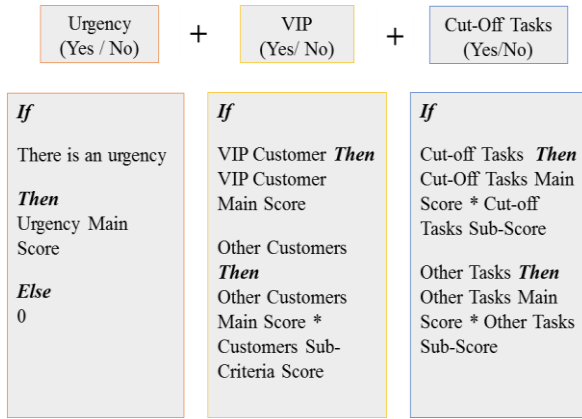
Figure 3. Final score calculation

4.2. Assignment stage

Parameters and decision variables of the model are listed as follows:

Index:

j:	index for tasks	$j=1,2,3,…,J$
i:	index for profile groups	$i=1,2,3,..,I$

Parameters:

α_{ji}: Competence level for profile group i for task j

a_{ji}: Ability matrix for profile group i for task j

b_j: Importance level of task j

tp_i: Available time for profile group i

k_i: Available employee number for profile group i

p: Planning period

t_j: Process time of task j

c: Minimum capacity usage

Decision Variables:

$$x_{ji}: \begin{cases} 1, & \text{if task } j \text{ assigned to profile group } i \\ 0, & \text{otherwise} \end{cases}$$

Proposed task assignment model is given as follow:

Objective Function 1:

$$Maximize: \left(\sum_{j=1}^{J} \sum_{i=1}^{I} x_{ji} * \alpha_{ji} \right) \qquad (1)$$

Eq. (1) tries to maximize the level of task assignments to appropriate profile groups.

Objective Function 2:

$$Maximize: \left(\sum_{j=1}^{J} \sum_{i=1}^{I} x_{ji} * b_j \right) \qquad (2)$$

Eq. (2) tries to maximize assignment level of higher priority tasks.

Objective Function 3:

$$Maximize: (c) \qquad (3)$$

Eq. (3) tries to maximize capacity usage of least occupied profile group. Capacity utilization rates are tried to be balanced.

Subject to:

$$x_{ji} \leq a_{ji} \qquad \forall i, \forall j \qquad (4)$$

$$\sum_{j=1}^{J} x_{ji} * t_j \leq tp_i \qquad \forall i \qquad (5)$$

$$\sum_{i=1}^{I} x_{ji} \leq 1 \qquad \forall j \qquad (6)$$

$$\sum_{i=1}^{I} k_i * p = tp_i \qquad \forall i \qquad (7)$$

$$\sum_{j=1}^{J} ((x_{ji} * t_j)/ tp_i) \geq c \qquad \forall i \qquad (8)$$

$$x_{ji} \in \{0,1\}, \quad \forall i, \forall j \qquad (9)$$

Eq. (4) tries to ensure that a task can be assigned to a proper profile group. Eq. (5) tries to ensure that available time of profile groups cannot be exceeded. Eq. (6) tries to ensure that each task should be assigned to a profile group. Eq. (7) gives the relation between the total available time and the number of employees in profile groups. Eq. (8) determines the minimum capacity usage of profile groups. Eq. (9) determines the range of variables.

5. Experimantal study

The model is developed by considering the problem of a private bank in Turkey and the related literature. One day banking data taken from this private bank is given in Figure 4, and some details are given below:
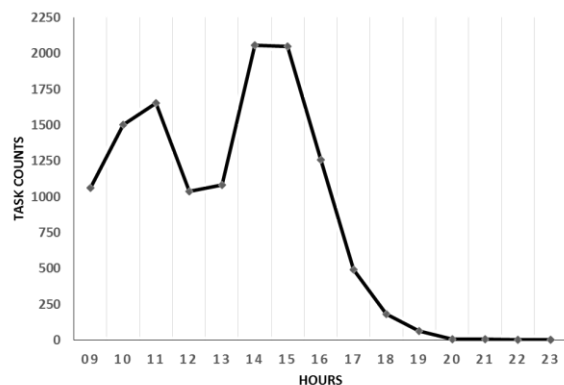
Figure 4. Hour based daily transactions

- Each new job progresses through a separate process. This study covers 6 different process types.

- Each incoming job consists of different tasks. For example; in terms of EFT; depending on the amount can consist of at least 2, up to 5 tasks. If the EFT amount is less than 1000 TL, only two task types are composed, while the amount is above 1000000 TL, five task types are formed.

- Similar tasks are grouped into specific task pools. The employee, assigned to this task pool, is able to do the different jobs such as EFT, remittance, etc. in this task pool.

- Each employee in the profile groups has similar competences.

- Each task type may be carried out by different profile groups.

5.1. Linear physical programming application and weight determination

First of all, optimal values are found for each objective function by solving the model by considering them one by one. Class intervals have been determined in the direction of optimum results.

The objective functions is classified as 2S (2nd soft class). Our preferences and target values for the three goals are as shown in Table 1. Table 2 shows the final weight deviations of performance criteria. Steps of the LPPWA are given below [35] and mathematical relations for weight determination algorithm can be found in [35].

Step 1   Start:

$\beta = 1,1; w_{p1}^+ = 0, w_{p1}^+ = 0, \tilde{z}^2 = small\ positive\ number\ (e.g.\ 0.1)$

$p=0$; $s=1$, n_{ek} = # soft criteria

Step 2 $p=p+1$

Step 3 $p=s+1$

Evaluate sequentially;

$\tilde{z}^s$, $\tilde{t}_{ps}^+$, $\tilde{t}_{ps}^-$, w_{ps}^+ , w_{ps}^- , $\tilde{w}_{ps}^+$, $\tilde{w}_{ps}^-$, $\tilde{w}_{min}$

If $\tilde{w}_{min}$ is smaller than the selected small positive number (e.g., 0.01), increase β and go to step 2.

Step 4   If $s \neq 5$ then go to step 3.

Step 5   If $p \neq n_{sc}$ then go to step 2.

Then, the objective function (to be maximized) is constructed as a weighted sum of deviations (d_{ps}) for all ranges and criteria.

Table 1. Management preferences concerned objectives (Target values).

Preference degree	g_1	g_2	g_3
Ideal	>2870	>3525	> 0.487
Desirable	2870 - 2670	3525 - 3300	0.487 – 0.467
Tolerable	2670 - 2470	3300 - 3100	0.467 – 0.447
Undesirable	2470 - 2270	3100 - 3000	0.447 – 0.427
Highly Undesirable	2270 - 2070	3000 - 2900	0.427 – 0.407
Unacceptable	<2070	<2900	< 0.407

Table 2. Normalized weight deviations of objectives.

	$\tilde{w}_{12}^-$	$\tilde{w}_{13}^-$	$\tilde{w}_{14}^-$	$\tilde{w}_{15}^-$
g_1	0.426086	0.043478	0.47826	0.052173
	$\tilde{w}_{22}^-$	$\tilde{w}_{23}^-$	$\tilde{w}_{24}^-$	$\tilde{w}_{25}^-$
g_2	0.371212	0.037878	0.5	0.090909
	$\tilde{w}_{32}^-$	$\tilde{w}_{33}^-$	$\tilde{w}_{34}^-$	$\tilde{w}_{35}^-$
g_3	0.4260869	0.0434782	0.47826	0.0521739

Our model in the LPP structure is given as follows:

- Piecewise Linear Archimedian Aggregate Function

$$min\ j = \sum_{p=1}^{3} \sum_{s=2}^{5} \left(\tilde{w}_{ps}^- d_{ps}^- + \tilde{w}_{ps}^+ d_{ps}^+ \right) \quad (10)$$

- Goal Constraints

$$g_1 = \left(\sum_{j=1}^{J} \sum_{i=1}^{I} x_{ji} * \alpha_{ji} \right) \quad (11)$$

$$g_2 = \left(\sum_{j=1}^{J} \sum_{i=1}^{I} x_{ji} * b_j \right) \quad (12)$$

$$g_3 = (c) \quad (13)$$

$$g_p + d_{ps}^- \leq t_{p(s-1)}^-; d_{ps}^- \geq 0; g_p \leq t_{p5}^- \quad (14)$$

(for all p classes 2S, $p=1,2,...,n_{sc}$, $s=2,...,5$)

- System Constraints (Hard constraints)

$$x_{ji} \leq a_{ji} \quad \forall i, \forall j \quad (15)$$

$$\sum_{j=1}^{J} x_{ji} * t_j \leq tp_i \quad \forall i \quad (16)$$

$$\sum_{i=1}^{I} x_{ji} \leq 1 \quad \forall j \quad (17)$$

$$\sum_{i=1}^{I} k_i * p = tp_i \quad \forall i \quad (18)$$

$$\sum_{j=1}^{J}((x_{ji} * t_j)/tp_i) \geq c \ \forall i \qquad (19)$$

$$x_{ji} \in \{0, 1\} \quad \forall i, \forall j \qquad (20)$$

The model is solved by using GAMS 25.0.1 solver, and results are given in Table 3.

Table 3. Results

	First Goal	Second Goal	Third Goal
Target Value	2683	3525	0.41
Preference	Desirable	Desirable	Highly Undesirable

Considering the numerical results, the first and second objective function are found in desirable range, and the third objective function is found in a highly undesirable range.

5.2. Results

In this study, GAMS 25.0.1 solver is used. The CPU time was 19 minutes and 32 seconds. Banking daily data is stored on Excel files and daily data was separated into hourly data. Therefore 12 separate datasets were obtained for each day. Then, datasets were tested on the proposed algorithm by using the program. In this study; only the busiest time zone (15:00 pm – 16:00 pm) data is used because of the continuous and large number of transactions coming to the banking system at that time interval. In this time zone, 11 different profile groups are available and each profile group has a different number of employees (see Table 4). According to data; it can be seen in Figure 5 that the capacity of the profile groups cannot be used in a balanced manner. While some profile groups use very small part of their capacities, some profile groups have had to work far beyond their capacity. When the Figure 5 is examined, it is seen that the capacity utilization rates of some profile groups are more than 100%. The reason of this situation can be explained as follows: The transactions performed by the profile groups are expressed in seconds and are based on standard transaction times. However, in order to complete the

transactions in busy profile groups, it is worked in periods well below the standard processing times. For example, in the first profile group, 47 transactions are completed. The standard processing time is 265 seconds. In this case; 47 transactions are completed in a total of 12,455 seconds. But, the capacity of this profile group is 7200 seconds. This conclusion is reached here. Employees in this profile group completed the transactions in an average of 153 seconds. They had to work faster than standart processing times to finish the assigned tasks.
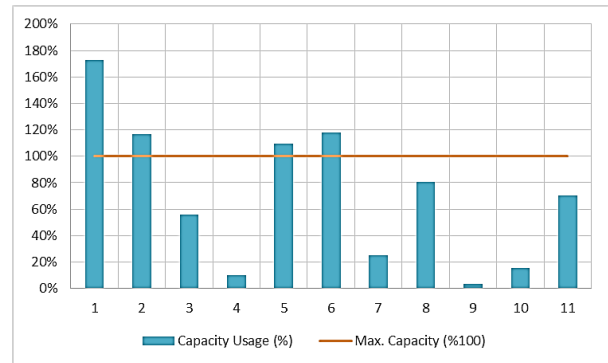
Figure 5. Capacity usage (%) in current situation

In the proposed solution, the capacity utilization level differences among the profile groups started to decrease and can be seen in Table 5. In the current situation, maximum capacity usage of any profile group could be 73% more than its own capacity as can be seen in Table 4. This unfair situation is tried to be balanced with the new methodology and maximum capacity utilization level among profile groups is not exceeded 100% with optimum solution (Table 5, Figure 6). As a result, the amount of unused idle capacity of the profile groups has decreased. As can be seen in Table 3, the result of the third objective function is highly undesirable because it may be due to the narrow range we have determined. We set the range between 0.407 and 0.487. Therefore; we wanted to observe the results by widening the ranges further. First, we set the lowest limit of the highly undesirable range to 0.30 as can be seen in Table 6. In this case; this value corresponds to the tolerable range from the ranges in Table 3 that we obtained earlier.

Table 4. Current situation

Profile Groups	Number of Employees	Profile Groups Capacity in Seconds	Number of Tasks	Total Demand Time in Seconds	Capacity Usage (%)
1	2	7200	47	12455	173%
2	9	32400	75	37885	117%
3	17	61200	114	34113	56%
4	19	68400	36	6713	10%
5	8	28800	232	31576	110%
6	38	136800	1199	161537	118%
7	36	129600	160	32855	25%
8	30	108000	82	86973	81%
9	10	36000	19	1283	4%
10	8	28800	26	4381	15%
11	4	14400	59	10095	70%

Table 5. Optimum solution

Profile Groups	Number of Employees	Profile Groups Capacity in Seconds	Number of Tasks	Total Demand Time in Seconds	Capacity Usage (%)
1	2	7200	38	7158	99%
2	9	32400	62	32054	99%
3	17	61200	82	25092	41%
4	19	68400	245	28555	42%
5	8	28800	263	27119	94%
6	38	136800	890	136778	100%
7	36	129600	335	62090	48%
8	30	108000	19	68400	63%
9	10	36000	55	14774	41%
10	8	28800	39	11934	41%
11	4	14400	21	5912	41%
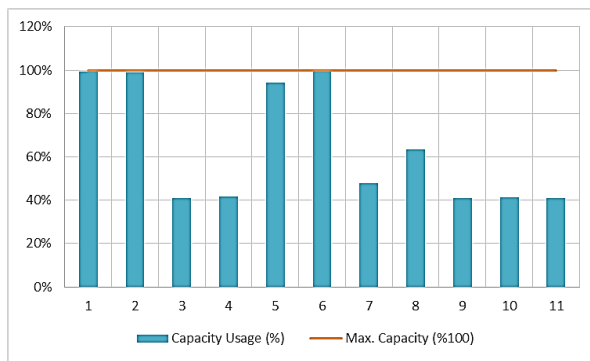
Figure 6. Capacity usage (%) in the proposed solution

When we solve the model for this range, the result for this objective function is found as 0.30, which means that it is highly undesirable. As can be seen in Table 6, we set the lowest limit of the highly undesirable range to 0.25 to extend the range a little further. When we solve the model again for this range, the result for this objective function is found as 0.25 which is highly undesirable.

Table 6. New Preference Values for the Third Goal

	Target values	Target values	Target values
Ideal	> 0.487	> 0.487	> 0.487
Desirable	0.487 – 0.45	0.487 – 0.44	0.487 – 0.48
Tolerable	0.45 – 0.40	0.44 – 0.38	0.48 – 0.47
Undesirable	0.40 – 0.35	0.38 – 0.32	0.47 – 0.46
Highly Undesirable	0.35 – 0.30	0.32 – 0.25	0.46 – 0.45
Unacceptable	< 0.30	< 0.25	< 0.45

It is seen that the minimum capacity utilization rates of the profile groups decrease significantly as the range values for the third objective function increase. It ignores the balance among profile groups. Therefore, we can observe that when we narrow the ranges, the minimum capacity utilization rate becomes higher. When we set the minimum target value to 0.45 for testing, the range is still fairly undesirable but a more balanced assignment takes place. The results can be

seen in Table 7.

Once the relevant tasks have been assigned to the relevant profile groups by proposed solution, the priority scores calculated in the first stage is taken into account. The tasks assigned to each profile group are sorted by ascending order according to the calculated priority score and these tasks are done by the appropriate employees defined in the profile groups, respectively.

Table 7. Capacity Usage (%)

Profile Groups	Minimum Target Value 0.30	Minimum Target Value 0.25	Minimum Target Value 0.45
1	99%	99%	93%
2	99%	99%	94%
3	30%	25%	45%
4	91%	100%	45%
5	100%	100%	94%
6	100%	100%	98%
7	30%	25%	45%
8	66%	73%	63%
9	30%	25%	45%
10	31%	26%	45%
11	30%	25%	45%

6. Conclusion

This study investigates personnel task assingment problem in central operational departments for banking sector. Although many methods have been proposed to address personel task assignment problem, there is no direct solution for this specific problem in the banking sector. Therefore, a two-step methodology has been proposed to solve this real life problem with the consideration of task priorities, task-profile group compability, capacity utilization balance of profile groups.

The proposed method consists of two stages. The first stage is about the prioritization of tasks. At this stage; customer types, transaction types, urgency status, task create times, processing times, cut-off times and SLA

times are taken into account, task priorities are found and the outputs of this stage are used in the second stage as inputs. The second stage is the part where tasks are assigned to profile groups or employees by considering competence, experience and other capabilities of employees. A multi-objective mathematical model is developed for this stage and the linear physical programming technique is used to solve this model.

In our study, real banking data is used and according to results, capacity usage levels of profile groups becomes more balanced and minimum capacity usage among them is increased to at least 41%. As a result, it has been observed that tasks are prioritized in a more precise way and more accurate and balanced task-employee assignments are obtained. There are no unassigned tasks when attempting to make a balanced assignment. When we evaluate the results of objective functions separately, the first and second objective function are found in desirable range, and the third objective function is found in a highly undesirable range.

In this study, completion times for different employees are assumed to be same. In a future study, variations in completion times can be taken into account. Also, number of tasks coming to task list can be forecasted and this can be added to proposed model as a new input. And then, we offered that tasks are assigned to the any available employees according to priority scores. In the future studies, scheduling algorithms can be used to create the tasks lists of the employees at this stage. Our proposed model gives optimal solution for small problem sets. However, it would be difficult to reach the optimum solution if the problem size increases. For larger size problem sets, heuristics /metaheuristics methods can be used.

Acknowledgments

References

[1] Feltl, H., & Raidl, G. R. (2004). An improved hybrid genetic algorithm for the generalized assignment problem, Nicosia, Cyprus: *Proceedings of the 2004 ACM Symposium on Applied Computing*.

[2] Kuhn, H. W, (1955). The Hungarian method for the assignment problem, *Naval Research Logistics*, 2, 83-97.

[3] Balachandran, K. R, (1972). Purchasing priorities in queues, *Management Science*, 18, 319-326.

[4] Mazzola, J. B., Neebe, A. W., & Dunn, C. V. R. (1989). Production planning of a flexible manufacturing system in a material requirements planning environment, *International Journal of Flexible Manufacturing Systems*, 1, 115-142.

[5] Ross, G. T., & Soland, R. M. (1977). Modeling facility location problems as generalized assignment problems, *Management Science*, 24, 345-357.

[6] Pentico, D. (2007). Assignment problems: a golden anniversary survey. *European Journal of Operational Research, Open Journal of Discrete Mathematics*, 176, 774-793.

[7] Osman, I.H. (1995). Heuristics for the generalized assignment problem: simulated annealing and tabu search approaches, *OR Spektrum*, 17, 211-225.

[8] Chu, P.C., & Beasley, J.E. (1997). A genetic algorithm for the generalized assignment problem, *Computers Operations Research*, 24, 17-23.

[9] Racer, M., & Amini, M.M. (1994). A robust heuristic for the generalized assignment problem, *Annals of Operations Research*, 50, 487-503.

[10] Laguna, M., Kelly, J.P., Gonzalez-Velarde, J.L., & Glover, F. (1995). Tabu search for the multilevel generalized assignment problem, *European Journal of Operational Research*, 82, 176-189.

[11] Diaz, J. A., & Fernandez, E. (2001). A tabu search heuristics for the generalized assignment problem, *European Journal of Operational Research*, 132, 22-38.

[12] Yagiura, M., Ibaraki, T., & Glover, F. (2004). An ejection chain approach for the generalized assignment problem, *INFORMS Journal on Computing*, pp. 133-151.

[13] Randall, M. (2004). Heuristics for ant colony optimisation using the generalised assignment problem, in: *Proceedings of IEEE Congress on Evolutionary Computation*, Portland, Oregon, USA, pp. 1916–1923.

[14] Lourenço, H.R., & Serra D. (2000). Adaptive search heuristics for the generalized assignment problem, *Mathware & Soft Computing*, 7, 1–15.

[15] Alfandari, L., Plateau, A., & Tolla, P. (2001). A two-phase path relinking algorithm for the generalized assignment problem, *4th International Conference of Metaheuristics*, Porto, Portugal, 175-179.

[16] Yagiura, M., Ibaraki, T., & Glover, F. (2006). A path relinking approach with ejection chains for the generalized assignment problem, *European Journal of Operational Research*, 169, 548-569.

[17] Haddadi, S., & Ouzia, H. (2001). An effective lagrangian heuristic for the generalized assignment problem, *INFOR: Information Systems and Operational Research*, 39: 351-356.

[18] Qu, G., Brown, D., & Li, N. (2019). Distributed greedy algorithm for multi-agent task assignment problem with submodular utility functions, *Automatica*, 105, 206-215.

[19] Jacyna, M., Izdebski, M., Szczepański, E., & Golda, P. (2018). The task assignment of vehicles for a production company, *Symmetry*, 10, 551.

[20] Demir, H. I., & Canpolat, O. (2018) Integrated process planning, WSPT scheduling and WSLK due-date assignment using genetic algorithms and evolutionary strategies, *An International Journal of*

Optimization and Control: Theories & Applications, Vol 8, No 1, pp. 73-83.

[21] Cattrysse, D.G., & Van Wassenhove, L.N. (1992). A survey of algorithms for the generalized assignment problem, *European Journal of Operational Research*, 60, 260–272.

[22] Mozzola, J. B. (1989). Generalized assignment with nonlinear capacity interaction, *Management Science*, 35.

[23] LeBlanc, L. J., Shtub, A., & Anandalingam, G. (1999). Formulating and solving production planning problems, *European Journal of Operational Research*, 112, 54–80.

[24] Mazzola, J.B., & Neebe, A.W. (1988). Bottleneck generalized assignment problem, *Engineering Cost and Production Economics*, 14, 61-65.

[25] Martello, S., & Toth, P. (1995). The bottleneck generalized assignment problem, *European Journal of Operational Research*, 83 (3), 621–638.

[26] Thomas, R. R., & Terry, P. H. (2010). A stochastic programming model for scheduling call centers with global service level agreements, *European Journal of Operational Research*, 207, 1608-1619.

[27] Rodney, B. W., & Ward, W. (2005). A staffing algorithm for call centers with skill-based routing, *Manufacturing & Service Operations Management*, 7, 276-294.

[28] Christian, H., & Rainer, K. (2010). Scheduling and staffing multiple projects with a multi-skilled workforce, *OR Spectrum*, 32:343–368.

[29] Krishnamoorthy, M., Ernts, A. T., & Baatar, D. (2012). Algorithms for large scale shift minimisation personnel task scheduling problems, *European Journal of Operational Research*, 219, 34-48.

[30] Cordeau, J. F., Laporte, G., Pasin, F., & Ropke, S. (2010). Scheduling technicians and tasks in a telecommunications company, *J Sched*, 13: 393–409.

[31] Hojati, M., & Patil, A.S. (2011). An integer linear programming-based heuristic for scheduling heterogeneous, part-time service employees, *European Journal of Operational Research*, 209, 37–50.

[32] Lin, H. T., Chen, Y. T., Chou, T. Y., & Liao, Y. C. (2012). Crew rostering with multiple goals: an empirical study, *Computers & Industrial Engineering*, 63, 483–493.

[33] Borenstein, Y., Shah, N., Tsang, E., Dorne, R., Alsheddy, A., & Voudouris, C. (2010). On the partitioning of dynamic workforce scheduling problems, *J Sched*, 13, 411–425.

[34] Messac, A., Gupta, S.M., & Akbulut, B. (1996). Linear physical programming: a new approach to multiple objective, *Optimization Transaction on Operation Research*, 8:39-59.

[35] Messac, A., Melachrinoudis, E., & Sukam, C. P. (2001). Mathematical and pragmatic perspectives of physical programming, *AIAA Journal*, 39(5):885-893.

[36] Onut S., Tuzkaya U.R., Tuzkaya G., & Gulsun B. (2011). A multi-objective energy resource allocation model for turkish manufacturing industry using linear physical programming, *International Journal of Innovative Computing Information and Control*, vol.7, pp.3147-3169.

[37] Gulsun B., Tuzkaya G., Tuzkaya U.R., & Onut S. (2009). An aggregate production planning strategy selection methodology based on linear physical programming, *International Journal of Industrial Engineering-Theory Applications and Practice*, vol.16, pp.135-146.

[38] Maria, A., Mattson, C., Yahaya, A., & Messac, A. (2003). Linear physical programming for production planning optimization, *Journal Engineering Optimization*, 35, pp. 19-37.

[39] Kucukbay, F., & Araz, C. (2016). Portfolio selection problem: a comparison of fuzzy goal programming and linear physical programming, *An International Journal of Optimization and Control: Theories & Applications*, Vol 6, No 2, pp. 115-120.

[40] Saaty, T.L. (1977). A scaling method for priorities in hierarchical structures, *Journal of Mathematical Psychology*, 15, 57-68.

Kenan Cetin received the B.Sc. degree in 2010 from the Department of Industrial Engineering from Sakarya University, Turkey. He is working as an R&D Specialist in Vakıfbank. His research interests are optimization algorithms, scheduling, artificial intelligence and data mining.

http://orcid.org/0000-0003-4894-8215

Gülfem Tuzkaya, Ph.D., is currently working as an Associate Professor in the Department of Industrial Engineering, Marmara University. Dr. G. Tuzkaya received her MSc. Degree in Industrial Engineering from Yildiz Technical University, in 2002, MBA degree from Istanbul Technical University, in 2005, and Ph.D. degree in Industrial Engineering from Yildiz Technical University, in 2008. She has been in Tilburg University, Netherland, as a visiting researcher in 2010. Her research interests are in the areas of reverse-forward logistics systems design, facility design and operations research applications for operations management problems.

http://orcid.org/0000-0001-7683-4405

Ozalp Vayvay received the M.Sc. and Ph.D. degrees in 1993 and 2000 from the Department of Industrial Engineering from Marmara University, Turkey respectively. He is working as a Professor at Business Administration Department of Marmara University. His

research interest includes supply chain management, quality management, and innovation management.
iD *http://orcid.org/0000-0003-0504-3395*

An International Journal of Optimization and Control: Theories & Applications (http://ijocta.balikesir.edu.tr)

RESEARCH ARTICLE

The problem with fuzzy eigenvalue parameter in one of the boundary conditions

Hülya Gültekin Çitil[*]

Department of Mathematics, Faculty of Arts and Sciences, Giresun University, Turkey
hulya.citil@giresun.edu.tr

ARTICLE INFO	ABSTRACT
	In this work, we study the problem with fuzzy eigenvalue parameter in one of the boundary conditions. We find fuzzy eigenvalues of the problem using the Wronskian functions $\underline{W}_\alpha(\lambda)$ and $\overline{W}_\alpha(\lambda)$. Also, we find eigenfunctions associated with eigenvalues. We draw graphics of eigenfunctions.

1. Introduction

Fuzzy logic is studied in many areas [1,2]. To solve many problems, Sturm-Liouville Theory is used in mathematical physics [3, 4]. Sturm-Liouville fuzzy problem was defined by Gültekin Çitil and Altınışık [5]. They studied Sturm-Liouville fuzzy problems with reel and fuzzy coefficients in the boundary conditions under the Hukuhara differentiability [6, 7]. Also, fuzzy eigenvalue problems were investigated under the approach of generalized differentiability in many papers [8, 9]. In the other hand, the fuzzy problem with eigenvalue parameter in the boundary condition was studied [10, 11]. But, eigenvalue parameter was not fuzzy in these papers. The problem with fuzzy eigenvalue parameter was defined and investigated by Gültekin Çitil [12].

This paper is on the problem with fuzzy eigenvalue parameter in one of the boundary conditions. That is, we concern the fuzzy eigenvalue problem

$$\tau u + [\lambda]^\alpha u = 0, t \in (a, b) \qquad (1)$$

$$[A]^\alpha u(a) + [\lambda]^\alpha [B]^\alpha u'(a) = 0, \qquad (2)$$

$$[C]^\alpha u(b) + [D]^\alpha u'(b) = 0, \qquad (3)$$

where $[A]^\alpha = \left[\underline{A}_\alpha, \overline{A}_\alpha\right]$, $[C]^\alpha = \left[\underline{C}_\alpha, \overline{C}_\alpha\right]$ are negative triangular fuzzy numbers, $[B]^\alpha = \left[\underline{B}_\alpha, \overline{B}_\alpha\right]$, $[D]^\alpha = \left[\underline{D}_\alpha, \overline{D}_\alpha\right]$ are positive triangular fuzzy numbers, $[\lambda]^\alpha = \left[\underline{\lambda}_\alpha, \overline{\lambda}_\alpha\right]$ is positive fuzzy eigenvalue parameter and $u(t, \lambda)$ is positive fuzzy function.

Definition 1. *[13] A fuzzy number is a mapping $u : \mathbb{R} \to [0, 1]$ satisfying the following properties:*
u is normal,
u is convex fuzzy set,
u is upper semi-continuous on $\mathbb{R}$,
$cl\{x\epsilon\mathbb{R} \mid u(x) > 0\}$ is compact, where cl denotes the closure of a subset.

We show the space of fuzzy sets with $\mathbb{R}_F$.

Definition 2. *[14] Let $u \in \mathbb{R}_F$. The α-level set of u is defined as*

$$[u]^\alpha = \{x \in \mathbb{R} \mid u(x) \geq \alpha\}, 0 < \alpha \leq 1$$

$$\tau = \frac{d^2}{dt^2},$$

---
*Corresponding Author

The α-level set of u is denoted as

$$[u]^\alpha = [\underline{u}_\alpha, \overline{u}_\alpha].$$

Definition 3. *[15]A fuzzy number u is called positive (negative), denoted by $u > 0$ $(u < 0)$, if its membership function $u(x)$ satisfies $u(x) = 0$, $\forall x < 0$ $(x > 0)$.*

Remark 1. *[14] The sufficient and necessary conditions for $[\underline{u}_\alpha, \overline{u}_\alpha]$ to define the parametric form of a fuzzy number as follows:*

$\underline{u}_\alpha$ is bounded monotonic increasing (nondecreasing) left-continuous function on $(0,1]$ and right-continuous for $\alpha = 0$,

$\overline{u}_\alpha$ is bounded monotonic decreasing (nonincreasing) left-continuous function on $(0,1]$ and right-continuous for $\alpha = 0$,

$\underline{u}_\alpha \leq \overline{u}_\alpha$, $0 \leq \alpha \leq 1$.

Definition 4. *[14] For $u, v \in \mathbb{R}_F$ and $\lambda \in \mathbb{R}$, the sum $u + v$ and the product λu are defined by $[u + v]^\alpha = [u]^\alpha + [v]^\alpha$, $[\lambda u]^\alpha = \lambda [u]^\alpha$ where means the usual addition of two intervals (subsets) of $\mathbb{R}$ and $\lambda [u]^\alpha$ means the usual product between a scalar and a subset of $\mathbb{R}$.*

Definition 5. *[16] Let $u, v \in \mathbb{R}_F$, $[u]^\alpha = [\underline{u}_\alpha, \overline{u}_\alpha]$, $[v]^\alpha = [\underline{v}_\alpha, \overline{v}_\alpha]$. The product uv is defined by*

$$[uv]^\alpha = [u]^\alpha [v]^\alpha, \ \forall \alpha \in [0,1],$$

where

$$[u]^\alpha [v]^\alpha = [\underline{u}_\alpha, \overline{u}_\alpha] [\underline{v}_\alpha, \overline{v}_\alpha] = [\underline{w}_\alpha, \overline{w}_\alpha],$$
$$\underline{w}_\alpha = \min \{\underline{u}_\alpha \underline{v}_\alpha, \underline{u}_\alpha \overline{v}_\alpha, \overline{u}_\alpha \underline{v}_\alpha, \overline{u}_\alpha \overline{v}_\alpha\},$$
$$\overline{w}_\alpha = \max \{\underline{u}_\alpha \underline{v}_\alpha, \underline{u}_\alpha \overline{v}_\alpha, \overline{u}_\alpha \underline{v}_\alpha, \overline{u}_\alpha \overline{v}_\alpha\}.$$

Definition 6. *[17] Let $u, v \in \mathbb{R}_F$. If there exists $w \in \mathbb{R}_F$ such that $u = v + w$, then w is called the Hukuhara difference of fuzzy numbers u and v, and it is denoted by $w = u \ominus v$.*

Definition 7. *[14, 18] Let $f : [a,b] \to \mathbb{R}_F$ and $t_0 \in [a,b]$. We say that f is Hukuhara differentiable at t_0, if there exists an element $f'(t_0) \in \mathbb{R}_F$ such that for all $h > 0$ sufficiently small, $\exists f(t_0 + h) \ominus f(t_0)$, $f(t_0) \ominus f(t_0 - h)$ and the limits hold*

$$\lim_{h \to 0} \frac{f(t_0 + h) \ominus f(t_0)}{h} = \lim_{h \to 0} \frac{f(t_0) \ominus f(t_0 - h)}{h}$$
$$= f'(t_0).$$

2. The fuzzy eigenvalues and fuzzy eigenfunctions of the problem

In this section, we investigate the fuzzy eigenvalues and the fuzzy eigenfunctions of the problem (1)-(3).

Let be $[\lambda]^\alpha = [\underline{\lambda}_\alpha, \overline{\lambda}_\alpha] = \left[\underline{k}_\alpha^2, \overline{k}_\alpha^2\right]$, $\underline{k}_\alpha > 0$, $\overline{k}_\alpha > 0$. Then, using the Hukuhara differentiability and fuzzy arithmetic, the general solution of the fuzzy differential equation (1) is

$$\underline{u}_\alpha(t, \lambda) = c_1(\alpha, \lambda) \cos(\underline{k}_\alpha t) + c_2(\alpha, \lambda) \sin(\underline{k}_\alpha t), \tag{4}$$

$$\overline{u}_\alpha(t, \lambda) = c_3(\alpha, \lambda) \cos(\overline{k}_\alpha t) + c_4(\alpha, \lambda) \sin(\overline{k}_\alpha t), \tag{5}$$

$$[u(t, \lambda)]^\alpha = [\underline{u}_\alpha(t, \lambda), \overline{u}_\alpha(t, \lambda)]. \tag{6}$$

Let

$$[\varphi(t, \lambda)]^\alpha = [\underline{\varphi}_\alpha(t, \lambda), \overline{\varphi}_\alpha(t, \lambda)]$$

be the solution of the equation (1) satisfying the conditions

$$u(a) = [\lambda]^\alpha [B]^\alpha, u'(a) = -[A]^\alpha \tag{7}$$

and

$$[\chi(t, \lambda)]^\alpha = [\underline{\chi}_\alpha(t, \lambda), \overline{\chi}_\alpha(t, \lambda)]$$

be the solution of the equation (1) satisfying the conditions

$$u(b) = [D]^\alpha, u'(b) = -[C]^\alpha \tag{8}$$

Then, $\underline{\varphi}_\alpha(t, \lambda)$, $\overline{\varphi}_\alpha(t, \lambda)$, $\underline{\chi}_\alpha(t, \lambda)$, $\overline{\chi}_\alpha(t, \lambda)$ can be shown as

$$\underline{\varphi}_\alpha(t, \lambda) = c_{11}(\alpha, \lambda) \cos(\underline{k}_\alpha t) + c_{21}(\alpha, \lambda) \sin(\underline{k}_\alpha t),$$

$$\overline{\varphi}_\alpha(t, \lambda) = c_{31}(\alpha, \lambda) \cos(\overline{k}_\alpha t) + c_{41}(\alpha, \lambda) \sin(\overline{k}_\alpha t),$$

$$\underline{\chi}_\alpha(t, \lambda) = c_{12}(\alpha, \lambda) \cos(\underline{k}_\alpha t) + c_{22}(\alpha, \lambda) \sin(\underline{k}_\alpha t),$$

$$\overline{\chi}_\alpha(t, \lambda) = c_{32}(\alpha, \lambda) \cos(\overline{k}_\alpha t) + c_{42}(\alpha, \lambda) \sin(\overline{k}_\alpha t).$$

For $[\varphi(t, \lambda)]^\alpha$, from the first condition in (7), since $[B]^\alpha = [\underline{B}_\alpha, \overline{B}_\alpha]$ is positive fuzzy number, we have

$$[\lambda]^\alpha [B]^\alpha = \left[\underline{k}_\alpha^2, \overline{k}_\alpha^2\right] [\underline{B}_\alpha, \overline{B}_\alpha] = \left[\underline{k}_\alpha^2 \underline{B}_\alpha, \overline{k}_\alpha^2 \overline{B}_\alpha\right].$$

Then, using the conditions (7), it is obtained

$$c_{11}(\alpha, \lambda)\cos(\underline{k}_\alpha a) + c_{21}(\alpha, \lambda)\sin(\underline{k}_\alpha a) = \underline{k}_\alpha^2 \underline{B}_\alpha, \tag{9}$$

$$c_{11}(\alpha, \lambda)\underline{k}_\alpha \sin(\underline{k}_\alpha a) - c_{21}(\alpha, \lambda)\underline{k}_\alpha \cos(\underline{k}_\alpha a) = \overline{A}_\alpha, \tag{10}$$

$$c_{31}(\alpha, \lambda)\cos(\overline{k}_\alpha a) + c_{41}(\alpha, \lambda)\sin(\overline{k}_\alpha a) = \overline{k}_\alpha^2 \overline{B}_\alpha, \tag{11}$$

$$c_{31}(\alpha, \lambda)\overline{k}_\alpha \sin(\overline{k}_\alpha a) - c_{41}(\alpha, \lambda)\overline{k}_\alpha \cos(\overline{k}_\alpha a) = \underline{A}_\alpha. \tag{12}$$

From (9)-(10),

$$c_{11}(\alpha, \lambda) = \frac{\underline{k}_\alpha^3 \underline{B}_\alpha \cos(\underline{k}_\alpha a) + \overline{A}_\alpha \sin(\underline{k}_\alpha a)}{\underline{k}_\alpha},$$

$$c_{21}(\alpha, \lambda) = \frac{\underline{k}_\alpha^3 \underline{B}_\alpha \sin(\underline{k}_\alpha a) - \overline{A}_\alpha \cos(\underline{k}_\alpha a)}{\underline{k}_\alpha}$$

are obtained. From (11)-(12), we have

$$c_{31}(\alpha, \lambda) = \frac{\overline{k}_\alpha^3 \overline{B}_\alpha \cos(\overline{k}_\alpha a) + \underline{A}_\alpha \sin(\overline{k}_\alpha a)}{\overline{k}_\alpha},$$

$$c_{41}(\alpha, \lambda) = \frac{\overline{k}_\alpha^3 \overline{B}_\alpha \sin(\overline{k}_\alpha a) - \underline{A}_\alpha \sin(\overline{k}_\alpha a)}{\overline{k}_\alpha}.$$

Then, the solution of the equation (1) satisfying the conditions (7) is

$$
\begin{aligned}
\underline{\varphi}_\alpha(t, \lambda) =\ & \big(\underline{k}_\alpha^2 \underline{B}_\alpha \cos(\underline{k}_\alpha a) \\
& + \frac{\overline{A}_\alpha}{\underline{k}_\alpha}\sin(\underline{k}_\alpha a)\big)\cos(\underline{k}_\alpha t) \\
& + \big(\underline{k}_\alpha^2 \underline{B}_\alpha \sin(\underline{k}_\alpha a) \\
& - \frac{\overline{A}_\alpha}{\underline{k}_\alpha}\cos(\underline{k}_\alpha a)\big)\sin(\underline{k}_\alpha t),
\end{aligned}
$$

$$
\begin{aligned}
\overline{\varphi}_\alpha(t, \lambda) =\ & \big(\overline{k}_\alpha^2 \overline{B}_\alpha \cos(\overline{k}_\alpha a) \\
& \frac{\underline{A}_\alpha}{\overline{k}_\alpha}\sin(\overline{k}_\alpha a)\big)\cos(\overline{k}_\alpha t) \\
& + \big(\overline{k}_\alpha^2 \overline{B}_\alpha \sin(\overline{k}_\alpha a) \\
& - \frac{\underline{A}_\alpha}{\overline{k}_\alpha}\cos(\overline{k}_\alpha a)\big)\sin(\overline{k}_\alpha t),
\end{aligned}
$$

$$[\varphi(t, \lambda)]^\alpha = [\underline{\varphi}_\alpha(t, \lambda), \overline{\varphi}_\alpha(t, \lambda)].$$

For $[\chi(t, \lambda)]^\alpha$, using the conditions (8), we have the equations

$$c_{12}(\alpha, \lambda)\cos(\underline{k}_\alpha b) + c_{22}(\alpha, \lambda)\sin(\underline{k}_\alpha b) = \underline{D}_\alpha, \tag{13}$$

$$c_{12}(\alpha, \lambda)\underline{k}_\alpha \sin(\underline{k}_\alpha b) - c_{22}(\alpha, \lambda)\underline{k}_\alpha \cos(\underline{k}_\alpha b) = \overline{C}_\alpha, \tag{14}$$

$$c_{32}(\alpha, \lambda)\cos(\overline{k}_\alpha b) + c_{42}(\alpha, \lambda)\sin(\overline{k}_\alpha b) = \overline{D}_\alpha, \tag{15}$$

$$c_{32}(\alpha, \lambda)\overline{k}_\alpha \sin(\overline{k}_\alpha b) - c_{42}(\alpha, \lambda)\overline{k}_\alpha \cos(\overline{k}_\alpha b) = \underline{C}_\alpha. \tag{16}$$

From (13)-(14),

$$c_{12}(\alpha, \lambda) = \frac{\underline{D}_\alpha \cos(\underline{k}_\alpha b) + \overline{C}_\alpha \sin(\underline{k}_\alpha b)}{\underline{k}_\alpha},$$

$$c_{22}(\alpha, \lambda) = \frac{\underline{D}_\alpha \sin(\underline{k}_\alpha b) - \overline{C}_\alpha \cos(\underline{k}_\alpha b)}{\underline{k}_\alpha}$$

are obtained. From (15)-(16), we have

$$c_{32}(\alpha, \lambda) = \frac{\overline{D}_\alpha \cos(\overline{k}_\alpha b) + \underline{C}_\alpha \sin(\overline{k}_\alpha b)}{\overline{k}_\alpha},$$

$$c_{42}(\alpha, \lambda) = \frac{\overline{D}_\alpha \sin(\overline{k}_\alpha b) - \underline{C}_\alpha \sin(\overline{k}_\alpha b)}{\overline{k}_\alpha}.$$

Then, solution of the equation (1) satisfying the conditions (8) is

$$
\begin{aligned}
\underline{\chi}_\alpha(t, \lambda) =\ & \Big(\frac{\underline{D}_\alpha}{\underline{k}_\alpha}\cos(\underline{k}_\alpha b) \\
& + \frac{\overline{C}_\alpha}{\underline{k}_\alpha}\sin(\underline{k}_\alpha b)\Big)\cos(\underline{k}_\alpha t) \\
& + \Big(\frac{\underline{D}_\alpha}{\underline{k}_\alpha}\sin(\underline{k}_\alpha b) \\
& - \frac{\overline{C}_\alpha}{\underline{k}_\alpha}\cos(\underline{k}_\alpha b)\Big)\sin(\underline{k}_\alpha t),
\end{aligned}
$$

$$
\begin{aligned}
\overline{\chi}_\alpha(t, \lambda) =\ & \Big(\frac{\overline{D}_\alpha}{\overline{k}_\alpha}\cos(\overline{k}_\alpha b) \\
& + \frac{\underline{C}_\alpha}{\overline{k}_\alpha}\sin(\overline{k}_\alpha b)\Big)\cos(\overline{k}_\alpha t) \\
& + \Big(\frac{\overline{D}_\alpha}{\overline{k}_\alpha}\sin(\overline{k}_\alpha b) \\
& - \frac{\underline{C}_\alpha}{\overline{k}_\alpha}\cos(\overline{k}_\alpha b)\Big)\sin(\overline{k}_\alpha t),
\end{aligned}
$$

$$[\chi(t, \lambda)]^\alpha = [\underline{\chi}_\alpha(t, \lambda), \overline{\chi}_\alpha(t, \lambda)].$$

Since the eigenvalues of the fuzzy boundary value problem (1)-(3) if and only if are consist of the zeros of functions $W\left(\underline{\varphi}_\alpha, \underline{\chi}_\alpha\right)(t,\lambda)$ and $W\left(\overline{\varphi}_\alpha, \overline{\chi}_\alpha\right)(t,\lambda)$ [5], we find Wronskian functions

$$W\left(\underline{\varphi}_\alpha, \underline{\chi}_\alpha\right)(t,\lambda) = \underline{\varphi}_\alpha(t,\lambda)\underline{\chi}'_\alpha(t,\lambda) \quad (17)$$
$$-\underline{\chi}_\alpha(t,\lambda)\underline{\varphi}'_\alpha(t,\lambda),$$

$$W\left(\overline{\varphi}_\alpha, \overline{\chi}_\alpha\right)(t,\lambda) = \overline{\varphi}_\alpha(t,\lambda)\overline{\chi}'_\alpha(t,\lambda) \quad (18)$$
$$-\overline{\chi}_\alpha(t,\lambda)\overline{\varphi}'_\alpha(t,\lambda).$$

Computing the values (17) and (18) and making the necessary operations, we obtain

$$W\left(\underline{\varphi}_\alpha, \underline{\chi}_\alpha\right)(\lambda) = \left(\frac{\overline{A}_\alpha\underline{D}_\alpha}{\underline{k}_\alpha}\right.$$
$$\left.-\underline{k}^2_\alpha\underline{B}_\alpha\overline{C}_\alpha\right)\cos\left(\underline{k}_\alpha(a-b)\right)$$
$$-\left(\underline{k}^2_\alpha\underline{B}_\alpha\underline{D}_\alpha\right.$$
$$\left.+\frac{\overline{A}_\alpha\overline{C}_\alpha}{\underline{k}_\alpha}\right)\sin\left(\underline{k}_\alpha(a-b)\right),$$

$$W\left(\overline{\varphi}_\alpha, \overline{\chi}_\alpha\right)(\lambda) = \left(\frac{\underline{A}_\alpha\overline{D}_\alpha}{\overline{k}_\alpha}\right.$$
$$\left.-\overline{k}^2_\alpha\overline{B}_\alpha\underline{C}_\alpha\right)\cos\left(\overline{k}_\alpha(a-b)\right)$$
$$-\left(\overline{k}^2_\alpha\overline{B}_\alpha\overline{D}_\alpha\right.$$
$$\left.\frac{\underline{A}_\alpha\underline{C}_\alpha}{\overline{k}_\alpha}\right)\sin\left(\overline{k}_\alpha(a-b)\right).$$

Example 1. *Consider the fuzzy eigenvalues and fuzzy eigenfunctions of the problem*

$$u'' + [\lambda]^\alpha u = 0, t \in (0,1) \quad (19)$$
$$-u(0) + [\lambda]^\alpha [2]^\alpha u'(0) = 0, \quad (20)$$
$$[-1]^\alpha u(1) + u'(1) = 0, \quad (21)$$

where $[A]^\alpha = -1$, $[B]^\alpha = [2]^\alpha = [1+\alpha, 3-\alpha]$, $[C]^\alpha = [-1]^\alpha = [-2+\alpha, -\alpha]$, $[D]^\alpha = 1$ and $[\lambda]^\alpha = [\underline{\lambda}_\alpha, \overline{\lambda}_\alpha]$ positive fuzzy eigenvalue parameter and $u(t,\lambda)$ is positive fuzzy function.

Let be $[\lambda]^\alpha = [\underline{\lambda}_\alpha, \overline{\lambda}_\alpha] = [\underline{k}^2_\alpha, \overline{k}^2_\alpha]$, $\underline{k}_\alpha > 0$, $\overline{k}_\alpha > 0$. Solution of the equation (19) satisfying the conditions (20) is

$$\underline{\varphi}_\alpha(t,\lambda) = \underline{k}^2_\alpha(1+\alpha)\cos(\underline{k}_\alpha t) + \frac{1}{\underline{k}_\alpha}\sin(\underline{k}_\alpha t),$$

$$\overline{\varphi}_\alpha(t,\lambda) = \overline{k}^2_\alpha(3-\alpha)\cos(\overline{k}_\alpha t) + \frac{1}{\overline{k}_\alpha}\sin(\overline{k}_\alpha t),$$

$$[\varphi(t,\lambda)]^\alpha = [\underline{\varphi}_\alpha(t,\lambda), \overline{\varphi}_\alpha(t,\lambda)]$$

and solution of the equation (19) satisfying the conditions (21) is

$$\underline{\chi}_\alpha(t,\lambda) = \left(\frac{1}{\underline{k}_\alpha}\cos(\underline{k}_\alpha)\right.$$
$$\left.-\frac{\alpha}{\underline{k}_\alpha}\sin(\underline{k}_\alpha)\right)\cos(\underline{k}_\alpha t)$$
$$+\left(\frac{1}{\underline{k}_\alpha}\sin(\underline{k}_\alpha)\right.$$
$$\left.+\frac{\alpha}{\underline{k}_\alpha}\cos(\underline{k}_\alpha)\right)\sin(\underline{k}_\alpha t),$$

$$\overline{\chi}_\alpha(t,\lambda) = \left(\frac{1}{\overline{k}_\alpha}\cos(\overline{k}_\alpha)\right.$$
$$\left.-\frac{(2-\alpha)}{\overline{k}_\alpha}\sin(\overline{k}_\alpha)\right)\cos(\overline{k}_\alpha t)$$
$$+\left(\frac{1}{\overline{k}_\alpha}\sin(\overline{k}_\alpha)\right.$$
$$\left.+\frac{(2-\alpha)}{\overline{k}_\alpha}\cos(\overline{k}_\alpha)\right)\sin(\overline{k}_\alpha t),$$

$$[\chi(t,\lambda)]^\alpha = [\underline{\chi}_\alpha(t,\lambda), \overline{\chi}_\alpha(t,\lambda)].$$

Then, it is obtained

$$W\left(\underline{\varphi}_\alpha, \underline{\chi}_\alpha\right)(\lambda) = \left(\underline{k}^2_\alpha\alpha(1+\alpha)\right.$$
$$\left.-\frac{1}{\underline{k}_\alpha}\right)\cos(\underline{k}_\alpha)$$
$$+\left(\underline{k}^2_\alpha(1+\alpha)\right.$$
$$\left.+\frac{\alpha}{\underline{k}_\alpha}\right)\sin(\underline{k}_\alpha),$$

$$W\left(\overline{\varphi}_\alpha, \overline{\chi}_\alpha\right)(\lambda) = \left(\overline{k}^2_\alpha(2-\alpha)(3-\alpha)\right.$$
$$\left.-\frac{1}{\overline{k}_\alpha}\right)\cos(\overline{k}_\alpha)$$
$$+\left(\overline{k}^2_\alpha(3-\alpha)\right.$$
$$\left.+\frac{(2-\alpha)}{\overline{k}_\alpha}\right)\sin(\overline{k}_\alpha).$$

Since the eigenvalues of the fuzzy boundary value problem (19)-(21) if and only if are consist of the zeros of functions $\underline{W}_\alpha(\lambda) = W\left(\underline{\varphi}_\alpha, \underline{\chi}_\alpha\right)(\lambda)$ and $\overline{W}_\alpha(\lambda) = W\left(\overline{\varphi}_\alpha, \overline{\chi}_\alpha\right)(\lambda)$, computing the values $\underline{k}_\alpha$ satisfying the equation $\underline{W}_\alpha(\lambda) = 0$ and $\overline{k}_\alpha$ satisfying the equation $\overline{W}_\alpha(\lambda) = 0$ for each $\alpha \in [0,1]$, we get infinitely many values as

$$\alpha = 0 \Rightarrow \begin{array}{ll} \underline{k}_1 = 0.915811, & \overline{k}_1 = 0.343085, \\ \underline{k}_2 = 3.17289, & \overline{k}_2 = 2.0719, \\ \underline{k}_3 = 6.28721, & \overline{k}_3 = 5.17844, \\ \cdots & \cdots \end{array}$$

$$\alpha = 0.2 \Rightarrow \begin{array}{ll} \underline{k}_1 = 0.808395, & \overline{k}_1 = 0.368214, \\ \underline{k}_2 = 2.97581, & \overline{k}_2 = 2.11559, \\ \underline{k}_3 = 6.08948, & \overline{k}_3 = 5.222, \\ \quad ... & \quad ... \end{array}$$

$$\alpha = 0.5 \Rightarrow \begin{array}{ll} \underline{k}_1 = 0.674971, & \overline{k}_1 = 0.413302, \\ \underline{k}_2 = 2.71138, & \overline{k}_2 = 2.19653, \\ \underline{k}_3 = 5.82291, & \overline{k}_3 = 5.30307, \\ \quad ... & \quad ... \end{array}$$

$$\alpha = 0.8 \Rightarrow \begin{array}{ll} \underline{k}_1 = 0.571662, & \overline{k}_1 = 0.470075, \\ \underline{k}_2 = 2.50229, & \overline{k}_2 = 2.30274, \\ \underline{k}_3 = 5.61159, & \overline{k}_3 = 5.41, \\ \quad ... & \quad ... \end{array}$$

$$\alpha = 1 \Rightarrow \begin{array}{ll} \underline{k}_1 = 0.516499, & \overline{k}_1 = 0.516499, \\ \underline{k}_2 = 2.39268, & \overline{k}_2 = 2.39268, \\ \underline{k}_3 = 5.50079, & \overline{k}_3 = 5.50079, \\ \quad ... & \quad ... \end{array}$$

We show that this values are $\underline{k}_n$ and $\overline{k}_n$, $k=1,2,...$ for each $\alpha \in [0,1]$. Then, the eigenvalues are $[\lambda_n]^\alpha = [\underline{\lambda}_{\alpha,n}, \overline{\lambda}_{\alpha,n}] = [\underline{k}^2_{\alpha,n}, \overline{k}^2_{\alpha,n}]$ with associated solutions

$$[\varphi_n(t,\lambda)]^\alpha = [\underline{\varphi}_{\alpha,n}(t,\lambda), \overline{\varphi}_{\alpha,n}(t,\lambda)],$$

$$\underline{\varphi}_{\alpha,n}(t,\lambda) = \underline{k}^2_{\alpha,n}(1+\alpha)\cos(\underline{k}_{\alpha,n}t) + \frac{1}{\underline{k}_{\alpha,n}}\sin(\underline{k}_{\alpha,n}t),$$

$$\overline{\varphi}_{\alpha,n}(t,\lambda) = \overline{k}^2_{\alpha,n}(3-\alpha)\cos(\overline{k}_{\alpha,n}t) + \frac{1}{\overline{k}_{\alpha,n}}\sin(\overline{k}_{\alpha,n}t)$$

and

$$[\chi_n(t,\lambda)]^\alpha = [\underline{\chi}_{\alpha,n}(t,\lambda), \overline{\chi}_{\alpha,n}(t,\lambda)],$$

$$\underline{\chi}_{\alpha,n}(t,\lambda) = \left(\frac{1}{\underline{k}_{\alpha,n}}\cos(\underline{k}_{\alpha,n}) - \frac{\alpha}{\underline{k}_{\alpha,n}}\sin(\underline{k}_{\alpha,n}) \right)\cos(\underline{k}_{\alpha,n}t) + \left(\frac{1}{\underline{k}_{\alpha,n}}\sin(\underline{k}_{\alpha,n}) + \frac{\alpha}{\underline{k}_{\alpha,n}}\cos(\underline{k}_{\alpha,n}) \right)\sin(\underline{k}_{\alpha,n}t),$$

$$\overline{\chi}_{\alpha,n}(t,\lambda) = \left(\frac{1}{\overline{k}_{\alpha,n}}\cos(\overline{k}_{\alpha,n}) - \frac{(2-\alpha)}{\overline{k}_{\alpha,n}}\sin(\overline{k}_{\alpha,n}) \right)\cos(\overline{k}_{\alpha,n}t) + \left(\frac{1}{\overline{k}_{\alpha,n}}\sin(\overline{k}_{\alpha,n}) + \frac{(2-\alpha)}{\overline{k}_{\alpha,n}}\cos(\overline{k}_{\alpha,n}) \right)\sin(\overline{k}_{\alpha,n}t).$$

When

$$\frac{\partial \underline{\varphi}_{\alpha,n}(t,\lambda)}{\partial \alpha} \geq 0, \quad \frac{\partial \overline{\varphi}_{\alpha,n}(t,\lambda)}{\partial \alpha} \leq 0, \quad (22)$$

$$\underline{\varphi}_{\alpha,n}(t,\lambda) \leq \overline{\varphi}_{\alpha,n}(t,\lambda),$$

$$\frac{\partial \underline{\chi}_{n,\alpha}(t,\lambda)}{\partial \alpha} \geq 0, \quad \frac{\partial \overline{\chi}_{n,\alpha}(t,\lambda)}{\partial \alpha} \leq 0, \quad (23)$$

$$\underline{\chi}_{n,\alpha}(t,\lambda) \leq \overline{\chi}_{n,\alpha}(t,\lambda),$$

for all $n = 1,2,..., [\varphi_n(t,\lambda)]^\alpha$ and $[\chi_n(t,\lambda)]^\alpha$ are valid $\alpha-$level sets. That is, $[\varphi_n(t,\lambda)]^\alpha$ and $[\chi_n(t,\lambda)]^\alpha$ are eigenfunctions when (22) and (23) are satisfied.

Now, we draw the graphics of $[\varphi_n(t,\lambda)]^\alpha$ and $[\chi_n(t,\lambda)]^\alpha$ for $\alpha = 0.2$ and $n = 2$.
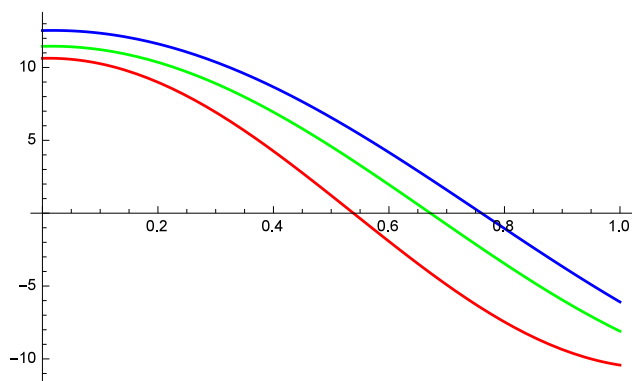

Figure 1. Graphic of $[\varphi_n(t,\lambda)]^\alpha$: Red $\rightarrow \underline{\varphi}_{\alpha,n}(t,\lambda)$, Blue $\rightarrow \overline{\varphi}_{\alpha,n}(t,\lambda)$, Green $\rightarrow \underline{\varphi}_{1,n}(t,\lambda) = \overline{\varphi}_{1,n}(t,\lambda)$.
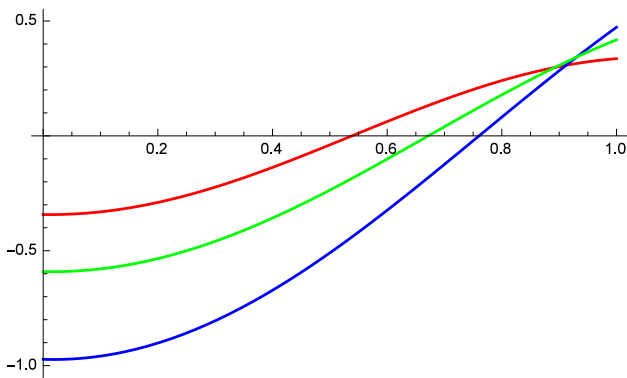
Figure 2. Graphic of $[\chi_n(t,\lambda)]^\alpha$: Red $\rightarrow$ $\underline{\chi}_{\alpha,n}(t,\lambda)$, Blue $\rightarrow \overline{\chi}_{\alpha,n}(t,\lambda)$, Green $\rightarrow \underline{\chi}_{1,n}(t,\lambda) = \overline{\chi}_{1,n}(t,\lambda)$.

In Figure 1, $[\varphi_n(t,\lambda)]^\alpha$ is a valid $\alpha-$level set for $t \in [0, 0.538478]$ and in Figure 2, is a valid $\alpha-$level set for $t \in [0.912106, 1]$, since the inequalities (23) and the solution is positive fuzzy function.

Then, the eigenfunctions are $[\varphi_n(t,\lambda)]^\alpha$ on $[0, 0.538478]$ and $[\chi_n(t,\lambda)]^\alpha$ on $[0.912106, 1]$ associated with eigenvalues $[\lambda_n]^\alpha = \left[\underline{\lambda}_{\alpha,n}, \overline{\lambda}_{\alpha,n}\right] = \left[\underline{k}_{\alpha,n}^2, \overline{k}_{\alpha,n}^2\right]$ for $\alpha = 0.2$ and $n = 2$.

3. Conclusion

In this work, we study the problem with fuzzy eigenvalue parameter in one of the boundary conditions. We find infinitely many eigenvalues for each $\alpha \in [0, 1]$. Also, we find solutions associated with eigenvalues. We draw graphics of solutions. But solutions are not valid $\alpha-$level sets every time. That is, solutions are valid fuzzy functions different interval for each $\alpha \in [0, 1]$. Thus, found solutions are solutions only in interval which they are valid fuzzy function. That is, found solutions are eigenfunctions only in interval which they are valid fuzzy function.

References

[1] Irkin, R., Yılmaz Özgür, N., Taş, N. (2018). Optimization of lactic acid bacteria viability using fuzzy soft set modelling. *An International Journal of Optimization and Control: Theories & Applications*, 8(2), 266-275.

[2] Karakaş, E., Özpalamutçu, H. (2019). A genetic algorithm for fuzzy order acceptance and scheduling problem. *An International Journal of Optimization and Control: Theories & Applications*, 9(2), 186-196.

[3] Fulton, C. T. (1977). Two point boundary value problems with eigenvalue parameter contained in the boundary conditions. *Proc. Soc. Edinburg*, 77A, 293-308.

[4] Binding, P. A., Browne, P. J., Watson, B. A. (2002). Sturm-Liouville problems with boundary conditions rationally dependent on the eigenparameter, II. *Journal of Computational and Applied Mathematics*, 148(1), 147-168.

[5] Gültekin Çitil, H., Altınışık, N. (2017). On the eigenvalues and the eigenfunctions of the Sturm-Liouville fuzzy boundary value problem. *Journal of Mathematical and Computational Science*, 7(4), 786-805.

[6] Gültekin Çitil, H., Altınışık, N. (2018). The examination of eigenvalues and eigenfunctions of the Sturm-Liouville fuzzy problem according to boundary conditions. *International Journal of Mathematical Combinatorics*, 1, 51-60.

[7] Gültekin Çitil, H., Altınışık, N. (2018). The eigenvalues and the eigenfunctions of the Sturm-Liouville fuzzy problem with fuzzy coefficient boundary conditions. *Journal of Science and Arts*, 4(45), 947-958.

[8] Gültekin Çitil, H. (2017). The eigenvalues and the eigenfunctions of the Sturm-Liouville fuzzy boundary value problem according to the generalized differentiability. *Scholars Journal of Physics, Mathematics and Statistics*, 4(4), 185-195.

[9] Ceylan, T., Altınışık, N. (2018). Eigenvalue problem with fuzzy coefficients of boundary conditions. *Scholars Journal of Physics, Mathematics and Statistics*, 5(2), 187-193.

[10] Gültekin Çitil, H. (2019). Important notes for a fuzzy boundary value problem. *Applied Mathematics and Nonlinear Sciences*, 4(2), 305–314.

[11] Ceylan, T., Altınışık, N. (2018). Fuzzy eigenvalue problem with eigenvalue parameter contained in the boundary condition. *Journal of Science and Arts*, 3(44), 589-602.

[12] Gültekin Çitil, H. (2019). Sturm-Liouville fuzzy problem with fuzzy eigenvalue parameter. *International Journal of Mathematical Modelling & Computations*, 9(3), 187- 195.

[13] Liu, H.-K. (2011). Comparison results of two-point fuzzy boundary value problems. *International Journal of Computational and Mathematical Sciences*, 5(1), 1-7.

[14] Khastan, A., Nieto, J. J. (2010). A boundary value problem for second order fuzzy differential equations. *Nonlinear Analysis*, 72, 3583-3593.

[15] Shirin, S., Saha, G. K. (2011). A new computational methodology to find appropriate solutions of fuzzy equations. *Mathematical Theory and Modeling*, 2(1), 1-10.

[16] Lakshmikantham, V., Mohapatra, R. N. (2003). *Theory of Fuzzy Differential Equations and Inclusions.* Taylor and Francis, London, New York.

[17] Puri, M. L., Ralescu D. A. (1983). Differentials of fuzzy functions. *Journal of Mathematical Analysis and Applications*, 91(2), 552-558.

[18] Bede, B. (2008). Note on "Numerical solutions of fuzzy differential equations by predictor-corrector method". *Information Sciences*, 178(7), 1917-1922.

Hülya Gültekin Çitil *is an Assistant Prof. Dr. at the Department of Mathematics, Faculty of Arts and Sciences, Giresun University, Turkey. She received her B.Sc. (2007) degree from Department of Mathematics, Faculty of Arts and Sciences, Ondokuz Mayıs University and M.Sc. (2010) degree and Ph.D. (2015) degree from Ondokuz Mayıs University, Turkey. She has many research papers about the fuzzy initial and boundary value problems and Sturm-Liouville fuzzy problems.*

http://orcid.org/0000-0002-3543-033X

RESEARCH ARTICLE

Dynamics of malaria-dengue fever and its optimal control

Nita H. Shah[*], Ankush H. Suthar, Ekta N. Jayswal

Department of Mathematics, Gujarat University, Ahmedabad, India-380009
nitahshah@gmail.com, ankush.suthar1070@gmail.com, jayswal.ekta1993@gmail.com

ARTICLE INFO	ABSTRACT
	The mosquito-borne infectious diseases like malaria and dengue are putative as important tropical infections and cause high morbidity and mortality around the world. In some cases, simultaneous coexistence of both the infections in one individual is seen which is very hard to distinguish as both diseases have almost similar symptoms. In this proposed article, dynamical system of non-linear differential equations is constructed with the help of mathematical modeling, which describe dynamics of the spread of these infectious diseases separately and concurrently. Basic reproduction number is evaluated to understand dynamical behaviour of the model. Local and global stability criteria have been deliberated rigorously. Control parameters are used to perceive effect of medication on these prevalent tropical diseases. Numerical simulations are used to observe effect of control parameters graphically.

1. Introduction

The present era witnesses the globalization of infectious diseases that occurs frequently by an unprecedented level. In this "globalized" environment of interdependent trade, travel, migration, and international economic markets, many factors now play an important role in the emergence and spread of infectious disease, which necessitates a coordinated, global response [17]. Mosquitoes are one of the deadliest insects in the world, with their ability to carry and spread disease to humans causes millions of deaths every year. Mosquito-borne infectious disease is accepted as one of the important tropical infections and is the focused topic in tropical medicine [23]. There are several tropical mosquito borne infections. Malaria and dengue are the two common mosquito infections that are easily spread and cause high morbidity and mortality for many patients around the world. Malaria is caused by Plasmodium parasites, which spreads through the bites of infected female Anopheles mosquitoes, called 'malaria vectors' [18]. Dengue is single positive-stranded RNA virus of the family Flaviviridae which is ingested by female mosquitoes (Aedes mosquito) during feeding [22]. The virus then infects the other mosquito and humans over its incubation period. Due to tremendous progress in malaria and dengue infection, the disease burden remains high mostly in subtropical and tropical areas [21].

Presence of infection in the body results in weakness in immune system, it increases the probability that individual gets infected by another infections. Hence there is a possibility that both malaria and dengue infection can be present in the individual at the same time (e.g., [4], [6], [8], [13], [21], [24], [30] or [13]). This scenario is called concurrent malaria-dengue infection. This overlapping of two different infections can result in more severe situations where both diagnosis and treatment of a patient may become difficult [10]. Initially, two cases of concurrent malaria and dengue infection were identified in July, 2005 and November, 2006 [4]. Malaria and dengue fever represent 2 major public health concerns in South America, whose 92% of area is covered by Amazon rain forest. According to the report in a French territory in South America, 0.99% from overall febrile patients are infected by malaria and dengue concurrently [4]. Malaria vectors and dengue vectors are habited in the forest [20] and in the city [7] respectively. Hence, overlapping of the habitat cannot be easily available and therefore concurrent malaria dengue infection cases are less in number.

Mathematical models relevant to the concurrent infections helps the researchers, biologists and public

[*]Corresponding author

166

health personnel to adopt improved and most effective strategies to control the diseases. Aldila D. and Agustin M. R. developed a nine-dimensional mathematical model to understand the spread of dengue and chikungunya in a closed population [1]. Isea R. & Lonngren K. E. presented two preliminary models that consist of the individual transmission dynamics of dengue, Chikungunya or Zika, and any possible co-infection between two diseases in the same population [12]. Sharomi et. al. developed a deterministic model which incorporates many of the essential biological and epidemiological features of HIV and tuberculosis and the synergistic interaction between them [25]. Silva C. J. & Torres D. F. proposed a population and introduced optimal treatment strategies for co-infection transmission dynamics of TB and HIV [26].

Some cases are reported where patients have symptoms of malaria and dengue both at the same time. In such situations, higher mortality rate is observed. On the basis of this observation, a mathematical model is constructed in the present work. Also two optimal controls are applied in the model in such a way that it helps to analyse malaria-dengue concurrent case and effect of recovery rate on the disease transmission. The paper is organized as follows. The malaria-dengue model construction will be discussed in section 2. Section 3 focuses on formulating basic reproduction number for concurrent malaria-dengue infection, moreover the equilibrium points of the given model are calculated. Local and global stability of all four equilibrium points are proved in section 4. Optimal control theory is introduced and applied to the model in section 5. The model is analysed numerically and graphically in the next section which provides better explanation of the analytic results.

2. Mathematical modeling

The environmental stress also damages the immune system and makes the individual weak to resist various kinds of infections. Motivated from this concurrent disease problem, we have proposed a compartmental model to analyze the spread of malaria and dengue infections individually and concurrently. The model subdivides the human population (N) into four mutually-exclusive compartments, namely susceptible individuals (S), malaria infected individuals (M), dengue infected individuals (D) and corresponding to two infectious agent class of recovered individuals is (R). Total recruitment rate in class of susceptible at time t is B. Susceptible individuals are infected by malaria infection with transmission rate α_1. The disease transmission from the class of susceptible individuals to the class of dengue infected individuals is taken as a saturated form with disease transmission rate α_2 and α_3 be the reciprocal of the half saturation constant. Therefore, from compartment S to D the disease

transmission form is taken as $\dfrac{\alpha_2 SD}{1+\alpha_3 D}$. The parameter α_4 represents the rate of the malaria infection giving rise to the dengue infection due to weak immunity. α_5 and α_6 are the rates at which the population infected by malaria and dengue are recovered respectively. μ is assumed as a natural death rate and μ_D be the dengue infection related death rate.

In Figure 1 the schematic diagram of the transmission of disease is shown. Here a concurrent disease case in which individual first get affected by dengue and then by malaria is ignored.
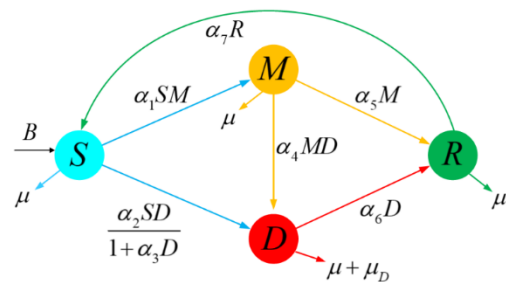
Figure 1. Schematic diagram of malaria-dengue model

On the basis these assumptions and figure 1, we formulate our model as:

$$\frac{dS}{dt} = B + \alpha_7 R - \alpha_1 SM - \frac{\alpha_2 SD}{1+\alpha_3 D} - \mu S$$

$$\frac{dM}{dt} = \alpha_1 SM - \alpha_4 MD - \alpha_5 M - \mu M$$

$$\frac{dD}{dt} = \frac{\alpha_2 SD}{1+\alpha_3 D} + \alpha_4 MD - \alpha_6 D - (\mu + \mu_D)D \qquad (1)$$

$$\frac{dR}{dt} = \alpha_6 D + \alpha_5 M - \alpha_7 R - \mu R$$

The initial conditions of the system (1) are $S(0) > 0$, $M(0) > 0$, $D(0) > 0$, $R(0) > 0$.

3. Basic reproduction number (R_0) and equilibrium

EnvironmentsNote that $S + M + D + R = N$ and all the compartments are taken positive. Summing all the equations of the system (1) gives,

$$\frac{d}{dt}(S + M + D + R) = B - \mu(S + M + D + R) - \mu_D D \geq 0$$

Hence, $\limsup_{t \to \infty}(S + M + D + R) \leq \dfrac{B}{\mu}$

Therefore, the feasible region for system (1) is:

$$\Lambda = \left\{ \begin{array}{c} (S + M + D + R)/(S + M + D + R) \leq \dfrac{B}{\mu}; \\ S \geq 0, M \geq 0, D \geq 0, R \geq 0 \end{array} \right\} \qquad (2)$$

Clearly the point $E_0 = (S_0, 0, 0, 0)$, where $S_0 = \dfrac{B}{\mu}$ is an equilibrium point of the system (1), which is called a disease free equilibrium point. The model has three more equilibrium points as follows,

I. Dengue free equilibrium point $E_1 = (S_1, M_1, 0, R_1)$

where, $S_1 = \dfrac{\alpha_5 + \mu}{\alpha_1}$, $M_1 = \dfrac{(\alpha_7 + \mu)k_1}{\alpha_1 \mu}$,

$R_1 = \dfrac{\alpha_5 k_1}{\alpha_1 \mu}$ and $k_1 = \dfrac{(B\alpha_1 - \alpha_5 \mu - \mu^2)}{\mu(\alpha_5 + \alpha_7 + \mu)}$

II. Malaria free equilibrium point $E_2 = (S_2, 0, M_2, R_2)$ where, $M_2 = k_2(\alpha_7 + \mu)$, $R_2 = \alpha_6 k_2$, where

$$S_2 = \frac{k_2 \left(\begin{array}{l} (\alpha_7 + \mu)((\mu_D + \alpha_6)(B\alpha_3 + \mu_D + \mu) \\ + \mu(\mu_D \mu + B\alpha_3 + \mu_D \alpha_6)) + \alpha_6 \mu(\alpha_6 + \mu) \end{array} \right)}{\mu(\mu_D + \mu) + \alpha_6 \mu - B\alpha_2} \text{ and}$$

$$k_2 = \frac{\mu(\mu_D + \mu) + \alpha_6 \mu - B\alpha_2}{\left(\begin{array}{l} (\alpha_7 + \mu)(\mu_D \alpha_3 \mu + \alpha_3 \mu(\alpha_6 + 1) + \alpha_2(\mu_D + \mu)) \\ + \alpha_2 \alpha_6 \mu \end{array} \right)}$$

III. Endemic equilibrium point $E^* = (S^*, M^*, D^*, R^*)$, where

$S^* = \dfrac{\alpha_4 k_3 + \alpha_5 + \mu}{\alpha_1}$, $D^* = k_3$,

$M^* = -\dfrac{(\alpha_7 + \mu)(\alpha_1 k_3 (\mu_D + \mu) + \mu(\alpha_4 k_3 + \alpha_5 + \mu) - B\alpha_1)}{\alpha_1 \mu(\alpha_5 + \alpha_7 + \mu)}$

$R^* = -\dfrac{\left(\begin{array}{l} \alpha_1 \alpha_5 k_3 (\mu_D + \mu) - k_3 \mu(\alpha_4 \alpha_5 - \alpha_1 \alpha_6) \\ -B\alpha_1 \alpha_5 + \alpha_5 \mu(\alpha_5 + \mu) \end{array} \right)}{\alpha_1 \mu(\alpha_5 + \alpha_7 + \mu)}$,

$k_3 = \text{Root of} \left\{ ((\alpha_7 + \mu)(\alpha_3 \alpha_4 (\mu_D \alpha_1 + \alpha_1 \mu + \alpha_4 \mu)) \right.$
$+ \alpha_1 \alpha_3 \alpha_4 \alpha_6 \mu) z^2 + ((\alpha_7 + \mu)((\alpha_1 \alpha_3 \mu + \alpha_1 \alpha_4)(\mu_D + \mu)$
$+ \alpha_3 \alpha_4 \mu(\alpha_5 + \mu) + \alpha_1 \alpha_3 (B\alpha_4 + \alpha_6 \mu)$
$+ \alpha_4 \mu(\alpha_4 - \alpha_2)) + \alpha_1 \alpha_3 \alpha_5 \mu(\alpha_6 + \mu)$
$+ \mu_D \alpha_1 \alpha_3 \alpha_5 \mu + \alpha_1 \alpha_4 \alpha_6 \mu - \alpha_2 \alpha_4 \alpha_5 \mu) z$
$+ (\alpha_7 + \mu)(\alpha_1 \mu(\alpha_6 + \mu) + \alpha_1 (\mu_D \mu - B\alpha_4)$
$+ \mu(\alpha_4 - \alpha_2)(\alpha_5 + \mu)) + \alpha_1 \alpha_5 \mu(\alpha_6 + \mu)$
$\left. - \alpha_2 \alpha_5 \mu(\alpha_5 + \mu) + \mu_D \alpha_1 \alpha_5 \mu \right\}$

Since the threshold parameter is useful in characterizing the spread of an infectious disease. Here, we use the next generation matrix ([9], [28], [3]) to obtain the expression of basic reproduction number R_0 for concurrent malaria-dengue infection.

Let $X = (S + M + D + R)$, then system (1) can be written as $X' = \mathscr{F}(X) - \mathscr{V}(X)$ such that,

$$\mathscr{F} = \begin{bmatrix} \alpha_1 SM \\ \dfrac{\alpha_2 SD}{1 + \alpha_3 D} + \alpha_4 MD \\ 0 \\ 0 \end{bmatrix},$$

$$\mathscr{V} = \begin{bmatrix} \alpha_4 MD + \alpha_5 M + \mu M \\ \alpha_6 D + \mu D + \mu_D D \\ -\alpha_6 D - \alpha_5 M + \alpha_7 R + \mu R \\ -B - \alpha_7 R + \alpha_1 SM + \dfrac{\alpha_2 SD}{1 + \alpha_3 D} + \mu S \end{bmatrix}$$

Let matrices $\mathcal{F}$ and $\mathcal{V}$ are be the Jacobian of $\mathscr{F}$ and $\mathscr{V}$ respectively around disease free equilibrium point (E_0):

$$\mathcal{F} = \begin{bmatrix} \dfrac{\alpha_1 B}{\mu} & 0 & 0 & 0 \\ 0 & \dfrac{\alpha_2 B}{\mu} & 0 & 0 \\ 0 & 0 & 0 & 0 \\ 0 & 0 & 0 & 0 \end{bmatrix},$$

$$\mathcal{V} = \begin{bmatrix} \alpha_5 + \mu & 0 & 0 & 0 \\ 0 & \mu + \mu_D + \alpha_6 & 0 & 0 \\ -\alpha_5 & -\alpha_6 & \alpha_7 + \mu & 0 \\ \dfrac{\alpha_1 B}{\mu} & \dfrac{\alpha_2 B}{\mu} & -\alpha_7 & \mu \end{bmatrix}$$

Here, the matrix $\mathcal{F}$ is related to the rate of increase of new individual in compartment and $\mathcal{V}$ to the rate of the diseases transmission in compartments.

The next generation matrix $K = (\mathcal{F} \mathcal{V}^{-1})$ have non negative eigenvalues. The basic reproduction number R_0 for the model is the spectral radius of $K = (\mathcal{F} \mathcal{V}^{-1})$, which is:

$$R_0 = \frac{\alpha_1 B}{\mu(\alpha_5 + \mu)} + \frac{\alpha_2 B}{\mu(\mu_D + \alpha_6 + \mu)} \qquad (3)$$

4. Stability analysis

This section includes stability results of all the equilibrium points of the proposed malaria-dengue model.

4.1. Local stability

Local stability of all the equilibrium points has been established by following theorems.

Theorem 1. *The disease free equilibrium point E_0 of model is locally asymptotically stable if it satisfy following two conditions.*

I. $\dfrac{\alpha_1 B}{\mu} > \alpha_5 + \mu$

II. $\dfrac{\alpha_2 B}{\mu} > \mu_D + \alpha_6 + \mu$

Proof. Jacobian matrix of the model around point E_0 is:

$$J(E_0) = \begin{bmatrix} -\mu & \dfrac{-\alpha_1 B}{\mu} & \dfrac{-\alpha_2 B}{\mu} & \alpha_7 \\[2mm] 0 & \dfrac{\alpha_1 B}{\mu} - \alpha_5 - \mu & 0 & 0 \\[2mm] 0 & 0 & \dfrac{\alpha_2 B}{\mu} - \mu_D - \alpha_6 - \mu & 0 \\[2mm] 0 & \alpha_5 & \alpha_6 & -\alpha_7 - \mu \end{bmatrix}$$

Eigenvalues of the matrix $J(E_0)$ are $\lambda_1^0 = -\mu$,

$\lambda_2^0 = \dfrac{\alpha_1 B}{\mu} - \alpha_5 - \mu$, $\lambda_3^0 = \dfrac{\alpha_2 B}{\mu} - \mu_D - \alpha_6 - \mu$,

$\lambda_4^0 = -(\alpha_7 + \mu)$.

Clearly all the eigenvalues are negative if $\dfrac{\alpha_1 B}{\mu} > \alpha_5 + \mu$ and $\dfrac{\alpha_2 B}{\mu} > \mu_D + \alpha_6 + \mu$, hence disease free equilibrium point is locally asymptotically stable under these conditions. □

Theorem 2. *The dengue free equilibrium point E_1 is locally asymptotically stable if it satisfy following two conditions.*

I. $B\alpha_1 > \mu(\alpha_5 + \mu)$

II. $\alpha_2(\alpha_5 + \mu) < \alpha_1(\mu_D + \mu)$ and $\alpha_6\mu > B\alpha_5$

Proof. Jacobian matrix of the model around point E_1 is:

$$J(E_1) = \begin{bmatrix} -n_1 - \mu & -n_5 - \mu & -n_2 & \alpha_7 \\[2mm] n_1 & 0 & -\dfrac{\alpha_4 n_1}{\alpha_1} & 0 \\[2mm] 0 & 0 & n_2 + \dfrac{\alpha_4 n_1}{\alpha_1} - \mu_D - \alpha_6 - \mu & 0 \\[2mm] 0 & \alpha_5 & \alpha_6 & -(\alpha_7 + \mu) \end{bmatrix}$$

Where, $n_1 = \dfrac{(B\alpha_1 - \alpha_5\mu - \mu^2)(\alpha_7 + \mu)}{\mu(\alpha_5 + \alpha_7 + \mu)}$ and

$n_2 = \dfrac{\alpha_2(\alpha_5 + \mu)}{\alpha_1}$.

Eigenvalues of the Jacobian matrix $J(E_1)$ are:

$\lambda_1^1 = -\mu$, $\lambda_2^1 = -\dfrac{1}{2\mu(\alpha_5 + \alpha_7 + \mu)}\left(\beta_1 - \sqrt{\beta_2}\right)$,

$\lambda_3^1 = -\dfrac{\left(\beta_1 + \sqrt{\beta_2}\right)}{2\mu(\alpha_5 + \alpha_7 + \mu)}$,

$\lambda_4^1 = -\dfrac{\begin{pmatrix} (\alpha_7 + \mu)\left(\alpha_1\mu(\mu_D + \mu)(1+\alpha_5) - B\alpha_1\alpha_5 \right. \\ + \alpha_1\alpha_6\mu + (\alpha_5 + \mu)(\alpha_4\mu - \alpha_2\mu(1+\alpha_5))) \end{pmatrix}}{\alpha_1\mu(\alpha_5 + \alpha_7 + \mu)}$

Where, $\beta_1 = (\alpha_7 + \mu)(B\alpha_1 + \mu\alpha_7)$,

$\beta_2 = (\alpha_7 + \mu)\left((\alpha_7 + \mu)\left((\alpha_7 + \mu)(4\mu^2(\alpha_7 + \mu) - 2B\alpha_1\mu)\right.\right.$

$\left. + 2\mu(\alpha_5 + \mu)(4\alpha_5\mu - B\alpha_1) + B\alpha_1(B\alpha_1 - 6\alpha_5\mu) + \alpha_7^2\mu^2\right)$

$\left. + 4\alpha_5^2\mu(-B\alpha_1 + \alpha_5 + \mu)\right)$

Eigenvalues λ_2^1 and λ_3^1 are complex when β_2 is negative, real part of both these eigenvalues are negative and when β_2 is positive, real part of both the eigenvalues λ_2^1 and λ_3^1 are negative when $\left(\beta_1 - \sqrt{\beta_2}\right) > 0$,

i.e $\left(\beta_1^2 - \beta_2\right) > 0$

$\beta_1^2 - \beta_2$

$= (\alpha_7 + \mu)\left((\alpha_7 + \mu)\left((\alpha_7 + \mu)4\mu(B\alpha_1 - \alpha_5\mu - \mu^2)\right.\right.$

$\left. + 8\alpha_5^2\mu(B\alpha_1 - \alpha_5\mu - \mu^2)\right) + 4\alpha_5^2\mu(B\alpha_1 - \alpha_5\mu - \mu^2))$

Hence, real part of eigenvalues λ_2^1 and λ_3^1 are negative when $B\alpha_1 > \mu(\alpha_5 + \mu)$.

$\lambda_4^1 = \dfrac{\begin{pmatrix} (\alpha_7 + \mu)\left(\mu(\alpha_4 - \alpha_2)(\alpha_5 + \mu) + \alpha_1\mu(\mu_D + \mu)\right. \\ -B\alpha_1\alpha_5 + \alpha_1\alpha_6\mu + \alpha_1\alpha_5\mu(\mu_D + \mu) - \alpha_2\alpha_5\mu(\alpha_5 + \mu)) \end{pmatrix}}{-\alpha_1\mu(\alpha_5 + \alpha_7 + \mu)}$

$\lambda_4^1 < 0$ when $\alpha_2(\alpha_5 + \mu) < \alpha_1(\mu_D + \mu)$ and $\alpha_6\mu > B\alpha_5$. Clearly, all the eigenvalues are negative under these conditions. Hence, the theorem. □

Theorem 3. *The malaria free equilibrium point E_2 is locally asymptotically stable if it satisfy following two conditions.*

I. $k_2(\alpha_7 + \mu)\alpha_4 + \dfrac{\alpha_1 n_3 k_2}{n_4} > \alpha_5 + \mu$

II. $\mu > n_6$, $\alpha_6 > n_5$ and $n_5^2 + n_6^2 > 2\mu n_6$

Proof. Jacobian matrix of the model around point E_2 is:

$$J(E_2) = \begin{bmatrix} n_6 - \mu & -\dfrac{\alpha_1 n_3 k_2}{n_4} & -n_5 & \alpha_7 \\[2mm] 0 & k_2(\alpha_7 + \mu)\alpha_4 + \dfrac{\alpha_1 n_3 k_2}{n_4} - \alpha_5 - \mu & 0 & 0 \\[2mm] -n_6 & -k_2(\alpha_7 + \mu)\alpha_4 & n_5 - \mu_D - \alpha_6 - \mu & 0 \\[2mm] 0 & \alpha_5 & \alpha_6 & -\alpha_7 - \mu \end{bmatrix}$$

Where, $n_3 = \mu(\mu_D + \mu) + \alpha_6\mu - B\alpha_2$,

$n_4 = (\alpha_7 + \mu)\left((\mu_D + \alpha_6)(B\alpha_3 + \mu_D + \mu)\right.$

$\left. + \mu(\mu_D\mu + B\alpha_3 + \mu_D\alpha_6)\right) + \alpha_6\mu(\alpha_6 + \mu)$,

$n_5 = \dfrac{-\alpha_2 n_2 k_2}{n_4(-k_2(\alpha_7 + \mu)\alpha_3 + 1)^2}$, $n_6 = \dfrac{\alpha_2 k_2(\alpha_7 + \mu)}{-n_5(\alpha_7 + \mu)\alpha_3 + 1}$.

Clearly, $\lambda_1^2 = k_2(\alpha_7 + \mu)\alpha_4 + \dfrac{\alpha_1 n_3 k_2}{n_4} - \alpha_5 - \mu$ is one of the eigen value of $J(E_2)$, hence characteristic equation is given by:

$Ch(x) = \left(x - k_2(\alpha_7 + \mu)\alpha_4 - \dfrac{\alpha_1 n_3 k_2}{n_4} + \alpha_5 + \mu\right)\phi(x)$

Where, $\phi(x) = x^3 + a_1 x^2 + a_2 x + a_3$

$a_1 = \alpha_7 + 3\mu - n_5 + \mu_D + \alpha_6 - n_6$,

$a_2 = (\alpha_7 + \mu)(\alpha_6 + \mu) + (\mu - n_6)(\mu_D + \alpha_6 + \alpha_7 + \mu)$
$\quad + (\mu - n_5)(\alpha_7 + 2\mu) - \mu n_6$,

$a_3 = (\mu - n_6)(\mu_D(\alpha_7 + \mu) + \mu(\alpha_6 + \alpha_7)) + \alpha_7 \mu(\alpha_6 - n_5)$
$\quad + \mu^2(\mu - n_5)$

$a_1 a_2 - a_3$
$= (\alpha_7 + \mu)\big(\mu_D(\mu_D \mu + \alpha_6) + (\alpha_6 + \alpha_7)(\mu_D + \alpha_6)\big)$
$\quad + (\mu - n_6)\big((\mu_D + 2\mu)(\mu_D + \alpha_6) + (\mu_D + \alpha_6)(\alpha_6 + \alpha_7)$
$\quad + (\alpha_7 + \mu)(\mu_D + 2\alpha_6 + \alpha_7) + \mu(\mu_D + \alpha_7)\big) + \mu_D \alpha_7 \mu$
$\quad + (\mu - n_5)\big((2\mu_D + 2\alpha_6 + \alpha_7)(\alpha_7 + \mu) + 2\mu(\mu_D + \alpha_6)$
$\quad + \mu(5\alpha_7 + 8\mu)\big) + n_6(\mu_D + \alpha_6)(n_5 + n_6 - 2\mu)$
$\quad + 4\mu n_6(n_5 - n_6) + (n_5 + n_6)(\alpha_7 n_5 + \alpha_7 n_6)$
$\quad + 2\mu(n_5^2 + n_6^2 - 2\mu n_6)$

$a_1, a_3 > 0$ and $a_1 a_2 > a_3$ if $\mu > n_6$, $\alpha_6 > n_5$ and $n_5^2 + n_6^2 > 2\mu n_6$. Hence, by applying Routh-Hurwitz criteria we can say all real roots of $Ch(x)$ are negative under these conditions. $\qquad\square$

Theorem 4. *The endemic equilibrium point E^* is locally asymptotically stable if it satisfy following two conditions.*

    I. $k_2(\alpha_7 + \mu)\alpha_4 + \dfrac{\alpha_1 n_3 k_2}{n_4} > \alpha_5 + \mu$

    II. $\mu > n_6$, $\alpha_6 > n_5$ and $n_5^2 + n_6^2 > 2\mu n_6$

Proof. Jacobian matrix of the model around point E^* is $J(E^*) = [x_{ij}]$.

Where, $x_{11} = -\alpha_1 M^* - \dfrac{\alpha_2 D^*}{D^* \alpha_3 + 1} - \mu$, $x_{12} = -\alpha_1 S^*$,

$x_{13} = \dfrac{-\alpha_2 S^*}{(D^* \alpha_3 + 1)^2}$, $x_{14} = \alpha_7$, $x_{21} = \alpha_1 M^*$,

$x_{22} = -D^* \alpha_4 + S^* \alpha_1 - \alpha_5 - \mu$, $x_{23} = -\alpha_4 M^*$, $x_{24} = 0$,

$x_{31} = \dfrac{\alpha_2 D^*}{D^* \alpha_3 + 1}$, $x_{32} = \alpha_4 D^*$, $x_{34} = 0$, $x_{41} = 0$, $x_{42} = \alpha_5$

$x_{33} = \dfrac{\alpha_2 S^*}{(D^* \alpha_3 + 1)^2} + \alpha_4 M^* - \mu_D - \alpha_6 - \mu$, $x_{43} = \alpha_6$,

$x_{44} = -\alpha_7 - \mu$

The characteristic equation of matrix $J(E^*)$ is $Ch^*(x) = x^4 + b_1 x^3 + b_2 x^2 + b_3 x + b_4 = 0$.

Where, $b_1 = -x_{44} - x_{33} - x_{22} - x_{11}$,

$b_2 = x_{11}x_{22} + x_{11}x_{33} + x_{11}x_{44} - x_{12}x_{21} - x_{13}x_{31} + x_{22}x_{33}$
$\quad + x_{22}x_{44} - x_{32}x_{23} + x_{33}x_{44}$,

$b_3 = -x_{11}x_{22}x_{33} - x_{11}x_{22}x_{44} + x_{11}x_{23}x_{32} - x_{11}x_{33}x_{44}$
$\quad + x_{12}x_{21}x_{33} + x_{12}(x_{21}x_{44} - x_{23}x_{31}) - x_{21}(x_{13}x_{32} - x_{14}x_{42})$
$\quad + x_{31}x_{13}x_{22} - x_{31}(x_{14}x_{43} - x_{13}x_{44}) - x_{22}x_{33}x_{44} + x_{23}x_{32}x_{44}$

$b_4 = x_{11}x_{44}(x_{22}x_{33} - x_{23}x_{32}) + x_{13}x_{44}(x_{12}x_{23} - x_{13}x_{22})$
$\quad + x_{21}x_{32}(x_{13}x_{44} - x_{14}x_{43}) + x_{21}x_{33}(x_{14}x_{42} - x_{12}x_{44})$
$\quad + x_{14}x_{31}(x_{22}x_{43} - x_{23}x_{42})$.

$b_2 > 0$ when x_{22}, x_{33} are negative.

$x_{22} < 0 \Leftrightarrow S^* \alpha_1 < \alpha_5 + \mu + D^* \alpha_4$ and

$x_{33} < 0 \Leftrightarrow \dfrac{\alpha_2 S^*}{(D^* \alpha_3 + 1)^2} + \alpha_4 M^* < \mu_D + \alpha_6 + \mu$.

$b_3 > 0$ when $\alpha_1 M^*(\alpha_7 - \mu) > \dfrac{\alpha_4 \alpha_2 D^* M^*}{D^* \alpha_3 + 1}$,

$\dfrac{\alpha_2 \alpha_4 S^* D^*}{(D^* \alpha_3 + 1)^2} > \alpha_7 \alpha_5$ and $\dfrac{\alpha_2 S^*(\alpha_7 + \mu)}{(D^* \alpha_3 + 1)^2} > \alpha_7 \alpha_6$.

$b_4 = x_{11}x_{44}(x_{22}x_{33} - x_{23}x_{32}) + x_{13}x_{44}(x_{12}x_{23} - x_{13}x_{22})$
$\quad + x_{21}x_{32}(x_{13}x_{44} - x_{14}x_{43}) + x_{21}x_{33}(x_{14}x_{42} - x_{12}x_{44})$
$\quad + x_{14}x_{31}(x_{22}x_{43} - x_{23}x_{42})$

and $b_4 > 0$ when,

$\alpha_1 \alpha_4 S^* M^* > \dfrac{\alpha_2 S^*}{(D^* \alpha_3 + 1)^2}\big(D^* \alpha_4 - S^* \alpha_1 + \alpha_5 + \mu\big)$,

$\dfrac{\alpha_2 S^*(\alpha_7 + \mu)}{(D^* \alpha_3 + 1)^2} > \alpha_7 \alpha_6$, $\alpha_7 \alpha_5 > \alpha_1 S^*(\alpha_7 + \mu)$,

$\alpha_4 \alpha_5 M^* > \big(D^* \alpha_4 - S^* \alpha_1 + \alpha_5 + \mu\big)\alpha_6$. $\qquad\square$

4.2. Global stability

To perform the global stability analysis of the disease free equilibrium we use the method developed by [5].

4.2.1. Global stability of disease-free equilibrium point (E_0)

The model system can be written as follows:

$$\frac{dX_{(0)}}{dt} = F_0(X_{(0)}, Z_{(0)})$$
$$\frac{dZ_{(0)}}{dt} = G_0(X_{(0)}, Z_{(0)}), \; G_0(X_{(0)}, 0) = 0 \tag{4}$$

Here $X_{(0)} = X_{(0)}(X_1^0) \in \mathbb{R}$ represents the number of uninfected individuals and $Z_{(0)} = Z_0(Y_1^0, Y_2^0, Y_3^0) \in \mathbb{R}^3$ denotes the number of infected individuals. According to this notation the disease-free equilibrium point is denoted by $E_0 = (S_0, 0)$.

Now as per the method given in [5], following two conditions will ensure global stability of the disease-free equilibrium point.

[H1] $\dfrac{dX_{(0)}}{dt} = F_0(X_{(0)}, 0)$, $E_0 = (X_0, 0)$ is globally asymptotically stable.

[H2] $G_0(X_{(0)}, Z_{(0)}) = B_1 M + \left[B_2 - \dfrac{\alpha_2 \alpha_3 DS^0}{1 + \alpha_3 D} \right] D + B_3 R - \hat{G}_0(X_{(0)}, Z_{(0)})$

    , where $\hat{G}_0(X_{(0)}, Z_{(0)}) \geq 0$ for $(X_{(0)}, Z_{(0)}) \in \Lambda$.

Here, $B_1 = D_M G_0(X_0, 0)$, $B_2 = D_D G_0(X_0, 0)$ and $B_3 = D_R G_0(X_0, 0)$ are matrix with non-negative off diagonal entries.

Lemma 1. *The fixed point $E_0 = (S_0, 0)$ is a globally*

asymptotically stable equilibrium of the system, provided $R_0 < 1$ and assumptions [H1] and [H2] are satisfied.

Theorem 5. *For $R_0 < 1$, the disease free equilibrium point is globally asymptotically stable.*

Proof. we begin by showing [H1] as $F_0(X_{(0)}, 0) = [B - \mu S]$ and $Ch_{(0)}(\lambda) = (\lambda + \mu) = 0$ is the characteristic polynomial of its Jacobian matrix. Since the polynomial have a negative root, $E_0 = (S_0, 0)$ is globally asymptotically stable.

Now, we have

$$G_0(X_{(0)}, Z_{(0)}) = (\alpha_1 S_0 - \mu)M + \left(\frac{\alpha_2 S_0}{1 + \alpha_3 D} - (\mu + \mu_D)\right)D - (\alpha_7 + \mu)R$$

$$- \left(\alpha_1 M(S_0 - S) + \frac{\alpha_2 D}{1 + \alpha_3 D} - (S_0 - S)\right)$$

$$= B_1 M + \left[B_2 - \frac{\alpha_2 \alpha_3 D S_0}{1 + \alpha_3 D}\right]D + B_3 R - \hat{G}_0(X_{(0)}, Z_{(0)})$$

Here, $\hat{G}_0(X, Z) \geq 0$ hence, the conditions (H1) and (H2) stated above are satisfied. $\square$

4.2.2. Global stability of dengue-free equilibrium point (E_1)

The model system can be written as

$$\frac{dX_{(1)}}{dt} = F_1(X_{(1)}, Z_{(1)})$$

$$\frac{dZ_{(1)}}{dt} = G_1(X_{(1)}, Z_{(1)}), \; G_1(X_{(1)}, 0) = 0 \tag{5}$$

Here $X_{(1)} = X_{(1)}(X_1^1, X_2^1, X_3^1) \in \mathbb{R}^3$ represents the number of uninfected individuals and $Z_{(1)} = Z_1(Y_1^1) \in \mathbb{R}$ denotes the number of infected individuals. According to this notation the Dengue free equilibrium point is denoted by $E_1 = (X_{(1)}^1, 0)$, where $X_{(1)}^1 = (S_1, M_1, R_1)$.

The following two conditions will ensure global stability of the dengue-free equilibrium point:

[H3] $\dfrac{dX_{(1)}}{dt} = F_1(X_{(1)}, 0)$, $\quad E_1 = (X_{(1)}^1, 0)$ is globally asymptotically stable.

[H4] $G_1(X_{(1)}, Z_{(1)}) = B_4 D - \dfrac{\alpha_2 \alpha_3 D S_1}{1 + \alpha_3 D} - \hat{G}_1(X_{(1)}, Z_{(1)})$,

where $\hat{G}_1(X_{(1)}, Z_{(1)}) \geq 0$ for $(X_{(1)}, Z_{(1)}) \in \Lambda$.

Here $B_4 = D_D G_1\left(X_{(1)}^1, 0\right)$ is a M-matrix.

Lemma 2. *The fixed point $E_1 = (X_{(1)}^1, 0)$ is a globally asymptotically stable equilibrium of the system, provided $R_0 < 1$ and assumptions [H3] and [H4] are satisfied.*

Theorem 6. *For $R_0 < 1$, the disease-free equilibrium point is globally asymptotically stable when*

$D\alpha_4 > S\alpha_1$.

Proof. we begin by showing [H3] as

$$F_1(X_{(1)}, 0) = \begin{bmatrix} B + \alpha_7 R - \alpha_1 SM - \mu S \\ \alpha_1 SM - \alpha_5 M - \mu M \\ \alpha_5 M - \alpha_7 R - \mu R \end{bmatrix} \text{ and}$$

$Ch_{(1)}(\lambda) = (\lambda^3 + c_1 \lambda^2 + c_2 \lambda + c_3) = 0$ is the characteristic polynomial of its Jacobian matrix. Where, $c_1 = (D\alpha_4 - S\alpha_1) + M\alpha_1 + \alpha_5 + \alpha_7 + 3\mu$,

$$c_2 = (D\alpha_4 - S\alpha_1)(\alpha_7 + 2\mu) + (M\alpha_1 + \alpha_7)(D\alpha_4 + \alpha_5)$$
$$+ 2\mu(M\alpha_1 + \alpha_5) + 2\mu(\alpha_7 + \mu) + \mu^2$$

$$c_3 = (\alpha_7 + \mu)\big(\mu(D\alpha_4 - S\alpha_1) + MD\alpha_1\alpha_4 + \alpha_5\mu\big)$$
$$+ M\alpha_1\mu(\alpha_5 + \alpha_7) + \mu^2(M\alpha_1 + \alpha_7) + \mu^3.$$

$$c_1 c_2 - c_3 = (D\alpha_4 - S\alpha_1)$$
$$\big((\alpha_7 + \mu)(D\alpha_4 + 2M\alpha_1 + 2\alpha_5 + \alpha_7 + 4\mu)$$
$$+ M\alpha_1(D\alpha_4 + \alpha_5)\big) + (\alpha_7 + 2\mu)\big(M\alpha_1(3\alpha_5 + M\alpha_1)$$
$$+ (\alpha_7 + 4\mu)(M\alpha_1 + \alpha_5) + 2\mu(\alpha_7 + 2\mu) + \alpha_5^2\big)$$
$$+ M^2\alpha_1^2(D\alpha_4 + \alpha_5) + S^2\alpha_1^2(\alpha_7 + \mu)$$
$$+ M\alpha_1\alpha_5(\alpha_5 + D\alpha_4) + 2DM\alpha_1\alpha_4\mu$$

$c_1, c_2 > 0$ and $c_1 c_2 - c_3 > 0$ if $D\alpha_4 > S\alpha_1$.

With the help of Routh-Hurwitz criteria it is clear that all the roots of the characteristic polynomial have negative real part when $D\alpha_4 > S\alpha_1$, hence $E_1 = (X_{(1)}^1, 0)$ is globally asymptotically stable under this condition.

Now,

$$G_1(X_{(1)}, Z_{(1)}) = \left(\frac{\alpha_2 S_1}{1 + \alpha_3 D} + \alpha_4 M_1 - \alpha_6 - (\mu + \mu_D)\right)D$$
$$- \left(\frac{\alpha_2 D}{1 + \alpha_3 D}(S_1 - S) + \alpha_4 D(M_1 - M)\right)$$
$$= \left(B_5 - \frac{\alpha_2 \alpha_3 D S_1}{1 + \alpha_3 D}\right)D - \hat{G}_1(X_{(1)}, Z_{(1)})$$

Here, $\hat{G}_1(X, Z) \geq 0$ hence, the conditions (H3) and (H4) stated above are satisfied. $\square$

4.2.3. Global stability of malaria-free equilibrium point (E_2)

The model system can be written as:

$$\frac{dX_{(2)}}{dt} = F_2(X_{(2)}, Z_{(2)})$$

$$\frac{dZ_{(2)}}{dt} = G_2(X_{(2)}, Z_{(2)}), \; G_2(X_{(2)}, 0) = 0 \tag{6}$$

Here $X_{(2)} = X_{(2)}(X_1^2, X_2^2, X_3^2) \in \mathbb{R}^3$ represents the number of uninfected individuals and $Z_{(2)} = Z_2(Y_1^2) \in \mathbb{R}$ denotes the number of infected individuals. According to this notation the Dengue free equilibrium point is denoted by $E_2 = (X_{(2)}^1, 0)$, where

$X^1_{(2)} = (S_2, D_2, R_2)$.

The following two conditions will ensure global stability of the malaria-free equilibrium point:

[H5] $\dfrac{dX_{(2)}}{dt} = F_2(X_{(2)}, 0)$, $E_2 = (X^1_{(2)}, 0)$ is globally asymptotically stable.

[H6] $G_2(X_{(2)}, Z_{(2)}) = B_5 M - \hat{G}_2(X_{(2)}, Z_{(2)})$, where

$$\hat{G}_2(X_{(2)}, Z_{(2)}) \geq 0 \text{ for } (X_{(2)}, Z_{(2)}) \in \Lambda.$$

Here $B_5 = D_M G_2\left(X^1_{(2)}, 0\right)$ is a M-matrix.

Lemma 3. *The fixed point $E_2 = (X^1_{(2)}, 0)$ is a globally asymptotically stable equilibrium of the system, provided $R_0 < 1$ and assumptions [H5] and [H6] are satisfied.*

Theorem 7. *For $R_0 < 1$, the disease-free equilibrium point is globally asymptotically stable if*
$$\dfrac{\alpha_2 S}{(1+\alpha_3 D)^2} < \alpha_6 + \mu + \mu_D.$$

Proof. we begin by showing [H5] as:

$$F_2(X_{(2)}, 0) = \begin{bmatrix} B + \alpha_7 R - \dfrac{\alpha_2 SD}{1+\alpha_3 D} - \mu S \\[2mm] \dfrac{\alpha_2 SD}{1+\alpha_3 D} - \alpha_6 D - (\mu + \mu_D)D \\[2mm] \alpha_6 D - \alpha_7 R - \mu R \end{bmatrix} \text{ and}$$

$Ch_{(2)}(\lambda) = (\lambda^3 + d_1 \lambda^2 + d_2 \lambda + d_3) = 0$ is the characteristic polynomial of its Jacobian matrix. Where, $d_1 = n_7 + n_8 + n_9$,

$d_2 = (n_9 + \mu)(n_7 + n_8) + n_7(\mu_D + \alpha_6) - \mu(\mu_D + \alpha_6 + \mu)$
and $d_3 = (n_7 - \mu)(\mu_D n_9 + n_9 \mu + \alpha_6 \mu) + n_8 n_9 \mu$

where, $n_7 = \dfrac{\alpha_2 D}{1+\alpha_3 D} + \mu$,

$n_8 = \dfrac{-\alpha_2 S}{(1+\alpha_3 D)^2} + \alpha_6 + \mu + \mu_D$ and $n_9 = \alpha_7 + \mu$.

$d_1 d_2 - d_3 = (n_7 - \mu)$
$$\left((n_7 + n_8)(\mu_D + \mu + \alpha_6) + \alpha_6(n_9 + \mu)\right)$$
$$+ n_7 n_8(n_9 + \mu) + n_8 n_9(n_7 + n_8)$$
$$+ n_7 n_9(n_7 + n_9) + n_8(n_8 \mu + n_9^2)$$

Clearly, $n_7 > \mu$ hence $d_3 > 0$ and $d_1 d_2 - d_3 > 0$. $d_1 > 0$

if $\dfrac{\alpha_2 S}{(1+\alpha_3 D)^2} < \alpha_6 + \mu + \mu_D$.

With the help of Routh-Hurwitz criteria it is clear that all the roots of the characteristic polynomial have negative real part, hence $E_2 = (X^1_{(2)}, 0)$ is globally asymptotically stable.

Now,

$G_2(X_{(2)}, Z_{(2)}) = (\alpha_1 S_2 - \alpha_4 D_2 - \alpha_5 - \mu)M$
$$-\left(\alpha_1(S_2 - S) + \alpha_4(D_2 - D)\right)M$$
$$= B_5 M - \hat{G}_2(X_{(2)}, Z_{(2)})$$

Here, $\hat{G}_2(X, Z) \geq 0$ hence, the conditions (H5) and (H6) stated above are satisfied. $\square$

4.2.4. Global stability of endemic equilibrium point (E^*)

We analyze global stability of an endemic equilibrium point through a geometric approach described in [16], [27] and [15]. To use this method let we modify our system (1) as follow:

$$\frac{dS}{dt} = B + \frac{\alpha_7(\alpha_6 D + \alpha_5 M)}{(\alpha_7 + \mu)} - \alpha_1 SM - \frac{\alpha_2 SD}{1+\alpha_3 D} - \mu S$$

$$\frac{dM}{dt} = \alpha_1 SM - \alpha_4 MD - \alpha_5 M - \mu M \qquad (7)$$

$$\frac{dD}{dt} = \frac{\alpha_2 SD}{1+\alpha_3 D} + \alpha_4 MD - \alpha_6 D - (\mu + \mu_D)D$$

Let $K \subset \mathbb{R}^3$ be a simply connected open set and $f \in C^1(K)$. Further suppose that $\varphi(t)$ be a solution to the following system,

$x' = f(x)$

(7) Suppose $P(x)$ be a matrix valued function on K and let $Q = P_f P^{-1} + PM^{[2]}P^{-1}$.

Here, the matrix P_f is:

$$\left(P_{ij}(x)\right)_f = \left(\frac{\partial P_{ij}(x)}{\partial x}\right).f(x) = \nabla P_{ij}.f(x).$$

Jacobian matrix of an arbitrary point is $M = [c_{ij}]$:

Where, $c_{11} = -\alpha_1 M - \dfrac{\alpha_2 D}{1+\alpha_3 D} - \mu$, $c_{12} = \dfrac{\alpha_7 \alpha_5}{\alpha_7 + \mu} - \alpha_1 S$,

$c_{13} = \dfrac{\alpha_7 \alpha_6}{\alpha_7 + \mu} - \dfrac{\alpha_2 S}{(1+\alpha_3 D)^2}$, $c_{21} = \alpha_1 M$, $c_{23} = -\alpha_4 M$,

$c_{22} = \alpha_1 S - \alpha_4 D - \alpha_5 - \mu$, $c_{31} = \dfrac{\alpha_2 D}{1+\alpha_3 D}$, $c_{32} = \alpha_4$,

$c_{33} = \dfrac{\alpha_2 S}{(1+\alpha_3 D)^2} + \alpha_4 M - \alpha_6 - (\mu + \mu_D)$.

The second additive compound matrix obtain from the Jacobian matrix M is $M^{[2]}$,

$$M^{[2]} = \begin{bmatrix} n_{10} & -\alpha_4 M & \dfrac{\alpha_2 S}{(1+\alpha_3 D)^2} - \dfrac{\alpha_7 \alpha_6}{\alpha_7 + \mu} \\[3mm] \alpha_4 & n_{11} & \dfrac{\alpha_7 \alpha_5}{\alpha_7 + \mu} - \alpha_1 S \\[3mm] -\dfrac{\alpha_2 D}{1+\alpha_3 D} & \alpha_1 M & n_{12} \end{bmatrix}$$

Where $n_{10} = \alpha_1 S - \alpha_4 D - \alpha_5 - 2\mu - \alpha_1 M - \dfrac{\alpha_2 D}{1+\alpha_3 D}$,

$$n_{11} = \frac{\alpha_2 S}{\left(1+\alpha_3 D\right)^2} + \alpha_4 M - \alpha_6 - 2\mu - \mu_D - \alpha_1 M - \frac{\alpha_2 D}{1+\alpha_3 D}$$

, and

$$n_{12} = \alpha_1 S - \alpha_4 D - \alpha_5 + \frac{\alpha_2 S}{\left(1+\alpha_3 D\right)^2} + \alpha_4 M - \alpha_6 - 2\mu - \mu_D$$

Next, consider the following system:

$$\frac{dz}{dt} = \Phi\left(\varphi(t)\right) z \tag{8}$$

And if (8) is stable then also the second compound equation $\frac{d\overline{z}}{dt} = M^{[2]}\left(\varphi(t)\right)\overline{z}$ is stable, moreover φ belong to a set in which $\left|P^{-1}\right|$ is bounded. A set $\overline{K}$ is absorbing with respect to (7) if solution exist for all $t \geq 0$ and $x(t, K_1) \subset \overline{K}$ for all t, where K_1 is any bounded subset of K.

To prove global stability through this approach we use techniques developed in [19].

Let, $P = \frac{1}{D} I_3$, where I_3 is an identity matrix of order 3. Hence, $P_f P^{-1} = -\frac{D'}{D} I_3$.

Next, $Q = P_f P^{-1} + P M^{[2]} P^{-1}$

$$= \begin{bmatrix} n_{10} - \dfrac{D'}{D} & -\alpha_4 M & \dfrac{\alpha_2 S}{\left(1+D\alpha_3\right)^2} - \dfrac{\alpha_7\alpha_6}{\alpha_7+\mu} \\[2ex] \alpha_4 & n_{11} - \dfrac{D'}{D} & \dfrac{\alpha_7\alpha_5}{\alpha_7+\mu} - \alpha_1 S \\[2ex] -\dfrac{\alpha_2 D}{1+\alpha_3 D} & \alpha_1 M & n_{12} - \dfrac{D'}{D} \end{bmatrix}$$

Where,

$$n_{10} - \frac{D'}{D} = \alpha_1 S - \alpha_4 D - \alpha_5 - \mu - \left(\alpha_1+\alpha_4\right)M - \frac{\alpha_2(S+D)}{1+\alpha_3 D}$$

$$n_{11} - \frac{D'}{D} = \frac{\alpha_3\alpha_2 SD}{\left(1+D\alpha_3\right)^2} - \alpha_1 S - \frac{\alpha_2 D}{1+\alpha_3 D} - \mu \text{ and}$$

$$n_{12} - \frac{D'}{D} = \frac{-\alpha_3\alpha_2 SD}{\left(1+D\alpha_3\right)^2} + \alpha_1 S - \alpha_4 D - \alpha_5 - \mu .$$

Let we define the following norm function as described in [2] for some $z = \left(z_1,\ z_2,\ z_3\right)$.

$$\|z\| = \begin{cases} \max\left\{\left|z_1\right|+\left|z_3\right|, \left|z_2\right|+\left|z_3\right|\right\} & \text{if } z_2 z_3 \geq 0 \\ \max\left\{\left|z_1\right|+\left|z_3\right|, \left|z_2\right|\right\} & \text{if } z_2 z_3 < 0 \end{cases}$$

Now we explore the existence of some $\chi > 0$, so that $D_+ \|z\| \leq -\chi\|z\|$. In this situation we have to analyses all eight possible cases.

Case 1   If $0 < z_1, z_2, z_3$ and $\left|z_1\right|+\left|z_3\right| > \left|z_2\right|+\left|z_3\right|$ then

$$\|z\| = \left|z_1\right|+\left|z_3\right| \text{ and } D_+\|z\| = D_+\left(\left|z_1\right|+\left|z_3\right|\right) = z_1' + z_3'$$

$$D_+\|z\| = \left[\alpha_1 S - \alpha_4 D - \alpha_5 - \mu - \left(\alpha_1+\alpha_4\right)M \right.$$
$$\left. - \frac{\alpha_2(S+D)}{1+\alpha_3 D} - \alpha_6 - \mu_D \right] z_1 + \left[-\alpha_4 M\right] z_2$$
$$+ \left[\frac{\alpha_2 S}{\left(D\alpha_3+1\right)^2} - \frac{\alpha_7\alpha_6}{\alpha_7+\mu}\right] z_3 + \left[-\frac{\alpha_2 D}{D\alpha_3+1}\right] z_1$$
$$+ \left[\alpha_1 M\right] z_2$$
$$+ \left[\frac{-\alpha_2\alpha_3 SD}{\left(D\alpha_3+1\right)^2} + \alpha_1 S - \alpha_4 D - \alpha_5 - \mu\right] z_3$$
$$\leq \left[\alpha_1 S - \alpha_4 D - \alpha_5 - \mu - \left(\alpha_1+\alpha_4\right)M - \frac{\alpha_2(S+D)}{1+\alpha_3 D} \right.$$
$$\left. - \alpha_6 - \mu_D\right]\left|z_1\right| + \left[\alpha_1 M - \alpha_4 M\right]\left|z_2\right|$$
$$+ \left[\frac{\alpha_2 S(1-\alpha_3 D)}{\left(D\alpha_3+1\right)^2} - \frac{\alpha_7\alpha_6}{\alpha_7+\mu} + \alpha_1 S - \alpha_4 D \right.$$
$$\left. - \alpha_5 - \mu\right]\left|z_3\right|$$

Since $\left|z_1\right| > \left|z_2\right|$, we get

$$\leq \left[\alpha_1 S - \alpha_4 D - \alpha_5 - \mu - \alpha_4 M - \frac{\alpha_2(S+D)}{1+\alpha_3 D} \right.$$
$$\left. - \alpha_6 - \mu_D\right]\left|z_1\right| + \left[\frac{\alpha_2 S(1-\alpha_3 D)}{\left(D\alpha_3+1\right)^2} - \frac{\alpha_7\alpha_6}{\alpha_7+\mu} \right.$$
$$\left. + \alpha_1 S - \alpha_4 D - \alpha_5 - \mu\right]\left|z_3\right|$$

$$D_+\|z\| \leq \max\left\{\alpha_1 S - \alpha_4 D - \alpha_5 - \mu - \alpha_4 M - \frac{\alpha_2(S+D)}{1+\alpha_3 D} \right.$$
$$- \alpha_6 - \mu_D, \frac{\alpha_2 S(1-\alpha_3 D)}{\left(D\alpha_3+1\right)^2} - \frac{\alpha_7\alpha_6}{\alpha_7+\mu} + \alpha_1 S - \alpha_4 D$$
$$\left. - \alpha_5 - \mu\right\}\|z\|$$

Case 2   If $0 < z_1, z_2, z_3$ and $\left|z_1\right|+\left|z_3\right| < \left|z_2\right|+\left|z_3\right|$ then

$$\|z\| = \left|z_2\right|+\left|z_3\right| \text{ and } D_+\|z\| = z_2' + z_3'$$

$$D_+\|z\| = \left[\alpha_4\right] z_1 + \left[-\alpha_1 M - \frac{\alpha_2\alpha_3 SD}{1+\alpha_3 D} - \frac{\alpha_2 D}{D\alpha_3+1} - \mu\right] z_2$$
$$+ \left[\frac{\alpha_7\alpha_5}{\alpha_7+\mu} - \alpha_1 S\right] z_3 + \left[-\frac{\alpha_2 D}{D\alpha_3+1}\right] z_1 + \left[\alpha_1 M\right] z_2$$
$$+ \left[\frac{-\alpha_2\alpha_3 SD}{\left(D\alpha_3+1\right)^2} + \alpha_1 S - \alpha_4 D - \alpha_5 - \mu\right] z_3$$
$$\leq \left[\alpha_4 - \frac{\alpha_2 D}{D\alpha_3+1}\right]\left|z_1\right| + \left[-\frac{\alpha_2\alpha_3 SD}{1+\alpha_3 D} - \frac{\alpha_2 D}{D\alpha_3+1} - \mu\right]\left|z_2\right|$$
$$+ \left[\frac{\alpha_7\alpha_5}{\alpha_7+\mu} - \frac{\alpha_2\alpha_3 SD}{\left(D\alpha_3+1\right)^2} - \alpha_4 D - \alpha_5 - \mu\right]\left|z_3\right|$$

Since $|z_1| < |z_2|$, we get

$$D_+\|z\| \leq \left[\alpha_4 - \frac{\alpha_2 D}{D\alpha_3 + 1} - \frac{\alpha_2\alpha_3 SD}{1 + \alpha_3 D} - \mu\right]|z_2|$$

$$+ \left[\frac{\alpha_7\alpha_5}{\alpha_7 + \mu} - \frac{\alpha_2\alpha_3 SD}{(D\alpha_3 + 1)^2} - \alpha_4 D - \alpha_5 - \mu\right]|z_3|$$

$$D_+\|z\| \leq \max\left\{\alpha_4 - \frac{\alpha_2 D}{D\alpha_3 + 1} - \frac{\alpha_2\alpha_3 SD}{1 + \alpha_3 D} - \mu, \frac{\alpha_7\alpha_5}{\alpha_7 + \mu}\right.$$

$$\left. - \frac{\alpha_2\alpha_3 SD}{(D\alpha_3 + 1)^2} - \alpha_4 D - \alpha_5 - \mu\right\}\|z\|$$

Case 3 If $z_1 < 0 < z_2, z_3$ and $|z_1| + |z_3| > |z_2| + |z_3|$ then

$$\|z\| = |z_1| + |z_3| \text{ and } D_+\|z\| = -z_1' + z_3'$$

$$D_+\|z\| = \left[-\alpha_1 S + \alpha_4 D + \alpha_5 + \mu + (\alpha_1 + \alpha_4)M\right.$$

$$\left. + \frac{\alpha_2(S + D)}{1 + \alpha_3 D} + \alpha_6 + \mu_D\right]z_1 + [\alpha_4 M]z_2$$

$$+ \left[-\frac{\alpha_2 S}{(D\alpha_3 + 1)^2} + \frac{\alpha_7\alpha_6}{\alpha_7 + \mu}\right]z_3 + \left[-\frac{\alpha_2 D}{D\alpha_3 + 1}\right]z_1$$

$$+ [\alpha_1 M]z_2 + \left[\begin{array}{l}\frac{-\alpha_2\alpha_3 SD}{(D\alpha_3 + 1)^2} + \alpha_1 S - \alpha_4 D \\ -\alpha_5 - \mu\end{array}\right]z_3$$

$$\leq \left[-\alpha_1 S + \alpha_4 D + \alpha_5 + \mu + (\alpha_1 + \alpha_4)M\right.$$

$$\left. + \frac{\alpha_2 S}{1 + \alpha_3 D} + \alpha_6 + \mu_D\right]|z_1| + [\alpha_1 M + \alpha_4 M]|z_2|$$

$$+ \left[\begin{array}{l}\frac{\alpha_7\alpha_6}{\alpha_7 + \mu} - \frac{\alpha_2 S(1 + \alpha_3 D)}{(D\alpha_3 + 1)^2} + \alpha_1 S - \alpha_4 D \\ -\alpha_5 - \mu\end{array}\right]|z_3|$$

Since $|z_1| > |z_2|$, we get

$$\leq \left[\begin{array}{l}-\alpha_1 S + \alpha_4 D + \alpha_5 + \mu + (2\alpha_1 + \alpha_4)M \\ +\alpha_4 M + \frac{\alpha_2 S}{1 + \alpha_3 D} + \alpha_6 + \mu_D\end{array}\right]|z_1|$$

$$+ \left[\begin{array}{l}\frac{\alpha_7\alpha_6}{\alpha_7 + \mu} - \frac{\alpha_2 S(1 + \alpha_3 D)}{(D\alpha_3 + 1)^2} + \alpha_1 S \\ -\alpha_4 D - \alpha_5 - \mu\end{array}\right]|z_3|$$

$$D_+\|z\| \leq \max\|z\|\left\{-\alpha_1 S + \alpha_4 D + \alpha_5 + \mu + (2\alpha_1 + \alpha_4)M\right.$$

$$+ \alpha_4 M + \frac{\alpha_2 S}{1 + \alpha_3 D} + \alpha_6 + \mu_D,$$

$$\left. \frac{\alpha_7\alpha_6}{\alpha_7 + \mu} - \frac{\alpha_2 S(1 + \alpha_3 D)}{(D\alpha_3 + 1)^2} + \alpha_1 S - \alpha_4 D - \alpha_5 - \mu\right\}\|z\|$$

Case 4 If $z_1 < 0 < z_2, z_3$ and $|z_1| + |z_3| < |z_2| + |z_3|$ then

$$\|z\| = |z_2| + |z_3| \text{ and } D_+\|z\| = z_2' + z_3'$$

$$D_+\|z\| = [\alpha_4]z_1 + \left[-\alpha_1 M - \frac{\alpha_2\alpha_3 SD}{1 + \alpha_3 D} - \frac{\alpha_2 D}{D\alpha_3 + 1} - \mu\right]z_2$$

$$+ \left[\frac{\alpha_7\alpha_5}{\alpha_7 + \mu} - \alpha_1 S\right]z_3 + \left[-\frac{\alpha_2 D}{D\alpha_3 + 1}\right]z_1 + [\alpha_1 M]z_2$$

$$+ \left[\frac{-\alpha_2\alpha_3 SD}{(D\alpha_3 + 1)^2} + \alpha_1 S - \alpha_4 D - \alpha_5 - \mu\right]z_3$$

$$\leq \left[\alpha_4 - \frac{\alpha_2 D}{D\alpha_3 + 1}\right]|z_1|$$

$$+ \left[-\frac{\alpha_2\alpha_3 SD}{1 + \alpha_3 D} - \frac{\alpha_2 D}{D\alpha_3 + 1} - \mu\right]|z_2|$$

$$+ \left[\frac{\alpha_7\alpha_5}{\alpha_7 + \mu} - \frac{\alpha_2\alpha_3 SD}{(D\alpha_3 + 1)^2} - \alpha_4 D - \alpha_5 - \mu\right]|z_3|$$

Since $|z_1| < |z_2|$, we get

$$D_+\|z\| \leq \left[\alpha_4 - \frac{\alpha_2 D}{D\alpha_3 + 1} - \frac{\alpha_2\alpha_3 SD}{1 + \alpha_3 D} - \mu\right]|z_2|$$

$$+ \left[\frac{\alpha_7\alpha_5}{\alpha_7 + \mu} - \frac{\alpha_2\alpha_3 SD}{(D\alpha_3 + 1)^2} - \alpha_4 D - \alpha_5 - \mu\right]|z_3|$$

$$D_+\|z\| \leq \max\left\{\alpha_4 - \frac{\alpha_2 D}{D\alpha_3 + 1} - \frac{\alpha_2\alpha_3 SD}{1 + \alpha_3 D} - \mu, \frac{\alpha_7\alpha_5}{\alpha_7 + \mu}\right.$$

$$\left. - \frac{\alpha_2\alpha_3 SD}{(D\alpha_3 + 1)^2} - \alpha_4 D - \alpha_5 - \mu\right\}\|z\|$$

Case 5 If $z_2 < 0 < z_1, z_3$ and $|z_1| + |z_3| > |z_2|$,

then $\|z\| = |z_1| + |z_3|$ and $D_+\|z\| = z_1' + z_3'$

$$D_+\|z\| = \left[\begin{array}{l}\alpha_1 S - \alpha_4 D - \alpha_5 - \mu - (\alpha_1 + \alpha_4)M \\ -\frac{\alpha_2(S + D)}{1 + \alpha_3 D} - \alpha_6 - \mu_D\end{array}\right]z_1$$

$$+ [-\alpha_4 M]z_2 + \left[\frac{\alpha_2 S}{(D\alpha_3 + 1)^2} - \frac{\alpha_7\alpha_6}{\alpha_7 + \mu}\right]z_3$$

$$+ \left[-\frac{\alpha_2 D}{D\alpha_3 + 1}\right]z_1 + [\alpha_1 M]z_2$$

$$+ \left[\frac{-\alpha_2\alpha_3 SD}{(D\alpha_3 + 1)^2} + \alpha_1 S - \alpha_4 D - \alpha_5 - \mu\right]z_3$$

$$\leq \left[\begin{array}{l}\alpha_1 S - \alpha_4 D - \alpha_5 - \mu - (\alpha_1 + \alpha_4)M \\ -\frac{\alpha_2(S + D)}{1 + \alpha_3 D} - \alpha_6 - \mu_D\end{array}\right]|z_1|$$

$$+ [\alpha_1 M - \alpha_4 M]|z_2| + \left[\frac{\alpha_2 S(1 - \alpha_3 D)}{(D\alpha_3 + 1)^2}\right.$$

$$\left. - \frac{\alpha_7\alpha_6}{\alpha_7 + \mu} + \alpha_1 S - \alpha_4 D - \alpha_5 - \mu\right]|z_3|$$

Since $|z_1| + |z_3| > |z_2|$, we get

$$\leq \left[\begin{array}{l} \alpha_1 S - \alpha_4 D - \alpha_5 - \mu - \alpha_4 M - \dfrac{\alpha_2(S+D)}{1+\alpha_3 D} \\ -\alpha_6 - \mu_D \end{array} \right] |z_1|$$

$$+ \left[\begin{array}{l} \dfrac{\alpha_2 S(1-\alpha_3 D)}{(D\alpha_3+1)^2} - \dfrac{\alpha_7 \alpha_6}{\alpha_7 + \mu} + \alpha_1(S+M) \\ -\alpha_4(D+M) - \alpha_5 - \mu \end{array} \right] |z_3|$$

$$D_+ \|z\| \leq \max \left\{ \alpha_1 S - \alpha_4 D - \alpha_5 - \mu - \alpha_4 M - \dfrac{\alpha_2(S+D)}{1+\alpha_3 D} \right.$$

$$-\alpha_6 - \mu_D, \; \dfrac{\alpha_2 S(1-\alpha_3 D)}{(D\alpha_3+1)^2} - \dfrac{\alpha_7 \alpha_6}{\alpha_7+\mu} + \alpha_1(S+M)$$

$$\left. -\alpha_4(D+M) - \alpha_5 - \mu \right\} \|z\|$$

Case 6 If $z_2 < 0 < z_1, z_3$ and $|z_1| + |z_3| < |z_2|$

then $\|z\| = |z_2|$ and

$$D_+ \|z\| = -z_2' = [-\alpha_4] z_1$$

$$+ \left[\alpha_1 M + \dfrac{\alpha_2 \alpha_3 SD}{1+\alpha_3 D} + \dfrac{\alpha_2 D}{D\alpha_3+1} + \mu \right] z_2$$

$$+ \left[\alpha_1 S - \dfrac{\alpha_7 \alpha_5}{\alpha_7 + \mu} \right] z_3$$

Since $|z_1| + |z_3| < |z_2|$, we get

$$D_+ \|z\| \leq \left[\begin{array}{l} \dfrac{\alpha_2 D}{D\alpha_3+1} + \dfrac{\alpha_2 \alpha_3 SD}{1+\alpha_3 D} - \dfrac{\alpha_7 \alpha_5}{\alpha_7+\mu} \\ +\alpha_1(M+S) - \alpha_4 + \mu \end{array} \right] \|z\|$$

Case 7 If $z_3 < 0 < z_1, z_2$ and $|z_1| + |z_3| > |z_2|$

then $\|z\| = |z_1| + |z_3|$ and

$$D_+ \|z\| = z_1' - z_3' = \left[\begin{array}{l} \alpha_1 S - \alpha_4 D - \alpha_5 - \mu - (\alpha_1 + \alpha_4) M \\ -\dfrac{\alpha_2(S+D)}{1+\alpha_3 D} - \alpha_6 - \mu_D \end{array} \right] z_1$$

$$+ [-\alpha_4 M] z_2 + \left[\dfrac{\alpha_2 S}{(D\alpha_3+1)^2} - \dfrac{\alpha_7 \alpha_6}{\alpha_7+\mu} \right] z_3$$

$$+ \left[\dfrac{\alpha_2 D}{D\alpha_3+1} \right] z_1 + [-\alpha_1 M] z_2$$

$$+ \left[\dfrac{\alpha_2 \alpha_3 SD}{(D\alpha_3+1)^2} - \alpha_1 S + \alpha_4 D + \alpha_5 + \mu \right] z_3$$

$$\leq \left[\begin{array}{l} \alpha_1 S - \alpha_4 D - \alpha_5 - \mu - (\alpha_1 + \alpha_4) M \\ -\dfrac{\alpha_2 S}{1+\alpha_3 D} - \alpha_6 - \mu_D \end{array} \right] |z_1|$$

$$+ [-\alpha_1 M - \alpha_4 M] |z_2|$$

$$+ \left[\begin{array}{l} \dfrac{\alpha_2 S(1+\alpha_3 D)}{(D\alpha_3+1)^2} - \dfrac{\alpha_7 \alpha_6}{\alpha_7+\mu} - \alpha_1 S + \alpha_4 D \\ +\alpha_5 + \mu \end{array} \right] |z_3|$$

Since $|z_1| + |z_3| > |z_2|$, we get

$$\leq \left[\begin{array}{l} \alpha_1 S - \alpha_4 D - \alpha_5 - \mu - (\alpha_1 + \alpha_4) M - \dfrac{\alpha_2 S}{1+\alpha_3 D} \\ -\alpha_6 - \mu_D \end{array} \right] |z_1|$$

$$+ \left[\begin{array}{l} \dfrac{\alpha_2 S(1+\alpha_3 D)}{(D\alpha_3+1)^2} - \dfrac{\alpha_7 \alpha_6}{\alpha_7+\mu} - \alpha_1(S+M) \\ -\alpha_4(M-D) + \alpha_5 + \mu \end{array} \right] |z_3|$$

$$D_+ \|z\| \leq \max \left\{ \alpha_1 S - \alpha_4 D - \alpha_5 - \mu - (\alpha_1 + \alpha_4) M \right.$$

$$-\dfrac{\alpha_2 S}{1+\alpha_3 D} - \alpha_6 - \mu_D, \; \dfrac{\alpha_2 S(1+\alpha_3 D)}{(D\alpha_3+1)^2} - \dfrac{\alpha_7 \alpha_6}{\alpha_7+\mu}$$

$$\left. -\alpha_1(S+M) - \alpha_4(M-D) + \alpha_5 + \mu \right\} \|z\|$$

Case 8 If $z_3 < 0 < z_1, z_2$ and $|z_1| + |z_3| < |z_2|$

then $\|z\| = |z_2|$ and

$$D_+ \|z\| = z_2' = [\alpha_4] z_1$$

$$+ \left[-\alpha_1 M - \dfrac{\alpha_2 \alpha_3 SD}{1+\alpha_3 D} - \dfrac{\alpha_2 D}{D\alpha_3+1} - \mu \right] z_2$$

$$+ \left[\dfrac{\alpha_7 \alpha_5}{\alpha_7 + \mu} - \alpha_1 S \right] z_3$$

Since $|z_1| + |z_3| < |z_2|$, we get

$$D_+ \|z\| \leq \left[\begin{array}{l} \dfrac{\alpha_2 \alpha_3 SD}{1+\alpha_3 D} - \dfrac{\alpha_2 D}{D\alpha_3+1} + \dfrac{\alpha_7 \alpha_5}{\alpha_7+\mu} \\ -\alpha_1(M+S) + \alpha_4 - \mu \end{array} \right] \|z\|$$

Combining all the eight cases, we got four independent inequality which are used in following theorem that proves the global stability of endemic eqlibrium point.

Theorem 8. *For $R_0 > 1$, the endemic equilibrium point E^* is globally asymptotically stable if the following inequality holds*

$$\max(\chi_1, \chi_2, \chi_3, \chi_4) < -\chi$$

Where,

$$\chi_1 = \max \left\{ \begin{array}{l} \alpha_4 - \dfrac{\alpha_2 D}{D\alpha_3+1} - \dfrac{\alpha_2 \alpha_3 SD}{1+\alpha_3 D} - \mu, \dfrac{\alpha_7 \alpha_5}{\alpha_7+\mu} \\ -\dfrac{\alpha_2 \alpha_3 SD}{(D\alpha_3+1)^2} - \alpha_4 D - \alpha_5 - \mu \end{array} \right\}$$

$$\chi_2 = \max \left\{ \alpha_1 S - \alpha_4 D - \alpha_5 - \mu - \alpha_4 M - \dfrac{\alpha_2(S+D)}{1+\alpha_3 D} \right.$$

$$-\alpha_6 - \mu_D, \; \dfrac{\alpha_2 S(1-\alpha_3 D)}{(D\alpha_3+1)^2} - \dfrac{\alpha_7 \alpha_6}{\alpha_7+\mu} + \alpha_1(S+M)$$

$$\left. -\alpha_4(D+M) - \alpha_5 - \mu \right\}$$

$$\chi_3 = \dfrac{\alpha_2 D}{D\alpha_3+1} + \dfrac{\alpha_2 \alpha_3 SD}{1+\alpha_3 D} - \dfrac{\alpha_7 \alpha_5}{\alpha_7+\mu} + \alpha_1(M+S) - \alpha_4 + \mu$$

$$\chi_4 = \dfrac{\alpha_2 \alpha_3 SD}{1+\alpha_3 D} - \dfrac{\alpha_2 D}{D\alpha_3+1} + \dfrac{\alpha_7 \alpha_5}{\alpha_7+\mu} - \alpha_1(M+S) + \alpha_4 - \mu$$

□

And χ is a positive number.

5. Optimal control

Mosquitoes are the most prolific killers of humans in the animal kingdom. One of the most ancient and deadly diseases that mosquitoes transmit are malaria and dengue. It has been hypothesized due to influences on immune responses that infection with malaria can alter to the course of infection of the dengue. An effective way to protect the people from dengue who are already affected by malaria is to control vector. Also medication pays a major role to control spread of vector borne diseases.

In present dynamical model, two bounded Lebesgue integrable controls are introduced say u_1 and u_2. u_1 control is to minimize concurrent infection cases by vector control and u_2 is a treatment control which helps to improve recovery rate. After applying control system (1) will take form as follow:

$$\frac{dS}{dt} = B + \alpha_7 R - \alpha_1 SM - \frac{\alpha_2 SD}{1 + \alpha_3 D} - \mu S$$

$$\frac{dM}{dt} = \alpha_1 SM - \alpha_4 MD - u_1 M - \alpha_5 M - \mu M$$

$$\frac{dD}{dt} = \frac{\alpha_2 SD}{1 + \alpha_3 D} + \alpha_4 MD + u_1 M - (\alpha_6 + u_2)D - (\mu + \mu_D)D$$

$$\frac{dR}{dt} = (\alpha_6 + u_2)D + \alpha_5 M - \alpha_7 R - \mu R$$

The objective function $J(u_i, \Omega)$ for the mathematical model along with the optimal control is given by:

$$J = \int_0^T (A_1 S^2 + A_2 M^2 + A_3 D^2 + A_4 R^2 + w_1 u_1^2 + w_2 u_2^2) dt$$

Here, Ω denotes set of all compartmental variables. A_i are small positive constants to keep a balance in the size of the respective compartments. w_1 and w_2 are positive weight parameter which is associated with the control u_1 and u_2. The objective of our work is to maximize the total number of recovered individual by optimizing control variables u_1 and u_2.

As, the weight parameters w_1 and w_2 are constant of the control rates applied as vector control and treatment control, from which the optimal control condition is normalized. Now, we will calculate the values of control variables from $t = 0$ to $t = T$ such that

$$J\left(u_1(t), u_2(t)\right) = optimum\{J(u_i, \Omega) / (u_1, u_2) \in \phi\}$$

Where ϕ is a smooth function on the interval $[0,1]$. The optimal controls denoted by u_1^* and u_2^* are founded by accumulating all the integrands of equation (4) using the lower bounds and upper bounds respectively with the results of Fleming and Rishel [11].

To optimize controls using the Pontryagin's principle we construct a Lagrangian function consisting of state equations and adjoint variables $\lambda_1, \lambda_2, \lambda_3, \lambda_4$ as follows:

$$L(\Omega, A) = A_1 S^2 + A_2 M^2 + A_3 D^2 + A_4 R^2 + w_1 u_1^2 + w_2 u_2^2$$

$$+ \lambda_1 \left(B + \alpha_7 R - \alpha_1 SM - \frac{\alpha_2 SD}{1 + \alpha_3 D} - \mu S \right)$$

$$+ \lambda_2 \left(\alpha_1 SM - \alpha_4 MD - u_1 M - \alpha_5 M - \mu M \right)$$

$$+ \lambda_3 \left(\frac{\alpha_2 SD}{1 + \alpha_3 D} + \alpha_4 MD + u_1 M - (\alpha_6 + u_2)D \right)$$

$$- (\mu + \mu_D)D \right) + \lambda_4 \left((\alpha_6 + u_2)D + \alpha_5 M \right.$$

$$- \alpha_7 R - \mu R \right)$$

The partially differentiation of the Lagrangian function with respect to each compartmental variable gives the adjoint equation variables $A_i = (\lambda_1, \lambda_2, \lambda_3, \lambda_4)$ corresponding to the system:

$$\dot{\lambda}_1 = -\frac{\partial L}{\partial S} = -2A_1 S + (\lambda_1 - \lambda_2)\alpha_1 M$$

$$+ (\lambda_1 - \lambda_3)\frac{\alpha_2 D}{1 + \alpha_3 D} + \mu \lambda_1$$

$$\dot{\lambda}_2 = -\frac{\partial L}{\partial M}$$

$$= -2A_2 M + (\lambda_1 - \lambda_2)\alpha_1 S + (\lambda_2 - \lambda_3)(\alpha_4 D + u_1)$$

$$+ (\lambda_2 - \lambda_4)\alpha_5 + \lambda_2 \mu - \frac{\lambda_3 \alpha_1 S}{1 + \alpha_3 D}$$

$$\dot{\lambda}_3 = -\frac{\partial L}{\partial D} = -2A_3 D + (\lambda_1 - \lambda_3)\frac{\alpha_2 S}{(1 + \alpha_3 D)^2}$$

$$+ (\lambda_2 - \lambda_3)\alpha_4 M + (\lambda_3 - \lambda_4)(\alpha_6 + u_2)$$

$$+ \lambda_3(\mu + \mu_D)$$

$$\dot{\lambda}_4 = -\frac{\partial L}{\partial R} = -2A_4 R + (\lambda_4 - \lambda_1)\alpha_7 + \lambda_4 \mu$$

The necessary conditions for Lagrangian function L to be optimal are, $\dot{u}_1 = 0$ and $\dot{u}_2 = 0$. Hence we get,

$$u_1 = \frac{1}{2w_1}(\lambda_2 - \lambda_3)M , \ u_2 = \frac{1}{2w_2}(\lambda_3 - \lambda_4)D$$

Formulated required optimal controls are:

$$u_1^* = \max\left\{a_1, \min\left(b_1, \frac{(\lambda_2 - \lambda_3)M}{2w_1}\right)\right\}$$

$$u_2^* = \max\left\{a_2, \min\left(b_2, \frac{(\lambda_3 - \lambda_4)D}{2w_2}\right)\right\}$$

Thus, analytical results for optimized controls have been visualised in simulation part.

6. Numerical simulation

Bifurcation analysis helps to demonstrate the qualitative information about the equilibrium point. Figure 2 shows backward bifurcation diagram where $R_C = 0.12$ is a critical point from which system's stability switches from unstable to stable state. If $R_C < R_0$, then for the point of R_0 backward bifurcation exists, moreover equilibrium coexist when $R_C < R_0 < 1$ [14], [29].
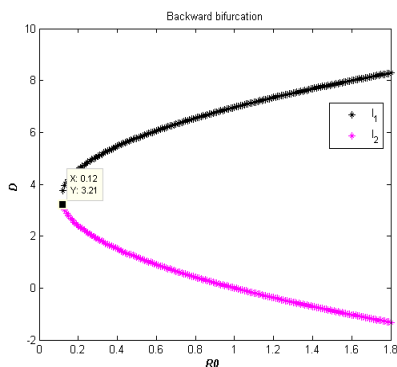

Figure 2. Bifurcation diagram for dengue infected individuals with R_0
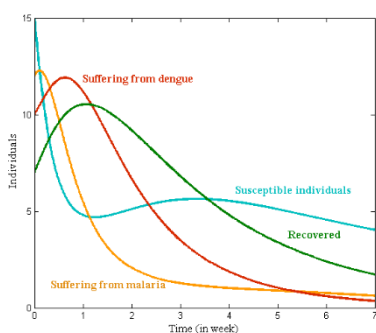
Figure 3. Time series of solution of malaria-dengue model

Figure 3 shows the flow of malaria-dengue model with time. It is observed that human immunity is more sensitive towards dengue compare to malaria infection moreover compare to dengue, recovery rate of malaria is higher. Hence we can say that medication is more effective on malaria infected compare to dengue infected. Compare to dengue, spread of malaria is easy to control by improving medication. Under proper medication both the diseases can be controlled in 7-8 weeks.
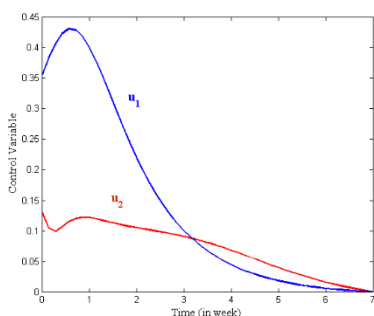
Figure 4. Variation in control variables with time

Figure 4 shows change in both the control variables needs to be done to stabilize the model. It is observed that initially 35% and 13%, u_1 and u_2 controls are needed to be applied respectively.
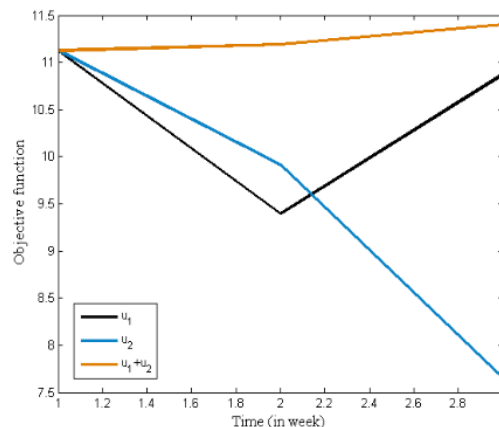
Figure 5. Change in objective function with time

Figure 5 gives change in objective function under influence of both the controls combine and individually which gives combine and individual effect of both the controls on malaria-dengue model. It is clearly visible that combine effect of controls gives more fruitful effect on the model compare to an individual effect.
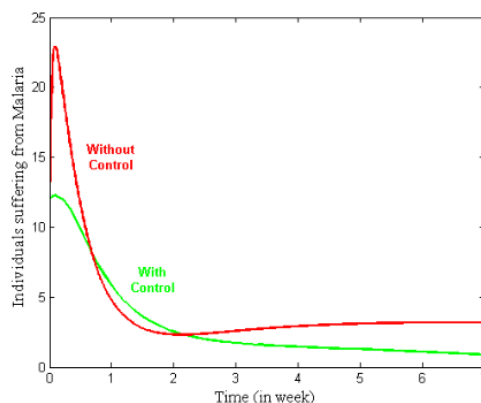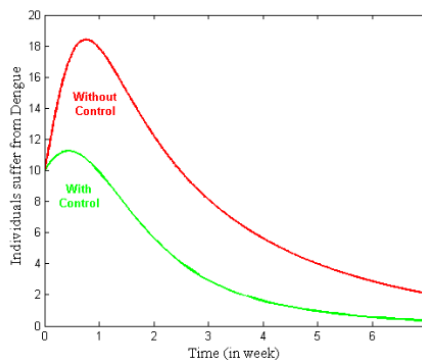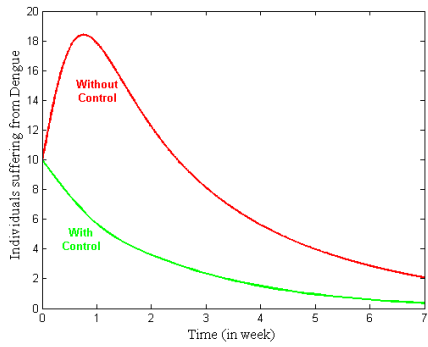

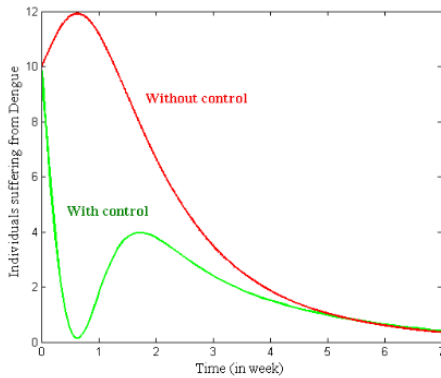**Figure 6.** Impact of u_1 control on class of malaria infected individuals

The simulation in figure 6 interprets that that chances to get infected by malaria decreases by 50% after applying *control* u_1.
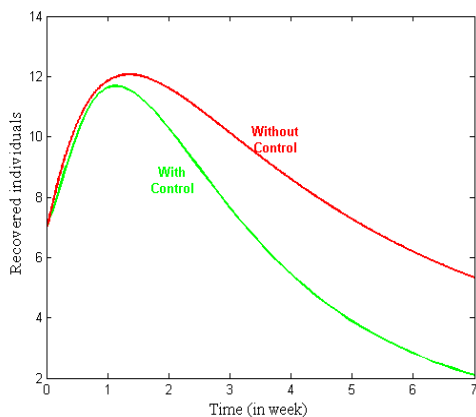

(a) Impact of u_1 control

(b) Impact of u_2 control

(c) Impact of both the controls

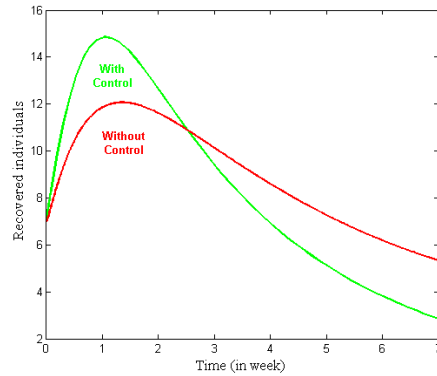**Figure 7.** Impact of controls on class of dengue infected individuals

From figure 7(a) and 7(b), it is clear that for class of dengue infected individuals u_2 control is more effective compare to u_1 control moreover it is visualised in figure 7(c) that combine effect of both the control is even more effective which shoews only medication is not enough to minimize dengue infaction case, different acts which minimize concurrent infaction case also have a significant effect.
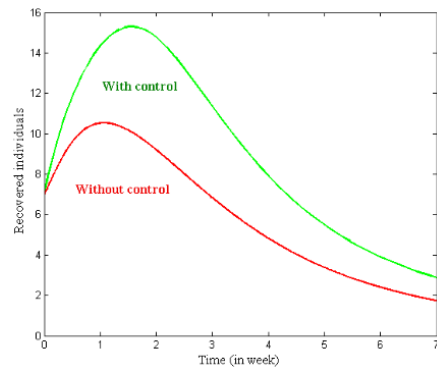

(b) Impact of u_1 control

Figure 8 shows separate and combine effect of both the controls on class of recovered individuals. From figure 8(c) we can observe better improvement in recovered class after applying both the controls at the same time. About 61% improvement is observed in recovery rate

white applying both the control together.

(b) Impact of u_2 control

(c) Impact of both the controls

Figure 8. Impact of controls on class of recovered individuals

Also figure 8(a) and 8(b) deplicate that compare to u_1 control, u_2 control gives better result which suggest that madication plays a major contribution to control the concurrent infection. Hence better medication facility and avaibility is good approach to control outbreak of malaria-dengue infections in endemic areas.

7. Conclusion

The fight against most deadly mosquito-borne diseases malaria and dengue is a challenge to the world. In the present study, the system of dynamical model for two different mosquito borne diseases is studied through the use of mathematical modeling. Moreover, Optimal control theory is also applied on the model to visualise the effect of controles on it. The model have four equilibrium points for four different possible cases including disease free society, case when only one individual infection is present and the case when both the diseases are present concurrently in society. It is proved that all four equilibrium points are local and globally asymptotically stable under some parametric conditions. The formula of basic reproduction number (R_0) used to calculate threshold value of the model. In this article, the basic reproduction number is formulated for malaria and dengue combinely, hence it

is unaffected by parameter α_4. Threshold value increases as value of parameters α_1 and α_2 is increases, and it decreases as α_5 and α_6 increases. Which simply means threshold value can be controled by improving recovery rates of both the diseases. Bifurcation analysis indicates that minimum rate of diseases spread is 12%. Threshold value signifies that there is 14.9% chance to get infected by malaria and dengue concurrently. In numerical simulation we have observed the effect of optimal controls individually as well as concurrently and more stability is observed when we apply both the controls at same time. Also it is analysed that 61% improvement in recovery rate is observed under the effect of both optimal controls, which suggest that vector control by using insecticide, treated mosquito nets and indoor residual spraying and medication to improve recovery are the main way to prevent and reduce malaria and dengue transmission.

Acknowledgments

References

[1] Aldila, D., & Agustin, M. R. (2018, March). A Mathematical Model Of Dengue-Chikungunya Co-Infection In A Closed Population. In *Journal of Physics: Conference Series* (Vol. 974, No. 1, p. 012001). IOP Publishing.

[2] Arino, J., McCluskey, C. C., & van den Driessche, P. (2003). Global results for an epidemic model with vaccination that exhibits backward bifurcation. *SIAM Journal on Applied Mathematics*, *64*(1), 260-276.

[3] Brauer, F., van den Driessche, P., & Wu, J. (2008). Mathematical Epidemiology. *lecture notes in mathematics-springer verlag-*, *1*(1945), 1-2.

[4] Carme, B., Matheus, S., Donutil, G., Raulin, O., Nacher, M., & Morvan, J. (2009). Concurrent dengue and malaria in Cayenne hospital, French Guiana. Emerging infectious diseases, 15(4), 668-671.

[5] Castillo-Chavez, C., Blower, S., van den Driessche, P., Kirschner, D., & Yakubu, A. A. (Eds.). (2002). *Mathematical approaches for emerging and reemerging infectious diseases: an introduction* (Vol. 1). Springer Science & Business Media.

[6] Charrel, R. N., Brouqui, P., Foucault, C., & De Lamballerie, X. (2005). Concurrent dengue and malaria. Emerging infectious diseases, 11(7), 1153-1154

[7] Cox, J., Grillet, M. E., Ramos, O. M., Amador, M., & Barrera, R. (2007). Habitat segregation of dengue vectors along an urban environmental gradient. *The American journal of tropical medicine and hygiene*, *76*(5), 820-826.

[8] Deresinski, S. (2006). Concurrent Plasmodium vivax malaria and dengue.

[9] Diekmann, O., Heesterbeek, J. A. P., & Metz, J. A. (1990). On the definition and the computation of the basic reproduction ratio R 0 in models for infectious diseases in heterogeneous populations. *Journal of mathematical biology*, *28*(4), 365-382.

[10] Epelboin, L., Hanf, M., Dussart, P., Ouar-Epelboin, S., Djossou, F., Nacher, M., & Carme, B. (2012). Is dengue and malaria co-infection more severe than single infections? A retrospective matched-pair study in French Guiana. *Malaria journal*, *11*(1), 142-149.

[11] Fleming, W. H., Rishel, R. W., Marchuk, G. I., Balakrishnan, A. V., Borovkov, A. A., Makarov, V. L., Rubinov, A.M., Liptser, R.S., Shiryayev, A.N., Krassovsky, N.N. & Subbotin, A. N. (1975). Applications of Mathematics. *Deterministic and Stochastic Optimal Control*.

[12] Isea, R., & Lonngren, K. E. (2016). A preliminary mathematical model for the dynamic transmission of Dengue, Chikungunya and Zika. *American Journal of Modern Physics and Application 2016; 3(2), 11-15.*

[13] Kaushik, R. M., Varma, A., Kaushik, R., & Gaur, K. J. (2007). Concurrent dengue and malaria due to Plasmodium falciparum and P. vivax. *Transactions of the Royal Society of Tropical Medicine and Hygiene*, *101*(10), 1048-1050.

[14] Khan, M. A., Islam, S., & Khan, S. A. (2014). Mathematical modeling towards the dynamical interaction of leptospirosis. *Applied Mathematics & Information Sciences*, *8*(3), 1049-1056.

[15] Kumari, N., & Sharma, S. (2018). Modeling the Dynamics of Infectious Disease Under the Influence of Environmental Pollution. *International Journal of Applied and Computational Mathematics*, *4*, 1-24.

[16] Li, M. Y., & Muldowney, J. S. (1996). A geometric approach to global-stability problems. *SIAM Journal on Mathematical Analysis*, *27*(4), 1070-1083.

[17] Mackey, T. K., & Liang, B. A. (2012). Lessons from SARS and H1N1/A: employing a WHO–WTO forum to promote optimal economic-public health pandemic response. *Journal of public health policy*, *33*(1), 119-130.

[18] Mahmoud, D. M., Hussein, H. M., El Gozamy, B. M. R., Thabet, H. S., Hassan, M. A., & Meselhey, R. A. A. (2019). Screening of Plasmodium parasite in vectors and humans in three villages in Aswan Governorate, Egypt. *Journal of Parasitic Diseases*, *43*(1), 158-163.

[19] McCluskey, C. C., & van den Driessche, P. (2004). Global analysis of two tuberculosis models. *Journal of Dynamics and Differential Equations*, *16*(1), 139-166.

[20] Obsomer, V., Defourny, P., & Coosemans, M. (2007). The Anopheles dirus complex: spatial distribution and environmental drivers. *Malaria Journal*, *6*(1), 26-40.

[21] Patel, S. K., Rajora, N., Kumar, S., Sahu, A., Kochar, S. K., Krishna, C. M., & Srivastava, S. (2019). Rapid discrimination of Malaria and Dengue Infected Patients Sera using Raman Spectroscopy. *Analytical chemistry*.

[22] Rodenhuis-Zybert, I. A., Wilschut, J., & Smit, J. M. (2010). Dengue virus life cycle: viral and host factors modulating infectivity. *Cellular and molecular life sciences*, *67*(16), 2773-2786.

[23] Rupali, P. (2019). Introduction to Tropical Medicine. *Infectious Disease Clinics*, *33*(1), 1-15.

[24] Santana, V. D. S., Lavezzo, L. C., Mondini, A., Terzian, A. C. B., Bronzoni, R. V. D. M., Rossit, A. R. B., Machado, R.L.D., Rahal, P., Nogueira, M.C.L. & Nogueira, M. L. (2010). Concurrent dengue and malaria in the Amazon region. *Revista da Sociedade Brasileira de Medicina Tropical,* 43(5), 508-511.

[25] Sharomi, O., Podder, C., Gumel, A., & Song, B. (2008). Mathematical analysis of the transmission dynamics of HIV/TB coinfection in the presence of treatment. *Mathematical Biosciences and Engineering*, *5*(1), 145-174.

[26] Silva, C. J., & Torres, D. F. (2015). A TB-HIV/AIDS coinfection model and optimal control treatment. *Discrete and Continuous Dynamical Systems*, 35(9), 4639-4663.

[27] Smith, R. A. (1986). Some applications of Hausdorff dimension inequalities for ordinary differential equations. *Proceedings of the Royal Society of Edinburgh Section A: Mathematics*, *104*(3-4), 235-259.

[28] Van den Driessche, P., & Watmough, J. (2002). Reproduction numbers and sub-threshold endemic equilibria for compartmental models of disease transmission. *Mathematical biosciences*, *180*(1-2), 29-48.

[29] Wangari, I. M., Davis, S., & Stone, L. (2016). Backward bifurcation in epidemic models: Problems arising with aggregated bifurcation parameters. *Applied Mathematical Modelling*, *40*(2), 1669-1675.

[30] Ward, D. I. (2006). A case of fatal Plasmodium falciparum malaria complicated by acute dengue fever in East Timor. *The American journal of tropical medicine and hygiene*, *75*(1), 182-185.

[31] Wiwanitkit, V. (2011). Concurrent malaria and dengue infection: a brief summary and comment. *Asian Pacific journal of tropical biomedicine*, *1*(4), 326-327.

Nita H. Shah is a Professor in the Department of Mathematics, Gujarat University, Ahmedabad. She has 25 years of research experience in inventory management, forecasting and information technology and information systems. She has published 375+ articles in international journals, including APJOR (Singapore), International Journal of Production Economics, OMEGA, CCERO (Belgium), ECPE (Romania), Measuring, Control & Simulation (France), JIOS (India), IJOMS (India), Industrial Engineering (India), European Journal of Operational Research, IJIR, IJOR, IJMOR, IJBPSCM.
http://orcid.org/0000-0003-1605-4778

Ankush H. Suthar is research scholar in Department of Mathematics, Gujarat University, India. He is working in dynamical systems and mathematical modeling of health problem related to infectious diseases. He has published 2-papers in JMCS and IJCER on transmission of deadly infectious diseases like Nipah-virus and swine-flu.
http://orcid.org/0000-0001-7583-450X

Ekta N. Jayswal is research scholar in Department of Mathematics, Gujarat University, India. She is working in finite dimensional dynamical systems and its stability. Her research interest is applications of mathematical modeling to resolve different environmental issues.
http://orcid.org/0000-0002-5888-2478

RESEARCH ARTICLE

Qualitative behavior of stiff ODEs through a stochastic approach

Hande Uslu[a] , Murat Sari[a*], Tahir Cosgun[a,b]

[a] Department of Mathematics, Yildiz Technical University, Turkey
[b] Department of Mathematics, Amasya University, Turkey
usluh@yildiz.edu.tr, sarim@yildiz.edu.tr, tahir.coskun@amasya.edu.tr

ARTICLE INFO	ABSTRACT
	In the last few decades, stiff differential equations have attracted a great deal of interest from academic society, because much of the real life is covered by stiff behavior. In addition to importance of producing model equations, capturing an exact behavior of the problem by dealing with a solution method is also handling issue. Although there are many explicit and implicit numerical methods for solving them, those methods cannot be properly applied due to their computational time, computational error or effort spent for construction of a structure. Therefore, simulation techniques can be taken into account in capturing the stiff behavior. In this respect, this study aims at analyzing stiff processes through stochastic approaches. Thus, a Monte Carlo based algorithm has been presented for solving some stiff ordinary differential equations and system of stiff linear ordinary differential equations. The produced results have been qualitatively and quantitatively discussed.

1. Introduction

Differential equations are used to model real-life systems by conserving their physical structures. There are different types of differential equations which have been named by according to their characteristics. Stiff differential equations are one of those. While developing a model of a system, it is necessary to consider suddenly occurred reactions with small time steps without neglecting that the system continue to behave over the whole-time interval. Stiff equations represent unstable behaviors for very small values. In other words, a model contains a point which decays or grows very rapidly than others. Despite natural restrictions of physical systems represented by stiff Ordinary Differential Equations (ODEs), they are commonly used in modelling various problems, through chemical reactions, while creating electrical circuits or studying in control theory etc. Not only modelling a stiff behavior but also solving the model accurately play a key role for capturing real-life behavior.

Stiffness was firstly named by Curtiss and Hirschfelder [1] in 1952. Although this explanation leads to be realized that almost all real-life problems include stiff property, the first efficient algorithm for solving the model equations was suggested relatively late, in 1976 by Shampine and Gear [2]. Finding exact solution for stiff problems is generally limited to simple cases and conventional numerical methods have to be reconstructed with small time steps for these types of problems. However, the increased number of steps might possibly cause an accumulation of error. This fact gives rise to a necessity of alternative approaches for stiff equations. In the last few decades, various implicit and explicit methods related to stiffness have been developed.

The explicit methods find a solution by using the current time information to produce later time information. However, implicit ones use the current and later time information at the same time. While analyzing stiff behavior, it should be taken into consideration how much small changes in the current time information affects the later time. Explicit methods generally do not work efficiently for catching the changing behavior in small step sizes or if they do, it converges very slowly than expected [3]. If the initial conditions cause a divergence in the solution, an explicit method requires impractically small step sizes to control the convergence. Although the implicit ones need more computation and requires sensitive implementations, they are properly applied to many stiff problems.

Even though an application area of numerical methods has a broad range, they are occasionally suffering from their restrictions. They may be seen to be efficient for the aim of the solving the problems iteratively, but these methods cannot be a first choice considering their computational time, computational error or effort spent for construction of a stiff structure. At this point, new approaches such that simulation techniques emerge by paying attention to these corresponding issues [4-5]. The Monte Carlo Method (MCM) is one of the basic simulation techniques [6-8]. It has been generally defined as a random sampling method for solving any model. Since this method uses basically random variables to represent the behavior of physical processes, it is classified as a stochastic approach.

The MCMs can be applied to a wide range of problems in three different ways; sampling, estimation and optimization [9-10]. This classification depends on aim and a way of building algorithm. If a researcher wants to use simulation to mimic the nature of the system by creating objects or unreal systems, sampling methods are more useful than the rest. Therefore, random sampling and estimation techniques are used in this study to observe the behavior of the stiff differential equations.

2. Implementation of the method

The main intention of this study is to capture the exact behavior of stiff differential equations by using simulation techniques. To achieve this, differential equations are described by using integrals since the Monte Carlo integration is based on random sampling [11-13]. This randomness comes from uniformly distributed pseudorandom numbers selected by a sample space. The method is named by rejection sampling which is used for generating random variables X with density function ρ. The main advantage of using rejection sampling is that sampling can be used even if the density function cannot be integrated analytically.

Let us then consider any first order differential equation in an implicit form:

$$\frac{dy}{dx} = F(x, y) \qquad (1)$$

where function F represent an arbitrary function with variables. After modifying the equation in this form, the algorithm needs a reference number which is chosen to do comparison in the related steps of the algorithm. The first reference number is generated by using initial conditions X_0 and Y_0 and this number should be revised for each iteration. The step size is determined by dividing uniformly the interval to m points. Let us call this reference number as Classification Number (*CN*) defined as follows

$$CN := \frac{dY}{dX} = F(X_n, Y_n) \qquad (2)$$

where $n = 0, 1, \dots, m$.

Next step, determination of upper and lower bounds for generating random numbers is expected to lead to more accurate estimation. The estimation can be made under the consideration of the physical realities of the problem. These bounds are determined by initial conditions. After determining an upper and a lower bound, random numbers can be created according to these bounds for making a comparison with the *CN*. To create random numbers, *rand* function of MATLAB can be used. This function generates different pseudorandom numbers between 0 and 1. They are known as pseudorandom since even if they act as a random number they are generated according to some artificial algorithm by the function. These random numbers between 0 and 1 are extended to the interval which determined by upper and lower bounds.

Then the comparison starts with created N positive random variables and N negative random variables by using *rand* function with respect to the *CN* of the algorithm. The way of implementation is given in the following pseudocode.

Pseudocode: Monte Carlo Based Algorithm for ODEs

---
1. Consider the differential equation $\frac{dY}{dX}$ as a function $\boldsymbol{F(X,Y)}$ and initial conditions as $\boldsymbol{X_0}$ and $\boldsymbol{Y_0}$.
2. Define $:= \frac{dY}{dx} = \boldsymbol{F(X_n, Y_n)}$.
3. Find the upper and lower boundaries, **U** and **L**, for the classifying random numbers.
4. Create **N** random numbers.
5. Initialize $\boldsymbol{X = X_0}$ and $\boldsymbol{Y = Y_0}$
6. while $(\boldsymbol{X < X_f})$
7. $CN = F(X, Y)$
8. if $\boldsymbol{CN} \geq 0$ then
     S ← the value of the random numbers $\leq \boldsymbol{CN}$
     $\boldsymbol{Y_{k+1}} \leftarrow \boldsymbol{Y_k} + U\frac{S}{N}\Delta X$
9. Else
     S ← the value of the random numbers $\geq \boldsymbol{CN}$
     $\boldsymbol{Y_{k+1}} \leftarrow \boldsymbol{Y_k} - L\frac{S}{N}\Delta X$
10.   end if
11.   end while

---

3. Illustrative examples

In this section, the predicted results of various differential equations by applying the current algorithm have been illustrated. In the examples, 100000 random samples are chosen for each iteration in the algorithm and the increment of time is taken to be 0.001. To justify the predicted results, comparison is made with both the *ode23s* based on a modified Rosenbrock formula of order 2 and the fourth order Runge-Kutta Method (RK4) as well as available analytical solutions. The two results are compared with each other by using the absolute error. Qualitative and quantitative behaviors have been exhibited by comparing with computational costs in detail. To compute the results, the codes have been produced in MATLAB 2018a

installed on a computer which has the properties of 2.3 GHz intel core i5 and 16 GB ram.

3.1. Example 1

Let us consider a first order stiff ODE with an initial condition,

$$\frac{dy}{dt} = -1000y + 3000 - 2000e^{-t}, y(0) = 0. \quad (3)$$

The exact solution of the differential equation is:

$$y(t) = 3 - 0.998e^{-1000t} - 2.002e^{-t}. \quad (4)$$

The Monte Carlo based algorithm is applied to Equation (3) by dividing the time axis uniformly. Qualitative results including the solution produced by the proposed algorithm, the exact solution and the absolute errors have been illustrated in Figure 1. The corresponding numerical results can be seen in Table 1.

It can be easily observed in Figure 2 that the stiffness occurs between the points 0 and 0.006, near to initial value. The initial deviation dampens fast due to the large value of coefficients. Despite the fact that each trial uses different set of random numbers to predict the results, each trial indicates the common feature at this stiff point. So the quantitative results are also close to each other. Even though quantitative results have slightly little deflections, qualitative results can be seen in good agreement with the exact results.
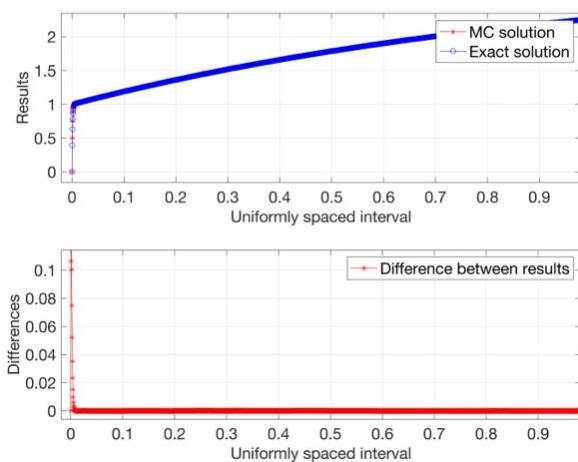

Figure 1. Comparison of the MC prediction and the exact solution of equation (3)

Computational time of the proposed algorithm is 0.5548 s for this set of trial. Moreover, the accuracy is expected to be improved by reasonably decreasing the step size of the interval. However, the small step size leads a large number of comparisons in the algorithm, so that increasing the computational cost. Even if there are higher computational costs for some complex problems, it is seen that the proposed algorithm is the accurate solver as one of the simulation techniques.

Table 1. Numerical results of Equation (3)

| Time t	Predicted Results	Exact Results	Absolute Errors
0.0005	0.49991771	0.39368315	0.10623456
0.0010	0.75242301	0.63285732	0.11956569
0.0015	0.87872659	0.77831685	0.10040974
0.0020	0.94166335	0.86693539	0.07472796
0.0025	0.97329583	0.92107792	0.05221791
0.0030	0.98957043	0.95430951	0.03526092
0.0035	0.99823965	0.97485776	0.02338189
0.0040	1.00283457	0.98771300	0.01512157
0.0045	1.00556209	0.99590198	0.00966011
0.0050	1.00740685	1.00126055	0.00614630
0.0100	1.01789819	1.01787492	0.00002327
0.0150	1.02777839	1.02780559	0.00002720
0.0200	1.03761332	1.03764225	0.00002893
0.0250	1.04739166	1.04742956	0.00003789
0.0500	1.09561564	1.09563869	0.00002305
0.2500	1.44096991	1.44084083	0.00012908
1.0000	2.26347104	2.26350536	0.00003432
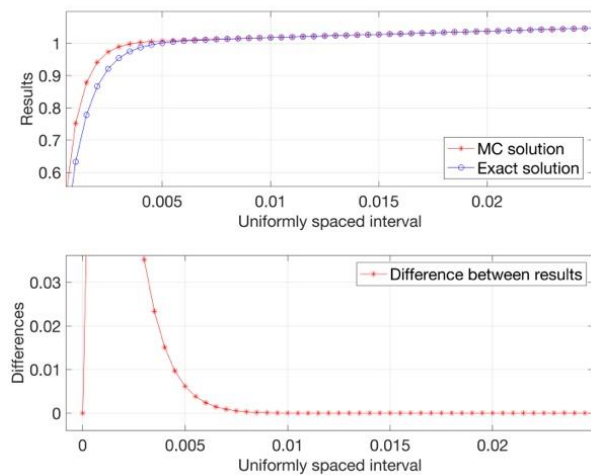
Figure 2. A closer view of Figure 1

3.2. Example 2

Let us now take a first order stiff ODE with an initial condition,

$$\frac{dy}{dt} = -1000y + \sin t, y(0) = 1/1000001. \quad (5)$$

Exact solution of the differential equation is then

$$y(t) = \frac{1000 \sin t + \cos t}{1000001}. \quad (6)$$

The proposed algorithm is applied to Equation (5) by dividing the time axis uniformly. The comparison of predicted results with the analytical solution of Equation (5) is given Figure 3 and the corresponding absolute errors are shown in Figure 4. Quantitative results of Equation (5) are exhibited in Table 2.

Unlike Example 1, from Figure 3 it can be seen that the solutions already computed are much closer to the exact solution for all points in the range. It can be seen from the absolute errors that the results are very accurately predicted by the current algorithm. Computational cost of the present algorithm is 0.2913 s for this set of trial. Even if the computational time of the algorithm seems to be higher than its rivals depending on random numbers, its accuracy level is relatively in good agreement with available analytical solution.
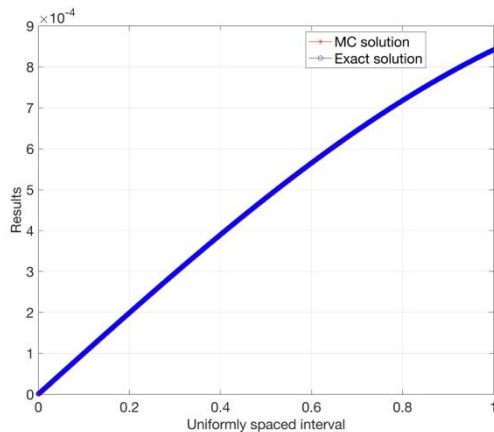
Figure 3. Comparison of the MC Prediction and the exact solution of equation (3)

Table 2. Numerical results of the first order stiff differential equation (5)

Time t	Predicted Results	Exact Results	Absolute Errors
0.0100	0.00000922	0.00001100	0.00000178
0.0500	0.00004920	0.00005098	0.00000178
0.1000	0.00009904	0.00010083	0.00000178
0.2000	0.00019788	0.00019965	0.00000177
0.3000	0.00029473	0.00029648	0.00000174
0.4000	0.00038866	0.00039034	0.00000168
0.5000	0.00047870	0.00048030	0.00000161
0.6000	0.00056397	0.00056547	0.00000150
0.7000	0.00064363	0.00064498	0.00000135
0.8000	0.00071679	0.00071805	0.00000126
0.9000	0.00078283	0.00078395	0.00000111
1.0000	0.00084103	0.00084201	0.00000098

3.3. Example 3

Now take a first order stiff differential equation system with initial conditions

$$\frac{dx}{dt} = -80.6x + 119.4y, \qquad x(0) = 1$$

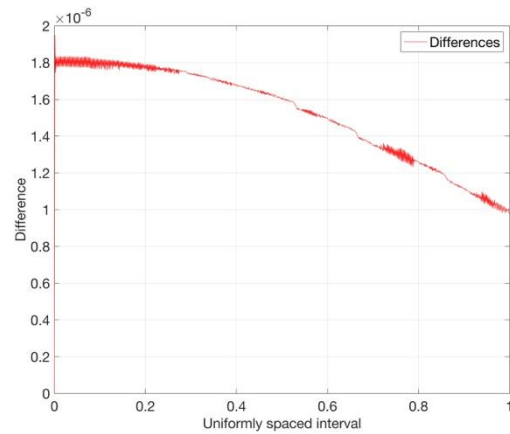$$\frac{dy}{dt} = 79.6x - 120.4y, \qquad y(0) = 2 \tag{7}$$

Figure 4. Absolute Errors of Equation (5)

The Monte Carlo based algorithm is applied to Equation (7) by dividing the time axis uniformly. The comparison of the results of the current algorithm with the ode23s results and a closer view can be seen in Figures 5 and 6, respectively. The corresponding differences are illustrated in Figure 7. Quantitative results of Equation (7) are exhibited in Table 3.

As seen in the corresponding figures, the deviations originating near to the initial conditions have arisen rapidly. Two different equations behave separately; one is increasing while the other one is decreasing. Though the solution remains close to the referenced solution curves in a large scale of vertical axis, the deviations may occur. However, the qualitative and quantitative results can be seen in good agreement with the *ode23s* results.

Even though *ode23s* is commonly accepted as one of the most suitable methods for properly capturing stiff behavior, the current method is seen to be as suitable as the *ode23s*. To support this, another suitable method, RK4 can be applied to this example. The difference between results of the simulation technique and the RK4 results are seen to be relatively small. Therefore, it has been claimed that the approach has ability to capture the stiff behavior. The predicted results have reasonable agreement with the results of *ode23s* and RK4 according to the Figure 8 and Table 3 and the differences between the predicted and *ode23s* solutions.

The computational costs of the current algorithm, *ode23s* and RK4 are 0.4214, 0.0180 and 0.1835 s, respectively. Despite the relatively higher computational cost of the proposed algorithm, the rest of its advantages is taken us to see attractiveness of the approach. In this respect, the computational cost can be sacrificed in simulation techniques in case of especially discrete and continuous methods have serious lack of accuracy or not existing solution for intricate problems.
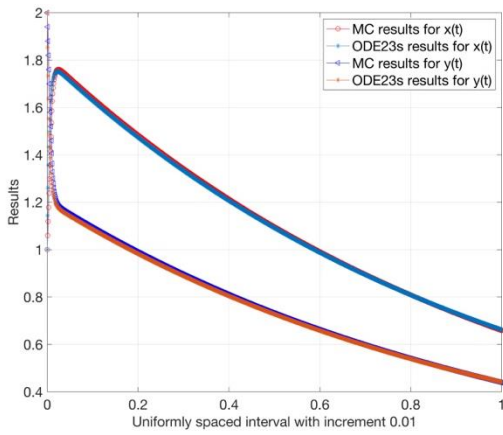
Figure 5. Comparison of the MC prediction results and the ode23s results of the first order stiff differential equation system (7)
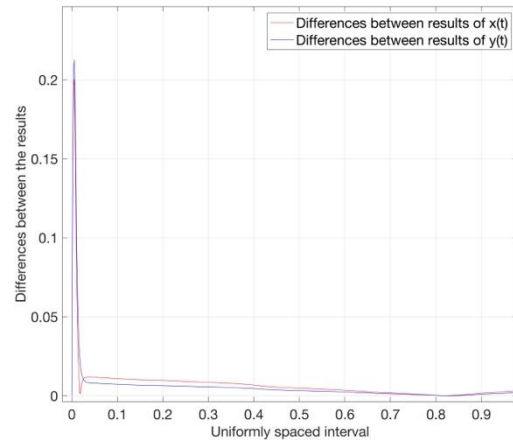

Figure 7. Differences between the MC prediction results and the ode23s results of Equation (7)
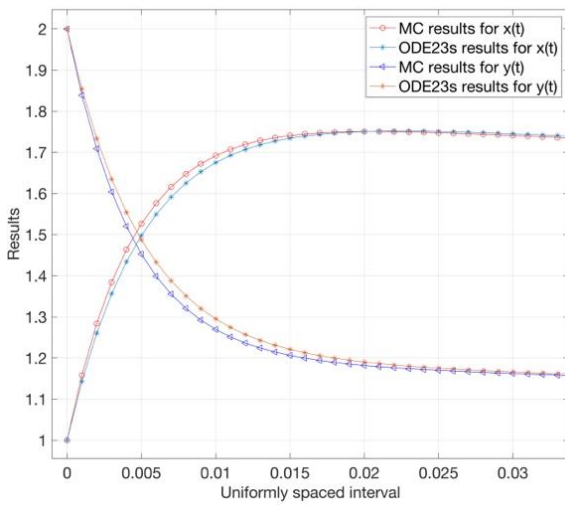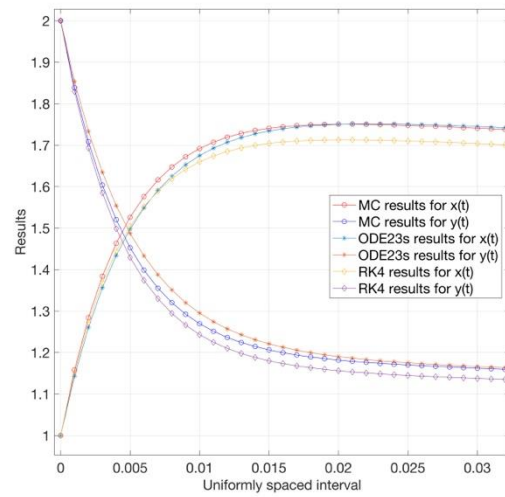

Figure 6. A closer view of Figure 5

Figure 8. Comparison of the MC results with the ode23s and RK4 results for the system of differential equations (7)

Table 3. Comparison of the predicted results with the *ode23s* and RK4 results

Time t	Predicted results for $x(t)$	*ode23s* solutions for $x(t)$	RK4 solutions for $x(t)$	Predicted results for $y(t)$	*ode23s* solutions for $y(t)$	RK4 solutions for $y(t)$
0.0010	1.15799020	1.14321714	1.15199238	1.83863000	1.85378436	1.82952707
0.0050	1.52630360	1.49780400	1.50433322	1.45274000	1.48723344	1.42945587
0.0100	1.69183400	1.67488571	1.66003934	1.26965000	1.29526379	1.24329043
0.0500	1.70742880	1.71222798	1.67279687	1.13853200	1.14145986	1.11337548
0.1000	1.62454282	1.62871297	1.59577436	1.08315800	1.08581070	1.06410479
0.2000	1.46892028	1.47366156	1.45219073	0.97910000	0.98244072	0.96835941
0.3000	1.32774952	1.33336946	1.32152638	0.88512200	0.88891302	0.88122894
0.4000	1.20073072	1.20643333	1.20261887	0.80063000	0.80428888	0.80193825
0.5000	1.08589966	1.09158143	1.09441035	0.72404000	0.72772096	0.72978193
0.6000	0.98283910	0.98766339	0.99593815	0.65544800	0.65844226	0.66411805
0.7000	0.88987552	0.89363829	0.90632622	0.59349800	0.59575886	0.60436243
0.8000	0.80615050	0.80856434	0.82477734	0.53775800	0.53904289	0.54998347
0.9000	0.73031200	0.73158939	0.75056602	0.48726200	0.48772626	0.50049739
1.0000	0.66218674	0.66193829	0.68303204	0.44193800	0.44129220	0.45546393

4. Conclusions and recommendations

In this study, a Monte Carlo based stochastic algorithm has been developed to discover the behavior of real-world processes governed by stiff differential equations. All qualitative and quantitative results produced by the present algorithm have been seen to be in good agreement with the real environment. Despite the effect of randomness to error, the current procedure has been seen to produce highly acceptable results. Even if reconstructing the conventional methods with small time steps for stiff problems is affordable, simulation techniques can be better choices for challenging problems. In real-life problems, when there are sudden deviations in the consequences of random movements, it is necessary to consider the current stochastic approach that can handle the rapidly changing behavior.

Acknowledgments

References

[1] Curtis, C.F. & Hirschfelder, J.O. (1950). *Integration of Stiff Equations.* Proceedings of the National Academy of Sciences of the United States of America*, 38(3), 235-243.

[2] Shampine, L.F. & Gear, C.W. (1976). *A User's View of Solving Ordinary Differential Equations.* Department of Computer Science University of Illinois at Urbana.

[3] Hairer, E. & Wanner, G. (2000). *Solving Ordinary Differential Equations II.* Springer*, Second Edition.

[4] Birge, J.R. & Louveaux, F. (2011). *Introduction to Stochastic Programming*. Springer Science and Business Media.

[5] Kroese, D.P. & Chan, J.C. (2016). *Statistical Modeling and Computation*. Springer.

[6] Rubinstein, R.Y. & Kroese, D.P. (2016). *Simulation and the Monte Carlo Method* (Vol. 10). John Wiley & Sons.

[7] Fishman, G. (2013). *Monte Carlo: Concepts, Algorithms, and Applications*. Springer Science and Business Media.

[8] Kroese, D.P., Taimre, T., & Botev, Z.I. (2013). *Handbook of Monte Carlo Methods* (Vol. 706). John Wiley and Sons.

[9] Chapra, C.S. (2017). *Applied Numerical Methods with MATLAB for Engineers and Scientists*. McGraw Hill.

[10] Dekking, F.M. (2005). *A Modern Introduction to Probability and Statistics: Understanding why and how*. Springer Science and Business Media.

[11] Uslu, H. (2018). *Behavior of First Order Differential Equations Through a Monte Carlo Based Algorithm*. MSc Thesis, Yildiz Technical University, Istanbul, Turkey.

[12] Sari, M., Uslu, H. & Cosgun, T. (2018). The Qualitative Behavior of Some Stiff ODEs Through Stochastic Methods. *The International Conference on Applied Mathematics in Engineering (ICAME'18),* Balikesir, Turkey.

[13] Uslu, H. & Sari, M. (2019). Monte Carlo based stochastic approach for first order nonlinear ODE systems. *Pamukkale Journal of Engineering Sciences*, 26(1), 133-139.

Hande Uslu is a Research Assistant in the Department of Mathematics at Yildiz Technical University, Istanbul Turkey. She received her BSc degree in Mathematics from Bogazici University in 2015, and MSc degree in Applied Mathematics from Yildiz Technical University, in 2018. She is currently continuing her PhD studies in Department of Mathematics at Yildiz Technical University. Her research interests are numerical solutions of differential equations, mathematical modelling, simulation techniques and stochastic processes.
https://orcid.org/0000-0002-1642-1120

Murat Sari is a Professor of Mathematics at Yildiz Technical University. He received the BSc degree from the Ondokuzmayis University in 1991, and the MPhil (transferred) and PhD degrees in Mathematics from University of South Wales, UK, in 1997 and 2000, respectively. His current research interests include numerical solutions of differential equations, simulation and computational methods, computational fluid dynamics, modelling of nonlinear behavior, economical modelling, and biomechanical/biomedical modelling. He has over 50 high-quality scientific papers, over 40 conference proceedings, and written/translated various chapters in some books. He is a reviewer for many international high-quality journals.
https://orcid.org/0000-0003-0508-2917

Tahir Cosgun has been working as a Research Assistant at Amasya University since 2012. He received BSc degree in Mathematics at Bogazici University (2012), and MSc degree in Mathematics at Amasya University (2015). Currently, he is doing his Ph.D. in Applied Mathematics at Yildiz Technical University. His main research interests are dynamical systems, stiff differential equations, numerical and analytical solutions of partial differential equations and integral equations.
https://orcid.org/0000-0003-2970-0863

RESEARCH ARTICLE

A modified crow search algorithm for the weapon-target assignment problem

Emrullah Sonuç [*]

ᵃ Department of Computer Engineering, Karabuk University, Turkey
esonuc@karabuk.edu.tr

ARTICLE INFO	ABSTRACT
	The Weapon-Target Assignment (WTA) problem is one of the most important optimization problems in military operation research. In the WTA problem, assets of defense aim the best assignment of each weapon to target for decreasing expected damage directed by the offense. In this paper, Modified Crow Search Algorithm (MCSA) is proposed to solve the WTA problem. In MCSA, a trial mechanism is used to improve the quality of solutions using parameter LIMIT. If the solution is not improved after a predetermined number of iterations, then MCSA starts with a new position in the search space. Experimental results on the different sizes of the WTA problem instances show that MCSA outperforms CSA in all problem instances. Also, MCSA achieved better results for 11 out of 12 problem instances compared with four state-of-the-art algorithms. The source codes of MCSA for the WTA are publicly available at http://www.3mrullah.com/MCSA.html

1. Introduction

Weapon-Target Assignment (WTA) problem is one of the most important optimization problems in military operation research. The WTA problem has two versions as the static weapon-target assignment problem (SWTA) and the dynamic weapon-target assignment problem (DWTA). The main difference between the SWTA and the DWTA is the timing of launching weapons to targets. In the DWTA, the launching of weapons is performed asynchronously, however in the SWTA, all weapons are launching at the same time and only once [1]. In the WTA problem, the aim is to minimize the damage caused by attacks of the targets. Hence, assets of the defense aim the best assignments for minimal damage after the engagement. Several exact and approximation algorithms [2–4] have recently involved in solving the WTA problem. Since the WTA is an NP-complete problem [5], exact algorithms can not solve large-scale WTA problems in polynomial time. To overcome this problem, metaheuristic algorithms are presented to solve the WTA problem. Metaheuristic algorithms provide a valid solution in a reasonable time [6].

In recent years, metaheuristic algorithms for solving optimization and engineering problems have attracted much attention in the literature. The development of nature-inspired metaheuristic algorithms has increased rapidly in the last decades [7]. These algorithms have good ability to solve global optimization problems even it is complex or high dimensional. The strategy of metaheuristic algorithms is to obtain a solution in a reasonable time for optimization problems which are naturally intricate and very hard to solve. This strategy is built on two main features: exploration and exploitation. In the exploration stage, the algorithm attempts to find a new solution in the search space. In the exploitation stage, the algorithm searches for the neighborhood of the highest quality solution so far to get better solutions. The balance of these two stages is highly important for the algorithm to be successful. The Crow Search Algorithm (CSA) [8] is a population-based metaheuristic algorithm inspired by the behavior of crows, has a good exploration and exploitation for optimization problems.

Many metaheuristic algorithms have been proposed for the WTA problem. Şahin and Leblebicioğlu [9] presented a Hierarchical Fuzzy Decision Maker method to achieve the best assignment for improving performance on the battlefield. The proposed method increased the approximation performance in comparison to exact and optimal methods. Wang et al. [10] developed a Grey Wolf Optimizer which is the

---

[*]Corresponding author

popular population-based algorithm in recent years, to solve the WTA problem. The problem was addressed as a binary problem and the algorithm was modified to a discrete method. According to results, Grey Wolf Optimizer resulted in good quality solutions for small-scale problems and proved that it is competitive for large-scale problems. Li et al. [11] have presented an Ant Colony Optimization for bi-objective the WTA problem. In their study, an optimization model for the WTA is designed which maximizes the expected damage of the enemy (first objective) and minimizes the cost of missiles (second objective). Due to the bi-objective model of the WTA, Ant Colony Optimization is modified to get a set of Pareto solutions. According to simulation results, the modified algorithm improved the performance of the pure one and produced better solutions. Sonuc et al. [12] have worked on a Simulated Annealing algorithm to solve the SWTA problem on GPU. The aim of the study was to obtain better solutions with less computational time compared to the solution of the serial algorithm. Computational results on problem instances have shown that the parallel algorithm was 250 times faster than a single-core CPU and improved the quality of solutions. Zhang et al. [13] have developed a hybrid method using Ant Colony Optimization and Genetic Algorithm to obtain fast convergence speed for the WTA problems. Implementation of Artificial Bee Colony algorithm which is inspired by intelligent behavior of honey bees, was proposed for solving the SWTA problem by Durgut et al. [14]. In the study, three local search operators were discussed and according to the results, the swap operator emerged as more effective than insertion and inversion operators. Kutucu et al. [15] presented a hybrid method with Artificial Bee Colony and Simulated Annealing for the SWTA. According to results on benchmark problems, the proposed algorithm was competitive and satisfactory compared to other metaheuristic algorithms for the WTA. To improve the ability of Ant Colony Optimization, an immune system based algorithm was developed to solve the WTA by Lee et al. [16]. According to the comparison results, the proposed algorithm has improved searching performance. Hu et al. [17] improved Ant Colony Optimization in the viewpoints of selection, updating and concentration interval and applied it to the WTA problem. The advantages of the proposed algorithm were faster convergence and better avoidance from local optima. Tokgöz et al. [18] presented combinatorial optimization techniques for WTA problems. Several heuristic algorithms were selected and applied to the WTA and the results proved that Variable Neighborhood Search and Simulated Annealing obtained better solutions than other algorithms. Li et al. [19] developed a decomposition-based evolutionary algorithm for multiobjective SWTA. According to experiments, the proposed method was effective and promising on generated scenarios. Also, real-time heuristics using Construction Heuristic, Quiz Problem Search Heuristic and Greedy Branch and Bound Heuristic, was presented by Kline et al. [20]. All three heuristics were used for comparison with existing heuristics in literature and the results outlined that the computational costs of the proposed methods are less expensive than the existing ones. Hocaoglu [21] aims to generate a model for air defense. The model answers to the question that is how many missiles are necessary to eliminate attacking from the offense. The model gives a better and faster than the Simulated Annealing algorithm.

This paper aims to improve the quality of solutions for the SWTA problem using a modified crow search algorithm (MCSA). MCSA is a population-based algorithm and obtained better solutions in less time compared to Simulated Annealing [1] which is an iterative heuristic algorithm. Besides, one agent searches a new solution in the search space for each iteration hence Simulated Annealing has a poor exploration compared to population-based metaheuristics. Also, MCSA was compared with the state-of-the-art algorithms and the experimental results were revealed that MCSA was improved quality of results in 6 of 12 problems. The rest of this paper is organized as follows. In Section 2, the model of the SWTA problem is illustrated and the formulation of the problem is presented. In Section 3, nature-inspired CSA is introduced. In Section 4, MCSA based on a trial mechanism is proposed. Experimental results on the WTA problems are presented to demonstrate the performance of improved CSA in Section 5. Finally, conclusion and future works are described in Section 6.

2. Problem formulation

According to the WTA model, which is a minimization optimization problem, assets of defense aim the best assignment of each weapon to target for decreasing expected damage directed by the offense. Each weapon has a destroying probability for each target and the expected damage for assets of defense is evaluated after engagement in the battlefield. An illustration of the WTA problem is presented in Figure 1.
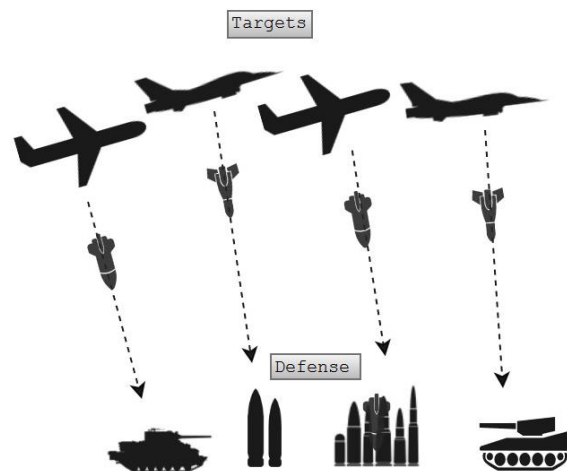

Figure 1. Illustration of the WTA problem.

Table 1 shows the explanation of each symbol for the WTA model. In general, a WTA problem for a defensive mission can be formulated as follows:

$$f(\pi) = \min \sum_{i=1}^{n} v_i \prod_{j=1}^{m} \left(1 - p_{ij}\right)^{x_{ij}} \quad (1)$$

$$s.\,t. \sum_{i=1}^{n} x_{ij} = 1, \quad j = 1, 2, ..., m. \quad (2)$$

Table 1. Definition of symbols for the WTA model.

Symbol	Explanation
n	the number of targets
m	the number of weapons
v_i	the value of the target i
p_{ij}	the probability of destroying by assigning the weapon j to the target i,
$x = [x_{ij}]$	the decision variable that is $n \times m$ matrix, where $x_{ij} = \begin{cases} 1 \text{ if weapon } j \text{ is assigned to target } i, \\ 0 \text{ otherwise} \end{cases}$

3. The crow search algorithm (CSA)

Crows live in flocks and can follow the other birds and steal the food they have stored in their nests. As a result of this follow-up, they can remember the location of other birds' hiding-place and find it whenever they want. The pseudocode of the CSA, which is inspired by the behavior of crows, is shown in Figure 2. CSA has an easy to implement structure and only needs two parameters. Implementation of CSA for optimization problems is an easy process since it has only two parameters: Awareness Probability (*AP*) and Flight Length (*FL*).

According to the strategy of CSA, the crow updates its position in two states. In the first state, each crow (*crow i*) selects a random crow (*crow j*) to steal food from its hiding place without being noticed. The decision to follow the selected crow is determined by the parameter *AP*. If the follow-up is carried out, the new position of the crow is determined according to Eq. (3) using the memory of *crow j* (m_j).

$$x^{i, iter+1} = x^{i, iter} + r_i \cdot fl^{i, iter} \cdot (m^{j, iter} - x^{i, iter}) \quad (3)$$

The second state is that *crow j* recognizes that is being followed by *crow i*. In this state, the crow moves to a new position in the search space. For the second state, the new position of the crow is defined as follows:

$$x^{i, iter+1} = \begin{cases} x^{i, iter+1} = x^{i, iter} + r_i \cdot fl^{i, iter} \cdot (m^{j, iter} - x^{i, iter}) & r_j \geq AP^{j, iter} \\ a \text{ random position} & otherwise \end{cases} \quad (4)$$

```
Initialize the crows population Xᵢ (i = 1, 2, ..., N)
Evaluate the position of each crow in the search space
Initialize the memory of each crow
while (iter < iter_max)
        for i = 1 : N (all N crows in the population)
                Randomly select one crow to follow (e.g. crow j)
                Set an awareness probability
                if rⱼ ≥ AP^(j,iter)
                        Update the position of the current crow by the Eq. (3)
                else
                        Generate a new position in the search space for the current crow
                end if
        end for
        Check if any crow goes beyond the search space and amend it
        Evaluate the new position of each crow
        Update the memory of each crow
end while
```

Figure 2. Pseudocode of the CSA.

4. The WTA problem using MCSA

The WTA problem is a combinatorial optimization problem and each weapon must be assigned to a target. This assignment is represented as a permutation in the problem. Also, this permutation represents a position in the search space for a crow. The aim is finding the best position (permutation) in the search space to minimize the objective function (Eq. (1)). CSA is modified to improve the quality of solutions using a new parameter called *LIMIT*. If a solution that represents a position in the search space, is not improved by a predetermined number of trials, then a new position is generated. This method is proposed by Karaboga et al. [22,23] for Artificial Bee Colony Algorithm to solve optimization problems. The implementation of MCSA for the SWTA problem is carried out through the following steps:

Step 1. Initialization of MCSA parameters.

Initialize the parameters: N, $iter_{max}$, FL, AP and number of non-improved trials *LIMIT*.

Step 2. Initialize permutation and memory of crows.

Randomly generate a permutation for each crow and memorize the initial permutations.

Step 3. Evaluate the objective function.

Compute objective function using its permutation for each crow.

Step 4. Generate a new permutation.

Generate a new permutation for *crow i* as follows:

Randomly select one other crow (*crow j*) to use its permutation. Generate a new position using the swap operator (see Figure 3.) for permutation of *crow j*. Thus, a new permutation of crow *i* is determined if $r_j \geq AP^{j,iter}$

. This procedure is repeated for all crows. Otherwise, it keeps its current permutation. This procedure is defined as follows:

$$x^{i,iter+1} = \begin{cases} new\ permutation\ with\ swapping & r_j \geq AP^{j,iter} \\ keep\ the\ current\ permutation & otherwise \end{cases} \quad (5)$$
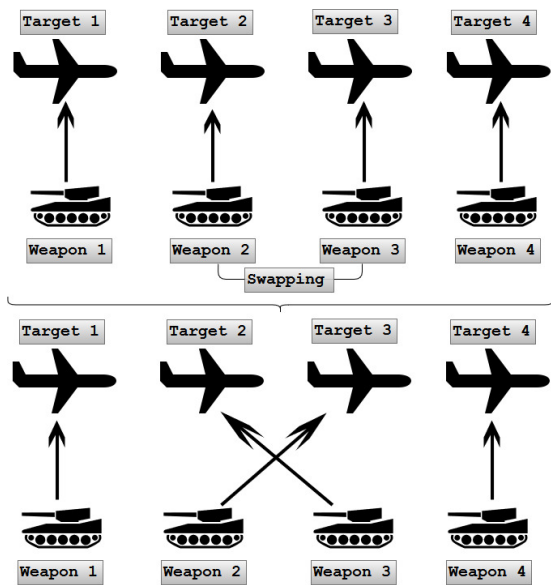

Figure 3. Illustration of swap operator for neighborhood solution.

Step 5. Evaluate the objective function of new permutations.

Compute the objective function of the new permutation for each crow.

Step 6. Update memory.

If the new objective function value of each crow is less than the memorized one, then update the memory of each crow using:

$$m^{i,iter+1} = \begin{cases} x^{i,iter+1} & f(x^{i,iter+1}) < f(m^{i,iter+1}) \\ m^{i,iter+1} & otherwise \end{cases} \quad (6)$$

Step 7. Check if the trial value is reached to LIMIT or not.

After a predetermined number of trials, if there is no improvement on the solutions for the population, generate a new permutation for each crow using the equation is as follows:

$$x^{i,iter+1} = \begin{cases} generate\ a\ random\ permutation & r_i > AP^{i,iter} \cdot fl^{i,iter} \\ keep\ the\ current\ permutation & otherwise \end{cases} \quad (7)$$

For each crow, the objective function value of the new permutation is computed.

Step 8. Evaluate the objective function and update memory.

Computation of objective function for each crow using its permutation. After computation, update the memory of crows.

Step 9. Check stop criterion.

Repeat Steps 4–8 until *iter_max* is reached.
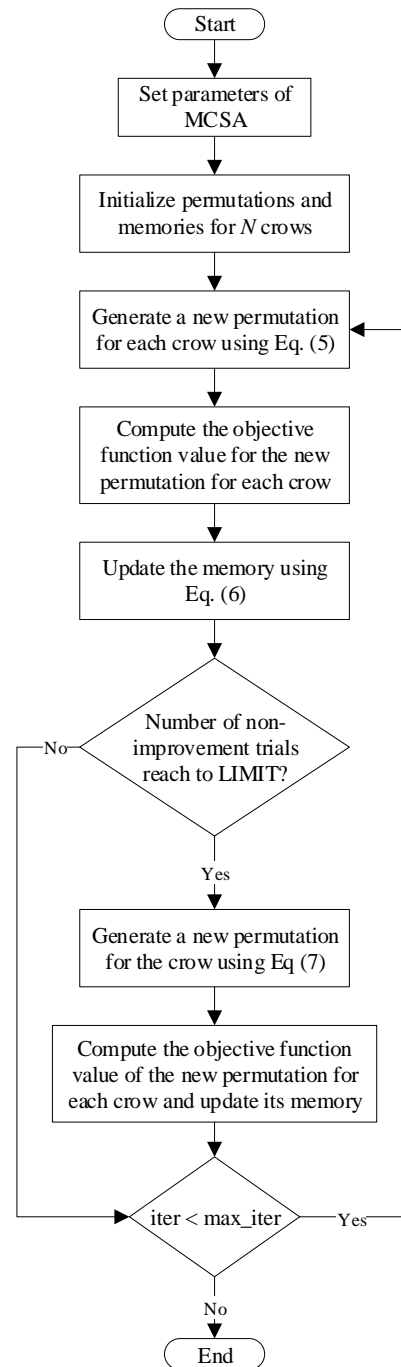
The flowchart of MCSA is presented in Figure 4.

Figure 4. Flowchart of the modified CSA for solving the WTA problem.

5. Experimental results

MCSA is tested on 12 problem instances (available at https://doi.org/10.17632/jt2ppwr62p.1) presented in [12]. Dimensions of problem instances are in the range 5 – 200 and listed in Table 2. The numerical experiments were performed on a PC with Intel(R) Core(TM) i7-5600U CPU @ 2.60 GHz, with 8.00 GB of RAM, running Windows 8 64-bit operating system. The codes of MCSA and CSA have been written in C under CodeBlocks IDE v17.12.
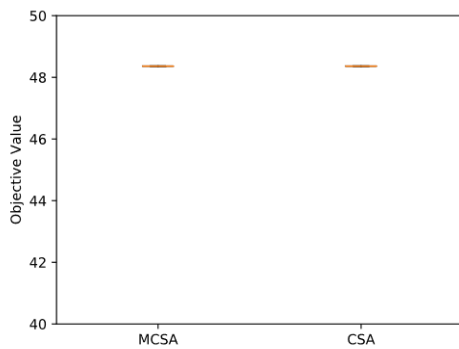
5.1. Comparison MCSA and CSA

Firstly, robustness of MCSA is tested in comparison with the pure CSA by using parameters which are $AP = 0.2$, $FL = 2$, $N = 20$, $ITERATION = 1000$ and $LIMIT = 10 \times$ size of problem (for MCSA only). Figure 5 shows the box plot of 10 independent runs for the problem instances from WTA1 to WTA12 with the aim of comparison between MCSA and CSA. The results show that MCSA outperforms CSA in all problem instances. Also, the box plots show that MCSA converges quickly to the optimal solutions as it has better values and fewer heights compared to CSA.
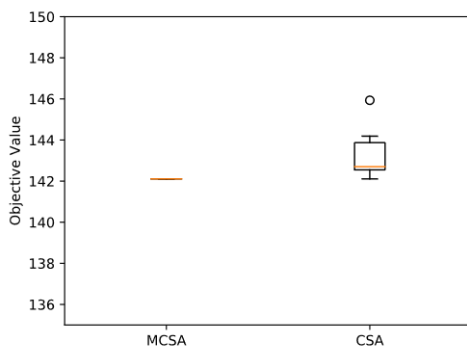
Table 2. The WTA problem instances.

Instance No	Number of Weapons	Number of Targets
#1	5	5
#2	10	10
#3	20	20
#4	30	30
#5	40	40
#6	50	50
#7	60	60
#8	70	70
#9	80	80
#10	90	90
#11	100	100
#12	200	200

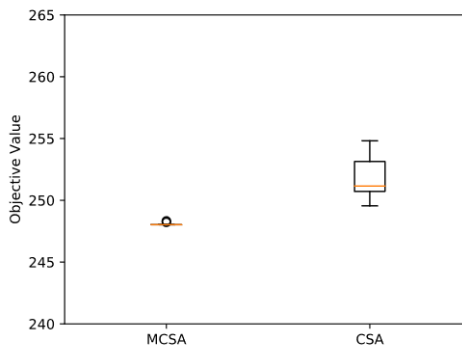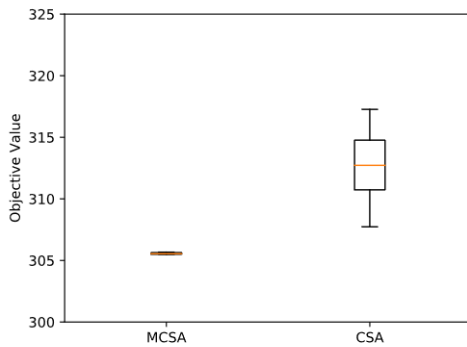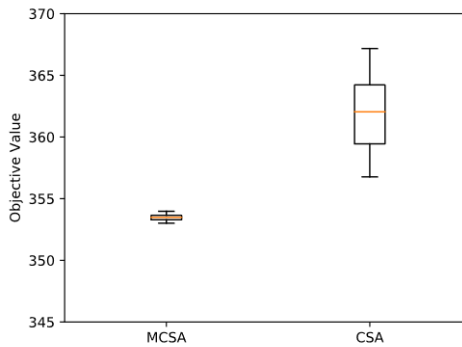**(a)** Box plot for WTA1.
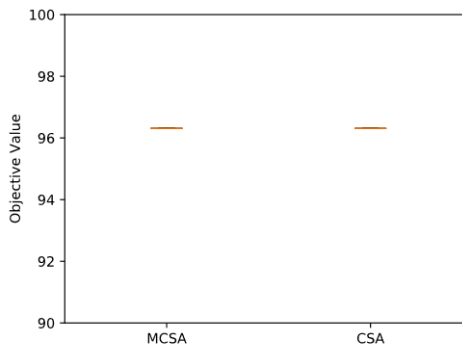
(b) Box plot for WTA2.

(c) Box plot for WTA3.

(d) Box plot for WTA4.

(e) Box plot for WTA5.

(f) Box plot for WTA6.

Figure 5. Box plots for comparing 10-runs results of MCSA and CSA on problem instances.

(g) Box plot for WTA7.

(h) Box plot for WTA8.

(i) Box plot for WTA9.

(j) Box plot for WTA10.

(k) Box plot for WTA11.
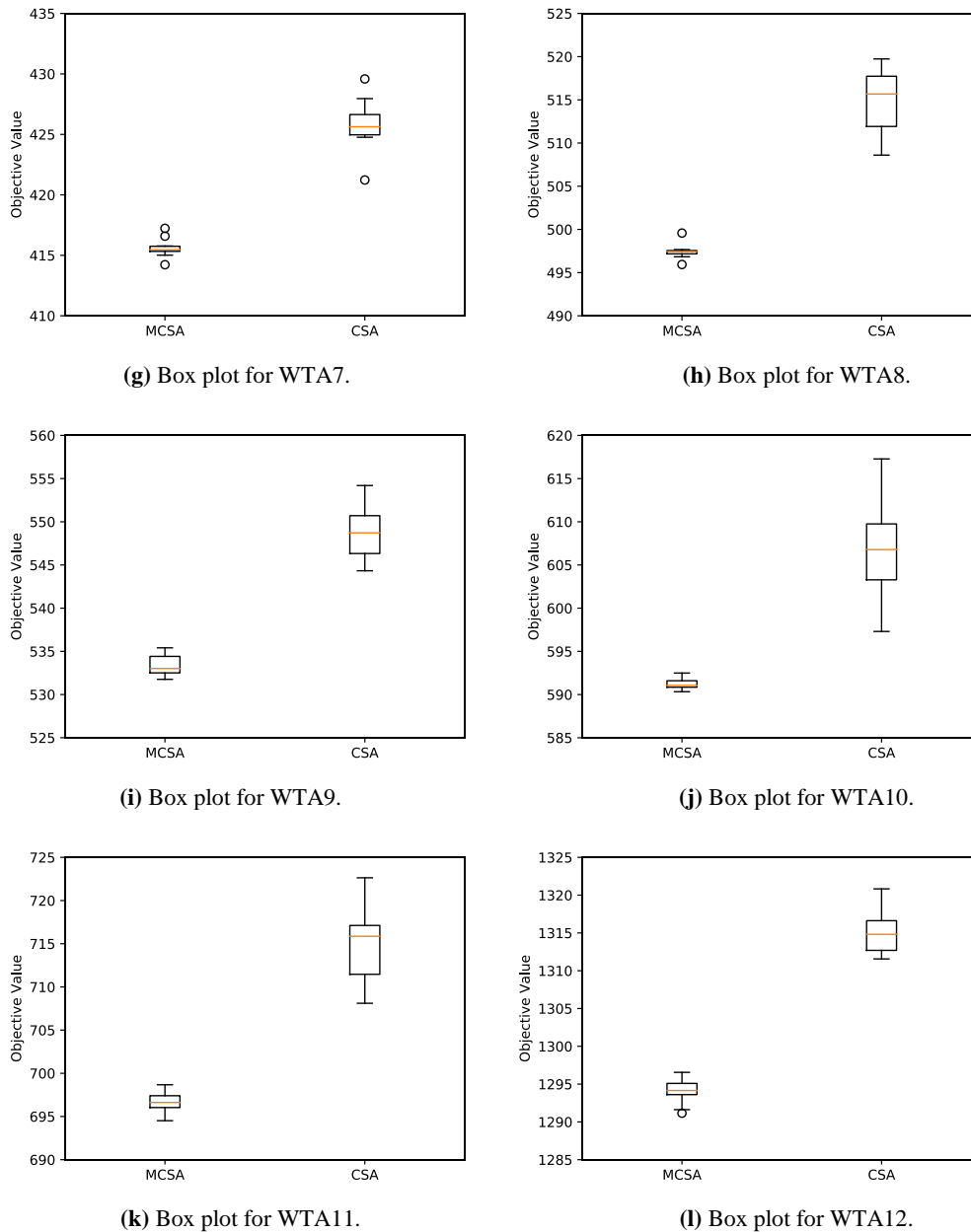

(l) Box plot for WTA12.

Figure 5 (cont). Box plots for comparing 10-runs results of MCSA and CSA on problem instances.

5.2. Comparison of MCSA with the state-of-the-art algorithms

MCSA was compared with four other metaheuristic algorithms for solving the WTA, which are ABC [14], ABC-SA [15], SA [12] and pure CSA. All parameters for the algorithms are given in Table 3. *LIMIT* parameter for MCSA is selected depending on problem size (see in Table 3) as suggested in [24]. With this tuning, *LIMIT* increases when the size of the WTA problem is increased.

The results of all metaheuristic algorithms are compared in terms of the best, mean, worst, median, standard deviation (SD) and time (seconds) in Table 4. However, median and SD values are not available for ABC and ABC-SA. The best results for each problem are shown in bold. Overall, MCSA obtained better results compared to other methods for 11 out of 12 problem instances. All algorithms can achieve the same best results for WTA1 and WTA2. The best result is the same on WTA3 and WTA4 for all algorithms except for CSA. Comparing the results obtained by all metaheuristic algorithms it can be inferred that all algorithms except CSA are successful in reaching the optimum of small size problems.

Table 3. Parameter settings for all algorithms.

ABC [13]		ABC-SA [14]		CSA		MCSA		SA [11]	
Parameter	**Value**	**Parameter**	**Value**	**Parameter**	**Value**	**Parameter**	**Value**	**Parameter**	**Value**
Iteration	200000	Iteration	200000	Iteration	200000	Iteration	200000	Initial Temperature	1000
Population Size	50	Population Size	50	Population Size	40	Population Size	40	Final Temperature	0.1
LIMIT	1000	LIMIT	1000	AP	0.2	AP	0.2	Cooling factor	0.99999
		Initial Temperature	N/A	FL	2	FL	2		
		Final Temperature	N/A			LIMIT	10 x Problem Size		
		Cooling factor	N/A						

Table 4 also shows that the worst value achieved by MCSA is better than the best values achieved by ABC, ABC-SA and CSA for WTA5 to WTA11, which means MCSA provides not only a good exploration but also a good exploitation. According to the results, pure CSA is not efficient yet to solve the WTA problem even if the problem size is small. SD of MCSA is lower than the pure CSA, which indicates that MCSA is a robust algorithm to solve the WTA. For WTA12, ABC-SA achieved the best result comparing to the other algorithms. MCSA is 0.25% worse than ABC-SA for WTA12 according to the best results.

Table 4. Comparison with the state-of-the-art algorithms on the problem instances.

Instance	Weapon	Target	Algorithm	Best	Mean	Worst	Median	SD	Time(sec)
WTA1	5	5	ABC [14]	**48.3640**	48.3640	48.3640	-	-	390.00
			ABC-SA [15]	**48.3640**	48.3640	48.3640	-	-	18.00
			CSA	**48.3640**	48.3640	48.3640	48.3640	0.00	5.20
			MCSA	**48.3640**	48.3640	48.3640	48.3640	0.00	4.42
			SA [12]	**48.3640**	48.3640	48.3640	48.3640	0.00	2985.92
WTA2	10	10	ABC [14]	**96.3123**	96.3123	96.3123	-	-	417.00
			ABC-SA [15]	**96.3123**	96.3123	96.3123	-	-	21.00
			CSA	**96.3123**	96.3123	96.3123	96.3123	0.00	7.10
			MCSA	**96.3123**	96.3123	96.3123	96.3123	0.00	5.39
			SA [12]	**96.3123**	96.3123	96.3123	96.3123	0.00	2841.04
WTA3	20	20	ABC [14]	**142.1070**	142.2480	142.8119	-	-	473.00
			ABC-SA [15]	**142.1070**	142.1070	142.1070	-	-	25.00
			CSA	**142.1070**	143.2052	145.9337	142.7028	1.15	10.92
			MCSA	**142.1070**	142.1070	142.1070	142.1070	0.00	7.56
			SA [12]	**142.1070**	142.1070	142.1070	142.1070	0.00	2752.49
WTA4	30	30	ABC [14]	**248.0285**	248.6854	249.2224	-	-	532.00
			ABC-SA [15]	**248.0285**	248.1678	248.4222	-	-	32.00
			CSA	249.5552	251.8021	254.8158	251.1550	1.79	14.35
			MCSA	**248.0285**	248.0781	248.3312	248.0285	0.10	9.86
			SA [12]	**248.0285**	248.0285	248.0285	248.0285	0.00	2754.31
WTA5	40	40	ABC [14]	305.8729	306.8570	307.4944	-	-	585.00
			ABC-SA [15]	**305.5016**	306.2735	307.1293	-	-	36.00
			CSA	307.7296	312.7559	317.2676	312.7247	2.79	18.78
			MCSA	**305.5016**	305.6046	305.9203	305.5016	0.15	12.70
			SA [12]	**305.5016**	305.5016	305.5016	305.5016	0.00	2760.78
WTA6	50	50	ABC [14]	353.3794	355.1488	356.8539	-	-	654.00
			ABC-SA [15]	353.0149	354.6901	357.2952	-	-	42.00
			CSA	356.7682	361.8349	367.1764	362.0425	3.05	22.60
			MCSA	**353.0102**	353.4104	353.6899	353.4893	0.26	14.86
			SA [12]	353.0767	353.3112	353.5702	353.2610	0.14	2790.03
WTA7	60	60	ABC [14]	414.4555	417.0145	420.1622	-	-	712.00
			ABC-SA [15]	414.7521	417.3107	420.6054	-	-	46.00
			CSA	421.2284	425.7957	429.5839	425.6336	2.09	26.38
			MCSA	**414.2222**	415.4017	416.8135	415.3838	0.82	17.48
			SA [12]	415.0528	415.4068	415.7079	415.4371	0.21	2787.45

Instance	Weapon	Target	Algorithm	Best	Mean	Worst	Median	SD	Time(sec)
WTA8	70	70	ABC [14]	498.0948	500.5102	504.3466	-	-	786.00
			ABC-SA [15]	496.9645	498.3417	500.6414	-	-	52.00
			CSA	508.5992	514.6464	519.7359	515.6737	3.67	30.24
			MCSA	**496.3095**	497.1012	498.1227	497.1297	0.55	19.84
			SA [12]	498.1049	498.5918	499.0167	498.5860	0.30	2841.02
WTA9	80	80	ABC [14]	534.4742	536.8911	541.8093	-	-	831.00
			ABC-SA [15]	531.4078	534.4042	536.5087	-	-	60.00
			CSA	544.3289	548.6797	554.1954	548.7232	2.88	33.99
			MCSA	**531.1592**	533.2647	536.3640	532.9782	1.46	22.26
			SA [12]	534.4408	535.4559	536.2618	535.5937	0.57	2868.79
WTA10	90	90	ABC [14]	592.9167	594.9403	598.3802	-	-	889.00
			ABC-SA [15]	590.4780	592.4761	595.1910	-	-	71.00
			CSA	597.3041	606.4188	617.2749	606.7811	5.52	37.88
			MCSA	**589.3209**	592.5042	594.5376	592.3725	1.52	24.37
			SA [12]	594.0639	595.3277	596.1228	595.6466	0.72	2812.57
WTA11	100	100	ABC [14]	698.4465	701.4467	707.7392	-	-	954.00
			ABC-SA [15]	694.8067	696.3017	700.4310	-	-	79.00
			CSA	708.1073	714.8838	722.6326	715.8635	4.41	41.60
			MCSA	**694.5009**	696.7299	698.3746	696.7235	1.34	29.08
			SA [12]	699.8357	701.0054	702.1189	701.2495	0.75	2805.83
WTA12	200	200	ABC [14]	1295.3142	1299.2044	1303.1223	-	-	1624.00
			ABC-SA [15]	**1287.0240**	1289.1600	1291.2790	-	-	124.00
			CSA	1311.5617	1314.9700	1320.8271	1314.8187	2.74	83.11
			MCSA	1290.2712	1294.4943	1296.3025	1294.8583	1.66	55.72
			SA [12]	1306.9126	1308.3382	1309.4616	1308.5187	0.86	2902.15

A comparison between MCSA and ABC-SA based on time is presented in Figure 6. Although it is not fair to compare MCSA and ABC-SA as we don't know some parameters and number of function evaluations, the capabilities of the used devices for running these two algorithms are approximately similar. It can be shown that the average run time for MCSA is better than ABC-SA.
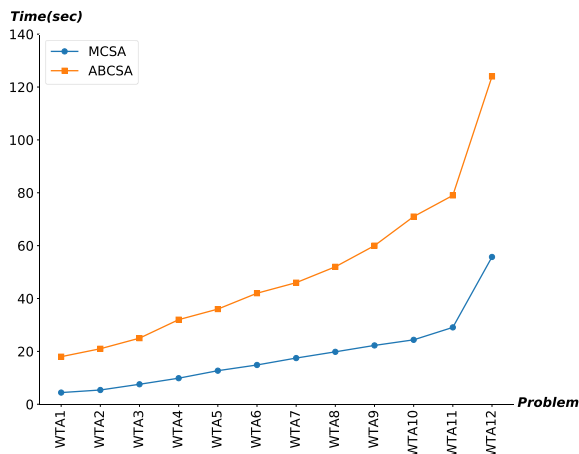

Figure 6. Time comparison between MCSA and ABC-SA for the WTA problem instances.

6. Conclusion and future works

This paper proposed a Modified Crow Search Algorithm (MCSA) for solving the static WTA problem. In MCSA, a trial mechanism that starts with a new position in the search space after a predetermined number of trials, has been adapted to the exploration phase. The number of trials defines as a parameter called *LIMIT*, is adjusted to the size of the problem. With this update, the exploitation stage of CSA is strengthened for combinatorial problems like the WTA. Experimental results of MCSA have been compared with four state-of-the-art algorithms on the WTA problem instances with different dimensions. In each problem, the numbers of the weapons and targets are equal and limited and this limitation occurs the size of the problem. According to the experimental results, MCSA achieved the best results on all problem instances except for only one and outperformed the state-of-the-art algorithms. In future works, MCSA can be combined with single solution based algorithms (hill-climbing, tabu search, simulated annealing, etc.), especially for the second state of CSA. Also, MCSA can be applied to solve dynamic WTA problem or other discrete optimization problems.

References

[1] Kline, A., Ahner, D., & Hill, R. (2018). The Weapon-Target Assignment Problem. *Computers & Operations Research*. https://doi.org/10.1016/j.cor.2018.10.015

[2] Ahuja, R. K., Kumar, A., Jha, K. C., & Orlin, J. B. (2007). Exact and Heuristic Algorithms for the Weapon-Target Assignment Problem. *Operations Research*, *55*(6), 1136–1146. https://doi.org/10.1287/opre.1070.0440

[3] Sikanen, T. (2008). Solving weapon target assignment problem with dynamic programming. *Independent Research Projects in Applied Mathematics*, 32.

[4] Ma, F., Ni, M., Gao, B., & Yu, Z. (2015). An efficient algorithm for the weapon target assignment problem. In *2015 IEEE International Conference on Information and Automation* (pp. 2093–2097). https://doi.org/10.1109/ICInfA.2015.7279633

[5] Lloyd, S. P., & Witsenhausen, H. S. (1986). Weapons allocation is NP-complete. In *1986 Summer Computer Simulation Conference* (pp. 1054–1058).

[6] Talbi, E.-G. (2009). *Metaheuristics: From Design to Implementation*. John Wiley & Sons.

[7] Sotoudeh-Anvari, A., & Hafezalkotob, A. (2018). A bibliography of metaheuristics-review from 2009 to 2015. *International Journal of Knowledge Based Intelligent Engineering Systems*, *22*(1), 83–95. https://doi.org/10.3233/KES-180376

[8] Askarzadeh, A. (2016). A novel metaheuristic method for solving constrained engineering optimization problems: Crow search algorithm. *Computers & Structures*, *169*, 1–12. https://doi.org/10.1016/j.compstruc.2016.03.001

[9] Şahin, M. A., & Leblebicioğlu, K. (2011). A Hierarchical Fuzzy Decision Maker for the Weapon Target Assignment. *IFAC Proceedings Volumes*, *44*(1), 8993–8998. https://doi.org/10.3182/20110828-6-IT-1002.00986

[10] Wang, J., Luo, P., Hu, X., & Zhang, X. (2018). A Hybrid Discrete Grey Wolf Optimizer to Solve Weapon Target Assignment Problems. *Discrete Dynamics in Nature and Society*. https://doi.org/10.1155/2018/4674920

[11] Li, Y., Kou, Y., Li, Z., Xu, A., & Chang, Y. (2017). A Modified Pareto Ant Colony Optimization Approach to Solve Biobjective Weapon-Target Assignment Problem. *International Journal of Aerospace Engineering*. https://doi.org/10.1155/2017/1746124

[12] Sonuc, E., Sen, B., & Bayir, S. (2017). A Parallel Simulated Annealing Algorithm for Weapon-Target Assignment Problem. *International Journal of Advanced Computer Science and Applications*, *8*(4). https://doi.org/10.14569/IJACSA.2017.080412

[13] Zhang, J., Wang, X., Xu, C., & Yuan, D. (2012). ACGA Algorithm of Solving Weapon—Target Assignment Problem. *Open Journal of Applied Sciences*, *02*(04), 74–77. https://doi.org/10.4236/ojapps.2012.24B018

[14] Durgut, R., Kutucu, H., & Akleylek, S. (2017). An Artificial Bee Colony Algorithm for Solving the Weapon Target Assignment Problem. In *Proceedings of the 7th International Conference on Information Communication and Management* (pp. 28–31). New York, NY, USA: ACM. https://doi.org/10.1145/3134383.3134390

[15] Kutucu, H., & Durgut, R. (2018). Silah Hedef Atama Problemi için Tavlama Benzetimli Bir Hibrit Yapay Arı Kolonisi Algoritması. *Süleyman Demirel Üniversitesi Fen Bilimleri Enstitüsü Dergisi*, *22*(Özel), 263. https://doi.org/10.19113/sdufbed.39561

[16] Lee, Z.-J., Lee, C.-Y., & Su, S.-F. (2002). An immunity-based ant colony optimization algorithm for solving weapon–target assignment problem. *Applied Soft Computing*, *2*(1), 39–47. https://doi.org/10.1016/S1568-4946(02)00027-3

[17] Hu, X., Luo, P., Zhang, X., & Wang, J. (2018). Improved Ant Colony Optimization for Weapon-Target Assignment. *Mathematical Problems in Engineering*. https://doi.org/10.1155/2018/6481635

[18] Tokgöz, A., & Bulkan, S. (2013). Weapon Target Assignment with Combinatorial Optimization Techniques. *International Journal of Advanced Research in Artificial Intelligence*, *2*(7). https://doi.org/10.14569/IJARAI.2013.020707

[19] Li, X., Zhou, D., Pan, Q., Tang, Y., & Huang, J. (2018). Weapon-Target Assignment Problem by Multiobjective Evolutionary Algorithm Based on Decomposition. *Complexity*. https://doi.org/10.1155/2018/8623051

[20] Kline, A. G., Ahner, D. K., & Lunday, B. J. (2018). Real-time heuristic algorithms for the static weapon target assignment problem. *Journal of Heuristics*. https://doi.org/10.1007/s10732-018-9401-1

[21] Hocaoğlu, M. F. (2019). Weapon target assignment optimization for land based multi-air defense systems: A goal programming approach. *Computers & Industrial Engineering*, *128*, 681–689. https://doi.org/10.1016/j.cie.2019.01.015

[22] Karaboga, D., & Basturk, B. (2007). A powerful and efficient algorithm for numerical function optimization: Artificial bee colony (ABC) algorithm. *Journal of Global Optimization*, *39*(3), 459–471. https://doi.org/10.1007/s10898-007-9149-x

[23] Akay, B. B., & Karaboga, D. (2017). Artificial bee colony algorithm variants on constrained optimization. *An International Journal of Optimization and Control: Theories & Applications (IJOCTA)*, *7*(1), 98–111. https://doi.org/10.11121/ijocta.01.2017.00342

[24] Sonuç, E. (2018). Artificial Bee Colony Algorithm for The Linear Ordering Problem. In *Proceeding Book of the International Conference on Advanced Technologi es, Computer Engineering and Science (ICATCES 2018)* (pp. 818–820). Safranbolu, Turkey.

Emrullah Sonuç *is currently working as an assistant professor at Department of Computer Engineering, Karabuk University, Karabuk, Turkey. He received M.Sc. and Ph.D. degrees from the Department of Computer Engineering, Karabuk University in 2012 and 2017, respectively. His current research interests are: Parallel and distributed computing, Evolutionary computation and Metaheuristic algorithms.*

http://orcid.org/0000-0001-7425-6963

RESEARCH ARTICLE

Application of spectral conjugate gradient methods for solving unconstrained optimization problems

Sulaiman Mohammed Ibrahim[a*], Usman Abbas Yakubu[b], Mustafa Mamat[a]

[a] Faculty of Informatics and Computing, University Sultan Zainal Abidin, Terengganu, Malaysia
[b] Department of Mathematics, Yusuf Maitama Sule University, Kano, Nigeria
sulaimanib@unisza.edu.my, usman.abbas84@yahoo.com, must@unisza.edu.my

ARTICLE INFO	ABSTRACT
	Conjugate gradient (CG) methods are among the most efficient numerical methods for solving unconstrained optimization problems. This is due to their simplicty and less computational cost in solving large-scale nonlinear problems. In this paper, we proposed some spectral CG methods using the classical CG search direction. The proposed methods are applied to real-life problems in regression analysis. Their convergence proof was establised under exact line search. Numerical results has shown that the proposed methods are efficient and promising.

1. Introduction

The spectral CG methods are among the most efficient variant of CG methods designed to solve large-scale problems. The methods possess the global convergent properties in addition to the sufficient descent condition. Moreso, the spectral CG methods are less expensive and requires less storage location. Some outstanding features of the spectral CG method are their simplicity in algebraic processes and development of computer codes [1]. Spectral CG method is formulated by combining the CG search direction and a scalar spectral parameter to form a new search direction. Birgin and Martinez [2], introduced a spectral CG method using standard secant equation [3].

Consider the following minimization problem.

$$min\, f(x), \qquad x \in R^n \qquad (1)$$

where $f: R^n \rightarrow R$ is continuous and differentiable, g_k is the gradient of $f(x)$ and the vector $x_0 \in R^n$ is known as the initial point. The CG method are iterative scheme of the form

$$x_{k+1} = x_k + \gamma_k d_k, \qquad k = 0,1,2,3,4,\ldots \qquad (2)$$

where the vector x_k is the current iterate, x_{k+1} is the new iteration point, and $\gamma_k > 0$ is the step-dimension obtained by the line search method defined as

$$\gamma_k = arg \min_{\gamma>0} f(x_k + \gamma d_k) \qquad (3)$$

also, d_k is the classical search direction given as

$$d_k = \begin{cases} -g_k, & if\ k = 0 \\ -g_k + \beta_k d_{k-1}, & if\ k \geq 1 \end{cases} \qquad (4)$$

$g_k = \nabla f(x)$, is the gradient and the parameter $\beta_k \in R$ is the CG coefficient that characterizes different CG methods. Some known CG coefficients are the Polak-Ribiére-Polyak (PRP) and Wei-Yao-Liu (WYL) methods with formulas as follows.

$$\beta_k^{PRP} = \frac{g_k^T(g_k - g_{k-1})}{\|g_{k-1}\|^2} \qquad (5)$$

$$\beta_k^{WYL} = \frac{g_k^T\left(g_k - \frac{\|g_k\|}{\|g_{k-1}\|}g_{k-1}\right)}{\|g_{k-1}\|^2} \leq \frac{2\|g_k\|^2}{\|g_{k-1}\|^2} \qquad (6)$$

where g_k and g_{k-1} are gradient vectors at points x_k, x_{k-1} respectively, and $\|.\|$ represent the Euclidian norm. The PRP method is regarded as the best CG method due to its rapid convergence. However, its convergence analysis for nonlinear function is

*Corresponding author

uncertain [12]. For further references on the CG and spectral CG methods, please refer to [4-14, 20, 26].

In this paper, the spectral PRP and spectral WYL CG methods are presented without the secant equation. Their performance is verified using the least square and trend line methods in regression analysis. The regression analysis is an important tool for the analysis of statistical data utilized in the field of economics, engineering, sciences and many more [15]. The analysis is use for forecasting and to comprehend the relation between dependent and independent variables in real life applications. The dependent variable is denoted by y and independent is denoted by x_j for $j = 1,2,3 \dots \dots, n, n > 0$, and e is an integer constant in the error term. The model is defined by

$$y = l(x_j + e), \qquad for \; x_j = x_1, x_2 \dots x_n \qquad (7)$$

and generalized as follows

$$y = u_0 + u_1 x_1 + u_2 x_2 + \dots \dots u_n x_n + e \qquad (8)$$

where $u_0, u_1, u_2, \dots \dots, u_n$ are the parameters for the regression analysis. The values of the parameters are estimate by using the nonlinear least square method defined by

$$\min E(u) = \sum_{j=1}^{n} (y_i - u_0 + y_1 x_{j1} + y_2 x_{j2} + \dots y_n x_{jn})^2 \qquad (9)$$

where y_i is the estimated data of jth response and $x_{j1}, x_{j2}, \dots \dots, x_{jn}$ are n data evaluation of the response variables [16]. The formula for predicting data in regression analysis is derive from calculating the relative error. However, the error is obtained by comparing the approximate value and actual value as described below

$$\text{Relative error} = \left| \frac{\text{Exact Value} - \text{Approximate Value}}{\text{Exact Value}} \right| \qquad (10)$$

The least square determines the best approximation models by comparing the total least square errors. The error is defined as

$$E_j = (u_0 + u_1 x) - y_j$$

The strategy of fitting the best line through the data would minimize the sum of the residual error squares for the data available. This problem is similar to the minimization problem in unconstrained optimization [17]. Thus, we employ the spectral PRP and WYL CG parameter to obtain the solution of the given unconstrained optimization problem.

2. Derivation of spectral CG methods

Spectral CG method was introduce by [2] with direction defined as $d_k = -\varphi_k g_k + \beta_k s_{k-1}$, where

$s_{k-1} = \gamma_{k-1} d_{k-1}$ and φ_k is a spectral scalar parameter. Motivated by the procedure of [5], we proposed the following search direction

$$d_k = \begin{cases} -g_k, & if \; k = 0 \\ -\varphi_k g_k + \beta_k^{PRP} d_{k-1}, & if \; k \geq 1 \end{cases} \qquad (11)$$

$$d_k = \begin{cases} -g_k, & if \; k = 0 \\ -\frac{1}{\emptyset_k} g_k + \beta_k^{WYL} d_{k-1}, & if \; k \geq 1 \end{cases} \qquad (12)$$

From (11), $d_k = -\varphi_k g_k + \beta_k^{PRP} d_{k-1} \rightarrow d_k - \beta_k^{PRP} d_{k-1} = -\varphi_k g_k$. Also, $d_k = -g_k$, then substituting equation (5) we have,

$$\varphi_k = 1 - \frac{g_k^T d_{k-1}}{g_{k-1}^T d_{k-1}} \qquad (13)$$

From equation (12), $d_k = -\frac{1}{\emptyset_k} g_k + \beta_k^{WYL} d_{k-1}$ which is rewritten as $d_k - \beta_k^{WYL} d_{k-1} = -\frac{1}{\emptyset_k} g_k$. This implies $\frac{1}{\emptyset_k} = \frac{d_k}{-g_k} + \frac{\beta_k^{WYL} d_{k-1}}{g_k}$. Substituting (6) in the equation, we have

$$\emptyset_k = \left(1 - \frac{2 g_k^T d_{k-1}}{g_{k-1}^T d_{k-1}}\right)^{-1} \qquad (14)$$

Recall that the orthogonality of gradients $g_k^T g_{k-1} = 0$ and thus, φ_k and $\emptyset_k$ are the new spectral parameters computed by exact line search procedure.

Algorithm 1.1 (Spectral CG method)

Step 1: Given a starting point $x_0 \in R^n$ set $k = 0$
Step 2: Compute β_k by (5) and (6)
Step 3: Compute d_k by (11) and (12). If $\|g_k\| = 0$, then stop.
Step 4: Compute γ_k by (3).
Step 5: Update the new point by the recurrence expression (2).
Step 6: If $f(x_{k+1}) < f(x_k)$ and $\|g_k\| < \varepsilon$ then stop, otherwise go to step 1 with $k = k + 1$.

3. The global convergence analysis of spectral CG methods

The Sufficient descent condition ensures that global convergence of iterative procedures or algorithm is achieved. Therefore, all CG methods must satisfy the following.

$$g_k^T d_k \leq -C \|g_k\|^2 \quad for \; k \geq 0 \; and \; C > 0 \qquad (15)$$

Theorem 1.1 *Suppose a CG method with search direction* (11), (12) *and* β_k^{PRP}, β_k^{WYL} *given by equation* (5), (6), *then condition* (15) *holds for*

all $k \geq 0$.

Proof. With β_k^{PRP}, we proceed by induction, since $g_0^T d_0 = -\|g_0\|^2$, the condition (15) satisfied as $k = 0$. Now we assume it is true for $k \geq 0$. Also, the inequality (15) as well hold.

From the search direction (11) multiply both sides by g_{k+1}^T and substitute parameter (13) gives

$$g_{k+1}^T d_{k+1} = -\left(1 - \frac{g_k^T d_{k-1}}{g_{k-1}^T d_{k-1}}\right)\|g_{k+1}\|^2 + \beta_k^{PRP} g_{k+1}^T d_k$$

It is known from the conjugacy conditions $g_{k+1}^T d_k = 0$. Hence for constant $C = 1$ condition (15) is true for $k + 1$. ■

Proof. With β_k^{WYL}, also by induction, since $g_0^T d_0 = -\|g_0\|^2$, the condition (15) satisfied as $k = 0$. Now we assume it is true for $k \geq 0$.
Also, the inequality (15) hold true, from the search direction (12) multiply both sides of the equation by g_{k+1}^T and substitute (14) gives

$$g_{k+1}^T d_{k+1} = -\left(1 - \frac{g_k^T d_{k-1}}{g_{k-1}^T d_{k-1}}\right)\|g_{k+1}\|^2 + \beta_k^{WYL} g_{k+1}^T d_k$$

Therefore, from the conjugacy conditions $g_{k+1}^T d_k = 0$. Hence for constant $C = 1$ condition (15) hold for $k + 1$. ■

The following assumptions are needed for the convergence analysis of the CG method.

Assumptions 1.1 *(i) A level set $\Omega = \{x \in R^n \mid f(x) \leq f(x_0)\}$ is bounded, the function f is continuously differentiable in a neighborhood N of the level set Ω and x_0 is a starting point.*
(ii) $g(x)$ is Lipschitz continuous in N that is $\exists$ a constant $L > 0$, such that $\|g(x) - g(y)\| \leq L\|x - y\|$ for any $x, y \in N$.

Lemma 1.1 *Suppose Assumption 1.1 hold and consider any recurrence expression (2) with search direction (11) and (12), γ_k computed using (3). Then Zoutendijk condition (16) holds.*

$$\sum_{k=0}^{\infty} \frac{(g_k^T d_k)^2}{\|d_k\|^2} < \infty \tag{16}$$

Proof: The proof of this Lemma is given in [18].

Theorem 1.2 *Suppose Assumptions 1.1 hold, for any CG sequence $\{x_k\}$, $\{d_k\}$ be given as spectral PRP, spectral WYL CG methods, γ_k determined by equation*

(3) and β_k in equation (5) and (6). Then

$$\lim_{k\to\infty} \|g_k\| = 0 \tag{17}$$

Proof. With β_k^{PRP}, from the search direction (11), square both sides of equation,

$$(d_{k+1} + \varphi_k g_{k+1})^2 = (\beta_k^{PRP} d_k)^2$$
$$\|d_{k+1}\|^2 = (\beta_k^{PRP})^2\|d_k\|^2 - 2\varphi_k g_{k+1}^T d_{k+1} - \varphi_k^2\|g_{k+1}\|^2 \tag{18}$$

Substituting (5) into (18) and recall that $g_{k+1}^T d_{k+1} = -C\|g_{k+1}\|^2$, rewrite equation (18) as

$$\|d_{k+1}\|^2 = \frac{\|g_{k+1}\|^4}{\|g_k\|^4}\|d_k\|^2 - \|g_{k+1}\|^2(\varphi_k^2 - 2C\varphi_k) \tag{19}$$

Multiply both sides of equation (19) by $\frac{\|g_{k+1}\|^2}{\|d_{k+1}\|^2}$, we get

$$\frac{\|d_{k+1}\|^2\|g_{k+1}\|^2}{\|d_{k+1}\|^2} = \frac{\|g_{k+1}\|^4}{\|d_{k+1}\|^2}\left((2C\varphi_k - \varphi_k^2) + \frac{\|g_k\|^4}{\|g_{k-1}\|^4}\|d_k\|^2\right) \tag{20}$$

From the theorem 1.1 the value of the constant $C = 1$ therefore, substituting equation (13) in (20) and note that from the conjugacy conditions $g_{k+1}^T d_k = 0$ we have,

$$\frac{\|d_{k+1}\|^2\|g_{k+1}\|^2}{\|d_{k+1}\|^2} \leq \frac{\|g_{k+1}\|^4}{\|d_{k+1}\|^2} \tag{21}$$

Thus, from the Lemma 1.1 above. It implies that Theorem 1.2 does not hold true, then $\lim_{k\to\infty} \frac{(g_{k+1}^T d_{k+1})^2}{\|d_{k+1}\|^2} = \infty$ and from equation (21) this is true $\infty \leq \frac{\|g_{k+1}\|^4}{\|d_{k+1}\|^2}$. So Theorem 1.2 is true for a sufficient large k. ■

Proof. With β_k^{WYL}, from the search direction equation (12), square both sides we have,

$$\left(d_{k+1} + \frac{1}{\emptyset_k} g_{k+1}\right)^2 = (\beta_k^{WYL} d_k)^2$$

$$\|d_{k+1}\|^2 = (\beta_k^{WYL})^2\|d_k\|^2 - \frac{2}{\emptyset_k} g_{k+1}^T d_{k+1} - \frac{1}{\emptyset^2}\|g_{k+1}\|^2 \tag{22}$$

Substituting equation (6) into (22) and recall that $g_{k+1}^T d_{k+1} = -C\|g_{k+1}\|^2$, rewrite (22) as

$$\|d_{k+1}\|^2 = \frac{4\|g_{k+1}\|^4}{\|g_k\|^4}\|d_k\|^2 + \frac{2C}{\emptyset_k}\|g_{k+1}\|^2 - \frac{1}{\emptyset_k^2}\|g_{k+1}\|^2 \tag{23}$$

Multiply both sides of (23) by $\frac{\|g_{k+1}\|^2}{\|d_{k+1}\|^2}$, we get

$$\frac{\|d_{k+1}\|^2\|g_{k+1}\|^2}{\|d_{k+1}\|^2} = \frac{\|g_{k+1}\|^4}{\|d_{k+1}\|^2}\left(\left(\frac{2C}{\emptyset_k} - \frac{1}{\emptyset_k^2}\right)\right.$$
$$\left. + \frac{4\|g_{k+1}\|^2}{\|g_k\|^4}\|d_k\|^2\right) \qquad (24)$$

From the theorem 1.1 the value of the constant $C = 1$ therefore, substituting (14) in (24) and note that from the conjugacy conditions $g_{k+1}^T d_k = 0$ we equally have,

$$\frac{\|d_{k+1}\|^2\|g_{k+1}\|^2}{\|d_{k+1}\|^2} = \frac{\|g_{k+1}\|^4}{\|d_{k+1}\|^2}\left(1 + \frac{4\|g_{k+1}\|^2}{\|g_k\|^4}\|d_k\|^2\right)$$

$$\frac{\|d_{k+1}\|^2\|g_{k+1}\|^2}{\|d_{k+1}\|^2} \leq \frac{\|g_{k+1}\|^4}{\|d_{k+1}\|^2} \qquad (25)$$

Thus, from the Lemma 1.1 above. It implies that Theorem 1.2 does not hold true, then $\lim_{k\to\infty}\frac{(g_{k+1}^T d_{k+1})^2}{\|d_{k+1}\|^2} = \infty$ and from equation (25) this is true $\infty \leq \frac{\|g_{k+1}\|^4}{\|d_{k+1}\|^2}$. So, Theorem 1.2 is true for a sufficient large k. ∎

4. Description of the real life application

In this section, the detailed description of the real-life problem considered are in Table 1. These problems were obtained from [19]. The approximate function for the nonlinear least square method is formed as follows

$$f(x) = -0.05690476x^2 + 0.68404762x + 0.13285714$$

Thus, the function $f(x)$ is use to approximate the value of y based on value of x, that is, the rate of drug abuse within the city from year 2009 to 2016. The least square method can easily be transformed into unconstrained minimization problems as follows

$$\min_{x \in R^n} f(x) = \sum_{j=1}^{n}\left((u_0 + u_1 x_j + u_2 x_j^2) - y_j\right)^2 \qquad (26)$$

The data set in Table 1 shows the rate of drug abuse among the youth with aged 18 to 25 in Kano city, Nigeria for the years 2009-2017. The statistical data was obtained yearly by the National Drug Law enforcement agency (NDLEA), Kano. From the Table 1, the x-variable represent the year of the operation while the y-variable represent the rate of drug abuse among the youth in the city. For the data fitting, only the data from 2009 to 2016 is been considered. The data for the year 2017 is reserved for the error analysis.

Table 1. Rate of Drug Abuse in Kano City for the Year 2009 to 2017 in Percentage

Number of Data (x)	Years	Rate of Drug Abuse (y)%
1	2009	0.78
2	2010	1.35
3	2011	1.59
4	2012	1.88
5	2013	1.95
6	2014	2.46
7	2015	2.26
8	2016	1.81
9	2017	1.83

Let the number of data x_j be the number of years and the value y_j be the rate of drug abuse in percentages. Then, the data from 2009 to 2016 are utilized to formulate the nonlinear quadric model for the least square method and the corresponding test function of unconstrained optimization problem. From the above problem, observation reveals that the data x_j and the value of y_j have parabolic relations with the regression function defined by (26) and the regression parameters u_0, u_1 and u_2.

$$\min_{x \in R^2} \sum_{j=1}^{n} E_j^2 = \sum_{j=1}^{n}\left((u_0 + u_1 x + u_2 x^2) - y_j\right)^2 \quad (27)$$

Similar transformation of the above least squares problem using the data from Table 1 for nonlinear quadratic unconstrained minimization model is

$$f(u_0, u_1, u_2) = (8u_0 + 36u_1 + 204u_2 - 14.08)^2 \qquad (28)$$

Equation (28) is similar to equation (27). Therefore, expanding (28) we have

$$f(u_0, u_1, u_2) = 64u_0^2 + 1296u_1^2 + 41616u_2^2$$
$$+ 576u_0 u_1 + 3264u_0 u_2 + 14688u_1 u_2 - 225.28u_0$$
$$- 1013.76u_1 - 5744.64u_2$$
$$+ 198.2464 \qquad (29)$$

However, the data for 2017 is excluded from the unconstrained optimization function so that it could be used to compute the relative errors of the predicted data. Therefore, the proposed spectral PRP and WYL CG methods are applied to solve the test function using exact line search technique. Table 2 and Table 3 shows the test results for the spectral PRP, spectral HS, spectral WYL and MSCG methods for some selected initial point.

Table 2. Numerical Results for SPRP, SWYL, MSCG and SHS Methods based on CPU Time.

Initial value	CPU Time			
	SPRP	SWYL	MSCG	SHS
(-5,-5,-5)	41.3119	49.5704	14.6685	0.00063
(-1,0,-1)	41.3443	44.2581	4.19763	0
(11,11,11)	97.317	103.905	5.58880	0
(-2,-2,-2)	41.3556	50.5668	4.55623	0

Table 3. Numerical Results for SPRP, SWYL, MSCG and SHS Methods based on Number of Iterations.

Initial value	Number of Iteration			
	SPRP	SWYL	MSCG	SHS
(-5,-5,-5)	10000	10000	2	0
(-1,0,-1)	10000	1000	3	NaN
(11,11,11)	1000	1000	2	NaN
(-2,-2,-2)	1000	1000	2	NaN

To avoid computing the values of u_0, u_1, u_2 using matrix inverse, we employ the Spectral PRP, Spectral WYL, SHS and MSCG using four initial points as presented in the Table 2 and Table 3. The iteration is terminated if the number of iterations exceed 10000 or if the method fails to solve a test problem and denoted the point of failure as 'NaN'. The approximation functions of the spectral CG methods is given in Table 4.

Table 4. Approximation Functions for Different Initial Point

Initial values	Methods	Approximate Function
	SPRP	$y = 0.5243x^2 + 31.9303x - 5$
(-5, -5, -5)	SWYL	$y = 0.5243x^2 + 31.9303x - 5$
	MSCG	NaN
	SHS	NaN
	SPRP	$y = 0.2142975x^2 + 6.6407718x - 1$
(-1, 0,-1)	SWYL	$y = 0.2142975x^2 + 6.6407718x - 1$
	MSCG	NaN
	SHS	NaN
	SPRP	$y = -0.7754x^2 - 69.2073x + 11$
(11, 11,11)	SWYL	$y = -0.7754x^2 - 69.2073x + 11$
	MSCG	NaN
	SHS	NaN
	SPRP	$y = 0.27574716x^2 + 12.96824x - 2$
(-2, -2,-2)	SWYL	$y = 0.27574716x^2 + 12.96824x - 2$
	MSCG	NaN
	SHS	NaN

4.1. Trend line method

The rate of drug abuse in Kano city, Nigeria is estimated using the least square method and the proposed spectral CG methods. The tread line is plotted based on the original data from Table 1 using Microsoft Excel software. The equation for the trend line is in the form of nonlinear quadratic equation. Based on the actual data, the index of drug abuse denoted by y is represented in the y-axis. The x-axis represent the year and denoted by x.
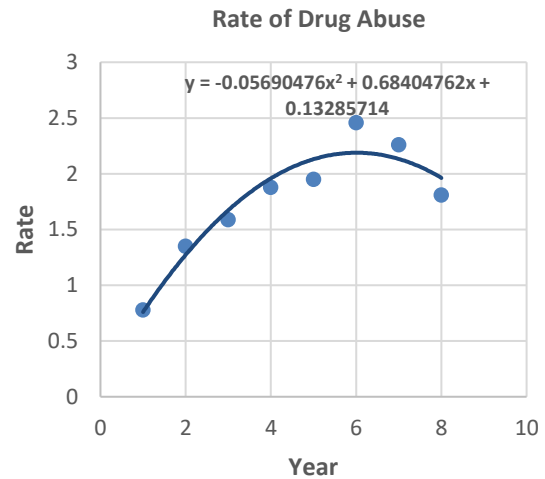

Figure 1. Nonlinear Quadratic Trend Line for Rate of Drug Abuse in Kano City

The functions of trend line and least square methods are compared with approximation functions obtained from the Spectral CG methods presented in Table 4.

5. Numerical result

Algorithm 1.1 have been tested on some benchmark problems and its performance are compared with RSPRP method [10], Wei-Yao-Liu (WYL) method [23], and Polak-Ribierre-Polyak (PRP) method [24] respectively. The comparisons are based on CPU time and number of iterations. The stopping criteria used is $\|g_k\| < \varepsilon$ where $\varepsilon = 10^{-6}$ as suggested by Hillstrom [21].

The set of standard test functions are considered from [1] and utilised with four different initial values. The codes are written on *MatlabR2015 subroutine* programming and run on an Intel® Core™ *i*5-3317U (1.7GHz with 4 GB (RAM)).

Table 5 and 6 presents the list of standard test problems with dimensions and initial points used to test the efficiency of the proposed spectral CG methods. The numerical performance of the proposed algorithms is presented in Figures 1.2 - 1.5 based on a number of iterations and CPU time. The maximum value of the percentage of probability $P_s(t)$ and the solver that reached the solution point foremost are regarded as the best performing CG methods for unconstrained optimization problems [25, 27].

Table 5. Standard Test Problems functions for Figure 2 and Figure 3

Functions	Dimensions	Initial Points
Trecanni	2	(3,3), (7,7), (11,11), (15,15)
Zettl	2	(10,10), (25,25), (100,100), (-100,-100)
Leon	2	(4,4), (-4,-4), (10,10), (-10,-10)
Quartic	4	(-3,-3), (5,-5), (15,15), (-20,-20)
Wood	4	(3,3), (-3,-3),(14,14),(-14,-14)
Hager	4	(2, 2), (10,10), (-10,-10),(15,15)
Fletcher	100	(13,13), (25,25),(40,40),(49,49)
Raydan	100	(2,2), (6,6), (8,8), (10,10)
Gen. Quartic	1000,10000, 50000,100000	(3,3), (5,5), (15,15), (-20,-20)
Freud. & Roth	4,10,100,500, 1000,10000, 50000,100000	(2,2), (5,5), (7,7), (-21,-21)
White and Holst	10,100,1000	(4,4), (-4,-4), (9,9), (-9,-9)
Shallow	100,1000, 10000	(100,100), (200,200), (300,300), (400,400)
Rosenbrock	2,4,10,100,1000, 10000,50000, 100000	(13,13), (25,25), (40,40), (49,49)

Table 6. Standard Test Problems functions for Figure 4 and Figure 5

| Functions	Dimensions	Initial Points
Trecanni	2	(5,5), (8,8), (-11,-11), (-15,-15)
Leon	2	(4,4), (-4,-4), (6,6), (-10,-10)
Extended Penalty	2,4,10,50	(2,2), (-2,-2), (5,5), (-5,-5)
Power	2,4,50,100	(5,5), (-5,-5), (100,100),(-100,-100)
Quadratic QF1	10,100,1000, 10000	(5,5), (-5,-5), (100,100),(-100,-100)
Ext. Quadratic Penalty QP1	10,100	(5,5), (-5,-5), (8,8), (-8,-8)
Ext. Quadratic Penalty QP2	10,100	(2,2), (6,6), (8,8), (10,10)
Himmelblau	10000	(2,2), (-2,-2), (25,25), (-25,-25)
Freud. & Roth	2,4,10,100,1000, 10000	(7,7), (11,11), (13,13), (25,25)
White and Holst	2,4,10,100,1000, 10000	(2,2), (5,5), (9,9), (-9,-9)
Shallow	2,4,10,100,1000, 10000	(100,100), (200,200), (400,400), (500,500)
Rosenbrock	2,4,10,100,1000, 10000	(5,5), (13,13), (20,20), (40,40)
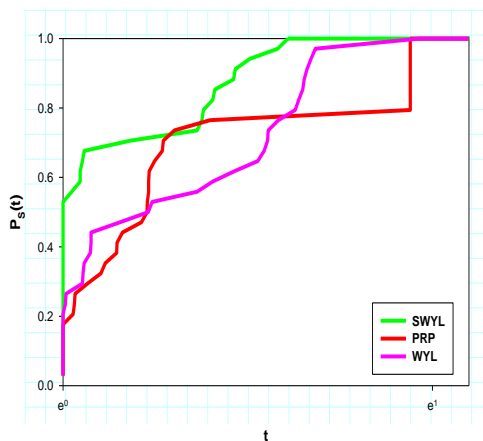
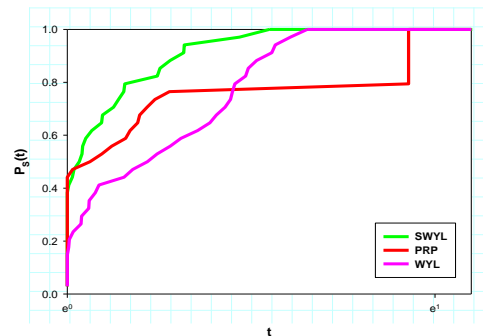**Figure 2.** Performance outline based on the number of iterations

Figure 3. Performance outline based on CPU time

Figure 4. Performance outline based on the number of iterations

From the results obtained, the SPRP and SWYL CG methods are able to solve the standard benchmark problems as compared to the existing methods used in the analysis. Similarly, the data for 2017 are estimated using the nonlinear unconstrained optimization model in Table 4. and the relative error for each model using equation (10) is presented in Table 7.
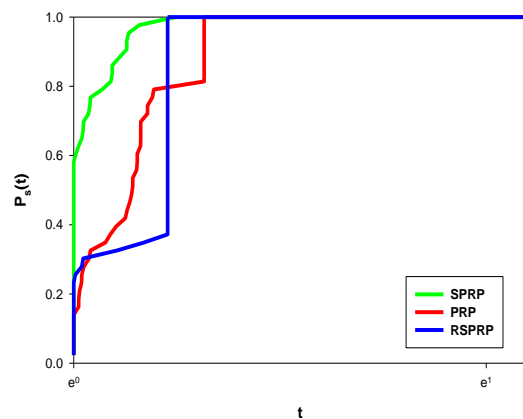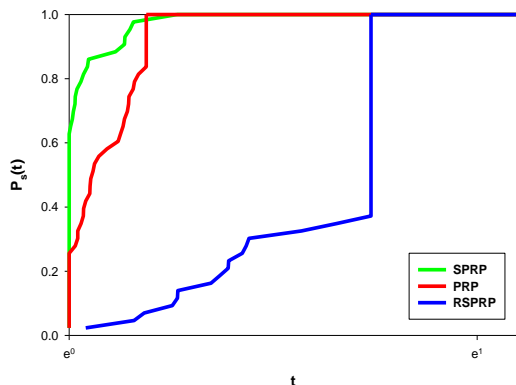
Figure 5. Performance outline based on CPU time

Table 7. Estimation Point and Relative Errors for 2017 Data

Models	Estimation Point	Relative Error
SPRP	1.130602014195	0.3821846916967
SWYL	1.130602014195	0.3821846916967
MSCG	NaN	NaN
SHS	NaN	NaN
Least Square	0.1686095216	0.907863649398907
Trend line	0.1686095216	0.907863649398907

The efficiency of each method is measure by equation (9). All the computations are carried out using Microsoft Excel 2016 and MATLAB 2015a *subroutine* programme. The model with the smallest relative error is considered the best model that estimate the rate of drug abuse in Kano city for the year 2017.

6. Conclusion

This paper focuses on the application of the spectral CG methods for unconstrained optimization. The proposed methods are compared with the classical WYL, PRP, least square and Trend line methods. The sum of relative error for the proposed spectral CG methods are computed based on four categories of initial values and three set of real numbers for nonlinear quadratic model. From the Table 7, the average relative error for the predicted data against the actual data 1.83 are calculated. The relative error for the data generated from nonlinear quadratic models of spectral PRP and spectral WYL methods are smaller compared to the least square and trend line models, which is around 0.3821846916967. The smallest relative error signifies the success of the spectral CG methods.

References

[1] Andrei, N. (2008). An unconstrained optimization test functions collection, *Advanced Modeling and Optimization,* 10, 147-161.

[2] Barzilai, J. & Borwein, J.M. (1988). Two-point step size gradient methods, *IMA J Numer Anal.* 8, 141-148.

[3] Birgin, E.G. & Martinez, J. M. (2011). A spectral conjugate gradient method for unconstrained optimization, *Applied Mathematics and Optimization,* 43 (2), 117-128.

[4] Yakubu, U.A. Mamat, M. Mohamad, A.M. Sukono, A.M. & Rivaie, M. (2018a). Secant free condition of a spectral PRP conjugate gradient method. *International Journal of Engineering & Technology,* 7 (3.28), 325 – 328.

[5] Yakubu, U.A. Mamat, M. Mohamad, A.M. Sukono, A.M. & Rivaie, M. (2018b). Modification on spectral conjugate gradient method for unconstrained optimization. *International Journal of Engineering & Technology*, 7 (3.28), 307 – 311.

[6] Yakubu, U.A. Mamat, M. Mohamad, A.M. Rivaie, M. & B.Y. Rabi'u. (2018d). Secant free condition of a spectral WYL and its global convergence properties. *Far East Journal of Mathematical science*, 12, 1889 – 1902.

[7] Yakubu, U.A. Mamat, M. Mohamad, A.M. Rivaie, M. & J. Sabi'u. (2018e). A recent modification on Dai-Liao conjugate gradient method for solving symmetric nonlinear equations. *Far East Journal of Mathematical science*, 12, 1961 – 1974.

[8] Zull, N. Rivaie, M. Mamat, M. Salleh, Z. & Amani, Z. (2015). Global convergence of a Spectral conjugate gradient by using strong Wolfe line search, *Applied Mathematical Sciences,* 9(63), 3105-3117.

[9] Hu, C. & Wan, Z. (2013). An Extended Spectral Conjugate Gradient Method for unconstrained optimization problems, *British Journal of Mathematics & Computer Science*, 3, 86-98.

[10] X. Wu. (2015). A new spectral Polak- Ribière -Polak conjugate gradient method, *ScienceAsia*. 41, 345-349.

[11] Sulaiman, I. M., Sukono, Sudradjat, S., and Mamat, M. (2019). New class of hybrid conjugate gradient coefficients with guaranteed descent and efficient line search. *IOP Conference Series: Materials Science and Engineering*, 621(012021), 1-7.

[12] *Mathematical Sciences* Issue 65-68, 3307-3319.

[13] W. W. Hager & H. Zhang. (2006). A survey of nonlinear conjugate gradient methods, Pacific Journal of Optimization, 2 (1), 35-58.

[14] Du, X. & Liu, J. (2011). Global convergence of a spectral HS conjugate gradient method, *Procedia Engineering*. 15, 1487 – 1492.

[15] Raydan, M. (1997). The Barzilai and J.M. Borwein gradient methods for the large scale unconstrained minimization in extreme problems, *SIAM Journal on Optimization,* 7 (1), 26-33.

[16] Batu, T., Dasgupta, S., Kumar, R., & Rubinfeld, R.

(2005). The complexity of approximating the entropy. *SIAM Journal on Computing*, 35(1): 132–150.

[17] Motulsky, H., & Christopoulos, A. (2004). *Fitting models to biological data using linear and nonlinear regression.* Oxford University Press, New York.

[18] Shirin, S., Mahmudul. H., & Laek, S.A. (2015). Age-Structured Population Projection of Bangladesh by Using a Partial Differential Model with Quadratic Polynomial Curve Fitting. *Journal of Applied Sciences,* 5: 542-551.

[19] Zoutendijk, G. (1970). Nonlinear programming, computational methods, in *J Abadie (ED), Integer and Nonlinear Programming*, North-Holland, Amsterdam, 37-86.

[20] Yakubu, U.A. (2019). *Enhancing spectral conjugate gradient method for solving unconstrained optimization problems*. PhD Thesis. University Sultan Zainal Abidin Kuala Terengganu, Malaysia.

[21] Yakubu, U.A. Mamat, M. Mohamad, A.M. Puspa, L.G. & Rivaie, M. (2018c). Secant free condition of a spectral Hestenes-Stiefel conjugate gradient method and its sufficient descent properties. *International Journal of Engineering & Technology*, 7 (3.28), 312 – 315.

[22] K.E. Hillstrom. (1977). A simulation test approach to the evaluation of the nonlinear optimization algorithm. *Journal ACM Trans.* Mathematics Software. 3 (4), 305-315.

[23] Dolan, E. & More, J.J. (2002). Benchmarking optimization software with performance profile, *Math. Prog*. Vol. 91, 201-213.

[24] Z. Wei, S. Yao, and L. Liu. (2006). The convergence properties of some new conjugate gradient methods, *Applied Mathematics and Computation*, Vol. 183(2), pp. 1341–1350.

[25] E. Polak & G. Ribiere. (1969). Note sur la convergence de directions conjug´ees, *Rev. Francaise Informat Recherche Opertionelle, 3e ann´ee*, Vol 16, pp. 35–43.

[26] Sulaiman, I. M. Mamat, M. Abashar, A. Rivaie M. (2015). The global convergence properties of an improved conjugate gradient method *Applied Mathematical Science*, 9(38), pp. 1857-1868.

[27] Powell, M.J.D. (1977). Restart procedures for the conjugate gradient method, Math. Program. 12, 241-254.

[28] Sulaiman, I. M., Mamat, M., Abashar, A., Zabidin, S. (2015): A Modified Nonlinear Conjugate Gradient Method for Unconstrained Optimization, Applied Mathematical Sciences 9(54), pp. 2671-2682.

[29] Aini, N. Rivaie, M. Mamat, M. and Sulaiman, I. M. (2019). A Hybrid of Quasi-Newton Method with CG Method for Unconstrained Optimization. J. Phys.: Conf. Ser. 1366(012079), 1-10.

Ibrahim Sulaiman Mohammed is currently a post-*doctoral researcher at Faculty of informatics and computing, Universiti Sultan Zainal Abidin (UniSZA), Malaysia from 2019 till date. He obtained his PhD from UniSZA in 2018 specializing in the field of fuzzy systems. He has published research papers in various international journals and attended international conferences. His research interest includes Numerical research, Fuzzy nonlinear systems, unconstrained optimization.*
 https://orcid.org/0000-0001-5246-6636

Usman Abbas Yakubu is a lecturer at Yusuf Maitama Sule University Kano, Nigeria. He obtained his PhD from Universiti Sultan Zainal Abidin (UniSZA), in 2019 specializing in the field of Computational Mathematics/ Unconstrained optimization. He has published research papers in various international journals and attended international conferences.
 https://orcid.org/0000-0002-6718-0523

Mustafa Mamat is currently a Professor of Computational and Applied Mathematics at Universiti Sultan Zainal Abidin, Malaysia since 2013. He obtained his PhD from UMT in 2007 specialization in optimization field. To date, he has successfully supervised more than 70 postgraduate students and published more than 260 research papers in various international journals. His research interest includes unconstrained optimization. Currently, he is the Editor in Chief for Malaysian Journal of Computing and Applied Mathematics and an editor for Indonesian Journal of Science and Technology.
 https://orcid.org/0000-0001-5358-3797

RESEARCH ARTICLE

A misalignment-adaptive wireless power transfer system using PSO-based frequency tracking

Fuat Kılıç [a] [*], Serkan Sezen [b], Seyit Ahmet Sis [c]

[a] Department of Mechatronics Engineering, Faculty of Engineering, Balıkesir University, Balıkesir, Turkey
[b] Department of Electrical & Energy, Uzunçiftlik Nuh Çimento Vocational School, Kocaeli University, Kocaeli, Turkey
[c] Department of Electrical & Electronics Engineering, Faculty of Engineering, Balıkesir University, Balıkesir, Turkey
fuatkilic@balikesir.edu.tr, serkan.sezen@kocaeli.edu.tr, seyit.sis@balikesir.edu.tr

ARTICLE INFO	ABSTRACT
	One of the major challenges in inductive wireless power transfer (WPT) systems is that the optimal frequency of operation may shift predominantly due to coupling variation as a result of so-called frequency splitting phenomenon. When frequency splitting occurs, two additional resonance frequencies split from the coupler's resonance frequency. Maximum power levels are observed at these split resonance frequencies; however, these frequencies are strongly-dependent on the coupling coefficient, hence the distance and alignment between the couplers. In addition to that, peak power values at these frequencies can be different from each other due to small impedance differences between the primary and secondary side resonant couplers, forming a local and a global maximum. Therefore, the WPT system should adaptively operate at the correct frequency for achieving maximum power transfer. In this paper, a metaheuristic Particle Swarm Optimization (PSO) based frequency tracking algorithm is proposed for use in WPT systems. The WPT system employs multi sub-coil flux pipe couplers, a full-bridge inverter which is driven by TMS320F28069 controller card and is suitable for high power charging applications. The control algorithm can accurately find the global maximum power point in case of frequency splitting with asymmetric peaks. The proposed frequency tracking algorithm operates only at the primary side based on measurement of the input power level. Therefore, no additional communication link is needed between the primary and the secondary side. Effectiveness of the proposed control method is validated by performing experiments under three different misalignment scenarios and compared to the traditional Perturb and Observe algorithm.

1. Introduction

Magnetic coupling based wireless power transfer (WPT) systems have been comprehensively investigated in recent years. The WPT finds its use in various applications such as mobile electronic devices [1], electric vehicles (EVs) [2, 3], robots [4, 5] and medical devices [6, 7]. Magnetically coupled coils, or so called couplers, are the major components in these systems determining the efficiency and power level delivered to the load. The WPT systems need to operate at one of the system's resonance frequencies for transferring the power in an efficient manner. However, temperature dependent variations in component values and load variations shift the resonance frequencies of the system. In this case, for guaranteeing maximum power delivery or maximum efficiency, a frequency tracking mechanism should be incorporated into the system.

Another important issue in WPT systems is so called frequency splitting phenomenon. Frequency splitting occurs when system operates at strongly coupled regime. In this regime, two more resonance frequencies emerge at lower and upper side of the isolated couplers' resonance frequency, making total of three resonance frequencies for the coupled system. The power values are maximum, same and independent of the coupling coefficient at these emerging split resonance frequencies; however, these frequencies are strongly-

---

[*]Corresponding author

dependent on the coupling variations. Furthermore, any small difference between the isolated resonance frequencies of the primary and secondary coils results in different peak power and efficiency values at these frequencies. Hence, a local and a global maximum for the delivered power levels are observed. Operating the system at a global maximum is important for reducing charging time, utilizing electrical power efficiently, reducing the losses in power electronic components and reactive power. Therefore, the WPT system should adopt itself to achieve maximum power delivery when resonance frequencies shift due to coupling coefficient variations.

Numerous works have been reported on realizing adaptive WPT systems. In [8], an impedance matching network is utilized to maximize power transfer by compensating the efficiency reduction due to coupling variations. This method necessitates changing the position of coils, making the system less practical for the implementation. In [9,10], authors again utilize matching circuits at both primary and secondary side; however, large number of passive elements increases the loss and the complexity of the system. In another work, zero crossing detector based phase angle is obtained by reading the voltage and current at the primary side to maximize the power transfer [11]. However, this method may become unstable if there is no resonance in the system. In another work [12], which is published by the authors of this manuscript, a flux-pipe coupler structure with three movable sub-coils is exploited for realizing an adaptive WPT system. The inductance value of the coupler is tuned by moving the position of the sub-coils to get back the system's resonance frequency shifted by the coupling variations. This solution, however, requires a complex mechanical mover and a dual side control [12].

In [13], authors propose a frequency tracking method based on simulated annealing algorithm for achieving maximum power transfer, but this algorithm is time inefficient and computationally dense [14]. Impedance matching and Perturb and Observe (PO) algorithm are implemented together in [15] for maximum power delivery to the load. In [16], power reduction due to resonance frequency shift caused by misalignment between primary and secondary coils is compensated by tracking the system's resonance frequency using again a PO algorithm. A drawback in PO algorithm, however, is that the algorithm may stuck at a local maximum rather than converging to the global maximum point. Ant Colony algorithm is also utilized for achieving maximum power transfer in [17]. Low converging speed and possibility of convergence to local maximum in large searching space are the main disadvantages in this algorithm [18]. In [19], derivation of power response is calculated and then the direction of frequency search is determined based on the sign of the derivation. As in PO algorithm, derivation method based algorithm may also stick to a local maximum rather than converging to the global maximum power point.

Particle Swarm Optimization (PSO) algorithm is another technique used in several adaptive WPT systems [20,21]. In [20], a software-defined, near-field WPT system is proposed where a particle swarm optimizer (PSO) is used to optimize the power transfer efficiency of the system. Matching network of the transmit and receive chain is controlled through the PSO algorithm to compensate for the efficiency reductions due to coupling variations [20]. However, the tuning range of the tunable components in matching circuits is limited and these components increase loss and complexity of the system. In [21], PSO algorithm is utilized in a frequency tracking controller to improve the power transfer efficiency of the WPT system. PSO algorithm's iterations are seems to be offline and does not consider the effect of dynamic variations on the system. In both [20] and [21], WPT systems operate in MHz range with a sinusoidal RF signal source and a power amplifier. MHz range WPT systems are not suitable for high power applications such as electric vehicle (EV) chargers.

In this paper, the Particle Swarm Optimization algorithm is implemented in a frequency tracking controller for use in misalignment adaptive WPT systems suitable for high power applications. The implemented frequency tracking system accurately finds the global maximum point without sticking to a local maximum under varying conditions. Therefore, the WPT system becomes insensitive to frequency splitting phenomenon caused by coupling variations. The algorithm needs only voltage and current measurement data at the resonant primary side coupler, making the proposed tracking system a simple primary side controller. The algorithm iteratively changes the switching frequency of the inverter. At each iteration, the controller calculates the power level at the input of the primary side resonant coupler. Iterations are online so that the algorithm does not stop and track the right frequency as long as the system is powered.

The paper is organized as follows: section 2 presents the frequency splitting phenomenon by analyzing a circuit model for a series-series (SS) compensated WPT system. Subsequently, PSO based frequency tracking algorithm is described in section 3. Finally, experimental setup and measurement results are presented in detail in section 4. Measurements are performed under three different scenarios with different misalignments and resonance conditions. For each scenario, a power vs frequency graph as an oscilloscope screenshot is obtained experimentally to show the frequency splitting phenomenon. Finally, accuracy of the PSO algorithm is proven by comparing the tracked frequency with the maximum power points shown in these graphs.

2. WPT system and mathematical model for maximum power delivery

In quite a few modern WPT applications (e.g electric vehicle chargers), separation between these primary

and secondary side couplers needs to be large enough (loosely coupled) and the system should be suitable for lateral and vertical misalignments between the couplers to some extent. One needs to compensate for this loose coupling by connecting compensation capacitors to both primary and secondary side couplers. Except recently introduced hybrid compensation schemes, there are four basic compensation topologies: series-series (SS), series-parallel (SP), parallel-series (PS) and parallel-parallel (PP). In this work, voltage-source inverter is utilized as a high power source hence series compensation is chosen for the primary side. Parallel compensation at the secondary side results in a k-dependent compensation capacitor at the primary side [24]. Therefore, series compensation scheme is chosen at the secondary side as well. Figure 1 shows a circuit model for a WPT system with an SS compensation topology. The components, $L_{1,2}$ and $R_{1,2}$ represent the self-inductances and loss resistances of the primary and secondary side couplers, respectively. C_1 and C_2 are the series connected compensation capacitors at primary and secondary sides, respectively. V_s and M are the RMS voltage level of the inverter and the mutual inductance between the couplers, respectively.
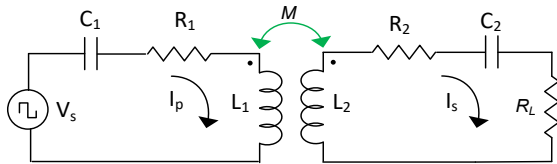

Figure 1. Circuit model for a WPT system with an SS compensation topology.

Analyzing the model in Figure 1 yields the following Eq. (1) for the power delivered to the load resistance, R_L, as function of source voltage (V_s) and lumped components as follows [25]:

$$P_L = \frac{(V_s \omega M)^2 R_L}{a^2 + b^2} \tag{1}$$

where

$$a = \begin{bmatrix} R_1(\omega L_2 - \frac{1}{\omega C_2}) \\ + (R_2 + R_L)(\omega L_1 - \frac{1}{\omega C_1}) \end{bmatrix} \tag{1.1}$$

and

$$b = \begin{bmatrix} R_1(R_2 + R_L) - (\omega L_1 - \frac{1}{\omega C_1}) \\ .(\omega L_1 - \frac{1}{\omega C_1}) + (\omega M)^2 \end{bmatrix} \tag{1.2}$$

The input impedance of the coupled system seen towards the resonant primary coupler (Figure 1) is as follows:

$$Z_{in} = (R_1 + j(\omega L_1 - \frac{1}{\omega C_1}) \\ + \frac{(\omega M)^2}{(R_2 + R_L + j(\omega L_2 - \frac{1}{\omega C_2}))} \tag{2}$$

Usually, WPT systems are realized with identical primary and secondary side couplers. In this case, one can simplify the model by assuming as $L_1 = L_2 = L$, $C_1 = C_2 = C$ and $R_1 = R_2 = R$. The resonance in a coupled system occurs at frequencies where imaginary part of Z_{in} becomes zero as given Eq. (3).

$$imag(Z_{in}) = (\omega L - \frac{1}{\omega C}) \\ . \left[1 - \frac{(\omega M)^2}{(R + R_L)^2 + (\omega L - \frac{1}{\omega C})^2} \right] = 0 \tag{3}$$

Solving Eq. (3) results in only one or three roots for ω for given conditions as shown in (4). As seen in (4), when the first condition (ωM ≤ R + RL) is satisfied, then the coupled system only exhibits a single resonance frequency of ω0, which is equal to the isolated resonance frequency of the couplers, and the system is said to be operating at the weakly-coupled regime. When the second condition (ωM > R + R_L) is satisfied, then two more resonance frequencies ω1, ω2 emerge along with the ω0. This phenomenon is called as frequency splitting, and the system is said to be operating at strongly-coupled regime. Maximum power to the load is delivered at system's resonance frequencies.

$$\omega = \begin{cases} \omega_0 = \frac{1}{\sqrt{LC}}, & \text{if } \omega M \leq R + R_L \\ \omega_0 = \frac{1}{\sqrt{LC}} \text{ and } \omega_1 = \omega_2 = \sqrt{\frac{C(R+R_L)^2 - 2L \mp \sqrt{C(R+R_L)^2 \left[C(R+R_L)^2 - 4L \right] + 4M^2}}{2C(M^2 - L^2)}}, & \text{if } \omega M > R + R_L \end{cases} \tag{4}$$

By plugging Eq. (4) into Eq. (1), the output power (P_L) at ω_0, ω_1 and ω_2 is simplified as follows:

$$P_L(\omega_0) = \frac{(V_s \omega M)^2 R_L}{(R(R + R_L) + (\omega M)^2)^2} \quad (5)$$

$$P_L(\omega_{1,2}) = \frac{V_s^2 R_L}{(2R + R_L)^2} \quad (6)$$

As seen in Eq. (5), the output power at ω_0 is quite dependent on the mutual inductance (M) between the couplers. That is, when a misalignment occurs between the primary and secondary side couplers, or the distance between them changes, P_L also changes. One needs to vary the inverter's voltage level to stabilize output power against varying coupling level. However, if system operates at the other resonance frequencies, ω_1 or ω_2, the output power is independent of M (as given in Eq. (6)), making the system insensitive to the coupling variations.
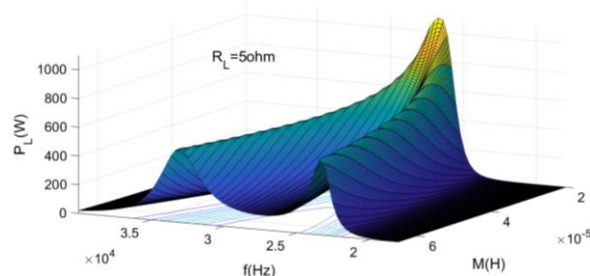
a) Sub-figure 1.
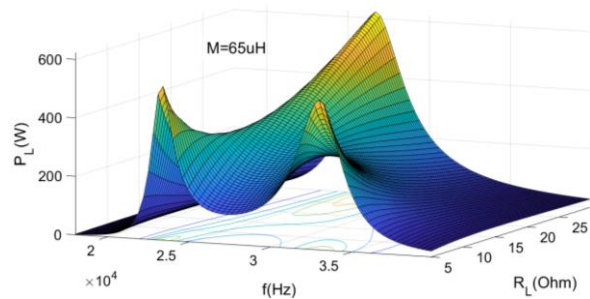
b) Sub-figure 2.

Figure 2. Output power's (PL's) variation as a function of f –M (a) , and f –RL (b)

It should be remembered that the ω_1 or ω_2 exist only at the strongly coupled regime and their values are dependent on M when the second condition in Eq. (4) is satisfied. Figure 2 shows simulated output power (P_L) using Eq. (1) as a function of f and M. Frequency splitting phenomenon is clearly observed in Figure 2. As seen in these graphs, any variation of M and R_L significantly changes the output power transferred to the load. Therefore, for a large power delivery to the load, system's frequency should be tuned to either ω_1 or ω_2 by applying a frequency tracking algorithm.

3. PSO based frequency tracking algorithm

3.1. Basics of PSO Algorithm

Particle Swarm Optimization (PSO) algorithm is inspired from the behaviors of swarm animals such as birds and fishes. Each individual animal in the swarm is called as particle and have the potential of exhibiting a solution to the problem to be solved. The particle looks for the best location in a three dimensional (3D) space [26]. A major advantage of PSO is its easier applicability to various different applications such as power systems, thermodynamics, image processing, proportional–integral–derivative (PID) control and machine learning as compared to other algorithms [27, 28]. PSO algorithm has several topologies and one of the most utilized topologies is a so called Von Neumann topology. In this topology, the particles are connected to one another in such a way that they communicate with each other from one point to the opposite point in a square pattern [29]. As in other topologies, Von Neumann topology based PSO algorithm is established on two principles; learning the previous knowledge and providing communication between the particles in the swarm. The Von Neumann topology consists of N element particles in a D dimensional space [30]. Each particle should achieve the best performance and all the particles should move towards the particle with the best performance [31]. Each particle has its own speed, and this speed is updated based on previous performance of the particle and the swarm. The algorithm initially produces random solutions and recursively update the locations of particles and search for the global maximum within the search space. By evaluating each individual particle, the best performance (P_{best}) and the particle associated with the best performance are stored in the memory. The inputs of the algorithm are varied until some of the goals are satisfied.

3.2. The application of PSO algorithm to frequency tracking in a WPT System

Figure 3 shows the vectorial movement of frequency-based particles in the PSO algorithm. The direction of particles depends on the best frequency per particle, the frequency at which maximum power is achieved in the whole swarm, previous frequency, current frequency and up-to-date frequency. Figure 4 shows algorithm's flow chart for frequency tracking to maximum power. This flow chart is elaborated under four main steps as follows:

Step I (Start): In this first step, optimization is launched by establishing an initial population. A frequency solution vector with Np elements is setup as given in Eq. (7). The initial vector is built on randomly chosen frequencies. The constants, $\gamma1$ and $\gamma2$, given in Eq. (8) and (9) are then determined based on c_1 and c_2 which satisfy the conditions given in Eq. (10) and (11).

$$f_r = [f_{r1}, f_{r2}, f_{r3}, ..., f_{rn}], \; n = 1, 2, 3, ..., N_p \quad (7)$$

$$\gamma_1 = r_1 c_1 \quad (8)$$

$$\gamma_2 = r_2 c_2 \quad (9)$$

$$c_1 + c_2 < 4 \quad (10)$$

$$\phi > 0.5(c_1 + c_2) - 1 \quad (11)$$

$\varnothing$ is a random variable of which values is limited to the 0-0.5 range. Similarly, r_1 and r_2 are also random variables limited to 0-1 range. The c_1 and c_2 are cognitive and social coefficients ranging between 0 and 2. The values of the aforementioned constants are utilized to update the frequency and power values in the next step.
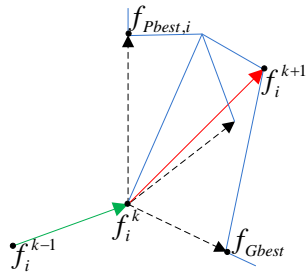

Figure 3. The vectorial movement of frequency-based particles in the PSO algorithm

The best individual particle frequency ($f_{pbest,r}$) and the best global frequency (f_{Gbest}) value within the whole swarm are randomly chosen as follows:

$$f_{Pbest,r} = [f_{Pbest1}, f_{Pbest2}, f_{Pbest3} \cdots f_{PbestN}],$$
$$n = 1, 2, 3, ..., N_p \quad (12)$$

$$f_{Gbest} = [0 - 1] \quad (13)$$

The f_{wpt}, f_{act}, P_{wpt}, and P_{act} variables shown in the flow chart are the stored frequency, up-to-date frequency, calculated power and up-to-date power, respectively.

Step II (Acquiring Measurement Data): Current and voltage values at the input of the WPT system are measured using hall effect based sensors as will be discussed in the next section. These measured data are acquired into the microcontroller and utilized as an input to the microcontroller. Subsequently, the power is calculated using measured voltage and current data. Once the condition in Eq. (14) is satisfied, the algorithm utilizes the best individual particle location to update the frequency as given in Eq. (15).

$$f_{i,j} > f_{Pbest\_i} \quad (14)$$

$$f_{Pbest\_i} = f_{i,j} \quad (15)$$

From the start of the algorithm, the best frequency (f_{Pbest}) for j_{th} iteration and i_{th} particle is stored in the memory. The best global frequency is also stored in the memory as f_{Gbest}.
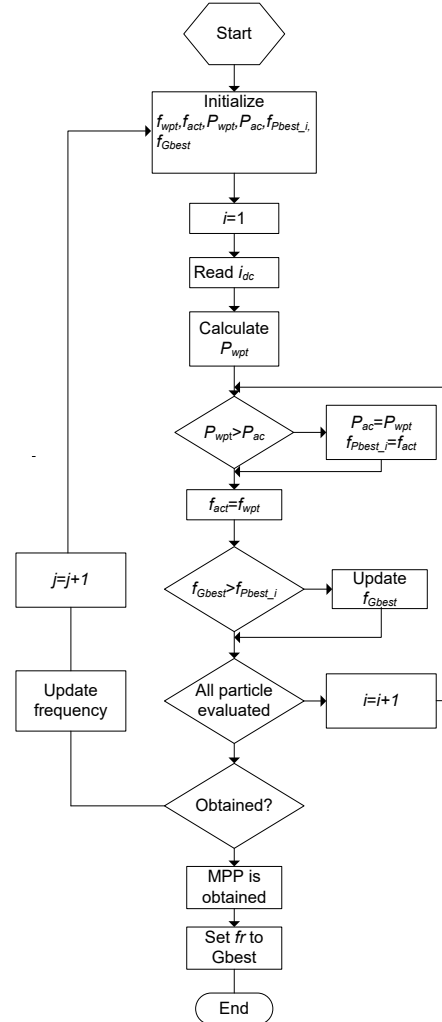

Figure 4. The flow chart for PSO based frequency tracking algorithm

Step III (Updating the Frequency Values): The stored f_{Pbest} and f_{Gbest} are plugged in to updated frequency expression as follows:

$$f_{i,j}(t+1) = f_{i,j}(t) + \delta_{i,j}(t+1) \quad (16)$$

$$\delta_{i,j}(t+1) = \phi\delta_{i,j}(t) + \gamma_1(f_{Pbest_i} - f_{i,j}(t))$$
$$+ \gamma_2(f_{Gbest} - f_{i,j}(t)) \quad (17)$$

The i, t, $f_{i,j}$, $f_{i,j}(t+1)$ and $\delta_{i,j}(t+1)$ are particle number, iteration number, current particle frequency, updated particle frequency and updated correction term.

Step IV (Checking the Maximum and Minimum Boundary Values): The maximum and minimum boundary values of updated frequencies are checked. If the boundary values are exceeded, higher and lower values, respectively, are taken into the program. According to flow chart, once initial values are

assigned, initial frequency value is sent to pulse width modulation (PWM) unit and then time based period is formed. The full-bridge inverter is driven by 50 % duty cycled PWM signal at a given frequency. The algorithm is run real-time and the frequency is recursively updated until it converges to the frequency at which power is maximized. The frequency range over which the algorithm make searching is from 10 kHz to 40 kHz.

4. Experimental setup and measurement results

An experimental WPT system is setup using a DC to AC high frequency inverter, flux-pipe couplers, series-connected capacitors and a heater load resistance (R_L). Figure 5 (a) and (b) show the block diagram and photo of experimental setup of the implemented WPT system, respectively. The experimental setup employs a microcontroller, gate-drive circuit, protection circuit and IGBT switches. The microcontroller is Texas Instruments' TMS320F28069 card and can be programmed via Matlab/Simulink. HCPL-3120 opto-coupler is utilized for driving the IGBTs with signals from microcontroller. Isolation between power and driver circuit is ensured by MURATA's MGJ2 series DC/DC converter. The dead time between the two switching signals of IGBTs on the same branch is set as 2 μs in the program. Currents are measured through hall-effect based LEM LA25-P and LEM LV25-P current and voltage sensors. The four IGBTs, in the inverter stage, are IXYS's hyper fast IXGH40N60B2D1 transistors.
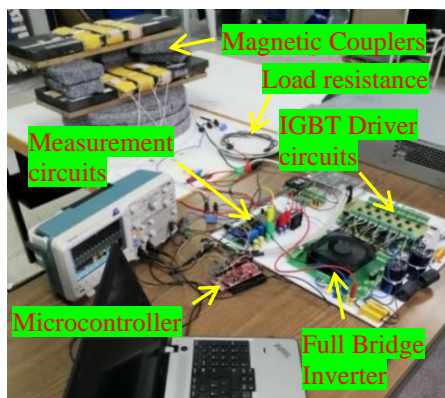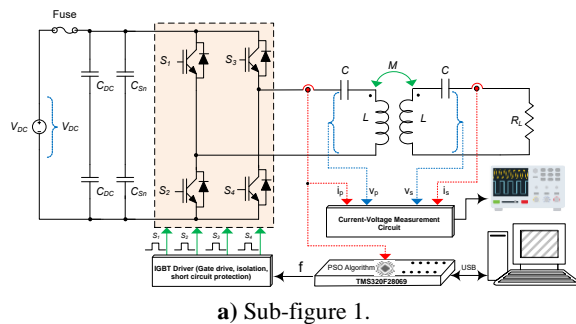
Two series connected 2200 µF/450V DC capacitors and a 1µF/1200V snubber capacitor, which is parallel to these two 2200 μF capacitors, are utilized at the DC bus node. The flux-pipe coupler utilized in this experiment is basically a helical structure with three sub-coils wound around a common ferrite core (Figure 5 (b)). The detailed simulation and measurement results of this coupler structure are out of scope of this paper and are reported elsewhere [12]. The list of component values and other details for the experimental setup are shown Table 1.

The proposed frequency tracking method is experimentally verified under three scenarios. In the first scenario, the couplers are perfectly aligned and separated with 100 mm vertical gap ($dz = 100$ mm). In the second scenario, the coupling coefficient between couplers is reduced by applying a 150 mm lateral misalignment along the coupler's longer side ($dy = 150$ mm). In the third scenario, the sub-coil separation (d_{sub}), which is originally 60 mm for each coupler, is changed in secondary side coupler until the self-inductance of the secondary side coupler increases to 185 µH from its original value of 170 µH. This final scenario results in moving the maximum power point from lower resonance frequency to the higher one. The difference between the power levels becomes also larger in this last scenario. A PO algorithm is also run in the last scenario and compared to the PSO algorithm. All three scenarios are sketched in Figure 6 and are summarized in Table 2.

a) Sub-figure 1.

b) Sub-figure 2.

Figure 5. Block diagram (a) and photo of experimental WPT system (b)

a) Scenario 1

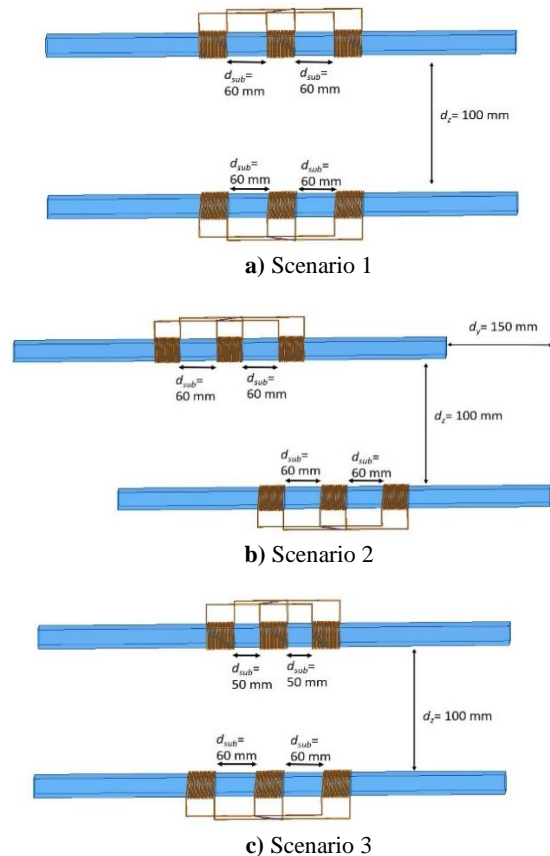
b) Scenario 2

c) Scenario 3

Figure 6. Three expermental scenarios with various coil and sub-coil orientations.

Table 1: Component values and other details of experimental setup

| Symbol	Parameter	Value
V_{DC}	DC rail voltage	50 V
C_{DC}	DC rail capacitors magnetic induction	2x2200 µF
C_{Sn}	DC rail snubber capacitors	2x1 µF
R_L	Load resistance	5Ω
$L_1=L_2$	Coupler inductances	170 µH
M	Mutual inductance	64,75 µH
$C_1=C_2$	Compensation capacitors	175 nF
$R_1=R_2$	Loss resistances	10 mΩ

Table 2: Details of experimental scenarios

| State	Scenario 1	Scenario 2	Scenario 3
Vertical separation (dz)	100mm	100mm	100mm
Lateral misalignment (dy)	0mm	150mm	0mm
Separation between sub-coils (d_{sub})	P.S.=60 S.S.=60 mm	P.S.=60 S.S.=60 mm	P.S.=60 S.S.=50 mm
Primary coupler self-inductance (L_1)	170 µH	170 µH	170 µH
Secondary coupler self-inductance (L_2)	170 µH	170 µH	185 µH
Mutual-inductance (M)	65 µH	50 µH	64 µH

(P.S.=Primary Side, S.S.=Secondary Side)

4.1. Scenario I

In scenario I, the couplers are perfectly aligned and separated with 100 mm vertical gap (dz = 100 mm). Before running PSO based frequency tracking algorithm, input power to the primary side resonant coupler and the inverter's switching frequency are scanned simultaneously in time to make sure that the system exhibits frequency splitting phenomenon. The switching frequency of the inverter is linearly increased from 10 kHz to 40 kHz with approximately 100 Hz increase at each time step. Figure 7 (a) shows oscilloscope screenshot of this scan. The data shown with cyan-colored line is the scanned input power and exhibits two peaks at approximately 24 kHz and 33 kHz, respectively. The data with maize-colored line is the scanned frequency. The PSO based frequency tracking algorithm is then utilized in microcontroller to drive the gates of IGBTs. Figure 7 (b) shows the oscilloscope screenshot of the PSO algorithm's performance for tracking the frequency of maximum power. In this graph (Figure 7 (b)), the instantaneous frequency searched by the PSO algorithm and the

corresponding input current are shown with maize and cyan colored lines, respectively.
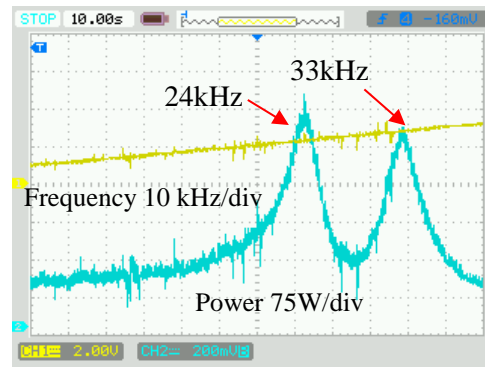
a) Sub-figure 1.
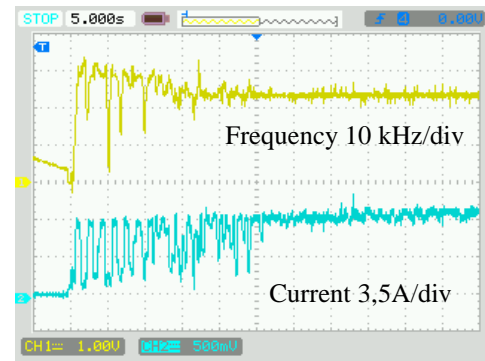
b) Sub-figure 2.

Figure 7. Oscilloscope screenshot for Scenario I for (a) scanning for input power to the primary side resonant coupler and the inverter's switching frequency and (b) performance of PSO algorithm

a) Sub-figure 1.

b) Sub-figure 2.

Figure 8. For 50 V DC bus voltage and 24 kHz switching frequency voltage (blue) and current (purple) at the (a) input and (b) load resistance (R_L).

One can read the searched frequency and input current level as well as the time using given kHz/div, A/div and s/div (on the top left of the graph) scales on the graphs. As seen in Figure 7 (b), the PSO algorithm finds the resonance frequency for maximum power as 24 kHz in approximately 25 seconds. The tracked 24 kHz agrees with the initial scanning results shown in Figure 7 (a), verifying the accuracy of PSO algorithm. The measured voltage and currents at the input and at the load resistance (R_L), when inverter operates at tracked 24 kHz, are shown as oscilloscope screenshots in Figure 8.

4.2. Scenario II

In this scenario, the coupling coefficient between couplers is reduced by applying a 150 mm lateral misalignment along the coupler's longer side ($dy = 150$ mm). As in scenario 1, first, input power to the primary side resonant coupler and the inverter's switching frequency are scanned simultaneously in time. Figure 9 (a) shows oscilloscope screenshot of this scan. The data shown with cyan-colored line is the scanned input power and exhibits two peaks at approximately 25.5 kHz and 31.5 kHz, respectively. The data with maize-colored line is the scanned frequency.
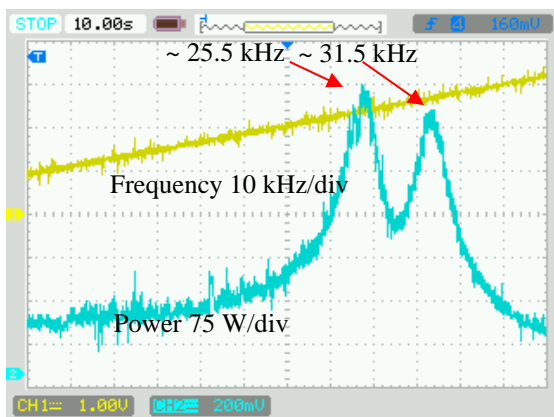
a) Sub-figure 1.
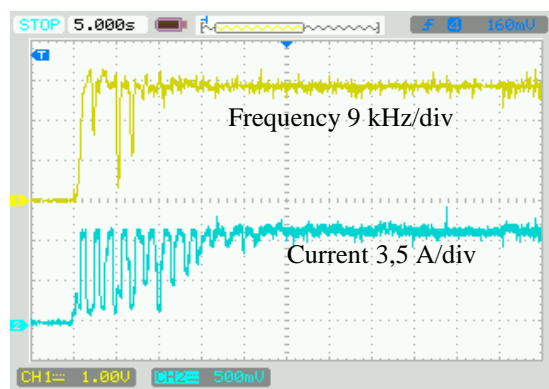
b) Sub-figure 2.

Figure 9. Oscilloscope screenshot for Scenario II for scanning for input power to the primary side resonant coupler (a) and the inverter's switching frequency and performance of PSO algorithm (b).
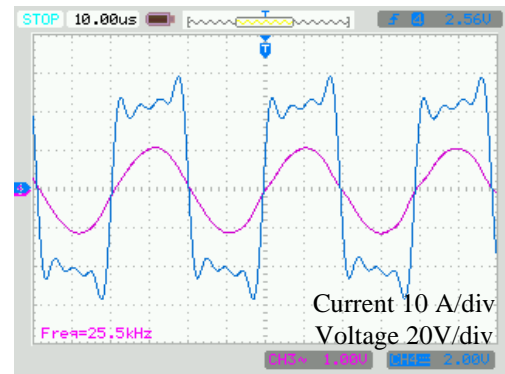
a) Sub-figure 1.
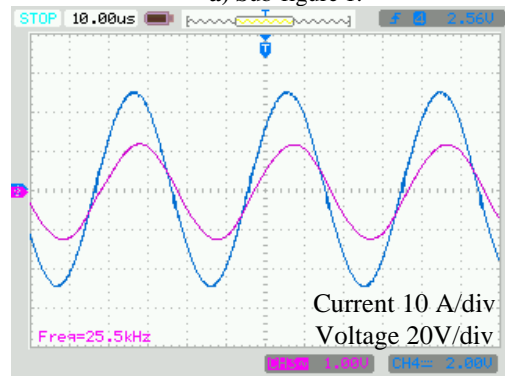
b) Sub-figure 2.

Figure 10. For 50 V DC bus voltage and 25.5 kHz switching frequency voltage (blue) and current (purple) at the input (a) and load resistance (R_L) (b).

As seen in Figure 9 (a), the resonance frequencies approach to one another when 150 mm misalignment is applied along the longer side of the couplers. This change in the resonance frequencies can be attributed to the decrease in the mutual inductance between the couplers. Figure 9 (b) shows the oscilloscope screenshot of the PSO algorithm's performance for tracking the frequency of maximum power. In this graph, the instantaneous frequency searched by the PSO algorithm and the corresponding input current are shown with maize an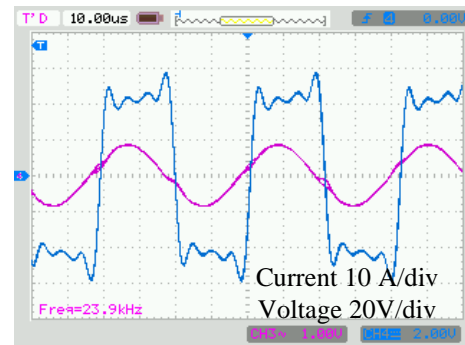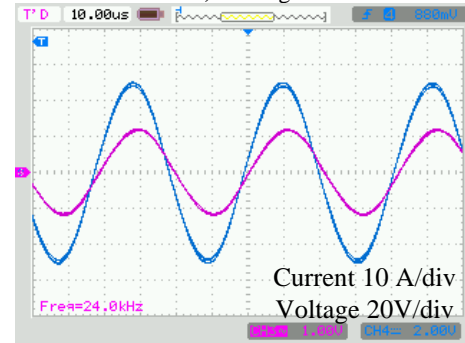d cyan colored lines, respectively. The PSO algorithm finds the resonance frequency for maximum power as 25.5 kHz in approximately 15 seconds. The tracked 25.5 kHz agrees with the frequency of global maximum power shown in Figure 9 (a)), verifying the accuracy of PSO algorithm. The measured voltage and currents at the input and at the load resistance (R_L), when inverter operates at tracked 25.5 kHz, are shown as oscilloscope screenshots in Figure 10.

4.3. Scenario III

In the third scenario, the sub-coil separation (d_{sub}), which is originally 60 mm for each coupler, is changed in secondary side coupler until the self-inductance of the secondary side coupler increases to 185 μH. Such a change results in switching the global power maximum from lower resonance frequency to the higher one as shown in Figure 11 (a).
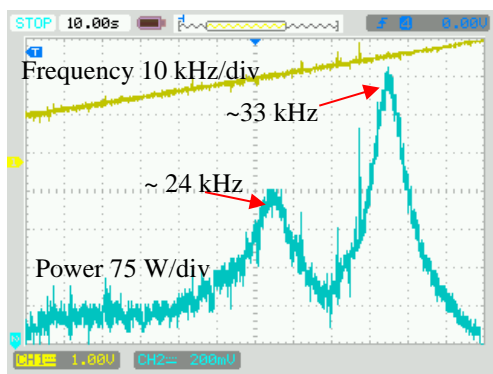
a) Sub-figure 1.
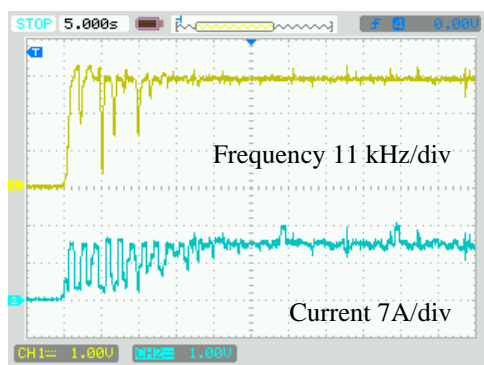
b) Sub-figure 2.

Figure 11. Oscilloscope screenshot for Scenario III for scanning for input power to the primary side resonant coupler and the inverter's switching frequency (a) and performance of PSO algorithm (b).

The data shown in Figure 11 (a) with cyan-colored line is the scanned input power and exhibits two peaks at approximately 24 kHz and 33 kHz, respectively. The data with maize-colored line is the scanned frequency. As seen in Figure 11 (b), algorithm converges in less than 20 seconds and finds the 33 kHz resonance frequency as the global maximum power point which agrees with Figure 11 (a). A major advantage of PSO algorithm is that it always converges to the global maximum and never stuck in a local maximum. To make a comparison, a PO algorithm is also run in the last scenario (scenario III). Figure 12 shows the oscilloscope screenshot of the PO algorithm's performance for tracking the frequency of maximum power.
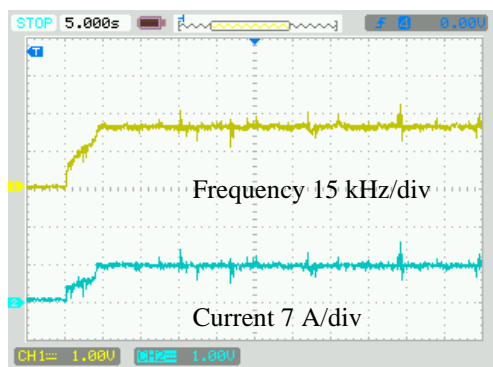

Figure 12. Performance of PO algorithm for scenario III
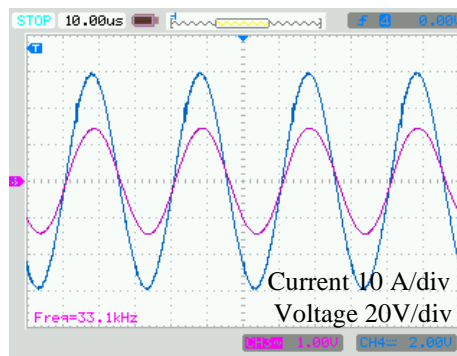
a) Sub-figure 1.
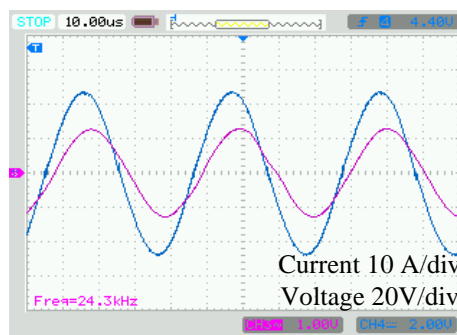
b) Sub-figure 2.

Figure 13. Voltage and current waveforms at load resistance (R_L) for scenario III (a) performance of PSO algorithm (b) performance of PO algorithm.

In Figure 12, within approximately ten seconds, the PO algorithm stucks in 24 kHz which is not the maximum power point. Although the PO algorithm converges faster than the PSO algorithm, the converged frequency does not guarantee the maximum power point. Figure 13 shows the oscilloscope screenshots of measured voltage and current waveforms on the load resistance (R_L) for both PSO and PO algorithms.

Performance data obtained for 3 different scenarios discussed in this article are summarized in Table 3. Comparison between PO and PSO algorithm has also been made for Scenario 3 to show incapability of PO algorithm tracking global maximum power point frequency . Although the PO algorithm converges faster than PSO algorihm, it stuck with the local maximum where input power (300 W) is much less than the global maximum (500 W) tracked by the PSO algorithm.

Table 3: Performance evaluation of algorithms

| Scenario | Frequency (kHz) | | Input Power (W) | Conv. Time (s) |
	Local/Global maximum	Tracked by algo.		
Scenario 1	33	24	PSO:23,9	PSO:405	PSO:15
Scenario 2	31,5	25,5	PSO:25,5	PSO:472	PSO:10
Scenario 3	24	33	PSO:33,1 PO:24,3	PSO:525 PO:300	PSO:15 PO:5

5. Conclusion

In this paper, a frequency tracking WPT system based on a PSO algorithm is presented. With the use of a PSO algorithm, inverter's frequency is tuned to a resonance frequency where maximum power is delivered to the load without sticking to a local maximum. An experimental WPT system is implemented under three different scenarios covering various misalignment and resonance conditions and compared with PO algorithm in misalignment scenario 3. The proposed PSO algorithm always converges to the resonance frequency of global maximum power in case frequency splitting. Furthermore, the proposed frequency tracking control method utilizes the current and voltage data at the primary side of the WPT system, making it a less complex single-sided controller. Therefore, no additional communication link between primary and secondary side is needed for maximizing the delivered power level. A potential future direction would be incorporating missing secondary side electronics such as a rectifier, a DC-DC converter, a battery management circuit and a battery to realize a complete WPT charger targeting a certain application such as an electric vehicle charger.

References

[1] Hui, S.Y. (2013). *Planar wireless charging technology for portable electronic products and Qi*. Proceeding of the IEEE, 101(6), 1290-1301.

[2] Wang, C.S., Stielau, O.H. & Covic, G.A. (2005) *Design considerations for a contactless electric vehicle battery charger.* IEEE Transactions on Industrial Electronics, 52(5), 1308-1314.

[3] Imura, T., Okabe, H. & Hori, Y. (2009). *Basic experimental study on helical antennas of wireless power transfer for electric Vehicles by using magnetic resonant couplings.* Proceedings of Vehicle Power and Propulsion Conference, Dearborn, IEEE, September, 936-940.

[4] Cho, I. K., Kim, S.M., Moon J.I., Yoon, J. H., Jeon, S.I. & Choi, J. I. (2013). *Wireless power transfer system for docent robot by using magnetic resonant coils*. Proceedings of IEEE 5th International Symposium on Microwave, Antenna, Propagation and EMC Technologies for Wireless Communications (MAPE), Chendu, October, 251-254.

[5] Deyle, T., & Reynolds, M. (2008). *Surface based wireless power transmission and bidirectional communication for autonomous robot swarms*. Proceedings of IEEE International Conference on Robotics and Automation (ICRA), Pasedana CA, May, 1036-1041.

[6] Li, X., Tsui, C.Y., & Ki, W.H. (2015). *A 13.56 MHz wireless power transfer system with reconfigurable resonant regulating rectifier and wireless power control for implantable medical devices.* IEEE Journal of Solid-State Circuits, 50(4), 978-989. Apr.

[7] Walk, J., Weber, J., Soell, C., Weigel, R., Fischer, G., & Ussmueller, T. (2014). *Remote powered medical implants for telemonitoring*. Proceeding of IEEE, 102(11), 1811-1832.

[8] Chaidee, E., Sangswang, A., Naetiladdanon, S. & Mujjalinvimut, E. (2017). *Maximum output power tracking for wireless power transfer system using impedance tuning*. IECON 43rd Annual Conference of the IEEE Industrial Electronics Society, Beijing, October- November, 6961-6966.

[9] Luo, Y., Yang, Y., Chen, S. & Wen, X. (2017). *A frequency-tracking and impedance-matching combined system for robust wireless power transfer*. International Journal of Antennas and Propagation. 2017,1-13.

[10] Barman, S.D., Reza, A.W., Kumar, N. & Anowar, T.I. (2015). *Two-side Impedance Matching for Maximum Wireless Power Transmission*. IETE Journal of Research, 62(4), 532-539.

[11] Liu, N. & Habetler, T.G. (2015). *Design of a universal inductive charger for multiple electric vehicle models*. IEEE Transactions on Power Electronics, 30(11), 6378-6390.

[12] Sis, S.A., Kilic, F. & Sezen, S. (2019). *Multi sub-coil flux pipe couplers and their use in a misalignment-adaptive wireless power transfer system*. Journal of Electromagnetic Waves and Applications. 33(14), 1890-1904.

[13] Lin, Z., Wang, J., Fang, Z., Hu, M., Cai, C. & Zhang, J. (2018). *Accurate maximum power tracking of wireless power transfer system based on simulated annealing algorithm*. IEEE Access. 6, 60881-60890.

[14] Hongbo, S. & Shuxia, L. (2008). *The comparison between genetic simulated annealing algorithm and antcolony optimization algorithm for ASP*. 4th International Conference on Wireless Communications, Networking and Mobile Computing, Dalian, IEEE, October, 1-6.

[15] Abreu, R.L., Pimenta, T.C. & Spadoti, D.H. (2017). *Self-tuning capacitance for impedance matching in wireless power transfer devices*. 29th International Conference on Microelectronics (ICM); Beirut, IEEE, December, 1-4.

[16] Jabri, I., Bouallegue, A. & Ghodbane, F. (2017). *Frequency and misalignment P&O controller for wireless battery charger*. International Conference on Green Energy Conversion Systems (GECS), Hammamet, IEEE, March, 1-6.

[17] Li, Y., Zhang, C., Yang, Q., Li, J., Zhang, Y., Zhang, X. & Xue, M. (2018). *Improved ant colony algorithm for adaptive frequency tracking control in WPT system*. IET Microwaves, Antennas and Propagation, 12(1), 23-28.

[18] Bai, J. & Li. S. (2011). *Improvement in Extension of Ant Colony Optimization and its appliance*. 3rd International Conference on Advanced Computer Control, Harbin, IEEE, January, 557-560.

[19] Ibrahim, M., Bernard, L., Pichon, L., Labour´e, E., Razek, A., Cayol, O., Ladas, D. & Irving, J. (2016). *Inductive Charger for Electric Vehicle: Advanced Modeling and Interoperability Analysis*. IEEE Transactions on Power Electronics, 31(12), 8096-8114.

[20] Schuetz, M., Georgiadis, A., Collado, A. & Fischer, G. (2015). *A particle swarm optimizer for tuning a software-defined, highly configurable wireless power transfer platform*. 2015 IEEE Wireless Power Transfer Conference (WPTC), Boulder, IEEE, May, 1-4.

[21] Wang, M., Feng, J., Shi, Y., Shen, M. & Jing, J. (2018). *A Novel PSO-Based Transfer Efficiency Optimization Algorithm for Wireless Power Transfer*. Progress in Electromagnetics Research. 85, 63-75.

[22] Covic, G.A., & Boys, J.T. (2013). *Inductive Power Transfer*. Proceedin of IEEE, 101(6),1276-1289.

[23] Budhia, M., Covic, G. & Boys, J. (2010). *A new ipt magnetic coupler for electric vehicle charging systems*. IECON 36th Annual Conference on IEEE Industrial Electronics Society, Glendale, November, 2487–2492.

[24] Siqi, L. and Mi, C.C. (2014). *Wireless power transfer for electric vehicle applications*. IEEE Journal of Emerging Selected Topics on Power Electronics. 3(1), 4-17.

[25] Heebl, Jason D., et al. "Comprehensive analysis and measurement of frequency-tuned and impedance-tuned wireless non-radiative power-transfer systems." *IEEE Antennas and Propagation Magazine* 56.4 (2014): 44-60.

[26] Kermadi, M., Salam, Z., Ahmed, J. & Berkouk, M. (2019). *An effective hybrid maximum power point tracker of photovoltaic arrays for complex partial shading conditions.* IEEE Transactions on Industrial Electronics. 66(9), 6990-7000.

[27] Ram, J.P., Pillai, D.S., Rajasekar, N. & Strachan, S.M. (2019). *Detection and identification of global maximum power point operation in solar PV applications using a hybrid ELPSO-P&O tracking technique*. IEEE Journal of Emerging Selected Topics on Power Electronics, Early Access, 1-14.

[28] Soufi, Y., Bechouat, M. & Kahla. S. (2018). *Particle swarm optimization based maximum power point tracking algorithm for photovoltaic energy conversion system*.15th International Multi-Conference on Systems, Signals & Devices (SSD), Hammamet, IEEE, March, 773-779.

[29] Calvinho, G., Pombo, J., Mariano, S. & Calado, M.R. (2018). *Design and implementation of MPPT system based on PSO algorithm*. International Conference on Intelligent Systems (IS), Funchal Madeira, IEEE, September, 733-738.

[30] Fahad, S., Mahdi, A.J., Tang, W.H., Huang, K. & Liu, Y. (2018). *Particle swarm optimization based DC-link voltage control for two stage grid connected PV inverter*. International Conference on Power System Technology, Guangzhou, IEEE, November, 733-738.

[31] Efendi, M.Z., Setiawan, R.E., Murdianto, F.D., Mubarok, R.H., Windarko, N.A. & Dirmawan, M. (2018). *A Performance evaluation of MPPT using modified PSO algorithm for battery charge application*. International Electronics Symposium on Engineering Technology and Applications (IES-ETA), Bali, IEEE, October, 8-12.

Fuat Kılıç received the B.S. and M.Sc. and Ph.D. degrees in electrical engineering from Kocaeli University, Kocaeli, Turkey, in 2001, 2003 and 2016, respectively. He is currently Assistant Professor with Balıkesir University in department of Mechatronics Engineering. His research interests include electrical machines, control theories, power electronics and renewable energy.
https://orcid.org/0000-0003-2502-3789

Serkan Sezen received the B.S., M.Sc. and Ph.D. degrees in Electrical Education from Kocaeli University, Kocaeli, Turkey, in 2003, 2006 and 2015 respectively. He is currently Assistant Professor at Department of Electric and Energy, Uzunçiftlik Nuh Çimento Vocational School, Kocaeli University. His research interests are renewable energy, power electronics, control theories and electrical machines.
http://orcid.org/0000- 0001-7273-7376

Seyit Ahmet Sis received the B.S. degree in electronics engineering from the The Gebze Institute of Technology, Kocaeli, Turkey, in 2005, the M.S. degree in electrical engineering from The Syracuse University, Syracuse, NY, and the Ph.D. degree from The University of Michigan at Ann Arbor in 2014. Since July 2014, he has been with The Balikesir University as a faculty member in the Electrical and Electronics Engineering Department. He is also working as a Senior Researcher with a part-time appointment at TÜBİTAK-BİLGEM since 2015. His current research interests include wireless power transfer systems, switchable and tunable microwave components and circuits, RF passive sensors and high efficiency power-amplifier design for wireless applications.
http://orcid.org/0000- 0002-3740-2391

RESEARCH ARTICLE

Modified operational matrix method for second-order nonlinear ordinary differential equations with quadratic and cubic terms

Burcu Gürbüz[a,b,c*] and Mehmet Sezer[d]

[a] Department of Computer Engineering, Üsküdar University, Turkey
[b] Institute of Mathematics, Johannes Gutenberg-University Mainz, Germany
[c] Jean Leray Mathematics Laboratory, University of Nantes, France
[d] Department of Mathematics Manisa Celal Bayar University, Turkey
burcu.gurbuz@uskudar.edu.tr, mehmet.sezer@cbu.edu.tr

ABSTRACT

In this study, by means of the matrix relations between the Laguerre polynomials, and their derivatives, a novel matrix method based on collocation points is modified and developed for solving a class of second-order nonlinear ordinary differential equations having quadratic and cubic terms, via mixed conditions. The method reduces the solution of the nonlinear equation to the solution of a matrix equation corresponding to system of nonlinear algebraic equations with the unknown Laguerre coefficients. Also, some illustrative examples along with an error analysis based on residual function are included to demonstrate the validity and applicability of the proposed method.

1. Introduction

Nonlinear differential equations and the related initial and boundary value problems play an important role in astrophysics, physics and engineering. In recent years, to solve these problems both analytically and numerically which have applications in various branches of pure and applied sciences, several numerical and analytical methods have been given. But it may not be possible to find the analytical solutions of such problems for all coefficient functions.

These type of mathematical models can be described by particular names such as Riccati equation, nonlinear equations of motion, Duffing's equation, Van Der Pol's equation, the equation of motion with quadratic damping, Emden's equation, Liouville's equation [1–5].

In this study, we consider the second-order nonlinear ordinary differential equations with quadratic and cubic terms:

$$\sum_{k=0}^{2} P_k(x) y^{(k)}(x) + \sum_{p=0}^{2} \sum_{q=0}^{p} Q_{pq}(x) y^{(p)}(x) y^{(q)}(x)$$

$$+ \sum_{p=0}^{2} \sum_{q=0}^{p} \sum_{r=0}^{q} Q_{pqr}(x) y^{(p)}(x) y^{(q)}(x) y^{(r)}(x)$$

$$= g(x), \quad 0 \le x \le b < \infty, \tag{1}$$

with the mixed conditions

$$\sum_{k=0}^{1} (a_{kj} y^{(k)}(0) + b_{kj} y^{(k)}(b)) = \lambda_j, \quad j = 0,1, \tag{2}$$

where $P_k(x), Q_{pq}(x), Q_{pqr}(x)$ and $g(x)$ are functions defined on the interval $0 \le x \le b < \infty$; a_{kj}, b_{kj} and λ_j are appropriate and real constants; $y(x)$ is an unknown function to be determined [6].

*Corresponding Author

In this study, we develop a new numerical methods to find the approximate solutions of Eq. (1) in the truncated Laguerre series form

$$y(x) \cong y_N(x) = \sum_{n=0}^{N} a_n L_n(x), \quad 0 \le x \le b < \infty, \tag{3}$$

where $a_n, n = 0, 1, ..., N, N \ge 2$ are the unknown Laguerre coefficients and $L_n(x), n = 0, 1, ..., N$ are the Laguerre functions of first kind defined by

$$L_n(x) = \sum_{k=0}^{n} \frac{(-1)^k}{k!} \binom{n}{k} x^k, \quad 0 \le x \le b < \infty. \tag{4}$$

2. Operational matrix relations

Firstly, let us write Eq. (1) in the form

$$L[y(x)] + N_2[y(x)] + N_3[y(x)] = g(x), \tag{5}$$

where the linear ordinary differential part

$$L[y(x)] = \sum_{k=0}^{2} P_k(x) y^{(k)}(x), \tag{6}$$

the nonlinear quadratic part

$$N_2[y(x)] = \sum_{p=0}^{2} \sum_{q=0}^{p} Q_{pq}(x) y^{(p)}(x) y^{(q)}(x), \tag{7}$$

and the nonlinear cubic part

$$N_3[y(x)] = \sum_{p=0}^{2} \sum_{q=0}^{p} \sum_{r=0}^{q} Q_{pqr}(x) y^{(p)}(x) y^{(q)}(x) y^{(r)}(x). \tag{8}$$

2.1. Matrix representation of linear ordinary differential part

Now, we consider Eq.(1) and find the matrix forms of each term in the equation. So, we convert Laguerre polynomial solution (3) to the matrix form as

$$y(x) = y^{(0)}(x) \cong \mathbf{L}(x)\mathbf{A},$$
$$y^{(1)}(x) = \mathbf{L}(x)\mathbf{C}\mathbf{A}, \tag{9}$$
$$y^{(2)}(x) = \mathbf{L}(x)\mathbf{C}^2\mathbf{A},$$

where

$$\mathbf{L}(x) = \begin{bmatrix} L_0(x) & L_1(x) & \cdots & L_N(x) \end{bmatrix},$$

$$\mathbf{C} = \begin{bmatrix} 0 & -1 & -1 & \cdots & -1 \\ 0 & 0 & -1 & \cdots & -1 \\ \vdots & \vdots & \vdots & \ddots & \vdots \\ 0 & 0 & 0 & \cdots & -1 \\ 0 & 0 & 0 & \cdots & 0 \end{bmatrix},$$

$$\mathbf{A} = \begin{bmatrix} a_0 & a_1 & \cdots & a_N \end{bmatrix}^T.$$

2.2. Matrix representation of nonlinear quadratic part

Now, we consider matrix representation of nonlinear quadratic part. So, we define the matrices with related to (7) and (9)

$$(y^{(0)}(x))^2 = \mathbf{L}(x)\overline{\mathbf{L}}(x)\overline{\mathbf{A}},$$
$$y^{(1)}(x)y^{(0)}(x) = \mathbf{L}(x)\mathbf{C}\overline{\mathbf{L}}(x)\overline{\mathbf{A}},$$
$$(y^{(1)}(x))^2 = \mathbf{L}(x)\mathbf{C}\overline{\mathbf{L}}(x)\overline{\mathbf{C}\mathbf{A}},$$
$$y^{(2)}(x)y^{(1)}(x) = \mathbf{L}(x)\mathbf{C}^2\overline{\mathbf{L}}(x)\overline{\mathbf{C}\mathbf{A}}, \tag{10}$$
$$y^{(2)}(x)y^{(0)}(x) = \mathbf{L}(x)\mathbf{C}^2\overline{\mathbf{L}}(x)\overline{\mathbf{A}},$$
$$(y^{(2)}(x))^2 = \mathbf{L}(x)\mathbf{C}^2\overline{\mathbf{L}}(x)\overline{\mathbf{C}^2\mathbf{A}},$$

where

$$\overline{\mathbf{L}}(x) = diag \begin{bmatrix} \mathbf{L}(x) & \mathbf{L}(x) & \cdots & \mathbf{L}(x) \end{bmatrix},$$
$$\overline{\mathbf{C}} = diag \begin{bmatrix} \mathbf{C} & \mathbf{C} & \cdots & \mathbf{C} \end{bmatrix},$$
$$\overline{\mathbf{A}} = \begin{bmatrix} a_0\mathbf{A} & a_1\mathbf{A} & \cdots & a_N\mathbf{A} \end{bmatrix}^T.$$

2.3. Matrix representation of nonlinear cubic part

Let us consider (8) as

$$N_3[y(x)] = \sum_{p=0}^{2} \sum_{q=0}^{p} \sum_{r=0}^{q} Q_{pqr}(x) y^{(p)}(x) y^{(q)}(x) y^{(r)}(x)$$
$$+ Q_{000}(x) y^{(0)}(x) y^{(0)}(x) y^{(0)}(x)$$
$$+ Q_{100}(x) y^{(1)}(x) y^{(0)}(x) y^{(0)}(x)$$
$$+ Q_{110}(x) y^{(1)}(x) y^{(1)}(x) y^{(0)}(x)$$
$$+ Q_{111}(x) y^{(1)}(x) y^{(1)}(x) y^{(1)}(x)$$
$$+ Q_{200}(x) y^{(2)}(x) y^{(0)}(x) y^{(0)}(x)$$
$$+ Q_{210}(x) y^{(2)}(x) y^{(1)}(x) y^{(0)}(x)$$
$$+ Q_{211}(x) y^{(2)}(x) y^{(1)}(x) y^{(1)}(x)$$
$$+ Q_{220}(x) y^{(2)}(x) y^{(2)}(x) y^{(0)}(x)$$
$$+ Q_{221}(x) y^{(2)}(x) y^{(2)}(x) y^{(1)}(x)$$
$$+ Q_{222}(x) y^{(2)}(x) y^{(2)}(x) y^{(2)}(x).$$

So, we define the matrices as

$$(y^{(0)}(x))^3 = \mathbf{L}(x)\overline{\mathbf{L}}(x)\overline{\overline{\mathbf{L}}}(x)\overline{\overline{\mathbf{A}}},$$
$$y^{(1)}(x)(y^{(0)}(x))^2 = \mathbf{L}(x)\mathbf{C}\overline{\mathbf{L}}(x)\overline{\overline{\mathbf{L}}}(x)\overline{\overline{\mathbf{A}}},$$
$$(y^{(1)}(x))^2 y^{(0)}(x) = \mathbf{L}(x)\mathbf{C}\overline{\mathbf{L}}(x)\overline{\mathbf{C}}\overline{\overline{\mathbf{L}}}(x)\overline{\overline{\mathbf{A}}},$$
$$(y^{(1)}(x))^3 = \mathbf{L}(x)\mathbf{C}\overline{\mathbf{L}}(x)\overline{\mathbf{C}}\overline{\overline{\mathbf{L}}}(x)\overline{\overline{\mathbf{CA}}},$$
$$y^{(2)}(x)(y^{(0)}(x))^2 = \mathbf{L}(x)\mathbf{C}^2\overline{\mathbf{L}}(x)\overline{\overline{\mathbf{L}}}(x)\overline{\overline{\mathbf{A}}},$$
$$y^{(2)}(x)y^{(1)}(x)y^{(0)}(x) = \mathbf{L}(x)\mathbf{C}^2\overline{\mathbf{L}}(x)\overline{\mathbf{C}}\overline{\overline{\mathbf{L}}}(x)\overline{\overline{\mathbf{A}}},$$

(11)

$$y^{(2)}(x)(y^{(1)}(x))^2 = \mathbf{L}(x)\mathbf{C}^2\overline{\mathbf{L}}(x)\overline{\mathbf{C}}\overline{\overline{\mathbf{L}}}(x)\overline{\overline{\mathbf{CA}}},$$
$$(y^{(2)}(x))^2 y^{(0)}(x) = \mathbf{L}(x)\mathbf{C}^2\overline{\mathbf{L}}(x)\overline{\mathbf{C}^2}\overline{\overline{\mathbf{L}}}(x)\overline{\overline{\mathbf{A}}},$$
$$(y^{(2)}(x))^2 y^{(1)}(x) = \mathbf{L}(x)\mathbf{C}^2\overline{\mathbf{L}}(x)\overline{\mathbf{C}^2}\overline{\overline{\mathbf{L}}}(x)\overline{\overline{\mathbf{CA}}},$$
$$(y^{(2)}(x))^3 = \mathbf{L}(x)\mathbf{C}^2\overline{\mathbf{L}}(x)\overline{\mathbf{C}^2}\overline{\overline{\mathbf{L}}}(x)\overline{\overline{\mathbf{C}^2\mathbf{A}}},$$

where

$$\overline{\overline{\mathbf{L}}}(x) = diag \begin{bmatrix} \overline{\mathbf{L}}(x) & \overline{\mathbf{L}}(x) & \cdots & \overline{\mathbf{L}}(x) \end{bmatrix},$$
$$\overline{\overline{\mathbf{C}}} = diag \begin{bmatrix} \overline{\mathbf{C}} & \overline{\mathbf{C}} & \cdots & \overline{\mathbf{C}} \end{bmatrix},$$
$$\overline{\overline{\mathbf{A}}} = \begin{bmatrix} a_0\overline{\mathbf{A}} & a_1\overline{\mathbf{A}} & \cdots & a_N\overline{\mathbf{A}} \end{bmatrix}^T.$$

3. Method of solution

Now, we define the collocation points as

$$x_i = \frac{b}{N}i, \;\; i = 0, 1, N; \;\; 0 \leq x_0 < x_1 < ... < x_N = b.$$

(12)

We substitute the collocation points (12) into Eq. (1), we have the system of matrix equations for $i = 0, 1, ..., N$,

$$\sum_{k=0}^{2} P_k(x_i)y^{(k)}(x_i) + \sum_{p=0}^{2}\sum_{q=0}^{p} Q_{pq}(x_i)y^{(p)}(x_i)y^{(q)}(x_i)$$
$$+ \sum_{p=0}^{2}\sum_{q=0}^{p}\sum_{r=0}^{q} Q_{pqr}(x_i)y^{(p)}(x_i)y^{(q)}(x_i)y^{(r)}(x_i)$$
$$= g(x_i), \quad 0 \leq x \leq b < \infty,$$

or briefly,

$$\sum_{k=0}^{2}\mathbf{P}_k\mathbf{Y}^{(k)} + \sum_{p=0}^{2}\sum_{q=0}^{p}\mathbf{Q}_{pq}\mathbf{Y}^{(p,q)}$$
$$+ \sum_{p=0}^{2}\sum_{q=0}^{p}\sum_{r=0}^{q}\mathbf{Q}_{pqr}\mathbf{Y}^{(p,q,r)}$$

(13)

$$= \mathbf{G}, \quad 0 \leq x \leq b < \infty,$$

where

$$\mathbf{P}_k = diag \begin{bmatrix} P_k(x_0) & P_k(x_1) & \cdots & P_k(x_N) \end{bmatrix},$$
$$\mathbf{Q}_{pq} = diag \begin{bmatrix} Q_{pq}(x_0) & Q_{pq}(x_1) & \cdots & Q_{pq}(x_N) \end{bmatrix},$$
$$\mathbf{Q}_{pqr} = diag \begin{bmatrix} Q_{pqr}(x_0) & Q_{pqr}(x_1) & \cdots & Q_{pqr}(x_N) \end{bmatrix},$$

and

$$\mathbf{Y}^{(k)} = \begin{bmatrix} y^{(k)}(x_0) \\ y^{(k)}(x_1) \\ \vdots \\ y^{(k)}(x_N) \end{bmatrix}, \;\; \mathbf{G} = \begin{bmatrix} g(x_0) \\ g(x_1) \\ \vdots \\ g(x_N) \end{bmatrix},$$

$$\mathbf{Y}^{(p,q,r)} = \begin{bmatrix} y^{(p)}(x_0)y^{(q)}(x_0)y^{(r)}(x_0) \\ y^{(p)}(x_1)y^{(q)}(x_1)y^{(r)}(x_1) \\ \vdots \\ y^{(p)}(x_N)y^{(q)}(x_N)y^{(r)}(x_N) \end{bmatrix},$$

$$\mathbf{Y}^{(p,q)} = \begin{bmatrix} y^{(p)}(x_0)y^{(q)}(x_0) \\ y^{(p)}(x_1)y^{(q)}(x_1) \\ \vdots \\ y^{(p)}(x_N)y^{(q)}(x_N) \end{bmatrix}.$$

By the other hand, we can write following matrix forms of the nonlinear quadratic and nonlinear cubic parts from (8) and (9) for $p, q, r = 0, 1, 2$

$$\mathbf{Y}^{(0,0)} = \mathbf{L}^*_{(0,0)}\overline{\mathbf{A}}, \;\; \mathbf{Y}^{(1,0)} = \mathbf{L}^*_{(1,0)}\overline{\mathbf{A}},$$
$$\mathbf{Y}^{(1,1)} = \mathbf{L}^*_{(1,1)}\overline{\mathbf{A}}, \;\; \mathbf{Y}^{(2,0)} = \mathbf{L}^*_{(2,0)}\overline{\mathbf{A}},$$
$$\mathbf{Y}^{(2,1)} = \mathbf{L}^*_{(2,1)}\overline{\mathbf{A}}, \;\; \mathbf{Y}^{(2,2)} = \mathbf{L}^*_{(2,2)}\overline{\mathbf{A}},$$

and

$$\mathbf{Y}^{(0,0,0)} = \mathbf{L}^*_{(0,0,0)}\overline{\overline{\mathbf{A}}}, \;\; \mathbf{Y}^{(1,0,0)} = \mathbf{L}^*_{(1,0,0)}\overline{\overline{\mathbf{A}}},$$
$$\mathbf{Y}^{(1,1,0)} = \mathbf{L}^*_{(1,1,0)}\overline{\overline{\mathbf{A}}}, \;\; \mathbf{Y}^{(1,1,1)} = \mathbf{L}^*_{(1,1,1)}\overline{\overline{\mathbf{A}}},$$
$$\mathbf{Y}^{(2,0,0)} = \mathbf{L}^*_{(2,0,0)}\overline{\overline{\mathbf{A}}}, \;\; \mathbf{Y}^{(2,1,0)} = \mathbf{L}^*_{(2,1,0)}\overline{\overline{\mathbf{A}}},$$
$$\mathbf{Y}^{(2,1,1)} = \mathbf{L}^*_{(2,1,1)}\overline{\overline{\mathbf{A}}}, \;\; \mathbf{Y}^{(2,2,0)} = \mathbf{L}^*_{(2,2,0)}\overline{\overline{\mathbf{A}}},$$
$$\mathbf{Y}^{(2,2,1)} = \mathbf{L}^*_{(2,2,1)}\overline{\overline{\mathbf{A}}}, \;\; \mathbf{Y}^{(2,2,2)} = \mathbf{L}^*_{(2,2,2)}\overline{\overline{\mathbf{A}}},$$

where

$$\mathbf{L}^*_{(0,0)} = \begin{bmatrix} \mathbf{L}(x_0)\overline{\mathbf{L}}(x_0) \\ \mathbf{L}(x_1)\overline{\mathbf{L}}(x_1) \\ \vdots \\ \mathbf{L}(x_N)\overline{\mathbf{L}}(x_N) \end{bmatrix},$$

$$\mathbf{L}^*_{(1,0)} = \begin{bmatrix} \mathbf{L}(x_0)\mathbf{C}\overline{\mathbf{L}}(x_0) \\ \mathbf{L}(x_1)\mathbf{C}\overline{\mathbf{L}}(x_1) \\ \vdots \\ \mathbf{L}(x_N)\mathbf{C}\overline{\mathbf{L}}(x_N) \end{bmatrix},$$

$$\mathbf{L}^*_{(1,1)} = \begin{bmatrix} \mathbf{L}(x_0)\mathbf{C}\overline{\mathbf{L}}(x_0)\overline{\mathbf{C}} \\ \mathbf{L}(x_1)\mathbf{C}\overline{\mathbf{L}}(x_1)\overline{\mathbf{C}} \\ \vdots \\ \mathbf{L}(x_N)\mathbf{C}\overline{\mathbf{L}}(x_N)\overline{\mathbf{C}} \end{bmatrix},$$

$$\mathbf{L}^*_{(2,0)} = \begin{bmatrix} \mathbf{L}(x_0)\mathbf{C}^2\overline{\mathbf{L}}(x_0) \\ \mathbf{L}(x_1)\mathbf{C}^2\overline{\mathbf{L}}(x_1) \\ \vdots \\ \mathbf{L}(x_N)\mathbf{C}^2\overline{\mathbf{L}}(x_N) \end{bmatrix},$$

$$\mathbf{L}^*_{(2,1)} = \begin{bmatrix} \mathbf{L}(x_0)\mathbf{C}^2\overline{\mathbf{L}}(x_0)\overline{\mathbf{C}} \\ \mathbf{L}(x_1)\mathbf{C}^2\overline{\mathbf{L}}(x_1)\overline{\mathbf{C}} \\ \vdots \\ \mathbf{L}(x_N)\mathbf{C}^2\overline{\mathbf{L}}(x_N)\overline{\mathbf{C}} \end{bmatrix},$$

$$\mathbf{L}^*_{(2,2)} = \begin{bmatrix} \mathbf{L}(x_0)\mathbf{C}^2\overline{\mathbf{L}}(x_0)\overline{\mathbf{C}^2} \\ \mathbf{L}(x_1)\mathbf{C}^2\overline{\mathbf{L}}(x_1)\overline{\mathbf{C}^2} \\ \vdots \\ \mathbf{L}(x_N)\mathbf{C}^2\overline{\mathbf{L}}(x_N)\overline{\mathbf{C}^2} \end{bmatrix};$$

$$\mathbf{L}^*_{(0,0,0)} = \begin{bmatrix} \mathbf{L}(x_0)\overline{\mathbf{L}}(x_0)\overline{\overline{\mathbf{L}}}(x_0) \\ \mathbf{L}(x_1)\overline{\mathbf{L}}(x_1)\overline{\overline{\mathbf{L}}}(x_1) \\ \vdots \\ \mathbf{L}(x_N)\overline{\mathbf{L}}(x_N)\overline{\overline{\mathbf{L}}}(x_N) \end{bmatrix},$$

$$\mathbf{L}^*_{(1,0,0)} = \begin{bmatrix} \mathbf{L}(x_0)\mathbf{C}\overline{\mathbf{L}}(x_0)\overline{\overline{\mathbf{L}}}(x_0) \\ \mathbf{L}(x_1)\mathbf{C}\overline{\mathbf{L}}(x_1)\overline{\overline{\mathbf{L}}}(x_1) \\ \vdots \\ \mathbf{L}(x_N)\mathbf{C}\overline{\mathbf{L}}(x_N)\overline{\overline{\mathbf{L}}}(x_N) \end{bmatrix},$$

$$\mathbf{L}^*_{(1,1,0)} = \begin{bmatrix} \mathbf{L}(x_0)\mathbf{C}\overline{\mathbf{L}}(x_0)\overline{\mathbf{C}}\overline{\mathbf{L}}(x_0) \\ \mathbf{L}(x_1)\mathbf{C}\overline{\mathbf{L}}(x_1)\overline{\mathbf{C}}\overline{\mathbf{L}}(x_1) \\ \vdots \\ \mathbf{L}(x_N)\mathbf{C}\overline{\mathbf{L}}(x_N)\overline{\mathbf{C}}\overline{\overline{\mathbf{L}}}(x_N) \end{bmatrix},$$

$$\mathbf{L}^*_{(1,1,1)} = \begin{bmatrix} \mathbf{L}(x_0)\mathbf{C}\overline{\mathbf{L}}(x_0)\overline{\mathbf{C}}\overline{\overline{\mathbf{L}}}(x_0)\overline{\overline{\mathbf{C}}} \\ \mathbf{L}(x_1)\mathbf{C}\overline{\mathbf{L}}(x_1)\overline{\mathbf{C}}\overline{\overline{\mathbf{L}}}(x_1)\overline{\overline{\mathbf{C}}} \\ \vdots \\ \mathbf{L}(x_N)\mathbf{C}\overline{\mathbf{L}}(x_N)\overline{\mathbf{C}}\overline{\overline{\mathbf{L}}}(x_N)\overline{\overline{\mathbf{C}}} \end{bmatrix},$$

$$\mathbf{L}^*_{(2,0,0)} = \begin{bmatrix} \mathbf{L}(x_0)\mathbf{C}^2\overline{\mathbf{L}}(x_0)\overline{\overline{\mathbf{L}}}(x_0) \\ \mathbf{L}(x_1)\mathbf{C}^2\overline{\mathbf{L}}(x_1)\overline{\overline{\mathbf{L}}}(x_1) \\ \vdots \\ \mathbf{L}(x_N)\mathbf{C}^2\overline{\mathbf{L}}(x_N)\overline{\overline{\mathbf{L}}}(x_N) \end{bmatrix},$$

$$\mathbf{L}^*_{(2,1,0)} = \begin{bmatrix} \mathbf{L}(x_0)\mathbf{C}^2\overline{\mathbf{L}}(x_0)\overline{\mathbf{C}}\overline{\overline{\mathbf{L}}}(x_0) \\ \mathbf{L}(x_1)\mathbf{C}^2\overline{\mathbf{L}}(x_1)\overline{\mathbf{C}}\overline{\overline{\mathbf{L}}}(x_1) \\ \vdots \\ \mathbf{L}(x_N)\mathbf{C}^2\overline{\mathbf{L}}(x_N)\overline{\mathbf{C}}\overline{\overline{\mathbf{L}}}(x_N) \end{bmatrix},$$

$$\mathbf{L}^*_{(2,1,1)} = \begin{bmatrix} \mathbf{L}(x_0)\mathbf{C}^2\overline{\mathbf{L}}(x_0)\overline{\mathbf{C}}\overline{\overline{\mathbf{L}}}(x_0)\overline{\overline{\mathbf{C}}} \\ \mathbf{L}(x_1)\mathbf{C}^2\overline{\mathbf{L}}(x_1)\overline{\mathbf{C}}\overline{\overline{\mathbf{L}}}(x_1)\overline{\overline{\mathbf{C}}} \\ \vdots \\ \mathbf{L}(x_N)\mathbf{C}^2\overline{\mathbf{L}}(x_N)\overline{\mathbf{C}}\overline{\overline{\mathbf{L}}}(x_N)\overline{\overline{\mathbf{C}}} \end{bmatrix},$$

$$\mathbf{L}^*_{(2,2,0)} = \begin{bmatrix} \mathbf{L}(x_0)\mathbf{C}^2\overline{\mathbf{L}}(x_0)\overline{\mathbf{C}^2}\overline{\overline{\mathbf{L}}}(x_0) \\ \mathbf{L}(x_1)\mathbf{C}^2\overline{\mathbf{L}}(x_1)\overline{\mathbf{C}^2}\overline{\overline{\mathbf{L}}}(x_1) \\ \vdots \\ \mathbf{L}(x_N)\mathbf{C}^2\overline{\mathbf{L}}(x_N)\overline{\mathbf{C}^2}\overline{\overline{\mathbf{L}}}(x_N) \end{bmatrix},$$

$$\mathbf{L}^*_{(2,2,1)} = \begin{bmatrix} \mathbf{L}(x_0)\mathbf{C}^2\overline{\mathbf{L}}(x_0)\overline{\mathbf{C}^2}\overline{\overline{\mathbf{L}}}(x_0)\overline{\overline{\mathbf{C}}} \\ \mathbf{L}(x_1)\mathbf{C}^2\overline{\mathbf{L}}(x_1)\overline{\mathbf{C}^2}\overline{\overline{\mathbf{L}}}(x_1)\overline{\overline{\mathbf{C}}} \\ \vdots \\ \mathbf{L}(x_N)\mathbf{C}^2\overline{\mathbf{L}}(x_N)\overline{\mathbf{C}^2}\overline{\overline{\mathbf{L}}}(x_N)\overline{\overline{\mathbf{C}}} \end{bmatrix},$$

$$\mathbf{L}^*_{(2,2,2)} = \begin{bmatrix} \mathbf{L}(x_0)\mathbf{C}^2\overline{\mathbf{L}}(x_0)\overline{\mathbf{C}^2}\overline{\overline{\mathbf{L}}}(x_0)\overline{\overline{\mathbf{C}^2}} \\ \mathbf{L}(x_1)\mathbf{C}^2\overline{\mathbf{L}}(x_1)\overline{\mathbf{C}^2}\overline{\overline{\mathbf{L}}}(x_1)\overline{\overline{\mathbf{C}^2}} \\ \vdots \\ \mathbf{L}(x_N)\mathbf{C}^2\overline{\mathbf{L}}(x_N)\overline{\mathbf{C}^2}\overline{\overline{\mathbf{L}}}(x_N)\overline{\overline{\mathbf{C}^2}} \end{bmatrix}.$$

Then the fundamental matrix equation is gained from (5)-(13)

$$\sum_{k=0}^{2}\mathbf{P}_k\mathbf{L}\mathbf{A} + \sum_{p=0}^{2}\sum_{q=0}^{p}\mathbf{Q}_{pq}\mathbf{L}^*_{(p,q)}\overline{\mathbf{A}}$$
$$+ \sum_{p=0}^{2}\sum_{q=0}^{p}\sum_{r=0}^{q}\mathbf{Q}_{pqr}\mathbf{L}^*_{(p,q,r)}\overline{\overline{\mathbf{A}}} \qquad (14)$$
$$= \mathbf{G}, \quad 0 \le x \le b < \infty,$$

Briefly, we can write Eq.(14) as

$$\mathbf{W}\mathbf{A} + \mathbf{V}\overline{\mathbf{A}} + \mathbf{Z}\overline{\overline{\mathbf{A}}} = \mathbf{G}, \qquad (15)$$

where

$$\mathbf{W} = \sum_{k=0}^{2} \mathbf{P}_k \mathbf{L} = [w_{i,j}]; \ i,j = 0,1,...,N,$$

$$\mathbf{V} = \sum_{p=0}^{2} \sum_{q=0}^{p} \mathbf{Q}_{pq} \mathbf{L}^*_{(p,q)} = [v_{i,j}]_{(N+1) \times (N+1)^2},$$

$$\mathbf{Z} = \sum_{p=0}^{2} \sum_{q=0}^{p} \sum_{r=0}^{q} \mathbf{Q}_{pqr} \mathbf{L}^*_{(p,q,r)} = [z_{i,j}]_{(N+1) \times (N+1)^3},$$

Moreover, fundamental matrix equation (15) can be written in the augmented matrix form

$$[\mathbf{W}; \mathbf{V}; \mathbf{Z} : \mathbf{G}]. \tag{16}$$

3.1. Matrix representation of the conditions

Let us define the matrix form of the conditions given by (2) can be written as

$$\text{for} \ \ j = 0, \ \ \mathbf{U}_0 = [y^{(0)}(0)] = \mathbf{L}(0),$$
$$\text{for} \ \ j = 1, \ \ \mathbf{U}_1 = [y^{(1)}(0)] = \mathbf{L}(0)\mathbf{C}.$$

Then, we have

$$\mathbf{U} = \begin{bmatrix} \mathbf{U}_0 \\ \mathbf{U}_1 \end{bmatrix}_{2 \times (N+1)},$$

$$\mathbf{O}_2 = \begin{bmatrix} 0 & 0 & \cdots & 0 \\ 0 & 0 & \cdots & 0 \end{bmatrix}_{2 \times (N+1)^2},$$

$$\mathbf{O}_3 = \begin{bmatrix} 0 & 0 & \cdots & 0 \\ 0 & 0 & \cdots & 0 \end{bmatrix}_{2 \times (N+1)^3},$$

or briefly,

$$[\mathbf{U}; \mathbf{O}_2; \mathbf{O}_3 : \lambda_j]. \tag{17}$$

Consequently, in order to find the Laguerre coefficients $a_n, (n = 0, 1, ..., N)$ related with the approximate solution (3) of the problem (1)-(2), by replacing the 2 row matrices (17) by the last 2 rows (or any 2 rows) of the augmented matrix (16), we obtain new augmented matrix

$$[\widetilde{\mathbf{W}}; \widetilde{\mathbf{V}}; \widetilde{\mathbf{Z}} : \widetilde{\mathbf{G}}]. \tag{18}$$

Thence the unknown Laguerre coefficients are calculated by solving (18) [7]- [8]. Therefore, the Laguerre polynomial solution can be acquired as

$$y_N(x) = \sum_{n=0}^{N} a_n L_n(x).$$

4. Error analysis

Definition 1 (Residual function). *We define the residual function $R_N(x_\alpha)$ for $x = x_\alpha \in [0,b]$*

$$R_N(x_\alpha) = \sum_{k=0}^{2} P_k(x_\alpha) y^{(k)}(x_\alpha)$$

$$+ \sum_{p=0}^{2} \sum_{q=0}^{p} Q_{pq}(x_\alpha) y^{(p)}(x_\alpha) y^{(q)}(x_\alpha)$$

$$+ \sum_{p=0}^{2} \sum_{q=0}^{p} \sum_{r=0}^{q} Q_{pqr}(x_\alpha) y^{(p)}(x_\alpha) y^{(q)}(x_\alpha) y^{(r)}(x_\alpha)$$

$$- g(x_\alpha) \cong 0$$

or

$$R_N(x_\alpha) \leq 10^{-k_\alpha}, \quad \text{for} \ k_\alpha \in \mathbb{Z}^+.$$

Then $|R_N(x_\alpha)|$ is called as the residual function on the interval $[0,b]$.

Theorem 1. *$|R_N(x_\alpha)|$ is the residual function on the interval $[0,b]$. Then*

$$\left| \int_0^b R_N(x)dx \right| \leq \int_0^b |R_N(x)| \, dx$$

So, that the upper bound of the mean error $\overline{R}_n$ is

$$|R_N(x)| \leq \frac{\int_0^b |R_N|(x)dx}{b} = \overline{R}_n.$$

Proof. In order to see the proof briefly, we consider the Mean Value Theorem and the definition below. Then

$$\left| \int_0^b R_N(x)dx \right| \leq \int_0^b |R_N(x)| \, dx$$

$$\left| \int_0^b R_N(x)dx \right| \leq b \, |R_N(c)|, \quad 0 \leq c \leq b$$

$$\left| \int_0^b R_N(x)dx \right| \leq b \, |R_N(c)| \leq \int_a^b |R_N(x)| \, dx$$

$$|R_N(x)| \leq \frac{\int_0^b |R_N|(x)dx}{b} = \overline{R}_n$$

$\square$

4.1. Algorithm

- **Step 0.** Input initial data: $P_k(x), Q_{pq}(x), Q_{pqr}(x)$ and $g(x)$. Determine the mixed conditions.

- **Step 1.** Set N where $N \in \mathbb{N}$.

- **Step 2.** Construct the matrices $\mathbf{L}(x), \mathbf{C}, \overline{\mathbf{L}}(x), \overline{\mathbf{C}}, \overline{\overline{\mathbf{L}}}(x), \overline{\overline{\mathbf{C}}}$ and $\mathbf{G}$ then $\mathbf{W}, \mathbf{V}, \mathbf{Z}$.

- **Step 3.** Define the collocation points $x_i = \frac{b}{N}i, \ i = 0, 1, ..., N$.

- **Step 4.** Compute $[\mathbf{W}; \mathbf{V}; \mathbf{Z} : \mathbf{G}]$.

- **Step 5.** Compute $[\mathbf{U}; \mathbf{O}_2; \mathbf{O}_3 : \lambda_j]$.

- **Step 6.** Construct the augmented matrix $[\tilde{\mathbf{W}}; \tilde{\mathbf{V}}; \tilde{\mathbf{Z}} : \tilde{\mathbf{G}}]$.

- **Step 7.** Input: the augmented matrix arguments, forward elimination, back substitution. Output: $\mathbf{A}$ (Solve the system by Gaussian elimination method).

- **Step 8.** Put arguments a_n in the truncated Laguerre series form.

- **Step 9.** Output data: the approximate solution $y_N(x)$.

- **Step 10.** Construct $y(x)$ is the exact solution of (1).

- **Step 11.** Stop when $R_N(x) \leq 10^{-k}$ where $k \in \mathbb{Z}^+$. Otherwise, increase N and return to Step 1.

5. Illustrative examples

In this section, some examples will be given to show applicability of our method. All the problems have been calculated and plotted by using Maple18 and MatlabR2014b.

Example 1. *First, we consider the second-order nonlinear ordinary differential equation with quadratic terms*

$$y''(x) + 2y'(x) + y(x) + y^2(x) - y''(x)y'(x) = 12\exp(x) + 2 \tag{19}$$

with the initial conditions

$$y(0) = 3, \quad y'(0) = 2. \tag{20}$$

The exact solution of (19)-(20) is $y(x) = 1 + 2\exp(x)$.

Table 1. $|R_N|$ comparison of Example 1. for different N values.

x	$|R_2|$	$|R_4|$	$|R_5|$
(0.0)	0.000000	0.000000	0.000000
(0.1)	0.341836E-4	0.530766E-5	0.450128E-6
(0.2)	0.280551E-3	0.281048E-4	0.194988E-5
(0.3)	0.971761E-3	0.563571E-4	0.318105E-5
(0.4)	0.236493E-3	0.671672E-4	0.339969E-5
(0.5)	0.474425E-2	0.525094E-4	0.365512E-5
(0.6)	0.842376E-2	0.476701E-4	0.530256E-5
(0.7)	0.137505E-2	0.162679E-3	0.552450E-5
(0.8)	0.211081E-1	0.617047E-3	0.104534E-4
(0.9)	0.309206E-1	0.177815E-2	0.808003E-4
(1.0)	0.436563E-1	0.420369E-2	0.282554E-3

Example 2. *Now, we consider the second-order nonlinear ordinary differential equation with cubic terms,*

$$y''(x) - y'(x)(1 - y^2(x)) + y(x) = (2 + \sin(x))\cos(x)\sin(x) + 1 \tag{21}$$

with the initial conditions

$$y(0) = y'(0) = 1. \tag{22}$$

The exact solution of (21)-(22) is $y(x) = 1 + \sin(x)$.

Table 2. $|R_N|$ comparison of Example 2. for different N values.

x	$|R_2|$	$|R_4|$	$|R_6|$
(0.0)	0.000000	0.000000	0.000000
(0.1)	0.516658E-7	0.554530E-9	0.551083E-12
(0.2)	0.213306E-8	0.243668E-10	0.241721E-11
(0.3)	0.494797E-8	0.597486E-10	0.593143E-11
(0.4)	0.905816E-8	0.114974E-10	0.114344E-11
(0.5)	0.145574E-8	0.193316E-10	0.192602E-11
(0.6)	0.215357E-8	0.298030E-9	0.297203E-11
(0.7)	0.300782E-7	0.432339E-9	0.430863E-10
(0.8)	0.402643E-7	0.599433E-9	0.595716E-10
(0.9)	0.521673E-7	0.802455E-9	0.793115E-10
(1.0)	0.658529E-7	0.444952E-8	0.234134E-9

6. Conclusion

In this study, we introduce a matrix method depending on Laguerre polynomials in order to solve a class of second-order nonlinear ordinary differential equations having quadratic and cubic terms numerically. Furthermore, the error analysis is given to show the accuracy of the method. The present method and its error analysis are applied

on some illustrative examples which have been shown by the tables.

The method has some significant advantages such as;

- The present method has short and concise computing procedure by writing the algorithm in Maple18.
- The technique gives an alternative way of solution to the second-order nonlinear ordinary differential equations which varies the other methods in literature.
- The present method has sufficient results when N is chosen large enough.

The method also can be developed and applied to differential functional integral equations, nonlinear functional integral equations and functional systems but some modifications are required [9]-[10].

References

[1] Fried, I. (1979). *Numerical solution of differential equations.* Academic Press, New York.

[2] Kells, L.M. (1960). *Elementary differential equations.* ISBN 07-033530-3.

[3] Jordan, D.W. and Smith, P. (2007). *Nonlinear ordinary differential equations: an introduction for Scientists and Engineers*, Fourth Edition. Oxford University Press, New York.

[4] King, A.C., Billingham, J. and Otto, S.R. (2003). *Differential equations: linear, nonlinear, ordinary, partial*, Cambridge University Press, New York.

[5] Rawashdeh, M.S. and Maitama, S. (2015). Solving nonlinear ordinary differential equations using the NDM. *Journal of Applied Analysis and Computation*, 5(1), 77-88.

[6] Yüksel, G., Gülsu, M. and Sezer, M. (2011). Chebyshev polynomial solutions of a class of second-order nonlinear ordinary differential equations. *Journal of Advanced Research in Scientific Computing*, 3(4), 11-24.

[7] Gürbüz, B. and Sezer, M. (2016). Laguerre polynomial solutions of a class of initial and boundary value problems arising in science and engineering fields. *Acta Physica Polonica A*, 130(1), 194-197.

[8] Gürbüz, B. and Sezer, M. (2014). Laguerre polynomial approach for solving Lane-Emden type functional differential equations. *Applied Mathematics and Computation*, 242, 255-264.

[9] Bülbül, B. and Sezer, M. (2013). Numerical solution of Duffing equation by using an improved Taylor matrix method. *Journal of Applied Mathematics*, 2013, 691614.

[10] Inc, M., Akgul, A. and Kılıçman, A. (2013). Numerical solutions of the second-order one-dimensional telegraph equation based on reproducing kernel Hilbert space method. *Abstract and Applied Analysis*, 2013, Hindawi.

Burcu Gürbüz *received her Ph.D. from the Department of Mathematics of Celal Bayar University in 2017 under the supervision of Prof. Dr. Mehmet SEZER in Applied Mathematics. Recently, she has been awarded as "2019 Young Visiting Research Fellow" from the Embassy of France and currently, she is a post-doctoral researcher at Institution of Mathematics in Johannes Gutenberg-University Mainz. She has worked as investigator in several national and international scientific research projects. Her main research interests ordinary and partial differential equations, integral and integro differential-difference equations, numerical methods, mathematical biology models and scientific computation. Ms. Gürbüz is a member of Turkish Math Society (TMD), Society for Mathematical Biology and European Society for Mathematical and Theoretical Biology (ESMTB).*
http://orcid.org/0000-0002-4253-5877

Mehmet Sezer *received his Ph.D. under the supervision of Prof. Dr. Süeda MORALI in the Department of Applied Mathematics at Ege University in 1982 and studied in the field of "Parabolic partial differential equations". In 1982, he was Assistant Professor at Faculty of Education (Balıkesir) of Uludağ University, Associate Professor in 1989, in 1995 Professor at Faculty of Education of Dokuz Eylül University. In 2004, Mathematics Professor at Faculty of Science at Muğla University and since 2012, he has been Applied Mathematics Professor at Faculty of Science at Celal Bayar University. His main research interests are ordinary and partial differential equations, integral and integro differential-difference equations, delay differential equations and their numerical solutions. Prof. Sezer has been reviewer for numerous influential journals, has published research articles related to differential equations, linear algebra, analytic geometry and calculus; and has been authored over 100 papers.*
http://orcid.org/0000-0002-7744-2574

RESEARCH ARTICLE

Fractional trapezium type inequalities for twice differentiable preinvex functions and their applications

Artion Kashuri[*] and Rozana Liko

Department of Mathematics, Faculty of Technical Science, University Ismail Qemali, Vlora, Albania
artionkashuri@gmail.com, rozanaliko86@gmail.com

ARTICLE INFO	ABSTRACT
	Trapezoidal inequalities for functions of divers natures are useful in numerical computations. The authors have proved an identity for a generalized integral operator via twice differentiable preinvex function. By applying the established identity, the generalized trapezoidal type integral inequalities have been discovered. It is pointed out that the results of this research provide integral inequalities for almost all fractional integrals discovered in recent past decades. Various special cases have been identified. Some applications of presented results to special means have been analyzed. The ideas and techniques of this paper may stimulate further research.

1. Introduction

The following inequality, named Hermite–Hadamard inequality, is one of the most famous inequalities in the literature for convex functions.

Theorem 1. *Let $f : I \subseteq \mathbb{R} \longrightarrow \mathbb{R}$ be a convex function and $a_1, a_2 \in I$ with $a_1 < a_2$. Then the following inequality holds:*

$$f\left(\frac{a_1 + a_2}{2}\right) \le \frac{1}{a_2 - a_1} \int_{a_1}^{a_2} f(x)dx \qquad (1)$$
$$\le \frac{f(a_1) + f(a_2)}{2}.$$

This inequality (1) is also known as trapezium inequality.

The trapezium inequality has remained an area of great interest due to its wide applications in the field of mathematical analysis. Authors of recent decades have studied (1) in the premises of newly invented definitions due to motivation of convex function. Interested readers see the references [1]–[16], [19, 20, 22, 23].

The aim of this paper is to establish trapezoidal type generalized integral inequalities for preinvex

functions. Interestingly, the special cases of presented results, are fractional integral inequalities. Therefore, it is important to summarize the study of fractional integrals. Let us recall some special functions and evoke some basic definitions as follows:

Definition 1. *[13] Let $f \in L[a_1, a_2]$. Then k–fractional integrals of order $\alpha, k > 0$ with $a_1 \ge 0$ are defined by*

$$I_{a_1^+}^{\alpha,k} f(x) = \frac{1}{k\Gamma_k(\alpha)} \int_{a_1}^x (x-t)^{\frac{\alpha}{k}-1} f(t)dt, \quad x > a_1$$

and

$$I_{a_2^-}^{\alpha,k} f(x) = \frac{1}{k\Gamma_k(\alpha)} \int_x^{a_2} (t-x)^{\frac{\alpha}{k}-1} f(t)dt, \quad a_2 > x.$$

For $k = 1$, k–fractional integrals give Riemann–Liouville integrals. For $\alpha = k = 1$, k–fractional integrals give classical integrals.

Definition 2. *[21] A set $S \subseteq \mathbb{R}^n$ is said to be invex set with respect to the mapping $\eta : S \times S \longrightarrow \mathbb{R}^n$, if $x + t\eta(y, x) \in S$ for every $x, y \in S$ and $t \in [0, 1]$.*

The invex set also termed as, an η–connected set.

---

*Corresponding Author

Definition 3. *Let $S \subseteq \mathbb{R}^n$ be an invex set with respect to $\eta : S \times S \longrightarrow \mathbb{R}^n$. A function $f : S \longrightarrow [0, +\infty)$ is said to be preinvex with respect to η, if for every $x, y \in S$ and $t \in [0, 1]$,*

$$f\big(x + t\eta(y, x)\big) \le (1 - t)f(x) + tf(y). \quad (2)$$

Also, let define a function $\varphi : [0, +\infty) \longrightarrow [0, +\infty)$ satisfying the following conditions:

$$\int_0^1 \frac{\varphi(t)}{t} dt < +\infty, \quad (3)$$

$$\frac{1}{A} \le \frac{\varphi(s)}{\varphi(r)} \le A \text{ for } \frac{1}{2} \le \frac{s}{r} \le 2 \quad (4)$$

$$\frac{\varphi(r)}{r^2} \le B \frac{\varphi(s)}{s^2} \text{ for } s \le r \quad (5)$$

$$\left| \frac{\varphi(r)}{r^2} - \frac{\varphi(s)}{s^2} \right| \le C|r - s| \frac{\varphi(r)}{r^2} \text{ for } \frac{1}{2} \le \frac{s}{r} \le 2, \quad (6)$$

where $A, B, C > 0$ are independent of $r, s > 0$. If $\varphi(r)r^\alpha$ is increasing for some $\alpha \ge 0$ and $\frac{\varphi(r)}{r^\beta}$ is decreasing for some $\beta \ge 0$, then φ satisfies (3)–(6), see [18]. Therefore, the left–sided and right–sided generalized integral operators are defined as follows:

$$_{a_1^+}I_\varphi f(x) = \int_{a_1}^x \frac{\varphi(x - t)}{x - t} f(t)dt, \quad x > a_1,$$

$$_{a_2^-}I_\varphi f(x) = \int_x^{a_2} \frac{\varphi(t - x)}{t - x} f(t)dt, \quad x < a_2.$$

The most important feature of generalized integrals is that; they produce Riemann–Liouville fractional integrals, k–Riemann–Liouville fractional integrals, Katugampola fractional integrals, conformable fractional integrals, Hadamard fractional integrals, etc.

Motivated by the above literatures, the main objective of this paper is to discover in section 2, an interesting identity in order to study some new bounds regarding general trapezoidal type integral inequalities. By using the established identity as an auxiliary result, some new estimates for trapezoidal type integral inequalities via generalized integrals are obtained. It is pointed out that some new fractional integral inequalities have been deduced from main results. In section 3, some applications to special means are given. In section 4, a briefly conclusion is provided as well. The ideas and techniques of this paper may stimulate further research in the field of integral inequalities.

2. Main results

Throughout this study, let $P = [ma_1, a_2]$ with $a_1 < a_2$, $m \in (0, 1]$ be an invex subset with respect to $\eta : P \times P \longrightarrow \mathbb{R}$. Also, for brevity, we define

$$\Lambda_{m,n}^{(1)}(t) = \int_0^t \Delta_{m,n}^{(1)}(s)ds, \quad (7)$$

$$\Delta_{m,n}^{(1)}(s) = \int_0^s \frac{\varphi\left(\frac{\eta(x,ma_1)}{n+1}u\right)}{u} du < +\infty, \quad (8)$$

where $\eta(x, ma_1) > 0$ and

$$\Lambda_{m,n}^{(2)}(t) = \int_0^t \Delta_{m,n}^{(2)}(s)ds, \quad (9)$$

$$\Delta_{m,n}^{(2)}(s) = \int_0^s \frac{\varphi\left(\frac{\eta(a_2,mx)}{n+1}u\right)}{u} du < +\infty, \quad (10)$$

where $\eta(a_2, mx) > 0$.

For establishing some new results regarding general fractional integrals we need to prove the following lemma.

Lemma 1. *Let $f : P \longrightarrow \mathbb{R}$ be a twice differentiable mapping on (ma_1, a_2). If $f'' \in L(P)$, then the following identity for generalized fractional integrals hold:*

$$\frac{\eta(x, ma_1)\Lambda_{m,n}^{(1)}(1)}{(n+1)\Delta_{m,n}^{(1)}(1)}$$

$$\times \frac{f'(ma_1) + f'(ma_1 + \eta(x, ma_1))}{2}$$

$$- \frac{f(ma_1) + f(ma_1 + \eta(x, ma_1))}{2} - \frac{1}{2\Delta_{m,n}^{(1)}(1)}$$

$$\times \left[_{(ma_1)^+}I_\varphi f\left(ma_1 + \frac{\eta(x, ma_1)}{n+1}\right) \right.$$

$$\left. + _{(ma_1 + \eta(x,ma_1))^-}I_\varphi f\left(ma_1 + \frac{n}{n+1}\eta(x, ma_1)\right) \right]$$

$$+ \frac{\eta(a_2, mx)\Lambda_{m,n}^{(2)}(1)}{(n+1)\Delta_{m,n}^{(2)}(1)}$$

$$\times \frac{f'(mx) + f'(mx + \eta(a_2, mx))}{2}$$

$$- \frac{f(mx) + f(mx + \eta(a_2, mx))}{2} - \frac{1}{2\Delta_{m,n}^{(2)}(1)}$$

$$\times \left[_{(mx)^+}I_\varphi f\left(mx + \frac{\eta(a_2, mx)}{n+1}\right) \right.$$

$$\left. + _{(mx + \eta(a_2,mx))^-}I_\varphi f\left(mx + \frac{n}{n+1}\eta(a_2, mx)\right) \right]$$

$$= \frac{\eta^2(x, ma_1)}{2(n+1)^2 \Delta_{m,n}^{(1)}(1)} \quad (11)$$

$$\times \int_0^1 \Lambda_{m,n}^{(1)}(t) \left[f''\left(ma_1 + \frac{(n+t)}{n+1}\eta(x, ma_1)\right) \right.$$

$$\left. - f''\left(ma_1 + \frac{(1-t)}{n+1}\eta(x, ma_1)\right) \right] dt$$

$$+\frac{\eta^2(a_2,mx)}{2(n+1)^2\Delta_{m,n}^{(2)}(1)}$$

$$\times\int_0^1\Lambda_{m,n}^{(2)}(t)\left[f''\left(mx+\frac{(n+t)}{n+1}\eta(a_2,mx)\right)\right.$$

$$\left.-f''\left(mx+\frac{(1-t)}{n+1}\eta(a_2,mx)\right)\right]dt.$$

We denote

$$I_{f,\Lambda_{m,n}^{(1)},\Lambda_{m,n}^{(2)},\Delta_{m,n}^{(1)},\Delta_{m,n}^{(2)}}(x,a_1,a_2)$$

$$=\frac{\eta^2(x,ma_1)}{2(n+1)^2\Delta_{m,n}^{(1)}(1)} \qquad (12)$$

$$\times\int_0^1\Lambda_{m,n}^{(1)}(t)\left[f''\left(ma_1+\frac{(n+t)}{n+1}\eta(x,ma_1)\right)\right.$$

$$\left.-f''\left(ma_1+\frac{(1-t)}{n+1}\eta(x,ma_1)\right)\right]dt$$

$$+\frac{\eta^2(a_2,mx)}{2(n+1)^2\Delta_{m,n}^{(2)}(1)}$$

$$\times\int_0^1\Lambda_{m,n}^{(2)}(t)\left[f''\left(mx+\frac{(n+t)}{n+1}\eta(a_2,mx)\right)\right.$$

$$\left.-f''\left(mx+\frac{(1-t)}{n+1}\eta(a_2,mx)\right)\right]dt.$$

Proof. Integrating by parts twice (12) and changing the variables of integration, we have

$$I_{f,\Lambda_{m,n}^{(1)},\Lambda_{m,n}^{(2)},\Delta_{m,n}^{(1)},\Delta_{m,n}^{(2)}}(x,a_1,a_2)$$

$$=\frac{\eta^2(x,ma_1)}{2(n+1)^2\Delta_{m,n}^{(1)}(1)}$$

$$\times\left\{\left.\frac{(n+1)\Lambda_{m,n}^{(1)}(t)f'\left(ma_1+\frac{(n+t)}{n+1}\eta(x,ma_1)\right)}{\eta(x,ma_1)}\right|_0^1\right.$$

$$-\frac{(n+1)}{\eta(x,ma_1)}$$

$$\times\int_0^1\Delta_{m,n}^{(1)}(t)f'\left(ma_1+\frac{(n+t)}{n+1}\eta(x,ma_1)\right)dt$$

$$+\left.\frac{(n+1)\Lambda_{m,n}^{(1)}(t)f'\left(ma_1+\frac{(1-t)}{n+1}\eta(x,ma_1)\right)}{\eta(x,ma_1)}\right|_0^1$$

$$-\frac{(n+1)}{\eta(x,ma_1)}$$

$$\times\int_0^1\Delta_{m,n}^{(1)}(t)f'\left(ma_1+\frac{(1-t)}{n+1}\eta(x,ma_1)\right)dt\right\}$$

$$+\frac{\eta^2(a_2,mx)}{2(n+1)^2\Delta_{m,n}^{(2)}(1)}$$

$$\times\left\{\left.\frac{(n+1)\Lambda_{m,n}^{(2)}(t)f'\left(mx+\frac{(n+t)}{n+1}\eta(a_2,mx)\right)}{\eta(a_2,mx)}\right|_0^1\right.$$

$$-\frac{(n+1)}{\eta(a_2,mx)}$$

$$\times\int_0^1\Delta_{m,n}^{(2)}(t)f'\left(mx+\frac{(n+t)}{n+1}\eta(a_2,mx)\right)dt$$

$$+\left.\frac{(n+1)\Lambda_{m,n}^{(2)}(t)f'\left(mx+\frac{(1-t)}{n+1}\eta(a_2,mx)\right)}{\eta(a_2,mx)}\right|_0^1$$

$$-\frac{(n+1)}{\eta(a_2,mx)}$$

$$\left.\times\int_0^1\Delta_{m,n}^{(2)}(t)f'\left(mx+\frac{(1-t)}{n+1}\eta(a_2,mx)\right)dt\right\}$$

$$=\frac{\eta^2(x,ma_1)}{2(n+1)^2\Lambda_{m,n}^{(1)}(1)}$$

$$\times\left\{\frac{(n+1)\Lambda_{m,n}^{(1)}(1)f'\left(ma_1+\eta(x,ma_1)\right)}{\eta(x,ma_1)}\right.$$

$$-\frac{(n+1)}{\eta(x,ma_1)}$$

$$\times\left[\frac{(n+1)\Delta_{m,n}^{(1)}(1)f\left(ma_1+\eta(x,ma_1)\right)}{\eta(x,ma_1)}\right.$$

$$-\frac{(n+1)}{\eta(x,ma_1)}$$

$$\left.\times\,_{(ma_1+\eta(x,ma_1))^-}I_\varphi f\left(ma_1+\frac{n}{n+1}\eta(x,ma_1)\right)\right]$$

$$+\frac{(n+1)\Lambda_{m,n}^{(1)}(1)f'\left(ma_1\right)}{\eta(x,ma_1)}$$

$$-\frac{(n+1)}{\eta(x,ma_1)}\times\left[\frac{(n+1)\Delta_{m,n}^{(1)}(1)f\left(ma_1\right)}{\eta(x,ma_1)}\right.$$

$$\left.\left.-\frac{(n+1)}{\eta(x,ma_1)}\times\,_{(ma_1)^+}I_\varphi f\left(ma_1+\frac{\eta(x,ma_1)}{n+1}\right)\right]\right\}$$

$$+\frac{\eta^2(a_2,mx)}{2(n+1)^2\Lambda_{m,n}^{(2)}(1)}$$

$$\times\left\{\frac{(n+1)\Lambda_{m,n}^{(2)}(1)f'\left(mx+\eta(a_2,mx)\right)}{\eta(a_2,mx)}\right.$$

$$-\frac{(n+1)}{\eta(a_2,mx)}$$

$$\times\left[\frac{(n+1)\Delta_{m,n}^{(2)}(1)f\left(mx+\eta(a_2,mx)\right)}{\eta(a_2,mx)}\right.$$

$$-\frac{(n+1)}{\eta(a_2,mx)}$$

$$\left.\times\,_{(mx+\eta(a_2,mx))^-}I_\varphi f\left(mx+\frac{n}{n+1}\eta(a_2,mx)\right)\right]$$

$$+\frac{(n+1)\Lambda_{m,n}^{(2)}(1)f'\left(mx\right)}{\eta(a_2,mx)}-\frac{(n+1)}{\eta(a_2,mx)}$$

$$\times\left[\frac{(n+1)\Delta_{m,n}^{(2)}(1)f(mx)}{\eta(a_2,mx)}\right.$$

$$-\frac{(n+1)}{\eta(a_2,mx)}\times {}_{(mx)^+}I_\varphi f\left(mx+\frac{\eta(a_2,mx)}{n+1}\right)\bigg\}$$

$$=\frac{\eta(x,ma_1)\Lambda_{m,n}^{(1)}(1)}{(n+1)\Delta_{m,n}^{(1)}(1)}$$

$$\times\frac{f'(ma_1)+f'(ma_1+\eta(x,ma_1))}{2}$$

$$-\frac{f(ma_1)+f(ma_1+\eta(x,ma_1))}{2}-\frac{1}{2\Delta_{m,n}^{(1)}(1)}$$

$$\times\left[{}_{(ma_1)^+}I_\varphi f\left(ma_1+\frac{\eta(x,ma_1)}{n+1}\right)\right.$$

$$\left.+{}_{(ma_1+\eta(x,ma_1))^-}I_\varphi f\left(ma_1+\frac{n}{n+1}\eta(x,ma_1)\right)\right]$$

$$+\frac{\eta(a_2,mx)\Lambda_{m,n}^{(2)}(1)}{(n+1)\Delta_{m,n}^{(2)}(1)}$$

$$\times\frac{f'(mx)+f'(mx+\eta(a_2,mx))}{2}$$

$$-\frac{f(mx)+f(mx+\eta(a_2,mx))}{2}-\frac{1}{2\Delta_{m,n}^{(2)}(1)}$$

$$\times\left[{}_{(mx)^+}I_\varphi f\left(mx+\frac{\eta(a_2,mx)}{n+1}\right)\right.$$

$$\left.+{}_{(mx+\eta(a_2,mx))^-}I_\varphi f\left(mx+\frac{n}{n+1}\eta(a_2,mx)\right)\right].$$

The proof of Lemma 1 is completed. $\square$

Remark 1. *Taking* $m=1, n=0, x=\frac{a_1+a_2}{2}$, $\eta(x,ma_1)=x-ma_1$, $\eta(a_2,mx)=a_2-mx$ *and* $\varphi(t)=t$ *in Lemma 1, we get*

$$I_{f,\Lambda_{1,0}^{(1)},\Lambda_{1,0}^{(2)},\Delta_{1,0}^{(1)},\Delta_{1,0}^{(2)}}\left(\frac{a_1+a_2}{2},a_1,a_2\right)$$

$$=\left(\frac{a_2-a_1}{2}\right)\qquad(13)$$

$$\times\left[\frac{f'(a_1)+2f'\left(\frac{a_1+a_2}{2}\right)+f'(a_2)}{2}\right]$$

$$-\left[\frac{f(a_1)+2f\left(\frac{a_1+a_2}{2}\right)+f(a_2)}{2}\right]$$

$$-\frac{2}{(a_2-a_1)}\int_{a_1}^{a_2}f(t)dt.$$

Theorem 2. *Let* $f:P\longrightarrow\mathbb{R}$ *be a twice differentiable mapping on* (ma_1,a_2). *If* $|f''|^q$ *is preinvex on* P *for* $q>1$ *and* $p^{-1}+q^{-1}=1$, *then the following inequality for generalized fractional integrals hold:*

$$\left|I_{f,\Lambda_{m,n}^{(1)},\Lambda_{m,n}^{(2)},\Delta_{m,n}^{(1)},\Delta_{m,n}^{(2)}}(x,a_1,a_2)\right|$$

$$\leq\frac{\eta^2(x,ma_1)}{2(n+1)^2\sqrt[q]{2(n+1)}\Delta_{m,n}^{(1)}(1)}\qquad(14)$$

$$\times\sqrt[p]{B_{\Lambda_{m,n}^{(1)}}(p)}$$

$$\times\left\{\sqrt[q]{|f''(ma_1)|^q+(2n+1)|f''(x)|^q}\right.$$

$$\left.+\sqrt[q]{(2n+1)|f''(ma_1)|^q+|f''(x)|^q}\right\}$$

$$+\frac{\eta^2(a_2,mx)}{2(n+1)^2\sqrt[q]{2(n+1)}\Delta_{m,n}^{(2)}(1)}\sqrt[p]{B_{\Lambda_{m,n}^{(2)}}(p)}$$

$$\times\left\{\sqrt[q]{|f''(mx)|^q+(2n+1)|f''(a_2)|^q}\right.$$

$$\left.+\sqrt[q]{(2n+1)|f''(mx)|^q+|f''(a_2)|^q}\right\},$$

where

$$B_{\Lambda_{m,n}^{(i)}}(p)=\int_0^1\left[\Lambda_{m,n}^{(i)}(t)\right]^p dt,\quad\forall i=1,2.\quad(15)$$

Proof. From Lemma 1, preinvexity of $|f''|^q$, Hölder's inequality and properties of the modulus, we have

$$\left|I_{f,\Lambda_{m,n}^{(1)},\Lambda_{m,n}^{(2)},\Delta_{m,n}^{(1)},\Delta_{m,n}^{(2)}}(x,a_1,a_2)\right|$$

$$\leq\frac{\eta^2(x,ma_1)}{2(n+1)^2\Delta_{m,n}^{(1)}(1)}$$

$$\times\left\{\int_0^1\Lambda_{m,n}^{(1)}(t)\left[\left|f''\left(ma_1+\frac{(n+t)}{n+1}\eta(x,ma_1)\right)\right|\right.\right.$$

$$\left.\left.+\left|f''\left(ma_1+\frac{(1-t)}{n+1}\eta(x,ma_1)\right)\right|\right]dt\right\}$$

$$+\frac{\eta^2(a_2,mx)}{2(n+1)^2\Delta_{m,n}^{(2)}(1)}$$

$$\times\left\{\int_0^1\Lambda_{m,n}^{(2)}(t)\left[\left|f''\left(mx+\frac{(1-t)}{n+1}\eta(a_2,mx)\right)\right|\right.\right.$$

$$\left.\left.+\left|f''\left(mx+\frac{(n+t)}{n+1}\eta(a_2,mx)\right)\right|\right]dt\right\}$$

$$\leq\frac{\eta^2(x,ma_1)}{2(n+1)^2\Delta_{m,n}^{(1)}(1)}\left(\int_0^1\left[\Lambda_{m,n}^{(1)}(t)\right]^p dt\right)^{\frac{1}{p}}$$

$$\times\left\{\left(\int_0^1\left|f''\left(ma_1+\frac{(n+t)}{n+1}\eta(x,ma_1)\right)\right|^q dt\right)^{\frac{1}{q}}\right.$$

$$\left.+\left(\int_0^1\left|f''\left(ma_1+\frac{(1-t)}{n+1}\eta(x,ma_1)\right)\right|^q dt\right)^{\frac{1}{q}}\right\}$$

$$+\frac{\eta^2(a_2,mx)}{2(n+1)^2\Delta_{m,n}^{(2)}(1)}\left(\int_0^1\left[\Lambda_{m,n}^{(2)}(t)\right]^p dt\right)^{\frac{1}{p}}$$

$$\times\left\{\left(\int_0^1\left|f''\left(mx+\frac{(1-t)}{n+1}\eta(a_2,mx)\right)\right|^q dt\right)^{\frac{1}{q}}\right.$$

$$+\left(\int_0^1\left|f''\left(mx+\frac{(n+t)}{n+1}\eta(a_2,mx)\right)\right|^q dt\right)^{\frac{1}{q}}\Bigg\}$$

$$\leq\frac{\eta^2(x,ma_1)}{2(n+1)^2\Delta_{m,n}^{(1)}(1)}\sqrt[p]{B_{\Lambda_{m,n}^{(1)}}(p)}$$

$$\times\Bigg\{\left[\int_0^1\left[\left(1-\frac{n+t}{n+1}\right)|f''(ma_1)|^q\right.\right.$$

$$\left.\left.+\frac{(n+t)}{n+1}|f''(x)|^q\right]dt\right]^{\frac{1}{q}}$$

$$+\left[\int_0^1\left[\left(1-\frac{1-t}{n+1}\right)|f''(ma_1)|^q\right.\right.$$

$$\left.\left.+\frac{(1-t)}{n+1}|f''(x)|^q\right]dt\right]^{\frac{1}{q}}\Bigg\}$$

$$+\frac{\eta^2(a_2,mx)}{2(n+1)^2\Delta_{m,n}^{(2)}(1)}\sqrt[p]{B_{\Lambda_{m,n}^{(2)}}(p)}$$

$$\times\Bigg\{\left[\int_0^1\left[\left(1-\frac{1-t}{n+1}\right)|f''(mx)|^q\right.\right.$$

$$\left.\left.+\frac{(1-t)}{n+1}|f''(a_2)|^q\right]dt\right]^{\frac{1}{q}}$$

$$+\left[\int_0^1\left[\left(1-\frac{n+t}{n+1}\right)|f''(mx)|^q\right.\right.$$

$$\left.\left.+\frac{(n+t)}{n+1}|f''(a_2)|^q\right]dt\right]^{\frac{1}{q}}\Bigg\}$$

$$=\frac{\eta^2(x,ma_1)}{2(n+1)^2\sqrt[q]{2(n+1)}\Delta_{m,n}^{(1)}(1)}\sqrt[p]{B_{\Lambda_{m,n}^{(1)}}(p)}$$

$$\times\Bigg\{\sqrt[q]{|f''(ma_1)|^q+(2n+1)|f''(x)|^q}$$

$$+\sqrt[q]{(2n+1)|f''(ma_1)|^q+|f''(x)|^q}\Bigg\}$$

$$+\frac{\eta^2(a_2,mx)}{2(n+1)^2\sqrt[q]{2(n+1)}\Delta_{m,n}^{(2)}(1)}\sqrt[p]{B_{\Lambda_{m,n}^{(2)}}(p)}$$

$$\times\Bigg\{\sqrt[q]{|f''(mx)|^q+(2n+1)|f''(a_2)|^q}$$

$$+\sqrt[q]{(2n+1)|f''(mx)|^q+|f''(a_2)|^q}\Bigg\}.$$

The proof of Theorem 2 is completed. □

We point out some special cases of Theorem 2.

Corollary 1. *Taking $p=q=2$ in Theorem 2, we have*

$$\left|I_{f,\Lambda_{m,n}^{(1)},\Lambda_{m,n}^{(2)},\Delta_{m,n}^{(1)},\Delta_{m,n}^{(2)}}(x,a_1,a_2)\right|$$

$$\leq\frac{\eta^2(x,ma_1)}{2(n+1)^2\sqrt{2(n+1)}\Delta_{m,n}^{(1)}(1)}\quad(16)$$

$$\times\sqrt{B_{\Lambda_{m,n}^{(1)}}(2)}$$

$$\times\Bigg\{\sqrt{|f''(ma_1)|^2+(2n+1)|f''(x)|^2}$$

$$+\sqrt{(2n+1)|f''(ma_1)|^2+|f''(x)|^2}\Bigg\}$$

$$+\frac{\eta^2(a_2,mx)}{2(n+1)^2\sqrt{2(n+1)}\Delta_{m,n}^{(2)}(1)}\sqrt{B_{\Lambda_{m,n}^{(2)}}(2)}$$

$$\times\Bigg\{\sqrt{|f''(mx)|^2+(2n+1)|f''(a_2)|^2}$$

$$+\sqrt{(2n+1)|f''(mx)|^2+|f''(a_2)|^2}\Bigg\}.$$

Corollary 2. *Taking $\varphi(t)=t$ in Theorem 2, we get*

$$\left|I_{f,\Lambda_{m,n}^{(1)},\Lambda_{m,n}^{(2)},\Delta_{m,n}^{(1)},\Delta_{m,n}^{(2)}}(x,a_1,a_2)\right|$$

$$\leq\frac{\eta^2(x,ma_1)}{4(n+1)^2\sqrt[q]{2(n+1)}\sqrt[p]{2p+1}}\quad(17)$$

$$\times\Bigg\{\sqrt[q]{|f''(ma_1)|^q+(2n+1)|f''(x)|^q}$$

$$+\sqrt[q]{(2n+1)|f''(ma_1)|^q+|f''(x)|^q}\Bigg\}$$

$$+\frac{\eta^2(a_2,mx)}{4(n+1)^2\sqrt[q]{2(n+1)}\sqrt[p]{2p+1}}$$

$$\times\Bigg\{\sqrt[q]{|f''(mx)|^q+(2n+1)|f''(a_2)|^q}$$

$$+\sqrt[q]{(2n+1)|f''(mx)|^q+|f''(a_2)|^q}\Bigg\}.$$

Corollary 3. *Taking $x=\frac{a_1+a_2}{2}$, $m=1$, $n=0$, $\eta(x,ma_1)=x-ma_1$ and $\eta(a_2,mx)=a_2-mx$ in Corollary 2, we obtain*

$$\left|I_{f,\Lambda_{1,0}^{(1)},\Lambda_{1,0}^{(2)},\Delta_{1,0}^{(1)},\Delta_{1,0}^{(2)}}\left(\frac{a_1+a_2}{2},a_1,a_2\right)\right|$$

$$\leq\frac{(a_2-a_1)^2}{8\sqrt[q]{2}\sqrt[p]{2p+1}}\quad(18)$$

$$\times\Bigg\{\sqrt[q]{|f''(a_1)|^q+\left|f''\left(\frac{a_1+a_2}{2}\right)\right|^q}$$

$$+\sqrt[q]{\left|f''\left(\frac{a_1+a_2}{2}\right)\right|^q+|f''(a_2)|^q}\Bigg\}.$$

Corollary 4. *Taking $\varphi(t)=\frac{t^\alpha}{\Gamma(\alpha)}$ in Theorem 2, we have*

$$\left|I_{f,\Lambda_{m,n}^{(1)},\Lambda_{m,n}^{(2)},\Delta_{m,n}^{(1)},\Delta_{m,n}^{(2)}}(x,a_1,a_2)\right|$$

$$\leq\frac{\eta^2(x,ma_1)}{4(n+1)^2\sqrt[q]{2(n+1)}\sqrt[p]{2p\alpha+1}}\quad(19)$$

$$\times\Bigg\{\sqrt[q]{|f''(ma_1)|^q+(2n+1)|f''(x)|^q}$$

$$+\sqrt[q]{(2n+1)|f''(ma_1)|^q+|f''(x)|^q}\Bigg\}$$

$$+\frac{\eta^2(a_2,mx)}{4(n+1)^2\sqrt[q]{2(n+1)}\sqrt[p]{2p\alpha+1}}$$

$$\times\Bigg\{\sqrt[q]{|f''(mx)|^q+(2n+1)|f''(a_2)|^q}$$

$$+\sqrt[q]{(2n+1)|f''(mx)|^q + |f''(a_2)|^q}\Big\}.$$

Corollary 5. *Taking* $\varphi(t) = \frac{t^{\frac{\alpha}{k}}}{k\Gamma_k(\alpha)}$ *in Theorem 2, we get*

$$\left|I_{f,\Lambda_{m,n}^{(1)},\Lambda_{m,n}^{(2)},\Delta_{m,n}^{(1)},\Delta_{m,n}^{(2)}}(x,a_1,a_2)\right|$$

$$\leq \frac{\eta^2(x,ma_1)}{4(n+1)^2\sqrt[q]{2(n+1)}\sqrt[p]{\frac{2p\alpha}{k}+1}} \tag{20}$$

$$\times\Big\{\sqrt[q]{|f''(ma_1)|^q + (2n+1)|f''(x)|^q}$$

$$+\sqrt[q]{(2n+1)|f''(ma_1)|^q + |f''(x)|^q}\Big\}$$

$$+\frac{\eta^2(a_2,mx)}{4(n+1)^2\sqrt[q]{2(n+1)}\sqrt[p]{\frac{2p\alpha}{k}+1}}$$

$$\times\Big\{\sqrt[q]{|f''(mx)|^q + (2n+1)|f''(a_2)|^q}$$

$$+\sqrt[q]{(2n+1)|f''(mx)|^q + |f''(a_2)|^q}\Big\}.$$

Corollary 6. *Taking* $\varphi(t) = t(a_2-t)^{\alpha-1}$ *and* $f(x)$ *is symmetric to* $x = \frac{ma_1+a_2}{2}$, *in Theorem 2, we obtain*

$$\left|I_{f,\Lambda_{m,n}^{(1)},\Lambda_{m,n}^{(2)},\Delta_{m,n}^{(1)},\Delta_{m,n}^{(2)}}\left(\frac{ma_1+a_2}{2},a_1,a_2\right)\right|$$

$$\leq \frac{\frac{\alpha\eta^2\left(\frac{ma_1+a_2}{2},ma_1\right)}{2(n+1)^2\sqrt[q]{2(n+1)}}\sqrt[p]{B^*_{\Lambda_{m,n}^{(1)}}(p)}}{\left[a_2^\alpha - \frac{(n+1)}{(\alpha+1)\eta\left(\frac{ma_1+a_2}{2},ma_1\right)}\left(a_2^{\alpha+1}-\left(a_2-\frac{\eta\left(\frac{ma_1+a_2}{2},ma_1\right)}{n+1}\right)^{\alpha+1}\right)\right]}$$

$$\tag{21}$$

$$\times\Big\{\sqrt[q]{|f''(ma_1)|^q + (2n+1)\left|f''\left(\frac{ma_1+a_2}{2}\right)\right|^q}$$

$$+\sqrt[q]{(2n+1)|f''(ma_1)|^q + \left|f''\left(\frac{ma_1+a_2}{2}\right)\right|^q}\Big\}$$

$$+\frac{\frac{\alpha\eta^2\left(a_2,m\frac{(ma_1+a_2)}{2}\right)}{2(n+1)^2\sqrt[q]{2(n+1)}}\sqrt[p]{B^*_{\Lambda_{m,n}^{(2)}}(p)}}{\left[a_2^\alpha - \frac{(n+1)}{(\alpha+1)\eta\left(a_2,m\frac{(ma_1+a_2)}{2}\right)}\left(a_2^{\alpha+1}-\left(a_2-\frac{\eta\left(a_2,m\frac{(ma_1+a_2)}{2}\right)}{n+1}\right)^{\alpha+1}\right)\right]}$$

$$\times\Big\{\sqrt[q]{\left|f''\left(m\frac{(ma_1+a_2)}{2}\right)\right|^q + (2n+1)|f''(a_2)|^q}$$

$$+\sqrt[q]{(2n+1)\left|f''\left(m\frac{(ma_1+a_2)}{2}\right)\right|^q + |f''(a_2)|^q}\Big\},$$

where

$$B^*_{\Lambda_{m,n}^{(1)}}(p) = \frac{1}{\alpha} \tag{22}$$

$$\times\int_0^1\left[a_2^\alpha t - \frac{(n+1)}{(\alpha+1)\eta\left(\frac{ma_1+a_2}{2},ma_1\right)}\right.$$

$$\left.\times\left(a_2^{\alpha+1}-\left(a_2-\frac{\eta\left(\frac{ma_1+a_2}{2},ma_1\right)t}{n+1}\right)^{\alpha+1}\right)\right]^p dt$$

and

$$B^*_{\Lambda_{m,n}^{(2)}}(p) = \frac{1}{\alpha} \tag{23}$$

$$\times\int_0^1\left[a_2^\alpha t - \frac{(n+1)}{(\alpha+1)\eta\left(a_2,m\frac{(ma_1+a_2)}{2}\right)}\right.$$

$$\left.\times\left(a_2^{\alpha+1}-\left(a_2-\frac{\eta\left(a_2,m\frac{(ma_1+a_2)}{2}\right)t}{n+1}\right)^{\alpha+1}\right)\right]^p dt.$$

Corollary 7. *Taking* $\varphi(t) = \frac{t}{\alpha}\exp\left[\left(-\frac{1-\alpha}{\alpha}\right)t\right]$ *for* $\alpha \in (0,1)$, *in Theorem 2, we have*

$$\left|I_{f,\Lambda_{m,n}^{(1)},\Lambda_{m,n}^{(2)},\Delta_{m,n}^{(1)},\Delta_{m,n}^{(2)}}(x,a_1,a_2)\right|$$

$$\leq \frac{(\alpha-1)\eta^2(x,ma_1)}{2(n+1)^2\sqrt[q]{2(n+1)}} \tag{24}$$

$$\times\frac{1}{\left\{\exp\left[\left(-\frac{1-\alpha}{\alpha}\right)\frac{\eta(x,ma_1)}{n+1}\right]-1\right\}}$$

$$\times\sqrt[p]{B^\diamond_{\Lambda_{m,n}^{(1)}}(p)}$$

$$\times\Big\{\sqrt[q]{|f''(ma_1)|^q + (2n+1)|f''(x)|^q}$$

$$+\sqrt[q]{(2n+1)|f''(ma_1)|^q + |f''(x)|^q}\Big\}$$

$$+\frac{(\alpha-1)\eta^2(a_2,mx)}{2(n+1)^2\sqrt[q]{2(n+1)}\left\{\exp\left[\left(-\frac{1-\alpha}{\alpha}\right)\frac{\eta(a_2,mx)}{n+1}\right]-1\right\}}$$

$$\times\sqrt[p]{B^\diamond_{\Lambda_{m,n}^{(2)}}(p)}$$

$$\times\Big\{\sqrt[q]{|f''(mx)|^q + (2n+1)|f''(a_2)|^q}$$

$$+\sqrt[q]{(2n+1)|f''(mx)|^q + |f''(a_2)|^q}\Big\},$$

where

$$B^\diamond_{\Lambda_{m,n}^{(1)}}(p) = \frac{1}{(\alpha-1)^p} \tag{25}$$

$$\times\int_0^1\left[\frac{(n+1)\alpha}{(\alpha-1)\eta(x,ma_1)}\right.$$

$$\left.\times\left\{\exp\left[\left(-\frac{1-\alpha}{\alpha}\right)\frac{\eta(x,ma_1)}{(n+1)}t\right]-(t+1)\right\}\right]^p dt$$

and

$$B^\diamond_{\Lambda_{m,n}^{(2)}}(p) = \frac{1}{(\alpha-1)^p} \tag{26}$$

$$\times\int_0^1\left[\frac{(n+1)\alpha}{(\alpha-1)\eta(a_2,mx)}\right.$$

$$\times \left\{ \exp\left[\left(-\frac{1-\alpha}{\alpha} \right) \frac{\eta(a_2, mx)}{(n+1)} t \right] - (t+1) \right\} \right]^p dt.$$

Theorem 3. *Let* $f : P \longrightarrow \mathbb{R}$ *be a twice differentiable mapping on* (ma_1, a_2). *If* $|f''|^q$ *is preinvex on* P *for* $q \geq 1$, *then the following inequality for generalized fractional integrals hold:*

$$\left| I_{f, \Lambda_{m,n}^{(1)}, \Lambda_{m,n}^{(2)}, \Delta_{m,n}^{(1)}, \Delta_{m,n}^{(2)}} (x, a_1, a_2) \right|$$
$$\leq \left(\frac{1}{n+1} \right)^{\frac{2q+1}{q}} \frac{\eta^2(x, ma_1)}{2\Delta_{m,n}^{(1)}(1)} \qquad (27)$$
$$\times \left(B_{\Lambda_{m,n}^{(1)}}(1) \right)^{1-\frac{1}{q}}$$
$$\times \left\{ \sqrt[q]{C_{\Lambda_{m,n}^{(1)}} |f''(ma_1)|^q + D_{\Lambda_{m,n}^{(1)}}(n)|f''(x)|^q} \right.$$
$$\left. + \sqrt[q]{D_{\Lambda_{m,n}^{(1)}}(n)|f''(ma_1)|^q + C_{\Lambda_{m,n}^{(1)}} |f''(x)|^q} \right\}$$
$$+ \left(\frac{1}{n+1} \right)^{\frac{2q+1}{q}} \frac{\eta^2(a_2, mx)}{2\Delta_{m,n}^{(2)}(1)} \left(B_{\Lambda_{m,n}^{(2)}}(1) \right)^{1-\frac{1}{q}}$$
$$\times \left\{ \sqrt[q]{C_{\Lambda_{m,n}^{(2)}} |f''(mx)|^q + D_{\Lambda_{m,n}^{(2)}}(n)|f''(a_2)|^q} \right.$$
$$\left. + \sqrt[q]{D_{\Lambda_{m,n}^{(2)}}(n)|f''(mx)|^q + C_{\Lambda_{m,n}^{(2)}} |f''(a_2)|^q} \right\},$$

where

$$C_{\Lambda_{m,n}^{(i)}} = \int_0^1 (1-t)\Lambda_{m,n}^{(i)}(t)dt, \quad \forall\, i = 1, 2 \quad (28)$$

$$D_{\Lambda_{m,n}^{(i)}}(n) = \int_0^1 (n+t)\Lambda_{m,n}^{(i)}(t)dt, \,\forall\, i = 1, 2 \quad (29)$$

and $B_{\Lambda_{m,n}^{(i)}}(1)$, $\forall\, i = 1, 2$, *are defined as in Theorem 2, where* $p = 1$.

Proof. From Lemma 1, preinvexity of $|f''|^q$, power mean inequality and properties of the modulus, we have

$$\left| I_{f, \Lambda_{m,n}^{(1)}, \Lambda_{m,n}^{(2)}, \Delta_{m,n}^{(1)}, \Delta_{m,n}^{(2)}} (x, a_1, a_2) \right|$$
$$\leq \frac{\eta^2(x, ma_1)}{2(n+1)^2 \Delta_{m,n}^{(1)}(1)}$$
$$\times \left\{ \int_0^1 \Lambda_{m,n}^{(1)}(t) \left[\left| f''\left(ma_1 + \frac{(n+t)}{n+1}\eta(x, ma_1) \right) \right| \right. \right.$$
$$\left. \left. + \left| f''\left(ma_1 + \frac{(1-t)}{n+1}\eta(x, ma_1) \right) \right| \right] dt \right\}$$
$$+ \frac{\eta^2(a_2, mx)}{2(n+1)^2 \Delta_{m,n}^{(2)}(1)}$$
$$\times \left\{ \int_0^1 \Lambda_{m,n}^{(2)}(t) \left[\left| f''\left(mx + \frac{(1-t)}{n+1}\eta(a_2, mx) \right) \right| \right. \right.$$

$$\left. \left. + \left| f''\left(mx + \frac{(n+t)}{n+1}\eta(a_2, mx) \right) \right| \right] dt \right\}$$
$$\leq \frac{\eta^2(x, ma_1)}{2(n+1)^2 \Delta_{m,n}^{(1)}(1)} \left(\int_0^1 \Lambda_{m,n}^{(1)}(t)dt \right)^{1-\frac{1}{q}}$$
$$\times \left\{ \left(\int_0^1 \Lambda_{m,n}^{(1)}(t) \left| f''\left(ma_1 + \frac{(n+t)}{n+1}\eta(x, ma_1) \right) \right|^q dt \right)^{\frac{1}{q}} \right.$$
$$\left. + \left(\int_0^1 \Lambda_{m,n}^{(1)}(t) \left| f''\left(ma_1 + \frac{(1-t)}{n+1}\eta(x, ma_1) \right) \right|^q dt \right)^{\frac{1}{q}} \right\}$$
$$+ \frac{\eta^2(a_2, mx)}{2(n+1)^2 \Delta_{m,n}^{(2)}(1)} \left(\int_0^1 \Lambda_{m,n}^{(2)}(t)dt \right)^{1-\frac{1}{q}}$$
$$\times \left\{ \left(\int_0^1 \Lambda_{m,n}^{(2)}(t) \left| f''\left(mx + \frac{(1-t)}{n+1}\eta(a_2, mx) \right) \right|^q dt \right)^{\frac{1}{q}} \right.$$
$$\left. + \left(\int_0^1 \Lambda_{m,n}^{(2)}(t) \left| f''\left(mx + \frac{(n+t)}{n+1}\eta(a_2, mx) \right) \right|^q dt \right)^{\frac{1}{q}} \right\}$$
$$\leq \frac{\eta^2(x, ma_1)}{2(n+1)^2 \Delta_{m,n}^{(1)}(1)} \left(B_{\Lambda_{m,n}^{(1)}}(1) \right)^{1-\frac{1}{q}}$$
$$\times \left\{ \left[\int_0^1 \Lambda_{m,n}^{(1)}(t) \right. \right.$$
$$\left. \times \left[\left(1 - \frac{n+t}{n+1} \right) |f''(ma_1)|^q + \frac{(n+t)}{n+1}|f''(x)|^q \right] dt \right]^{\frac{1}{q}}$$
$$+ \left[\int_0^1 \Lambda_{m,n}^{(1)}(t) \right.$$
$$\left. \left. \times \left[\left(1 - \frac{1-t}{n+1} \right) |f''(ma_1)|^q + \frac{(1-t)}{n+1}|f''(x)|^q \right] dt \right]^{\frac{1}{q}} \right\}$$
$$+ \frac{\eta^2(a_2, mx)}{2(n+1)^2 \Delta_{m,n}^{(2)}(1)} \left(B_{\Lambda_{m,n}^{(2)}}(1) \right)^{1-\frac{1}{q}}$$
$$\times \left\{ \left[\int_0^1 \Lambda_{m,n}^{(2)}(t) \right. \right.$$
$$\left. \times \left[\left(1 - \frac{1-t}{n+1} \right) |f''(mx)|^q + \frac{(1-t)}{n+1}|f''(a_2)|^q \right] dt \right]^{\frac{1}{q}}$$
$$+ \left[\int_0^1 \Lambda_{m,n}^{(2)}(t) \right.$$
$$\left. \left. \times \left[\left(1 - \frac{n+t}{n+1} \right) |f''(mx)|^q + \frac{(n+t)}{n+1}|f''(a_2)|^q \right] dt \right]^{\frac{1}{q}} \right\}$$
$$= \left(\frac{1}{n+1} \right)^{\frac{2q+1}{q}} \frac{\eta^2(x, ma_1)}{2\Delta_{m,n}^{(1)}(1)} \left(B_{\Lambda_{m,n}^{(1)}}(1) \right)^{1-\frac{1}{q}}$$
$$\times \left\{ \sqrt[q]{C_{\Lambda_{m,n}^{(1)}} |f''(ma_1)|^q + D_{\Lambda_{m,n}^{(1)}}(n)|f''(x)|^q} \right.$$

$$+ \sqrt[q]{D_{\Lambda_{m,n}^{(1)}}(n)|f''(ma_1)|^q + C_{\Lambda_{m,n}^{(1)}}|f''(x)|^q}\Bigg\}$$

$$+ \left(\frac{1}{n+1}\right)^{\frac{2q+1}{q}} \frac{\eta^2(a_2, mx)}{2\Delta_{m,n}^{(2)}(1)} \left(B_{\Lambda_{m,n}^{(2)}}(1)\right)^{1-\frac{1}{q}}$$

$$\times \Bigg\{ \sqrt[q]{C_{\Lambda_{m,n}^{(2)}}|f''(mx)|^q + D_{\Lambda_{m,n}^{(2)}}(n)|f''(a_2)|^q}$$

$$+ \sqrt[q]{D_{\Lambda_{m,n}^{(2)}}(n)|f''(mx)|^q + C_{\Lambda_{m,n}^{(2)}}|f''(a_2)|^q}\Bigg\}.$$

The proof of Theorem 3 is completed. □

We point out some special cases of Theorem 3.

Corollary 8. *Taking $q = 1$ in Theorem 3, we have*

$$\left|I_{f,\Lambda_{m,n}^{(1)},\Lambda_{m,n}^{(2)},\Delta_{m,n}^{(1)},\Delta_{m,n}^{(2)}}(x, a_1, a_2)\right|$$

$$\leq \frac{1}{(n+1)^3}\Bigg\{ \frac{\eta^2(x, ma_1)}{2\Delta_{m,n}^{(1)}(1)} \quad (30)$$

$$\times \left(C_{\Lambda_{m,n}^{(1)}} + D_{\Lambda_{m,n}^{(1)}}(n)\right)\left[|f''(ma_1)| + |f''(x)|\right]$$

$$+ \frac{\eta^2(a_2, mx)}{2\Delta_{m,n}^{(2)}(1)}$$

$$\times \left(C_{\Lambda_{m,n}^{(2)}} + D_{\Lambda_{m,n}^{(2)}}(n)\right)\left[|f''(mx)| + |f''(a_2)|\right]\Bigg\}.$$

Corollary 9. *Taking $\varphi(t) = t$ in Theorem 3, we get*

$$\left|I_{f,\Lambda_{m,n}^{(1)},\Lambda_{m,n}^{(2)},\Delta_{m,n}^{(1)},\Delta_{m,n}^{(2)}}(x, a_1, a_2)\right|$$

$$\leq \left(\frac{1}{n+1}\right)^{\frac{2q+1}{q}} \frac{\eta^2(x, ma_1)}{12\sqrt[q]{4}} \quad (31)$$

$$\times \Bigg\{ \sqrt[q]{|f''(ma_1)|^q + (4n+3)|f''(x)|^q}$$

$$+ \sqrt[q]{(4n+3)|f''(ma_1)|^q + |f''(x)|^q}\Bigg\}$$

$$+ \frac{\eta^2(a_2, mx)}{12\sqrt[q]{4}}$$

$$\times \Bigg\{ \sqrt[q]{|f''(mx)|^q + (4n+3)|f''(a_2)|^q}$$

$$+ \sqrt[q]{(4n+3)|f''(mx)|^q + |f''(a_2)|^q}\Bigg\}.$$

Corollary 10. *Taking $x = \frac{a_1+a_2}{2}$, $m = 1$, $n = 0$, $\eta(x, ma_1) = x - ma_1$ and $\eta(a_2, mx) = a_2 - mx$ in Corollary 9, we obtain*

$$\left|I_{f,\Lambda_{1,0}^{(1)},\Lambda_{1,0}^{(2)},\Delta_{1,0}^{(1)},\Delta_{1,0}^{(2)}}\left(\frac{a_1+a_2}{2}, a_1, a_2\right)\right|$$

$$\leq \left(\frac{1}{n+1}\right)^{\frac{2q+1}{q}} \frac{(a_2 - a_1)^2}{48\sqrt[q]{4}} \quad (32)$$

$$\times \Bigg\{ \sqrt[q]{|f''(a_1)|^q + 3\left|f''\left(\frac{a_1+a_2}{2}\right)\right|^q}$$

$$+ \sqrt[q]{3|f''(a_1)|^q + \left|f''\left(\frac{a_1+a_2}{2}\right)\right|^q}$$

$$+ \sqrt[q]{\left|f''\left(\frac{a_1+a_2}{2}\right)\right|^q + 3|f''(a_2)|^q}$$

$$+ \sqrt[q]{3\left|f''\left(\frac{a_1+a_2}{2}\right)\right|^q + |f''(a_2)|^q}\Bigg\}.$$

Corollary 11. *Taking $\varphi(t) = \frac{t^\alpha}{\Gamma(\alpha)}$ in Theorem 3, we have*

$$\left|I_{f,\Lambda_{m,n}^{(1)},\Lambda_{m,n}^{(2)},\Delta_{m,n}^{(1)},\Delta_{m,n}^{(2)}}(x, a_1, a_2)\right|$$

$$\leq \left(\frac{1}{n+1}\right)^{\frac{2q+1}{q}} \quad (33)$$

$$\times \frac{\Gamma(\alpha+1)}{2\Gamma(\alpha+3)}\sqrt[q]{\frac{\Gamma(\alpha+3)}{\Gamma(\alpha+4)}}\eta^2(x, ma_1)$$

$$\times \Bigg\{ \sqrt[q]{|f''(ma_1)|^q + [n(\alpha+3) + (\alpha+2)]|f''(x)|^q}$$

$$+ \sqrt[q]{[n(\alpha+3) + (\alpha+2)]|f''(ma_1)|^q + |f''(x)|^q}\Bigg\}$$

$$+ \left(\frac{1}{n+1}\right)^{\frac{2q+1}{q}} \frac{\Gamma(\alpha+1)}{2\Gamma(\alpha+3)}\sqrt[q]{\frac{\Gamma(\alpha+3)}{\Gamma(\alpha+4)}}\eta^2(a_2, mx)$$

$$\times \Bigg\{ \sqrt[q]{|f''(mx)|^q + [n(\alpha+3) + (\alpha+2)]|f''(a_2)|^q}$$

$$+ \sqrt[q]{[n(\alpha+3) + (\alpha+2)]|f''(mx)|^q + |f''(a_2)|^q}\Bigg\}.$$

Corollary 12. *Taking $\varphi(t) = \frac{t^{\frac{\alpha}{k}}}{k\Gamma_k(\alpha)}$ in Theorem 3, we get*

$$\left|I_{f,\Lambda_{m,n}^{(1)},\Lambda_{m,n}^{(2)},\Delta_{m,n}^{(1)},\Delta_{m,n}^{(2)}}(x, a_1, a_2)\right|$$

$$\leq \left(\frac{1}{n+1}\right)^{\frac{2q+1}{q}} \quad (34)$$

$$\times \frac{\Gamma_k(\alpha+k)}{2\Gamma_k(\alpha+2k)}\sqrt[q]{\frac{\Gamma_k(\alpha+k+2)}{\Gamma_k(\alpha+k+3)}}\eta^2(x, ma_1)$$

$$\times \Bigg\{ \sqrt[q]{|f''(ma_1)|^q + \left[n\left(\frac{\alpha}{k}+3\right) + \left(\frac{\alpha}{k}+2\right)\right]|f''(x)|^q}$$

$$+ \sqrt[q]{\left[n\left(\frac{\alpha}{k}+3\right) + \left(\frac{\alpha}{k}+2\right)\right]|f''(ma_1)|^q + |f''(x)|^q}\Bigg\}$$

$$+ \left(\frac{1}{n+1}\right)^{\frac{2q+1}{q}}$$

$$\times \frac{\Gamma_k(\alpha+k)}{2\Gamma_k(\alpha+2k)}\sqrt[q]{\frac{\Gamma_k(\alpha+k+2)}{\Gamma_k(\alpha+k+3)}}\eta^2(a_2, mx)$$

$$\times\left\{\sqrt[q]{|f''(mx)|^q + \left[n\left(\frac{\alpha}{k}+3\right)+\left(\frac{\alpha}{k}+2\right)\right]|f''(a_2)|^q}\right.$$

$$\left.+\sqrt[q]{\left[n\left(\frac{\alpha}{k}+3\right)+\left(\frac{\alpha}{k}+2\right)\right]|f''(mx)|^q + |f''(a_2)|^q}\right\}.$$

Remark 2. *Applying our Theorems 2 and 3, for $n \in \mathbb{N}^*$ and appropriate choices of function $\varphi(t) = t$; $\varphi(t) = \frac{t^\alpha}{\Gamma(\alpha)}$; $\frac{t^{\frac{\alpha}{k}}}{k\Gamma_k(\alpha)}$; $\varphi(t) = t(a_2-t)^{\alpha-1}$, where $f(x)$ is symmetric to $x = \frac{ma_1+a_2}{2}$ and $m \in (0,1]$ is a fixed number; $\varphi(t) = \frac{t}{\alpha}\exp\left[\left(-\frac{1-\alpha}{\alpha}\right)t\right]$, for $\alpha \in (0,1)$; such that $\eta(x,ma_1) = x - ma_1$ and $\eta(a_2,mx) = a_2 - mx, \forall\, x \in P$, we can deduce some new general fractional integral inequalities. We omit their proofs and the details are left to the interested readers.*

3. Applications to special means

Consider the following special means for different real numbers α, β and $\alpha\beta \neq 0$, as follows:

(1) The arithmetic mean:
$$A := A(\alpha, \beta) = \frac{\alpha + \beta}{2},$$

(2) The harmonic mean:
$$H := H(\alpha, \beta) = \frac{2}{\frac{1}{\alpha} + \frac{1}{\beta}},$$

(3) The logarithmic mean:
$$L := L(\alpha, \beta) = \frac{\beta - \alpha}{\ln|\beta| - \ln|\alpha|},$$

(4) The generalized log–mean:
$$L_r := L_r(\alpha, \beta) = \left[\frac{\beta^{r+1} - \alpha^{r+1}}{(r+1)(\beta-\alpha)}\right]^{\frac{1}{r}},$$

    where $r \in \mathbb{Z} \setminus \{-1, 0\}$.

It is well known that L_r is monotonic nondecreasing over $r \in \mathbb{Z}$ with $L_{-1} := L$. In particular, we have the following inequality $H \leq L \leq A$. Now, using the theory results in section 2, we give some applications to special means for different real numbers.

Proposition 1. *Let $a_1, a_2 \in \mathbb{R} \setminus \{0\}$, where $a_1 < a_2$ and $x \in [a_1, a_2]$. Then for $r \in \{2, 3, \dots\}$, where $q > 1$ and $p^{-1} + q^{-1} = 1$, the following inequality hold:*

$$\left| r\left(\frac{a_2 - a_1}{2}\right)\left[A\left(a_1^{r-1}, a_2^{r-1}\right) + A^{r-1}(a_1, a_2)\right]\right.$$

$$\left. - \left[A\left(a_1^r, a_2^r\right) + A^r(a_1, a_2)\right] - 2L_r^r(a_1, a_2)\right|$$

$$\leq \frac{r(r-1)(a_2 - a_1)^2}{8\sqrt[p]{2p+1}} \qquad (35)$$

$$\times\left\{\sqrt[q]{A\left(|a_1|^{q(r-2)}, \left|\frac{a_1+a_2}{2}\right|^{q(r-2)}\right)}\right.$$

$$\left.+\sqrt[q]{A\left(\left|\frac{a_1+a_2}{2}\right|^{q(r-2)}, |a_2|^{q(r-2)}\right)}\right\}.$$

Proof. Applying Theorem 2 for $x = \frac{a_1+a_2}{2}$, $m = 1$, $n = 0$, $\eta(x, ma_1) = x - ma_1, \eta(a_2, mx) = a_2 - mx$, $f(x) = x^r$ and $\varphi(t) = t$, one can obtain the result immediately. $\qquad\square$

Proposition 2. *Let $a_1, a_2 \in \mathbb{R} \setminus \{0\}$, where $a_1 < a_2$ and $x \in [a_1, a_2]$. Then, for $q > 1$ and $p^{-1} + q^{-1} = 1$, the following inequality hold:*

$$\left|\left(\frac{a_1 - a_2}{2}\right)\left[\frac{1}{H\left(a_1^2, a_2^2\right)} + \frac{1}{A^2(a_1, a_2)}\right]\right.$$

$$\left. - \left[\frac{1}{H(a_1, a_2)} + \frac{1}{A(a_1, a_2)}\right] - \frac{2}{L(a_1, a_2)}\right|$$

$$\leq \frac{(a_2 - a_1)^2}{4\sqrt[p]{2p+1}} \qquad (36)$$

$$\times\left\{\frac{1}{\sqrt[q]{H\left(|a_1|^{3q}, \left|\frac{a_1+a_2}{2}\right|^{3q}\right)}}\right.$$

$$\left.+\frac{1}{\sqrt[q]{H\left(\left|\frac{a_1+a_2}{2}\right|^{3q}, |a_2|^{3q}\right)}}\right\}.$$

Proof. Applying Theorem 2 for $x = \frac{a_1+a_2}{2}$, $m = 1$, $n = 0$, $\eta(x, ma_1) = x - ma_1, \eta(a_2, mx) = a_2 - mx$, $f(x) = \frac{1}{x}$ and $\varphi(t) = t$, one can obtain the result immediately. $\qquad\square$

Proposition 3. *Let $a_1, a_2 \in \mathbb{R} \setminus \{0\}$, where $a_1 < a_2$ and $x \in [a_1, a_2]$. Then, for $r \in \{2, 3, \dots\}$ and $q \geq 1$, the following inequality hold:*

$$\left| r\left(\frac{a_2 - a_1}{2}\right)\left[A\left(a_1^{r-1}, a_2^{r-1}\right) + A^{r-1}(a_1, a_2)\right]\right.$$

$$\left. - \left[A\left(a_1^r, a_2^r\right) + A^r(a_1, a_2)\right] - 2L_r^r(a_1, a_2)\right|$$

$$\leq \frac{r(r-1)(a_2 - a_1)^2}{48\sqrt[q]{2}} \qquad (37)$$

$$\times\left\{\sqrt[q]{A\left(3|a_1|^{q(r-2)}, \left|\frac{a_1+a_2}{2}\right|^{q(r-2)}\right)}\right.$$

$$\left.+\sqrt[q]{A\left(3\left|\frac{a_1+a_2}{2}\right|^{q(r-2)}, |a_1|^{q(r-2)}\right)}\right.$$

$$+ \sqrt[q]{A\left(3|a_2|^{q(r-2)}, \left|\frac{a_1+a_2}{2}\right|^{q(r-2)}\right)}$$

$$+ \sqrt[q]{A\left(3\left|\frac{a_1+a_2}{2}\right|^{q(r-2)}, |a_2|^{q(r-2)}\right)}\Bigg\}.$$

Proof. Applying Theorem 3 for $x = \frac{a_1+a_2}{2}$, $m = 1$, $n = 0$, $\eta(x, ma_1) = x - ma_1$, $\eta(a_2, mx) = a_2 - mx$, $f(x) = x^r$ and $\varphi(t) = t$, one can obtain the result immediately. $\qquad\square$

Proposition 4. *Let $a_1, a_2 \in \mathbb{R} \setminus \{0\}$, where $a_1 < a_2$ and $x \in [a_1, a_2]$. Then for $q \geq 1$, the following inequality hold:*

$$\left| \left(\frac{a_1 - a_2}{2}\right) \left[\frac{1}{H\left(a_1^2, a_2^2\right)} + \frac{1}{A^2\left(a_1, a_2\right)} \right] \right.$$
$$\left. - \left[\frac{1}{H\left(a_1, a_2\right)} + \frac{1}{A\left(a_1, a_2\right)} \right] - \frac{2}{L\left(a_1, a_2\right)} \right|$$

$$\leq \sqrt[q]{\frac{3}{2}} \frac{(a_2 - a_1)^2}{24} \tag{38}$$

$$\times \Bigg\{ \frac{1}{\sqrt[q]{H\left(3|a_1|^{3q}, \left|\frac{a_1+a_2}{2}\right|^{3q}\right)}}$$

$$+ \frac{1}{\sqrt[q]{H\left(3\left|\frac{a_1+a_2}{2}\right|^{3q}, |a_1|^{3q}\right)}}$$

$$+ \frac{1}{\sqrt[q]{H\left(3|a_2|^{3q}, \left|\frac{a_1+a_2}{2}\right|^{3q}\right)}}$$

$$+ \frac{1}{\sqrt[q]{H\left(3\left|\frac{a_1+a_2}{2}\right|^{3q}, |a_2|^{3q}\right)}} \Bigg\}.$$

Proof. Applying Theorem 3 for $x = \frac{a_1+a_2}{2}$, $m = 1$, $n = 0$, $\eta(x, ma_1) = x - ma_1$, $\eta(a_2, mx) = a_2 - mx$, $f(x) = \frac{1}{x}$ and $\varphi(t) = t$, one can obtain the result immediately. $\qquad\square$

Remark 3. *Applying our Theorems 2 and 3 for $x = \frac{a_1+a_2}{2}$, $m = 1$, $n = 0$, $\eta(x, ma_1) = x - ma_1$, $\eta(a_2, mx) = a_2 - mx$ and appropriate choices of function $\varphi(t) = \frac{t^\alpha}{\Gamma(\alpha)}$, $\frac{t^{\frac{\alpha}{k}}}{k\Gamma_k(\alpha)}$, $\varphi(t) = t(a_2 - t)^{\alpha-1}$, where $f(x)$ is symmetric to $x = \frac{a_1+a_2}{2}$, $\varphi(t) = \frac{t}{\alpha} \exp\left[\left(-\frac{1-\alpha}{\alpha}\right) t\right]$, for $\alpha \in (0, 1)$, such that $|f''|^q$ to be preinvex, we can deduce some new general fractional integral inequalities using above special means. We omit their proofs and the details are left to the interested readers.*

4. Conclusion

It is expected that from the results obtained, and following the methodology applied, additional special functions may also be evaluated. Future works can be developed in the area of numerical analysis using the theorems and corollaries presented. The authors hope that the ideas and techniques of this paper will inspire interested readers working in this fascinating field.

Acknowledgments

References

[1] Aslani, S.M. Delavar, M.R. and Vaezpour, S.M. (2018). Inequalities of Fejér type related to generalized convex functions with applications. *Int. J. Anal. Appl.*, 16(1), 38–49.

[2] Chen, F.X. and Wu, S.H. (2016). Several complementary inequalities to inequalities of Hermite–Hadamard type for s–convex functions. *J. Nonlinear Sci. Appl.*, 9(2), 705–716.

[3] Chu, Y.M. Khan, M.A. Khan, T.U. and Ali, T. (2016). Generalizations of Hermite–Hadamard type inequalities for MT–convex functions. *J. Nonlinear Sci. Appl.*, 9(5), 4305–4316.

[4] Dahmani, Z. (2010). On Minkowski and Hermite–Hadamard integral inequalities via fractional integration. *Ann. Funct. Anal.*, 1(1), 51–58.

[5] Delavar, M.R. and Dragomir, S.S. (2017). On η–convexity. *Math. Inequal. Appl.*, 20, 203–216.

[6] Delavar, M.R. and De La Sen, M. (2016). Some generalizations of Hermite–Hadamard type inequalities. *SpringerPlus*, 5(1661).

[7] Dragomir, S.S. and Agarwal, R.P. (1998). Two inequalities for differentiable mappings and applications to special means of real numbers and trapezoidal formula. *Appl. Math. Lett.*, 11(5), 91–95.

[8] Khan, M.A. Chu, Y.M. Kashuri, A. Liko, R. and Ali, G. (2018). New Hermite–Hadamard inequalities for conformable fractional integrals. *J. Funct. Spaces*, Article ID 6928130, 9.

[9] Khan, M.A. Khurshid, Y. and Ali, T. (2017). Hermite–Hadamard inequality for fractional integrals via η–convex functions. *Acta Math. Univ. Comenianae*, 79(1), 153–164.

[10] Liu, W.J. (2014). Some Simpson type inequalities for h–convex and (α, m)–convex

functions. *J. Comput. Anal. Appl.*, 16(5), 1005–1012.

[11] Liu, W. Wen, W. and Park, J. (2016). Hermite–Hadamard type inequalities for MT–convex functions via classical integrals and fractional integrals. *J. Nonlinear Sci. Appl.*, 9, 766–777.

[12] Mihai, M.V. (2013). Some Hermite–Hadamard type inequalities via Riemann–Liouville fractional calculus. *Tamkang J. Math*, 44(4), 411–416.

[13] Mubeen, S. and Habibullah, G.M. (2012). k–Fractional integrals and applications. *Int. J. Contemp. Math. Sci.*, 7, 89–94.

[14] Noor, M.A. Noor, K.I. Awan, M.U. and Khan, S. (2014). Hermite–Hadamard inequalities for s–Godunova–Levin preinvex functions. *J. Adv. Math. Stud.*, 7(2), 12–19.

[15] Omotoyinbo, O. and Mogbodemu, A. (2014). Some new Hermite–Hadamard integral inequalities for convex functions. *Int. J. Sci. Innovation Tech.*, 1(1), 1–12.

[16] Özdemir, M.E. Dragomir, S.S. and Yildiz, C. (2013). The Hadamard's inequality for convex function via fractional integrals. *Acta Mathematica Scientia*, 33(5), 153–164.

[17] Sarikaya, M.Z. and Ertuğral, F. (2020). On the generalized Hermite–Hadamard inequalities. *Annals of the University of Craiova–Mathematics and Computer Science Series*, in press.

[18] Sarikaya, M.Z. and Yildirim, H. (2007). On generalization of the Riesz potential. *Indian Jour. of Math. and Mathematical Sci.*, 3(2), 231–235.

[19] Set, E. Noor, M.A. Awan, M.U. and Gözpinar, A. (2017). Generalized Hermite–Hadamard type inequalities involving fractional integral operators. *J. Inequal. Appl.*, 169, 1–10.

[20] Wang, H. Du, T.S. and Zhang, Y. (2017). k–fractional integral trapezium–like inequalities through (h, m)–convex and (α, m)–convex mappings. *J. Inequal. Appl.*, 2017(311), 20.

[21] Weir, T. and Mond, B. (1988). Preinvex functions in multiple objective optimization. *J. Math. Anal. Appl.*, 136, 29–38.

[22] Zhang, X.M. Chu, Y.M. and Zhang, X.H. (2010). The Hermite–Hadamard type inequality of GA–convex functions and its applications. *J. Inequal. Appl.*, Article ID 507560, 11.

[23] Zhang, Y. Du, T.S. Wang, H. Shen, Y.J. and Kashuri, A. (2018). Extensions of different type parameterized inequalities for generalized (m, h)–preinvex mappings via k–fractional integrals. *J. Inequal. Appl.*, 2018(49), 30.

Artion Kashuri *received his PhD degree from University Ismail Qemali of Vlora in 2016 in the area of Analysis. His research areas are Mathematical Inequalities, Applied Mathematics, Fractional Calculus, Quantum Calculus, etc. He has vast experience of teaching such as Differential Equations, Numerical Analysis, Calculus, Real Analysis, Complex Analysis, Topology, etc. He has more than 100 published papers in international reputation indexed journals. His current position is Lecturer in University Ismail Qemali, Department of Mathematics.*
http://orcid.org/0000-0003-0115-3079

Rozana Liko *received her PhD degree from University Ismail Qemali of Vlora in 2018 in the area of Applied Mathematics. Her research areas are Mathematical Inequalities, Applied Mathematics, etc. She has vast experience of teaching such as Probability and Statistics, Calculus, Linear Algebra, Real Analysis, etc. She has more than 50 published papers in international reputation indexed journals. Her current position is Lecturer in University Ismail Qemali, Department of Mathematics.*
http://orcid.org/0000-0003-2439-8538

IJOCTA
An International Journal of
Optimization and Control:
Theories & Applications
2010

RESEARCH ARTICLE

Using matrix stability for variable telegraph partial differential equation

Mahmut Modanli[a], Bawar Mohammed Faraj[b*] and Faraedoon Waly Ahmed[c]

[a] Department of Mathematics, Harran University, Turkey
[b] Computer Science Department, University of Halabja,Iraq
[c] Department of Physics, University of Halabja,Iraq
mmodanli@harran.edu.tr, bawarm.faraj@uoh.edu.iq, faraidun.ahmad@uoh.edu.iq

ARTICLE INFO

ABSTRACT

The variable telegraph partial differential equation depend on initial boundary value problem has been studied. The coefficient constant time-space telegraph partial differential equation is obtained from the variable telegraph partial differential equation throughout using Cauchy-Euler formula. The first and second order difference schemes were constructed for both of coefficient constant time-space and variable time-space telegraph partial differential equation. Matrix stability method is used to prove stability of difference schemes for the variable and coefficient telegraph partial differential equation. The variable telegraph partial differential equation and the constant coefficient time-space telegraph partial differential equation are compared with the exact solution. Finally, approximation solution has been found for both equations. The error analysis table presents the obtained numerical results.

1. Introduction

Partial differential equations have several applications in engineering, finance, physics and seismology [1–3]. They have several approximation methods which are different from each other. Some of these methods are solvable with respect to variables time and space. The space- heat equations were presented by difference schemes in previous works [4–6]. The partial differential equations depend on time were worked on in some papers [7–9], The telegraph partial differential equations is a special equation of the partial differential equations. In the literature, Telegraph equations can be defined based on time and space. Many important studies have been done on these equations in [10–12]. The telegraph partial differential equations were solved by difference schemes and methods in [13–16].

*Corresponding Author

In this paper, the initial boundary value problem for variable coefficient partial differential equation is investigated

$$
\begin{cases}
\frac{\partial}{\partial t}\left(\alpha(t)u_t(t,x)\right) - \frac{\partial}{\partial x}\left(\beta(x)u_x(t,x)\right) + pu(t,x) \\
= f(t,x),\ 0 < t < T,\ 0 < x < L \\
u(0,x) = \varphi(x), \quad u_t(0,x) = \psi(x), \quad 0 \le t \le T, \\
u(t,0) = g_1(t), \quad u(t,L) = g_2(t), \quad 0 \le x \le L.
\end{cases}
\tag{1}
$$

Here, $\alpha(t)$, $\beta(x)$ are variable as to t, x, respectively. Now, we shall construct first order difference scheme. Then, we will prove the stability estimates for this problem.

2. First and second order difference schemes for variable telegraph partial differential equation

If taking as $\alpha(t) = t^2$, $\beta(x) = x^2$ and $p = 1$ in the formula (1), this formula can be written as follow

$$\begin{cases} t^2 u_{tt}(t,x) + 2t u_t(t,x) - x^2 u_{xx}(t,x) - 2x u_x(t,x) \\ + u(t,x) = f(t,x), \ 1 < t < e^T, \ 1 < x < e^L \\ u(0,x) = In(\varphi(x)), u_t(0,x) = In(\psi(x)), \\ u(t,0) = u(t,L) = 0, \quad 1 \le t \le e^T, \ 1 \le x \le e^L. \end{cases}$$ (2)

This equation represents a variable time-space telegraph partial differential equation. It is not easy to find out the analytical solution of this equation.

Therefore, if the Cauchy-Euler formula is applied to the last part of the equation separately for the x and t variables, the formula (2) can be written as

$$\begin{cases} u_{tt}(t,x) + u_t(t,x) - u_{xx}(t,x) - u_x(t,x) + u(t,x) \\ = f(t,x), \ 0 < t < T, \ 0 < x < L \\ u(0,x) = \varphi(x), \quad u_t(0,x) = \psi(x), \quad 0 \le t \le T, \\ u(t,0) = u(t,L) = 0, \quad 0 \le x \le L. \end{cases}$$ (3)

The problem (3) is a coefficient time-space telegraph partial differential equation.

Now, we shall construct the first and the second order of accuracy difference scheme for the equation (2). In the first step, we consider the set $w_{\tau,h} = [0,1]_\tau \times [0,\pi]_h$ of a family of grid points depending on the small parameters τ and h. To evaluate difference scheme for problem (2), the following formula

$$[0,1]_\tau \times [0,\pi]_h = \{(t_k, x_n) : t_k = k\tau, 0 \le k \le N,$$
$$N\tau = 1, x_n = nh, 0 \le n \le M; Mh = \pi\},$$

is used. For the formula (2), we get the first order difference scheme

$$\begin{cases} t_k^2 \dfrac{u_n^{k+1} - 2u_n^k + u_n^{k-1}}{\tau^2} + 2t_k \dfrac{u_n^{k+1} - u_n^k}{\tau} \\ -x_n^2 \dfrac{u_{n+1}^k - 2u_n^k + u_{n-1}^k}{h^2} - 2x_n \dfrac{u_{n+1}^k - u_{n-1}^k}{2h} \\ +u_n^k = f_n^k, \quad x_n = nh, \ t_k = k\tau, \\ 1 \le k \le N-1, \ 1 \le n \le M-1, \\ u_0^k = u_M^k = 0, \ u_n^0 = In(\varphi(x_n)), \ 0 \le k \le N \\ \dfrac{u_n^1 - u_n^0}{\tau} = In(\psi(x_n)), \ 0 \le n \le M, \end{cases}$$ (4)

and the second order difference scheme for the formula (2)

$$\begin{cases} t_k^2 \dfrac{u_n^{k+1} - 2u_n^k + u_n^{k-1}}{\tau^2} + 2t_k \dfrac{u_n^{k+1} - u_n^{k-1}}{2\tau} \\ -\dfrac{x_n^2}{2} \dfrac{u_{n+1}^{k+1} - 2u_n^{k+1} + u_{n-1}^{k+1}}{h^2} \\ -\dfrac{x_n^2}{2} \dfrac{u_{n+1}^{k-1} - 2u_n^{k-1} + u_{n-1}^{k-1}}{h^2} \\ -\dfrac{x_n}{2} \dfrac{u_{n+1}^{k+1} - u_{n-1}^{k+1}}{h} - \dfrac{x_n}{2} \dfrac{u_{n+1}^{k-1} - u_{n-1}^{k-1}}{h} \\ +\dfrac{1}{2} u_n^{k+1} + \dfrac{1}{2} u_n^{k-1} = f_n^k, \\ x_n = nh, \ t_k = k\tau, \ 1 \le k \le N-1, \ 1 \le n \le M-1, \\ \dfrac{u_n^1 - u_n^0}{\tau} = In(\psi(x_n)) + \dfrac{\tau}{2} \dfrac{u_n^2 - 2u_n^1 + u_n^0}{\tau^2}, \\ u_n^0 = In(\varphi(x_n)), u_0^k = u_M^k = 0, \\ 0 \le k \le N, \ 0 \le n \le M. \end{cases}$$ (5)

Similarly, the first order difference schemes for the formula (3) are

$$\begin{cases} \dfrac{u_n^{k+1} - 2u_n^k + u_n^{k-1}}{\tau^2} + \dfrac{u_n^{k+1} - u_n^k}{\tau} - \dfrac{u_{n+1}^k - 2u_n^k + u_{n-1}^k}{h^2} \\ -\dfrac{u_{n+1}^k - u_{n-1}^k}{2h} + u_n^k = f_n^k, \quad x_n = nh, \ t_k = k\tau, \\ 1 \le k \le N-1, \ 1 \le n \le M-1, \\ u_0^k = u_M^k = 0, \ u_n^0 = \varphi(x_n), \ \dfrac{u_n^1 - u_n^0}{\tau} = \psi(x_n), \\ 0 \le k \le N, \ 0 \le n \le M, \end{cases}$$ (6)

and the second order difference schemes

$$\begin{cases} \dfrac{u_n^{k+1} - 2u_n^k + u_n^{k-1}}{\tau^2} + \dfrac{u_n^{k+1} - u_n^{k-1}}{2\tau} \\ -\dfrac{1}{2} \dfrac{u_{n+1}^{k+1} - 2u_n^{k+1} + u_{n-1}^{k+1}}{h^2} \\ -\dfrac{1}{2} \dfrac{u_{n+1}^{k-1} - 2u_n^{k-1} + u_{n-1}^{k-1}}{h^2} \\ -\dfrac{1}{4} \dfrac{u_{n+1}^{k+1} - u_{n-1}^{k+1}}{h} - \dfrac{1}{4} \dfrac{u_{n+1}^{k-1} - u_{n-1}^{k-1}}{h} \\ +\dfrac{1}{2} u_n^{k+1} + \dfrac{1}{2} u_n^{k-1} = f_n^k, \\ x_n = nh, \ t_k = k\tau, \ 1 \le k \le N-1, \ 1 \le n \le M-1, \\ u_n^0 = \varphi(x), \ \dfrac{u_n^1 - u_n^0}{\tau} = \psi(x) + \dfrac{\tau}{2} \dfrac{u_n^2 - 2u_n^1 + u_n^0}{\tau^2}, \\ u_0^k = u_M^k = 0, \ 0 \le k \le N, \ 0 \le n \le M. \end{cases}$$ (7)

The formula (4) is rewritten as

$$\left(\frac{t_k^2}{\tau^2} + 2\frac{t_k}{\tau}\right)u_n^{k+1} + \left(-\frac{x_n^2}{h^2} - \frac{x_k}{h}\right)u_{n+1}^k$$
$$+ \left(-2\frac{t_k^2}{\tau^2} - 2\frac{t_k}{\tau} + 1 + 2\frac{x_n^2}{h^2}\right)u_n^k \qquad (8)$$
$$+ \left(-\frac{x_n^2}{h^2} + \frac{x_n}{h}\right)u_{n-1}^k + \left(\frac{t_k^2}{\tau^2}\right)u_n^{k-1} = f_n^k.$$

Then, the last formula can be written as

$$au_n^{k+1} + bu_{n+1}^k + cu_n^k + du_{n-1}^k + eu_n^{k-1} = f_n^k. \quad (9)$$

Here,

$$a = \frac{t_k^2}{\tau^2} + 2\frac{t_k}{\tau}, \; b = -\frac{x_n^2}{h^2} - \frac{x_k}{h},$$

$$c = -2\frac{t_k^2}{\tau^2} - 2\frac{t_k}{\tau} + 1 + 2\frac{x_n^2}{h^2},$$

$$d = -\frac{x_n^2}{h^2} + \frac{x_n}{h} \;\text{ and }\; e = \frac{t_k^2}{\tau^2}.$$

From the formula (9), the following matrices' formulas are obtained as

$$AU^{k+1} + BU^k + CU^{k-1} = \phi^k. \qquad (10)$$

where, A, B and C are $(N+1) \times (N+1)$ matrix, U^{k+1}, U^k, U^{k-1} and $\phi^k = F_n^k$ is $(N+1) \times 1$ vector as the following

$$A = a \begin{bmatrix} 0 & 0 & 0 & \dots & 0 & 0 & 0 \\ 0 & 1 & 0 & \dots & 0 & 0 & 0 \\ 0 & 0 & 1 & \dots & 0 & 0 & 0 \\ \vdots & \vdots & \vdots & \ddots & \vdots & \vdots & \vdots \\ 0 & 0 & 0 & \dots & 1 & 0 & 0 \\ 0 & 0 & 0 & \dots & 0 & 1 & 0 \\ 0 & 0 & 0 & \dots & 0 & 0 & 0 \end{bmatrix}_{(N+1)\times(N+1)},$$

$$(11)$$

$$B = \begin{bmatrix} c & b & 0 & 0 & \dots & 0 & 0 & 0 & 0 \\ d & c & b & 0 & \dots & 0 & 0 & 0 & 0 \\ 0 & d & c & b & \dots & 0 & 0 & 0 & 0 \\ 0 & 0 & d & c & \dots & 0 & 0 & 0 & 0 \\ \vdots & \vdots & \vdots & \vdots & \ddots & \vdots & \vdots & \vdots & \vdots \\ 0 & 0 & 0 & 0 & \dots & c & b & 0 & 0 \\ 0 & 0 & 0 & 0 & \dots & d & c & b & 0 \\ 0 & 0 & 0 & 0 & \dots & 0 & d & c & b \\ 0 & 0 & 0 & 0 & \dots & 0 & 0 & d & c \end{bmatrix}_{(N+1)\times(N+1)}$$

$$(12)$$

$$C = e \begin{bmatrix} 1 & 0 & 0 & \dots & 0 & 0 & 0 \\ 0 & 1 & 0 & \dots & 0 & 0 & 0 \\ 0 & 0 & 1 & \dots & 0 & 0 & 0 \\ \vdots & \vdots & \vdots & \ddots & \vdots & \vdots & \vdots \\ 0 & 0 & 0 & \dots & 1 & 0 & 0 \\ 0 & 0 & 0 & \dots & 0 & 1 & 0 \\ 0 & 0 & 0 & \dots & 0 & 0 & 1 \end{bmatrix}_{(N+1)\times(N+1)},$$

$$(13)$$

$$U^{k-1} = \begin{bmatrix} u_0^{k-1} \\ u_1^{k-1} \\ u_2^{k-1} \\ \vdots \\ u_{N-1}^{k-1} \\ u_N^{k-1} \end{bmatrix}_{(N+1)\times1} \quad U^k = \begin{bmatrix} u_0^k \\ u_1^k \\ u_2^k \\ \vdots \\ u_{N-1}^k \\ u_N^k \end{bmatrix}_{(N+1)\times1}$$

$$U^{k+1} = \begin{bmatrix} u_0^{k+1} \\ u_1^{k+1} \\ u_2^{k+1} \\ \vdots \\ u_{N-1}^{k+1} \\ u_N^{k+1} \end{bmatrix}_{(N+1)\times1.}$$

Modified Gauss elimination method is applied to solve the above difference equations. After that, a solution of the matrix equation is looked for as the following form

$$u_j = \alpha_{j+1}u_{j+1} + \beta_{j+1}; \; u_M = 0; \; j = M-1, \dots, 2, 1. \quad (14)$$

Using boundary conditions, the formula

$$u_0 = \alpha_1 u_1 + \beta_1 = 0$$

is obtained. Then, α_1 is obtained the $(N+1) \times (N+1)$ zero matrix and β_1 is obtained the $(N+1) \times 1$ zero column vector. Using the formula (14), the following formula is found

$$Au_{j+1} + B[\alpha_{j+1}u_{j+1} + \beta_{j+1}] + C[\alpha_j u_j + \beta_j] = \phi_j,$$

$$Au_{j+1} + B[\alpha_{j+1}u_{j+1} + \beta_{j+1}] + C[\alpha_j[\alpha_{j+1}u_{j+1} + \beta_{j+1}] + \beta_j] = \phi_j,$$

$$Au_{j+1} + B\alpha_{j+1}u_{j+1} + B\beta_{j+1} + C\alpha_j\alpha_{j+1}u_{j+1} + C\alpha_j\beta_{j+1} + C\beta_j = \phi_j,$$

$$[A + B\alpha_{j+1} + C\alpha_j\alpha_{j+1}]u_{j+1} + B\beta_{j+1}$$
$$+ C\alpha_j\beta_{j+1} + C\beta_j = \phi_j,$$

and then also

$$[A + B\alpha_{j+1} + C\alpha_j\alpha_{j+1}]u_{j+1} = 0$$
and   (15)
$$B\beta_{j+1} + C\alpha_j\beta_{j+1} + C\beta_j = \phi_j.$$

From the (15), the formulas are found

$$\alpha_{j+1} = -(B + C\alpha_j)^{-1}A,$$

and

$$\beta_{j+1} = (B + C\alpha_j)^{-1}(D\phi - C\beta_j), \quad j = 1, 2, \ldots, M-1.$$

Here, α_j is $(N+1) \times (N+1)$ zero matrix and β_j is $(N+1) \times 1$ zero column vector.

Now, we shall prove the stability estimate by applying the method of analyzing the eigenvalues of the iteration matrices of the schemes for the formula (4). For this, we express $\|A\| = \|A\|_\infty = \max\limits_{1 \le k \le N-1}\left[\sum_{i=1}^{N-1}|a_{km}|\right]$, where $A = [a_{km}]_{(N-1) \times (N-1)}$, I is unit matrix.

Let $\rho(A)$ be the spectral radius of a matrix A, which means the maximum of the absolute value of the eigenvalues of the matrix A. We can write the following theorem.

Theorem 1. *If* $-2\dfrac{t_k^2}{\tau^2} - 2\dfrac{t_k}{\tau} + 1 + 2\dfrac{x_n^2}{h^2} > 0$, *then, the difference scheme (4) is stable.*

Proof. From the method [18], we should prove that $\rho(\alpha_n) < 1$, $1 \le n \le M$.

$\rho(\alpha_1) = 0 < 1$ is clearly.

$$\rho(\alpha_2) = \left\|-BA^{-1}\right\| \le \|-B\|\left\|A^{-1}\right\|$$

$$= \|B\| \frac{1}{\min\limits_{1 \le k \le N-1}\left\{|a_{kk}| - \sum\limits_{\substack{m \ne k, \\ m=1}}^{N-1}|a_{km}|\right\}}$$

$$= \frac{\left|-2\dfrac{t_k^2}{\tau^2} - 2\dfrac{t_k}{\tau} + 1 + 2\dfrac{x_n^2}{h^2}\right|}{\left|\dfrac{t_k^2}{\tau^2} + \dfrac{t_k}{\tau}\right|}$$

$$+ \frac{\left|-\dfrac{x_n^2}{h^2} - \dfrac{x_k}{h}\right| + \left|-\dfrac{x_n^2}{h^2} + \dfrac{x_k}{h}\right|}{\left|\dfrac{t_k^2}{\tau^2} + \dfrac{t_k}{\tau}\right|}$$

$$= \frac{-2\dfrac{t_k^2}{\tau^2} - 2\dfrac{t_k}{\tau} + 1 + 2\dfrac{x_n^2}{h^2} - \dfrac{x_n^2}{h^2} - \dfrac{x_k}{h} - \dfrac{x_n^2}{h^2} + \dfrac{x_k}{h}}{\dfrac{t_k^2}{\tau^2} + \dfrac{t_k}{\tau}}$$

$$= \frac{1 - 2\dfrac{t_k^2}{\tau^2} - 2\dfrac{t_k}{\tau}}{\dfrac{t_k^2}{\tau^2} + \dfrac{t_k}{\tau}}$$

$$= \frac{1 - 2(k^2 + k)}{(k^2 + k)} \le 1, \ k = 1, 2, \ldots M.$$

If $\rho(\alpha_n) < 1$, let us calculate $\rho(\alpha_{n+1})$ for the formula (3) and procedure [19]. We know that $\alpha_{ni} = \rho(\alpha_n)$ and $0 \le \rho(\alpha_n) < 1$ for $2 \le i \le N+1$. Then, we can obtain that $\rho(\alpha_{n+1}) < 1$. Thus, the proof of the theorem is completed. $\square$

For the stability estimate of the second order difference schemes formula (5), a similar procedure can be used. The stability estimates of the formulas (6) and (7) were given in the [13], [17].

Now let's find the approximate solutions of a few examples for the application of these theoretical expressions.

3. Numerical experiments

In this section, some numerical example for the telegraph partial differential equation by the first and second order difference schemes method will be present. We can calculate the maximum norm of the error of the numerical solution as

$$E_M^N = \max\limits_{1 \le k \le N-1, 1 \le n \le M-1}|u(t_k, x_n) - u_n^k|.$$

Where $u(t_k, x_n)$ represents the exact solution and u_n^k represents numerical solution at points (t_k, x_n). Result of calculations tell us the second order has more accurate than the first order of accuracy difference scheme.

Example 1. *Consider the following initial boundary value problem for Telegraph partial differential equation*

$$\begin{cases} u_{tt}(t,x) + u_t(t,x) - u_{xx}(t,x) - u_x(t,x) + u(t,x) \\ = \cos(x-t) - \sin(x)\cos(t),\ 0 < t < 1,\ \ 0 < x < \pi, \\ u(0,x) = -\sin(x),\ \ u_t(0,x) = 0, \\ \ u(t,0) = u(t,\pi) = 0, 0 \le t \le 1,\ 0 \le x \le \pi. \end{cases}$$
$$(16)$$

Using the Laplace transform method, the exact solution of the problem (16) is $u(x,t) = -\sin(x)\cos(t)$. Error analysis Table 1 is shown the approximation solution of the problem (16).

Table 1. Error analysis for exact and approximation solution for example 16.

$\tau = 1/N,$ $h = \pi/M$	First Order Difference Scheme	Second Order Difference Scheme
$N = M = 20$	1.1102×10^{-2}	1.8527×10^{-3}
$N = M = 50$	3.8794×10^{-3}	2.9979×10^{-4}
$N = M = 100$	1.8400×10^{-3}	7.5204×10^{-5}
$N = M = 200$	8.9448×10^{-4}	1.8815×10^{-5}
$N = M = 400$	4.4078×10^{-4}	4.7025×10^{-6}
$N = M = 600$	2.9241×10^{-4}	2.0896×10^{-6}

Example 2. *Investigate the following initial boundary value problem for Telegraph partial differential equation*

$$\begin{cases} u_{tt}(t,x) + u_t(t,x) - u_{xx}(t,x) - u_x(t,x) + u(t,x) \\ = (x^2 - 2x - 2)e^{-t} + \pi(1-x)e^{-t}, \\ \ 0 < t < 1,\ 0 < x < \pi, \\ u(0,x) = x(x-\pi),\ \ u_t(0,x) = -x(x-\pi), \\ u(t,0) = u(t,\pi) = 0,\ \ 0 \le t \le 1,\ 0 \le x \le \pi. \end{cases}$$
$$(17)$$

The exact solution of the problem (17) is $u(x,t) = (x^2 - \pi x)e^{-t}$. Error analysis Table 2 is shown the approximation solution of the problem (17).

Table 2. Error analysis for exact and approximation solution for example 17.

$\tau = 1/N,$ $h = \pi/M$	First Order Difference Scheme	Second Order Difference Scheme
$N = M = 20$	3.7052×10^{-2}	2.1852×10^{-3}
$N = M = 50$	1.5780×10^{-2}	3.5362×10^{-4}
$N = M = 100$	8.0644×10^{-3}	8.8693×10^{-5}
$N = M = 200$	4.0783×10^{-3}	2.2207×10^{-5}
$N = M = 400$	2.0505×10^{-3}	5.5558×10^{-6}
$N = M = 600$	1.3695×10^{-3}	2.4698×10^{-6}

The exact and approximate solution of these examples are also presented in the following figures.
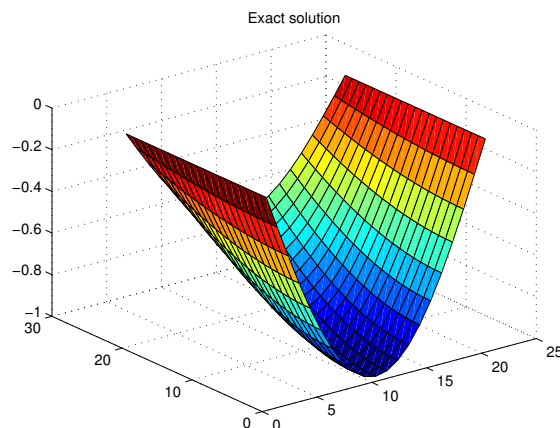

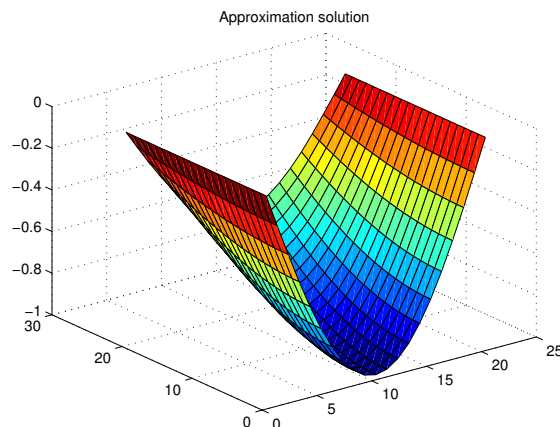**Figure 1.** Figure of exact solution for problem16, where N=M=20.

Figure 2. Figure of approximation solution for problem 16, where N=M=20.

Remark 1. *Using the first order difference scheme formula (4), we obtain the the following numerical results for the problem (2) and example (17). For example; Taking $N = 21, M = 20$, we obtain maxerror $= 8.7021 \times 10^{-1}$. For these values, the figures are the added as follow:*
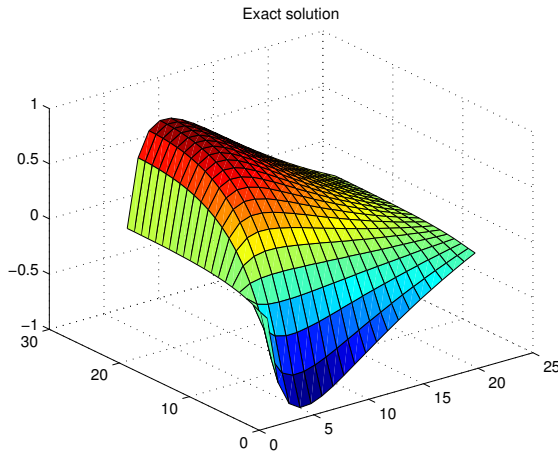

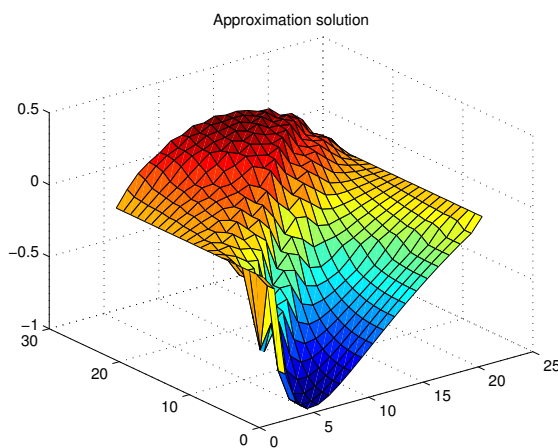**Figure 3.** Figure of exact solution for problem(2) and example (16), where N=21, M=20.

Figure 4. Figure of approximation solution for problem(2) and example (16), where N=21, M=20.

Remark 2. *The following results are obtained through using the Cauchy-Euler formula:*
i. The non-uniform region becomes a smooth region. And this is easier made calculation of the Matlab program.
ii. This also provides to obtain more appropriate and beautiful numerical results.

4. Conclusion

In this paper, the variable telegraph partial differential equation has been investigated. Then, this equation is transformed to the constant coefficient via using Cauchy-Euler formula. For this equation, we construct the first and second order difference schemes. Stability estimate is proved for these difference schemes. The exact and approximate solution of the problem were compared to obtain the error analysis in the maximum norm. Numerical examples show that this method is appropriate for this problem.

Acknowledgments

References

[1] Çelik, C., & Duman, M.(2012). Crank-Nicolson method for the fractional diffusion equation with the Riesz fractional derivative. *Journal of computational physics*, 231(4), 1743-1750.

[2] Gorial, I. I. (2011). Numerical methods for fractional reaction-dispersion equation with Riesz space fractional derivative. *Engineering and Technology Journal*, 29(4), 709-715.

[3] Jafari, H., & Daftardar-Gejji, V. (2006). Solving linear and nonlinear fractional diffusion and wave equations by Adomian decomposition. *Applied Mathematics and Computation*, 180(2), 488-497.

[4] Karatay, I., Bayramoglu, ŞR., & Şahin, A. (2011). Implicit difference approximation for the time fractional heat equation with the nonlocal condition. *Applied Numerical Mathematics*, 61(12), 1281-1288.

[5] Su, L., Wang, W., & Yang, Z. (2009). Finite difference approximations for the fractional advection-diffusion equation. *Physics Letters A*, 373(48), 4405-4408.

[6] Tadjeran, C., Meerschaert, M. M., Scheffler, H.P.(2006). A second order accurate numerical approximation for the fractional diffusion equation. *Journal of computational physics*, 213(1), 205-213.

[7] Nouy, A. (2010). A priori model reduction through proper generalized decomposition for solving time-dependent partial differential equations. *Computer Methods in Applied Mechanics and Engineering*, 199(23-24), 1603-1626.

[8] Wu, J. (1996). *Theory and applications of partial functional differential equations*, Springer-Verlag, New York.

[9] Pontryagin, L. S. (2018). *Mathematical theory of optimal processes*, Routledge, London.

[10] He, J. H. (2008). Recent development of the homotopy perturbation method. *Topological methods in nonlinear analysis*, 31(2), 205-209.

[11] Holmes, E. E., Lewis, M. A., Banks, J. E., & Veit, R. R. (1994). Partial differential equations in ecology: spatial interactions and population dynamics. *Ecology*, 75(1), 17-29.

[12] Dehghan, M., Shokri, A. (2008). A numerical method for solving the hyperbolic telegraph equation. *Numerical Methods for Partial Differential Equations*, 24(4), 1080-1093.

[13] Faraj, B., & Modanli, M. (2017). Using difference scheme method for the numerical solution of telegraph partial differential equation. *Journal of Garmian University*, 3, 157-163.

[14] Ashyralyev, A., & Modanli, M. (2015). An operator method for telegraph partial differential and difference equations. *Boundary Value Problems*, 41(1), 1-17.

[15] Ashyralyev, A., & Modanli, M. (2015). Nonlocal boundary value problem for telegraph equations. *AIP Conference Proceedings,* 1676(1), 020078-1 - 020078-4.

[16] Ashyralyev A, & Modanli, M. (2014). A numerical solution for a telegraph equation. *AIP Conference Proceedings*, 1611(1), 300-304.

[17] Faraj, B. M. (2018). *Difference scheme methods for telegraph partial differential equations.* MSc Thesis. Harran University.

[18] Smith, G. D. (1985). *Numerical solution of partial differential equations: finite difference methods.* Oxford university press.

[19] Richtmyer, R. D., & Morton, K. W. (1994). *Difference methods for initial-value problems*, Krieger Publishing Co., 2nd ed., Portland, USA.

Mahmut Modanli *is an associate professor in applied mathematics holding PhD at Department of Mathematics, Faculty of Arts and Sciences, Harran University, Şanlıurfa, 63010, Turkey.*
http://orcid.org/0000-0002-7743-3512

Bawar Mohammed Faraj *is an assistant lecturer holding Msc in applied mathematics at Computer science department, College of Science, University of Halabja, Halabja, 46018, Iraq.*
http://orcid.org/0000-0002-7543-2890

Faraedoon Waly Ahmed *is an assistant lecturer holding Msc in electrical engineering at Department of Physics, college of Science, University of Halabja, Halabja, 46018, Iraq.*
http://orcid.org/0000-0003-3016-6274

IJOCTA
An International Journal of
Optimization and Control:
Theories & Applications
2010

RESEARCH ARTICLE

Numerical investigation of nonlinear generalized regularized long wave equation via delta-shaped basis functions

Ömer Oruç*

Eğil Vocational and Technical Anatolian High School, Diyarbakır, Turkey
omeroruc0@gmail.com

ARTICLE INFO	ABSTRACT
	In this study we will investigate generalized regularized long wave (GRLW) equation numerically. The GRLW equation is a highly nonlinear partial differential equation. We use finite difference approach for time derivatives and linearize the nonlinear equation. Then for space discretization we use delta-shaped basis functions which are relatively few studied basis functions. By doing so we obtain a linear system of equations whose solution is used for constructing numerical solution of the GRLW equation. To see efficiency of the proposed method four classic test problems namely the motion of a single solitary wave, interaction of two solitary waves, interaction of three solitary waves and Maxwellian initial condition are solved. Further, invariants are calculated. The results of numerical simulations are compared with exact solutions if available and with finite difference, finite element and some collocation methods. The comparison indicates that the proposed method is favorable and gives accurate results.

1. Introduction

Consider following generalized equation

$$u_t + \alpha u_x + \epsilon \left(u^p\right)_x - \mu u_{xxt} - \gamma u_{xx} = 0, \qquad (1)$$
$$-\infty < x < \infty, \ t > 0$$

in which t is time, x is spatial variable and u is the amplitude, and $\alpha \geq 0$, $\epsilon \geq 0$, $\mu \geq 0$, $\gamma \geq 0$, $p \geq 2$. The Eq. (1) presents a lot of mathematical models according to the values of α, ϵ, μ, γ [1] for instance :

- if $\alpha = 0$, $\epsilon = 0$, $\mu = 0$, $\gamma \neq 0$ then Eq. (1) corresponds to heat equation,
- if $\alpha \neq 0$, $\epsilon = 0$, $\mu = 0$, $\gamma = 0$ then Eq. (1) corresponds to wave equation,
- if $\alpha = 0$, $\epsilon \neq 0$, $\mu = 0$, $\gamma \neq 0$, $p = 2$ then Eq. (1) corresponds to viscous Burgers' equation,

- if $\alpha = 1$, $\epsilon \neq 0$, $\mu \neq 0$, $\gamma = 0$, $p = 2$ then Eq. (1) corresponds regularized long wave (RLW) equation,
- if $\alpha = 1$, $\epsilon \neq 0$, $\mu \neq 0$, $\gamma = 0$, $p > 2$ then Eq. (1) corresponds generalized regularized long wave (GRLW) equation.

In this paper, we will study GRLW equation numerically. The GRLW equation was first proposed by Peregrine [2, 3] for description of an undular bore and then by Benjamin et al. [4] GRLW equation suggested as a model for long waves with small amplitudes on the surface of water in a channel. Since the GRLW equation can be a model for a lot of real life phenomena such as plasma waves [5] and shallow water waves [2] it is crucial to develop efficient methods for solving this equation. Since analytical solutions of the GRLW equation are available only for limited initial and boundary conditions it is inevitable for

---

*Corresponding Author

looking at numerical methods. Due to highly non-linear structure of the GRLW equation, developing efficient numerical methods for this equation also is a challenging work.

GRLW equation includes RLW and modified RLW equation for certain values of p. There are a vast of studies related to both RLW and modified RLW equations, see for example [6–14] and references therein. On the other hand for the GRLW equation literature is not so rich. But, nevertheless there are some studies related to the GRLW equation. For example, the GRLW equation has been solved using Sinc-collocation method [16], Wang et al. [17] used a meshless method for the GRLW equation, element-free kp-Ritz method has been used by Guo et al. [18] for solving the GRLW equation, Kang et al. [19] used a second-order Fourier pseudospectral method for the GRLW equation, compact finite difference method and finite difference method have been used in [20, 21], respectively. Roshan [22], used a Petrov-Galerkin method for the GRLW equation. B-spline finite element method has been used in [23], a collocation method with cubic B-splines is used in [6], Karakoc and Zeybek [24] used septic B-spline collocation method, more recently local momentum-preserving algorithms [25] are developed for the GRLW equation.

We will investigate numerical solution of the GRLW equation given in following form;

$$u_t + u_x + p(p+1)u^p u_x - \mu u_{xxt} = 0, \quad a \le x \le b \tag{2}$$

with Dirichlet boundary conditions $u(a,t) = u(b,t) = 0$ by employing finite difference and delta-shaped basis functions.

The paper is organized as follows. In Section 2, a brief information about delta-shaped basis functions is given. In section 3, time discretization with finite difference and space discretization with delta-shaped basis functions are described. The results of numerical simulations are presented in Section 4. Finally, the paper is concluded in Section 5.

2. Delta-shaped basis functions

Delta-shaped basis functions (DBFs) have been derived by Reutskiy [26] from Fourier series of Dirac-delta function and were used for simulating a set of scattered data in both regular and irregular domains successfully. Since then DBFs have been used in some studies for numerical solution of partial differential equations. For instance, DBFs are used for solving Helmholtz-type equations in [27, 28], Hon and Yang used DBFs for

default barrier model [29], one-dimensional Stefan problems are solved by DBFs [30], numerical solution of the Schrödinger equations are obtained by using DBFs [31], DBFs are used for solving ill-posed nonhomogeneous elliptic boundary value problems [32], recently a pseudo spectral method based on DBFs is developed in [33] for solving modified Burgers equation. We briefly introduce delta-shaped basis functions, in the sequel [29, 31]. Consider following Sturm-Liouville eigenvalue problem

$$\begin{cases} -\frac{d^2\phi}{dx^2} = \lambda\phi, & x \in (-1,1), \\ \phi(-1) = \phi(1) = 0. \end{cases}$$

Let $(\phi_n(x), \lambda_n)$ be a solution to the above Sturm-Liouville eigenvalue problem. Clearly, $\phi_n(x) = \sin\left(n\pi\frac{x+1}{2}\right)$, $\lambda_n = \left(\frac{n\pi}{2}\right)^2$ and further

$$\int_{-1}^{1} \phi_m(x)\phi_n(x)dx = \delta_{mn} = \begin{cases} 1, & m = n, \\ 0, & m \ne n. \end{cases}$$

That means, eigenfunctions $\{\phi_n(x)\}_{n=1}^{\infty}$ form an orthogonal system on interval $[-1, 1]$ and furthermore Dirac's delta function can be expressed as follows

$$\delta(x - \xi) = \sum_{n=1}^{\infty} \phi_n(\xi)\phi_n(x). \tag{3}$$

The series in Eq. (3), can be used with some regularization techniques [30] to derive smooth delta-shaped function $I_{M,\chi}(x,\xi)$. Otherwise the series in Eq. (3) diverges at any point in the interval $[-1,1]$ [26]. Here we consider Riesz regularization approach and thus the regularized delta-shaped functions are in the following form

$$I_{M,\chi}(x,\xi) = \sum_{n=1}^{M} \left(1 - \frac{n^2}{(M+1)^2}\right)^{\chi} \phi_n(\xi)\phi_n(x). \tag{4}$$

The parameters M and χ may be think of as shape parameters since they form the properties of delta-shaped functions. The parameter M is responsible for scaling, as M increases the support of basis function decreases. This can be seen in left column of Fig. 1. The parameter χ responsible for regularizing, if $\chi = 0$ i.e. when there is no regularization, basis function shows oscillating behavior on its support. On the other hand if χ increases basis function gets smoother. We show this situation in right column of Fig. 1. We should note that choosing optimal values of shape
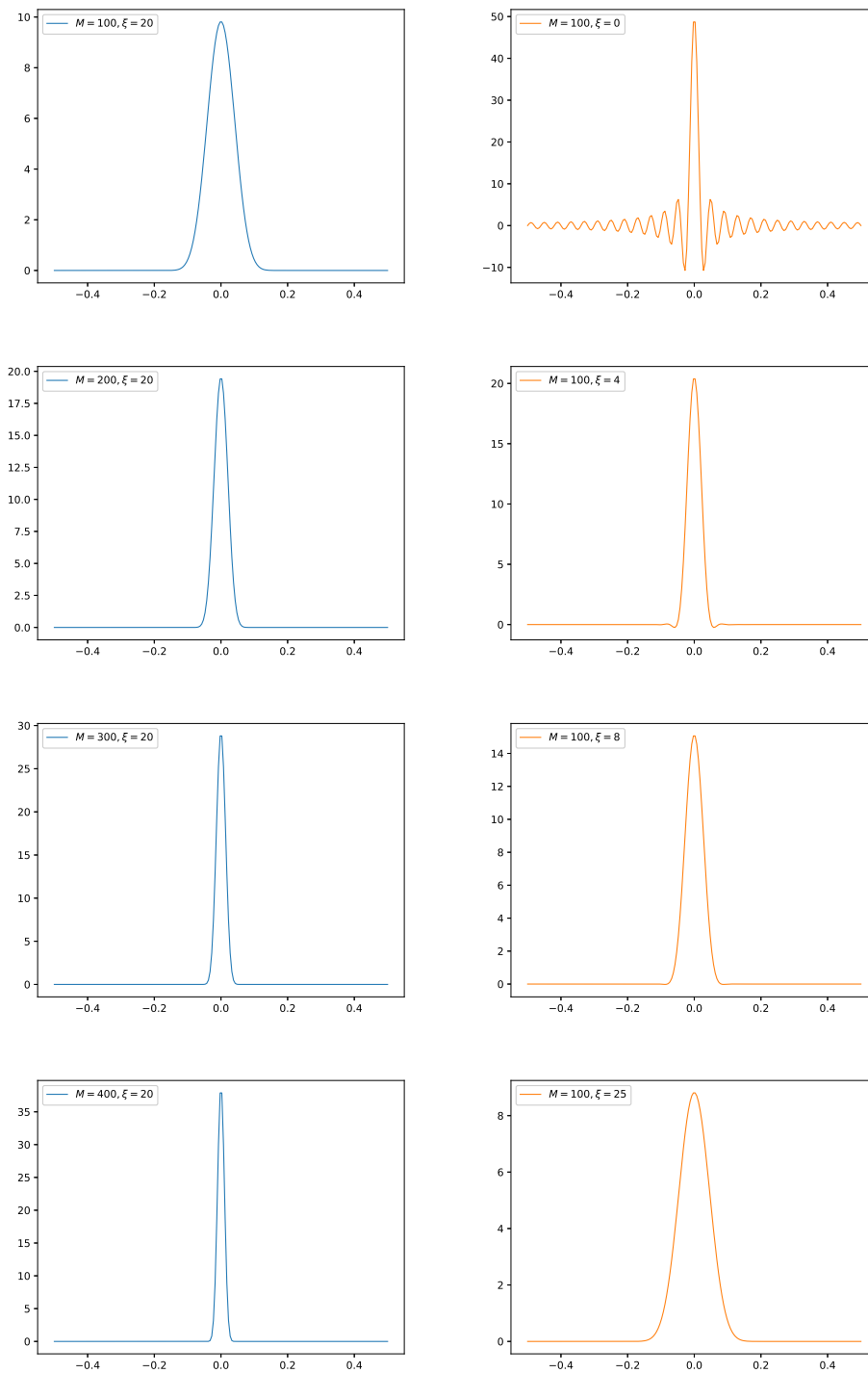
Figure 1. Effect of M and χ with center $\xi = 0$ on delta-shaped functions.

parameters for delta-shaped functions is still an open problem.

3. Solution method for GRLW equation

In this section, we describe time discretization and space discretization for the GRLW equation. We start with time discretization.

3.1. Time discretization by finite differences

We take GRLW equation as

$$u_t + u_x + \epsilon u^p u_x - \mu u_{xxt} = 0, \quad a \leq x \leq b,\ t > 0 \tag{5}$$

with initial condition

$$u(x,0) = f(x),$$

and boundary conditions

$$u(a,t) = g_1(t), \ u(b,t) = g_2(t), \ t \geq 0, \qquad (6)$$

where $\epsilon = p(p+1) > 0$, $\mu > 0$ and $f(x), g_1(t)$ and $g_2(t)$ are prescribed functions. We use forward Euler formula for time derivatives and utilize $\theta-$weighted $(0 \leq \theta \leq 1)$ scheme between time levels j and $j+1$ as

$$\frac{u^{j+1} - u^j}{\Delta t} + \theta \left[(u_x)^{j+1} + \epsilon \left(u^p u_x \right)^{j+1} \right]$$
$$+ (1 - \theta) \left[(u_x)^j + \epsilon \left(u^p u_x \right)^j \right] \qquad (7)$$
$$- \frac{\mu}{\Delta t} \left((u_{xx})^{j+1} - (u_{xx})^j \right) = 0$$

where Δt is time step size and $t^{j+1} = t^j + \Delta t$, $u^{j+1} = u(x, t^{j+1})$. Following [16], the nonlinear term $(u^p u_x)^{j+1}$ can be linearized as

$$(u^p u_x)^{j+1} \simeq (u^p u_x)^j + \Delta t \left[(u_t^p)^j u_x^j + (u^p)^j (u_{xt})^j \right]$$
$$+ \mathcal{O}(\Delta t^2)$$
$$= (u^p u_x)^j$$
$$+ \Delta t \left[\frac{(u^p)^{j+1} - (u^p)^j}{\Delta t} u_x^j + (u^p)^j \frac{u_x^{j+1} - u_x^j}{\Delta t} \right]$$
$$+ \mathcal{O}(\Delta t^2)$$
$$\simeq (u^p)^j u_x^{j+1} + p \left(u^{p-1} \right)^j u_x^j u^{j+1} - p (u^p)^j u_x^j. \qquad (8)$$

Now by plugging Eq. (8) into the Eq. (7) we obtain time discretized scheme as follows [16].

$$u^{j+1}$$
$$+ \Delta t \theta \left[u_x^{j+1} + \epsilon \left((u^p)^j u_x^{j+1} + p \left(u^{p-1} \right)^j u_x^j u^{j+1} \right) \right]$$
$$- \mu (u_{xx})^{j+1}$$
$$= u^j + \Delta t \left[\epsilon ((p+1)\theta - 1) (u^p)^j u_x^j - (1-\theta) u_x^j \right]$$
$$- \mu (u_{xx})^j$$
$$(9)$$

In numerical calculations we select $\theta = \frac{1}{2}$ which corresponds famous Crank-Nicolson approach.

3.2. Space discretization with DBFs

Let us assume the solution $u(x)$ can be approximated by the linear combination of DBFs as follows

$$u^{j+1}(x) = \sum_{i=1}^{N} \lambda_i^{j+1} I_{M,\chi}(x, \xi_i). \qquad (10)$$

Then first and second order derivatives can be found simply as

$$\frac{d}{dx} u^{j+1}(x) = \sum_{i=1}^{N} \lambda_i^{j+1} \frac{d}{dx} I_{M,\chi}(x, \xi_i), \qquad (11)$$

$$\frac{d^2}{dx^2} u^{j+1}(x) = \sum_{i=1}^{N} \lambda_i^{j+1} \frac{d^2}{dx^2} I_{M,\chi}(x, \xi_i), \qquad (12)$$

Substituting Eqs. (10)-(12) into the Eq. (9) we obtain

$$\sum_{i=1}^{N} \lambda_i^{j+1} \left(I_{M,\chi}(x, \xi_i) + \Delta t \theta \left[\frac{d}{dx} I_{M,\chi}(x, \xi_i) \right. \right.$$
$$\left. + \epsilon \left((u^p)^j \frac{d}{dx} I_{M,\chi}(x, \xi_i) + p \left(u^{p-1} \right)^j u_x^j I_{M,\chi}(x, \xi_i) \right) \right]$$
$$\left. - \mu \frac{d^2}{dx^2} I_{M,\chi}(x, \xi_i) \right)$$
$$= \Delta t \left[\epsilon ((p+1)\theta - 1) (u^p)^j u_x^j - (1-\theta) u_x^j \right]$$
$$+ u^j - \mu (u_{xx})^j$$
$$(13)$$

Discretizing Eq. (13) at collocation points $a = x_1 < x_2 < ... < x_N = b$ and imposing boundary conditions (6) we can obtain a linear system of equations with size of $N \times N$ whose solution gives expansion coefficients λ_i. Then by using these coefficients in the (10) numerical solution can be found for each time step. The centers ξ_i are different from collocation points but for convenience we take ξ_i same as collocation points. For starting simulation, right hand side of the Eq. (13) must be calculated from initial condition.

We also should note that $I_{M,\chi}(x, \xi)$ vanishes near the boundaries $x = \pm 1$. Thus centers and collocation points should not be near the boundary in $[-1, 1]$. To overcome this issue, as pointed out in [26], considered partial differential equations should be redefined in subdomain $[-0.5, 0.5]$ by some scaling and transformation operations.

4. Numerical experiments

To indicate the performance of the proposed method we will use the error norms L_2 and L_∞ defined by

$$L_2 = \left\| u_i^{\text{exact}} - u_i^{\text{num}} \right\|_2$$

$$\simeq \left(\Delta x \sum_{i=1}^{N} \left| u_i^{\text{exact}} - u_i^{\text{num}} \right|^2 \right)^{1/2}$$

$$L_\infty = \left\| u_i^{\text{exact}} - u_i^{\text{num}} \right\|_\infty \simeq \max_i \left| u_i^{\text{exact}} - u_i^{\text{num}} \right|$$

and invariants [23]:

- Conservation of mass

$$I_1 = \int_a^b u \, dx = \Delta x \sum_{i=1}^{N} u_i,$$

- Conservation of momentum

$$I_2 = \int_a^b \left(u^2 + \mu u_x^2 \right) dx$$

$$= \Delta x \sum_{i=1}^{N} \left[(u_i)^2 + \mu \left((u_x)_i \right)^2 \right],$$

- Conservation of energy

$$I_3 = \int_a^b \left(u^4 - \mu u_x^2 \right) dx = \Delta x \sum_{i=1}^{N} \left(u_i^4 - \mu \left((u_x)_i \right)^2 \right).$$

Further, we calculate the convergence orders by the following formulae

$$C_1 = \frac{\log \left(\frac{L_{\infty,2}(2\Delta t, N)}{L_{\infty,2}(\Delta t, N)} \right)}{\log 2}, \qquad C_2 = \frac{\log \left(\frac{L_{\infty,2}(\Delta t, N)}{L_{\infty,2}(\Delta t, 2N)} \right)}{\log 2}$$

We denote absolute differences of I_1, I_2, I_3 between initial time $t = 0$ and final time $t = \text{t} - \text{final}$ as $|\Delta I_i| = |I_i^{\text{t-final}} - I_i^{\text{t-initial}}|$, $i = 1, 2, 3$. In all numerical simulations we choose $\theta = 0.5$ and we take $M = 2N + 100$, $\chi = M/40$ for single solitary wave problem, $M = 2N + 300$, $\chi = M/100$ for interaction of two-three solitary waves problem and $M = 5N + 100$, $\chi = M/100$ for Maxwellian problem. Numerical calculations have been done in Python environment [34, 35] with a desktop computer (Linux OS, NumPy version 1.15.1, Intel i7-8750H, 8GB RAM). Graphical outputs in this study were generated by Matplotlib package [36].

4.1. Single solitary wave motion

We investigate motion of single solitary given as

$$u(x, 0) = \sqrt[p]{\frac{c(p+2)}{2p} \sec h^2 \left(\frac{p}{2} \sqrt{\frac{c}{\mu(c+1)}} (x - x_0) \right)}.$$

To this end, we calculate the error norms L_2, L_∞ and the invariants I_1, I_2, I_3 for constant values of $x_0 = 40$, $\mu = 1$, $0 \leq x \leq 100$ and for various

values of Δt, c, p, N. Firstly, to see convergence of the present method in space we fix $\Delta t = 0.0001$ and we increase number of collocation points, obtained results are reported in Table 1. As it can be seen from the table by increasing number of collocation points the errors decrease. Later, we set $N = 400$ and decrease time step size to see convergence in temporal variable. Obtained results are given in Table 2 where one can see that by halving the time step size the errors decrease and convergence orders are about two which is theoretical convergence order of Crank-Nicolson method.

In Table 3, for $N = 100$, $c = 0.1$, $\Delta t = 0.05$ and $p = 2, 3$ the error norms are given at different final times with CPU times taken during simulation. Accuracy of the results can be seen from the table. Table 4 indicates variation in the invariants for $N = 400$, $\Delta t = 0.1$, $c = 0.1$ and $p = 2, 3$ at different final times. From the table one can conclude that the proposed method can conserve invariants quite good.

In Tables 5 and 6 the invariants and errors are calculated and compared with ones of septic B-spline collocation method [24] for $\Delta t = 0.01$, $\mu = 1$, $p = 4$, $c = 0.3$ and $N = 250$ (in case of the present method), $h = 0.1$ (in case of the method of [24]). Absolute differences of I_1, I_2, I_3 between initial time $t = 0$ and final time $t = 10$ are approximately $2e - 07$, $2e - 06$, $2e - 06$, respectively for the method of [24] while these differences are approximately $2e - 07$, $4e - 07$, $1.2e - 06$, respectively for the present method. In Table 7, a comprehensive comparison between B-spline finite element [23], cubic B-spline collocation [6], Petrov-Galerkin [22], septic B-spline collocation [24] methods and the present method is given for $p = 2, 3, 4$. For present method we take $N = 250$ while for the other methods space step size h is taken as 0.2 and 0.1. From the table it is clearly seen that for $p = 3$ lowest errors are obtained by the present method and for $p = 2, 4$ lowest errors are obtained by the method of [24]. Finally in Table 8 a comparison with compact finite difference [20] is given for $\Delta t = c = 0.1$ where accuracy of the present method is obvious.

In Figs. 2 and 3, motion of single solitary waves are given for $p = 3$, $c = 1.2$ and $p = 4$, $c = 4/3$, respectively. It can be seen that at $t = 0$ the solitary wave is located at $x_0 = 40$ and as time goes the single solitary wave moves rightward with constant speed and with almost invariable amplitude.

Table 1. Error norms and convergence orders for $c = 4/3$, $p = 4$ and increasing values of N at $t = 0.1$.

N	L_2	L_∞	C_2 for L_2	C_2 for L_∞
40	7.154182e-01	4.146875e-01	-	-
80	1.528925e-01	1.253767e-01	2.2263	1.7258
160	1.141233e-03	8.628014e-04	7.0658	7.1830
320	1.912428e-05	2.386172e-05	5.8990	5.1763

Table 2. Error norms and convergence orders for $c = 4/3$, $p = 4$ and decreasing values of Δt at $t = 1$.

Δt	L_2	L_∞	C_1 for L_2	C_1 for L_∞
1/10	5.540555e-02	3.539277e-02	-	-
1/20	1.409159e-02	9.028174e-03	1.9752	2.0136
1/40	3.494540e-03	2.234878e-03	2.0117	2.0142
1/80	8.792614e-04	5.534720e-04	1.9907	2.0136

Table 3. Error norms and CPU times for $N = 100$, $c = 0.1$, $\Delta t = 0.05$, $x_0 = 40$ on $0 \le x \le 100$ at different times.

| Time | $p = 2$ | | $p = 3$ | | CPU time |
	L_2	L_∞	L_2	L_∞	
$t = 2$	1.396342e-05	5.698786e-06	3.618557e-05	1.747289e-05	0.03
$t = 4$	2.732318e-05	1.146938e-05	7.126962e-05	3.143534e-05	0.04
$t = 6$	4.059471e-05	1.720380e-05	1.060434e-04	4.661107e-05	0.04
$t = 8$	5.360908e-05	2.260812e-05	1.401759e-04	6.109345e-05	0.05
$t = 10$	6.632761e-05	2.753908e-05	1.736471e-04	7.520650e-05	0.06

Table 4. Invariants on $0 \le x \le 100$ for $N = 400$, $\Delta t = 0.1$, $c = 0.1$ at different final times.

| t | $p = 2$ | | | $p = 3$ | | | CPU time |
	I_1	I_2	I_3	I_1	I_2	I_3	
0	3.294918	0.683426	0.024121	4.062584	1.133875	0.092900	0.00
2	3.294919	0.683426	0.024121	4.062584	1.133874	0.092899	0.33
4	3.294920	0.683426	0.024121	4.062585	1.133873	0.092899	0.38
6	3.294919	0.683425	0.024121	4.062585	1.133872	0.092898	0.42
8	3.294919	0.683425	0.024121	4.062584	1.133871	0.092896	0.48
10	3.294918	0.683425	0.024121	4.062583	1.133871	0.092895	0.53

Table 5. Invariants and their comparison on $0 \le x \le 100$ for $N = 250$, $\Delta t = 0.01$, $\mu = 1$, $p = 4$, $c = 0.3$

| | [24] (second) | Present | [24] (second) | Present | [24] (second) | Present |
t	I_1	I_1	I_2	I_2	I_3	I_3
0	3.7592865	3.7592300	1.7300239	1.7300029	0.2894189	0.2894090
2	3.7592865	3.7592300	1.7300244	1.7300028	0.2894183	0.2894091
4	3.7592865	3.7592299	1.7300250	1.7300027	0.2894178	0.2894097
6	3.7592864	3.7592299	1.7300254	1.7300026	0.2894174	0.2894100
8	3.7592864	3.7592299	1.7300256	1.7300025	0.2894171	0.2894101
10	3.7592863	3.7592298	1.7300259	1.7300024	0.2894169	0.2894102

4.2. The interaction of two solitary waves

In this subsection, we examine interaction of two solitary waves, namely we consider the Eq. (2) with following initial condition

$$u(x,0) = \sum_{i=1}^{2} \sqrt[p]{\frac{c_i(p+2)}{2p}} \operatorname{sec} h^2 \left(\frac{p}{2} \sqrt{\frac{c_i}{\mu(c_i+1)}} (x - x_i) \right)$$

Table 6. Invariants and their comparison on $0 \leq x \leq 100$ for $N = 250$, $\Delta t = 0.01$, $\mu = 1$, $p = 4$, $c = 0.3$

t	[24] (first) $L_2 \times 10^4$	[24] (second) $L_2 \times 10^4$	Present $L_2 \times 10^4$	[24] (first) $L_\infty \times 10^4$	[24] (second) $L_\infty \times 10^4$	Present $L_\infty \times 10^4$
2	0.25417530	0.19937853	0.2803098	0.13193138	0.09833776	0.1510377
4	0.50867400	0.39600506	0.5629237	0.25511505	0.19527926	0.2957829
6	0.76378746	0.59159317	0.8494472	0.37848569	0.29108460	0.4345260
8	1.01967310	0.78622772	1.1406822	0.50227119	0.38611041	0.5756090
10	1.27628477	0.98004530	1.4373113	0.62645346	0.48083798	0.7138410

Table 7. Comparison of the results on $0 \leq x \leq 100$ for $\mu = 1$ at $t = 10$.

		$p = 2$, $c = 1$ $\Delta t = 0.025$, $h = 0.2$	$p = 3$, $c = 0.3$ $\Delta t = 0.01$, $h = 0.1$	$p = 4$, $c = 0.3$ $\Delta t = 0.01$, $h = 0.1$
I_1	Present method, $N = 250$	4.44288292	3.67755181	3.75922990
	Collocation+PA-CN (cubic) [23]	4.44000000	-	-
	Collocation-CN (cubic) [23]	4.44200000	-	-
	Collocation (cubic) [6]	4.44288000	-	-
	Petrov–Galerkin (quintic) [22]	4.44288000	3.67755000	3.75923000
	Collocation (septic) [24]	4.44286610	3.67760690	3.75928630
	Present method, $N = 250$	3.29978116	1.56574072	1.73000240
	Collocation+PA-CN (cubic) [23]	3.29600000	-	-
	Collocation-CN (cubic) [23]	3.29900000	-	-
	Collocation (cubic) [6]	3.29983000	-	-
I_2	Petrov–Galerkin (quintic) [22]	3.29981000	1.56574000	1.72999000
	Collocation (septic) [24]	3.29971510	1.56576200	1.73002590
	Present method, $N = 250$	1.41416306	0.22683878	0.28941022
	Collocation+PA-CN (cubic) [23]	1.41100000	-	-
	Collocation-CN (cubic) [23]	1.41300000	-	-
I_3	Collocation (cubic) [6]	1.41420000	-	-
	Petrov–Galerkin (quintic) [22]	1.41416000	0.22683700	0.28940600
	Collocation (septic) [24]	1.41431220	0.22684460	0.28941690
	Present method, $N = 250$	3.91431278	0.06900426	0.14368290
	Collocation+PA-CN (cubic) [23]	20.30000000	-	-
	Collocation-CN (cubic) [23]	16.39000000	-	-
$L_2 \times 10^3$	Collocation (cubic) [6]	9.30196000	-	-
	Petrov–Galerkin (quintic) [22]	3.00533000	0.07197600	0.12253900
	Collocation (septic) [24]	2.57148152	0.07851367	0.09800453
	Present method, $N = 250$	2.00191759	0.03304418	0.07169059
	Collocation+PA-CN (cubic) [23]	11.20000000	-	-
	Collocation-CN (cubic) [23]	9.24000000	-	-
$L_\infty \times 10^3$	Collocation (cubic) [6]	5.43718000	-	-
	Petrov–Galerkin (quintic) [22]	1.68749000	0.03772280	0.06620700
	Collocation (septic) [24]	1.34021078	0.03650124	0.04808379

which describes propagation of two waves with different amplitudes, one placed at x_1 and the other placed at x_2.

First numerical simulation have been done with the following values $p = 2$, $c_1 = 4$, $c_2 = 1$, $x_1 = 25$, $x_2 = 55$, $\Delta t = 0.025$, $\mu = 1$ on the interval $0 \leq x \leq 250$. The results obtained are reported in Table 9 and are compared with Petrov-Galerkin [22] and septic B-spline collocation [24] methods.

From the table we can see that the invariants obtained by the present method are compatible with the ones of [22], [24]. In Fig. 4, interaction of the solitary waves are depicted.

Second simulation have been done with $p = 3$, $c_1 = 48/5$, $c_2 = 6/5$, $x_1 = 20$, $x_2 = 50$, $\Delta t = 0.01$, $0 \leq x \leq 120$ and $\mu = 1$. The obtained results are reported and compared with the results of [22] and [24] in Table 10. Variations in the invariants I_1, I_2, I_3 are approximately $2.0e - 06$, 0.111,

Table 8. Comparison of the results on $0 \le x \le 100$, $\mu = 1$, $x_0 = 40$ and $\Delta t = c = 0.1$.

|		$p = 1$				$p = 2$			
		I_1	I_2	L_2	L_∞	I_1	I_2	L_2	L_∞
$t = 2$	[20], $h = 0.1$	1.989963	0.196378	0.013774	0.005403	3.29492	0.649425	0.039859	0.018973
	Present, $N = 250$	1.989964	0.202616	0.000011	0.000004	3.294919	0.683426	0.000055	0.000023
$t = 4$	[20], $h = 0.1$	1.989964	0.197220	0.012347	0.004610	3.29492	0.653939	0.036136	0.015780
	Present, $N = 250$	1.989965	0.202616	0.000022	0.000008	3.294920	0.683426	0.000109	0.000047
$t = 6$	[20], $h = 0.1$	1.989964	0.198076	0.010985	0.003841	3.29492	0.658616	0.032839	0.013296
	Present, $N = 250$	1.989965	0.202616	0.000032	0.000012	3.294919	0.683425	0.000162	0.000070
$t = 8$	[20], $h = 0.1$	1.989963	0.198947	0.009737	0.003158	3.29492	0.663465	0.030230	0.011791
	Present, $N = 250$	1.989964	0.202616	0.000043	0.000016	3.294919	0.683425	0.000214	0.000093
$t = 10$	[20], $h = 0.1$	1.989962	0.199832	0.008677	0.002656	3.29492	0.668494	0.028541	0.011065
	Present, $N = 250$	1.989963	0.202616	0.000053	0.000020	3.294918	0.683425	0.000265	0.000113
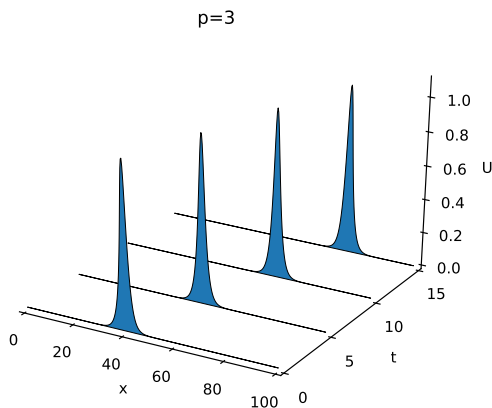
Figure 2. Motion of single solitary wave at $t = 0, 5, 10, 15$ for $N = 400$, $\Delta t = 0.05$ and $p = 3$.
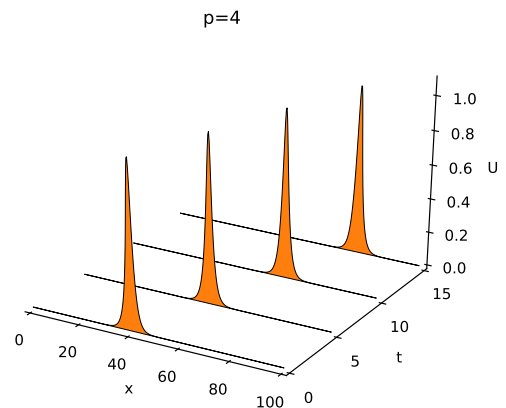
Figure 3. Motion of single solitary wave at $t = 0, 5, 10, 15$ for $N = 400$, $\Delta t = 0.05$ and $p = 4$.

Table 9. Comparison of the results for $p = 2$, $c_1 = 4$, $c_2 = 1$, $x_1 = 25$, $x_2 = 55$, $\Delta t = 0.025$, $\mu = 1$ on $0 \le x \le 250$ at different final times.

		$t = 0$	$t = 4$	$t = 8$	$t = 12$	$t = 16$	$t = 20$
I_1	Present method, $N = 400$	11.4676982	11.4677197	11.4676926	11.4676587	11.4676037	11.4674483
	[24] Collocation (second), $h = 0.2$	11.4676542	11.4676484	11.466 884 9	11.4676777	11.4676555	11.4676452
	[22] Petrov–Galerkin (quintic), $h = 0.2$	11.4677000	11.4677000	11.4677000	11.4677000	11.4677000	11.4677000
	Present method, $N = 400$	14.6290652	14.6194206	14.6068263	14.6029824	14.5933673	14.5831979
I_2	[24] Collocation (second), $h = 0.2$	14.6292089	14.6277880	14.1400014	14.6803731	14.6442435	14.6309639
	[22] Petrov–Galerkin (quintic), $h = 0.2$	14.6286000	14.6292000	14.6229000	14.6299000	14.6295000	14.6299000
	Present method, $N = 400$	22.8816460	22.8411085	22.7875495	22.7753681	22.7381963	22.6975609
	[24] Collocation (second), $h = 0.2$	22.8803575	22.8817784	23.3695650	22.8291933	22.8653229	22.8786025
	[22] Petrov–Galerkin (quintic), $h = 0.2$	22.8788000	22.8811000	22.8798000	22.8803000	22.8805000	22.8806000

0.45 respectively for the present method. Fig. 10 shows the interaction of the solitary waves.

4.3. The interaction of three solitary waves

The Eq. (2) with initial condition

$$u(x,0) = \sum_{i=1}^{3} \sqrt[p]{\frac{c_i(p+2)}{2p}} \sec h^2 \left(\frac{p}{2} \sqrt{\frac{c_i}{\mu(c_i+1)}} (x - x_i) \right)$$
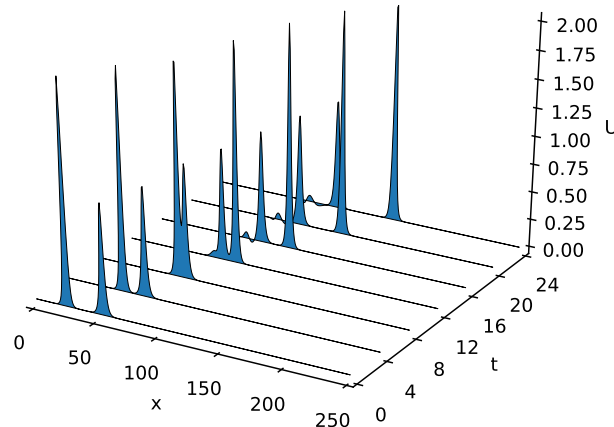
Figure 4. Interaction of two solitary waves for $N = 400$, $p = 2$, $c_1 = 4$, $c_2 = 1$, $x_1 = 25$, $x_2 = 55$, $\Delta t = 0.025$, and $\mu = 1$ at $t = 0, 4, 8, 12, 16, 20$.

Table 10. Comparison of the results for $p = 3$, $c_1 = 48/5$, $c_2 = 6/5$, $x_1 = 20$, $x_2 = 50$, $\Delta t = 0.01$, $\mu = 1$ on $0 \leq x \leq 120$ at different final times.

		$t = 0$	$t = 2$	$t = 3$	$t = 4$	$t = 5$	$t = 6$
I_1	Present method, $N = 400$	9.6907416	9.6907408	9.6907405	9.6907403	9.6907398	9.6907396
	[24] Collocation (second), $h = 0.1$	9.6907772	9.6881175	9.6850972	9.6860154	9.6847993	9.6834620
	[22] Petrov–Galerkin (quintic), $h = 0.1$	9.6907500	9.6907400	9.6907400	9.6907400	9.6907400	9.6907400
I_2	Present method, $N = 400$	12.9443811	12.9034856	12.8814687	12.8721151	12.8526253	12.8331028
	[24] Collocation (second), $h = 0.1$	12.9443914	12.9390629	12.3046064	12.9703128	13.0538036	13.0027533
	[22] Petrov–Galerkin (quintic), $h = 0.1$	12.9444000	12.9452000	12.9379000	12.9453000	12.9457000	12.9454000
I_3	Present method, $N = 400$	17.0187240	16.8733431	17.5959108	16.7459006	16.5917866	16.5602450
	[24] Collocation (second), $h = 0.1$	17.0186758	17.0240043	17.6584608	16.9927544	16.9092637	16.9603139
	[22] Petrov–Galerkin (quintic), $h = 0.1$	17.0184000	16.9835000	17.0591000	16.9261000	16.8781000	16.9113000

is considered in this subsection. The above initial condition describes movement of three solitary waves with different amplitudes in same direction. For numerical simulation, we choose $0 \leq x \leq 100$, $\mu = 1$, $c_1 = 0.6$, $c_2 = 0.3$, $c_3 = 0.15$, $x_1 = 15$, $x_2 = 35$, $x_3 = 60$ and different values of Δt and p. In Table 11, we calculate the invariants for $N = 400$, $p = 2$, $\Delta t = 0.1$ and compare the results with compact finite difference method [20]. In the same table we give absolute difference of the invariants approximately, between initial time $t = 0$ and final time $t = 10$ where it can be seen that the present method conserves invariants better than the method of [20]. In Tables 12, 13 the invariants and their changes are given for $N = 400$, $\Delta t = 0.05$ and $p = 3, 4$ respectively. From these tables we can conclude that the present method can conserve invariants successfully. Finally the interaction of three solitary waves are shown in Figs. 6 and 7.

4.4. Maxwellian inital condition

Finally, in this subsection we consider the Eq.(2) with

$$u(x, 0) = e^{-(x^2)}, \quad -20 \leq x \leq 60$$

Maxwellian initial condition. In this case, it is known that solution depends on μ [15, 21]. Let us assume μ_c be some critical value. If $\mu \gg \mu_c$ then the solution shows rapidly oscillating behavior without breaking up into solitons. When $\mu < \mu_c$ the solution forms solitons based on the value of μ. Lastly if $\mu = \mu_c$ a leading soliton with oscillating tail occurs. We perform numerical simulations for various values of $\mu = 0.1$, 0.05 0.025, 0.01. In first simulation we consider the case $p = 3$. We
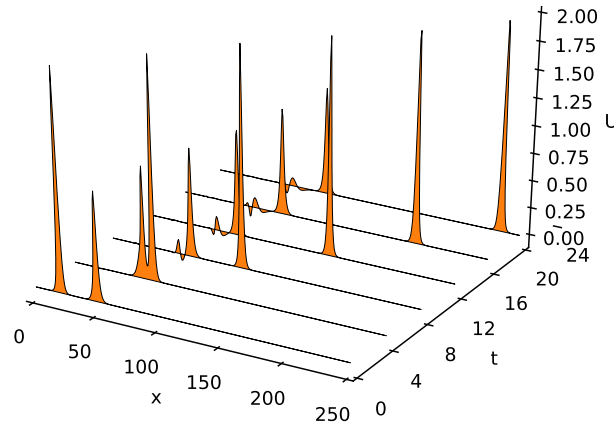
Figure 5. Interaction of two solitary waves for $N = 400$, $p = 3$, $c_1 = 48/5$, $c_2 = 6/5$, $x_1 = 20$, $x_2 = 50$, $\Delta t = 0.025$, and $\mu = 1$ at $t = 0, 4, 8, 12, 16, 20$.

Table 11. Invariants and their changes for $p = 2$ and $\Delta t = 0.1$.

t	[20], $h = 0.1$			Present, $N = 400$		
	I_1	I_2	I_3	I_1	I_2	I_3
0	10.9245	4.4191	0.740798	10.9245437	4.4191243	0.7407977
2	10.9245	3.8743	0.505953	10.9246354	4.4190394	0.7407469
4	10.9246	4.0302	0.573556	10.9246419	4.4189527	0.7406946
6	10.9245	4.2342	0.669611	10.9246165	4.4188661	0.7406418
8	10.9245	4.5023	0.812142	10.9245872	4.4187793	0.7405883
10	10.9244	4.8697	1.039870	10.9245403	4.4186918	0.7405338
$\lvert\Delta I_i\rvert \rightarrow$	1.0e-04	0.45060	0.29907	3.4e-06	4.325e-04	2.639e-04

Table 12. Invariants and their changes for $p = 3$, $N = 400$ and $\Delta t = 0.05$.

t	I_1	I_2	I_3	CPU time
0	11.1945795	4.8882472	0.7971747	0.00
2	11.1946512	4.8881944	0.7972071	0.25
4	11.1946551	4.8881413	0.7972680	0.34
6	11.1946323	4.8880883	0.7973291	0.43
8	11.1946040	4.8880352	0.7974067	0.51
10	11.1945561	4.8879819	0.7975176	0.60
$\lvert\Delta I_i\rvert \rightarrow$	9.5100e-05	2.6530e-04	3.4290e-04	

Table 13. Invariants and their changes for $p = 4$, $N = 400$ and $\Delta t = 0.05$.

t	I_1	I_2	I_3	CPU time
0	11.4706872	5.3297106	0.9191609	0.00
2	11.4707529	5.3295569	0.9192072	0.25
4	11.4707560	5.3294031	0.9193171	0.35
6	11.4707341	5.3292498	0.9194077	0.42
8	11.4707057	5.3290969	0.9195143	0.51
10	11.4706562	5.3289442	0.9196717	0.61
$\lvert\Delta I_i\rvert \rightarrow$	3.1000e-05	7.6640e-04	5.1080e-04	

take $N = 400$, $\Delta t = 0.005$ for the present method.

We give changes in the invariants and their comparison with results of septic B-spline collocation
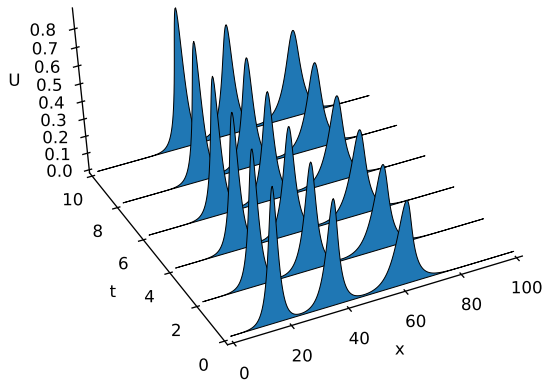
Figure 6. Interaction of three solitary waves for $p = 3$, $N = 400$, $\mu = 1$, $c_1 = 0.6$, $c_2 = 0.3$, $c_3 = 0.15$, $x_1 = 15$, $x_2 = 35$ and $x_3 = 60$ at $t = 0, 2, 4, 6, 8, 10$.
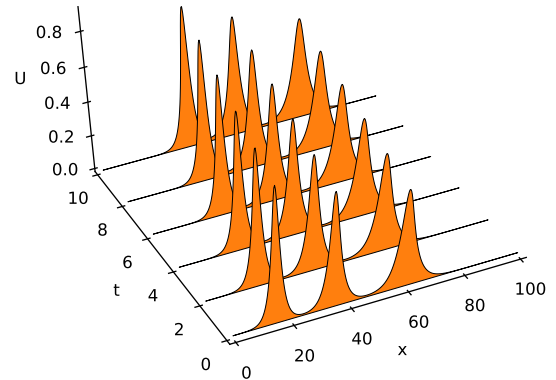
Figure 7. Interaction of three solitary waves for $p = 4$, $N = 400$, $\mu = 1$, $c_1 = 0.6$, $c_2 = 0.3$, $c_3 = 0.15$, $x_1 = 15$, $x_2 = 35$ and $x_3 = 60$ at $t = 0, 2, 4, 6, 8, 10$.

Table 14. Invariants and their comparison for $p = 3$, $N = 400$, $\Delta t = 0.005$ and different values of μ.

		Present	[24]		Present	[24]		Present	[24]
	t	I_1	I_1		I_2	I_2		I_3	I_3
$\mu = 0.1$	0	1.772454	1.772453		1.378646	1.378645		0.760896	0.760895
	2	1.772766	1.772452		1.379399	1.548191		0.607357	0.591349
	4	1.772561	1.772451		1.378142	1.546329		0.604010	0.593211
	6	1.772610	1.772449		1.378273	1.545540		0.603203	0.594000
$\lvert\Delta I_1\rvert \rightarrow$		0.000156	4.0e-06	$\lvert\Delta I_2\rvert \rightarrow$	0.000373	0.166895	$\lvert\Delta I_3\rvert \rightarrow$	0.157693	0.166895
$\mu = 0.05$	0	1.772454	1.772453		1.315980	1.315979		0.823561	0.823561
	2	1.772215	1.772376		1.312421	1.514843		0.639867	0.624697
	4	1.772022	1.772272		1.311619	1.514131		0.639441	0.625409
	6	1.773135	1.772168		1.317028	1.513035		0.648906	0.626505
$\lvert\Delta I_1\rvert \rightarrow$		0.000681	0.000285	$\lvert\Delta I_2\rvert \rightarrow$	0.001048	0.197056	$\lvert\Delta I_3\rvert \rightarrow$	0.174655	0.197056
$\mu = 0.025$	0	1.772454	1.772453		1.284647	1.284646		0.854894	0.854894
	2	1.782801	1.768943		1.332664	1.502469		0.815844	0.637071
	4	1.774529	1.764956		1.302657	1.501801		0.754045	0.637740
	6	1.754215	1.761477		1.222551	1.498994		0.589541	0.640546
$\lvert\Delta I_1\rvert \rightarrow$		0.018239	0.010976	$\lvert\Delta I_2\rvert \rightarrow$	0.062096	0.214348	$\lvert\Delta I_3\rvert \rightarrow$	0.265353	0.214348
$\mu = 0.01$	0	1.772454	1.772453		1.265847	1.265847		0.873694	0.873693
	2	1.733125	1.720433		1.172092	1.456451		0.616309	0.683090
	4	1.711463	1.706008		1.120066	1.450265		0.541076	0.689276
	6	1.731412	1.700567		1.196719	1.451593		0.733945	0.687947
$\lvert\Delta I_1\rvert \rightarrow$		0.041042	0.071886	$\lvert\Delta I_2\rvert \rightarrow$	0.069128	0.185746	$\lvert\Delta I_3\rvert \rightarrow$	0.139749	0.185746

method in Table 14. Further, for $p = 4$ the results obtained are reported in Table 15.

Graphics of numerical solutions for various values of parameter μ are given in Figs. 8 and 9. Breaking of solitons can be observed from the Figs. 8 and 9.

5. Conclusion

In this paper, delta-shaped functions combined with the finite difference and a linearization approach are used for numerically solving generalized regularized long wave equation.

The present method has been tested on four classic problems and its accuracy has been assessed

Table 15. Invariants and their comparison for $p = 4$, $N = 400$, $\Delta t = 0.005$ and different values of μ

|		$p = 4$							
		Present	[24]		Present	[24]		Present	[24]
	t	I_1	I_1		I_2	I_2		I_3	I_3
$\mu = 0.1$	0	1.772454	1.772453		1.378646	1.378645		0.760896	0.760895
	2	1.772594	1.772110		1.376700	1.591837		0.474657	0.547703
	4	1.772315	1.771702		1.375158	1.588948		0.467131	0.550592
	6	1.774090	1.771297		1.381579	1.587779		0.469617	0.551761
$\lvert\Delta I_1\rvert \rightarrow$		0.001636	0.001156	$\lvert\Delta I_2\rvert \rightarrow$	0.002933	0.209134	$\lvert\Delta I_3\rvert \rightarrow$	0.291279	0.209134
$\mu = 0.05$	0	1.772454	1.772453		1.315980	1.315979		0.823561	0.823561
	2	1.765624	1.753662		1.293771	1.535874		0.512686	0.603666
	4	1.772599	1.741625		1.321959	1.528679		0.551366	0.610862
	6	1.755506	1.733910		1.265309	1.523490		0.481081	0.616050
$\lvert\Delta I_1\rvert \rightarrow$		0.016948	0.038543	$\lvert\Delta I_2\rvert \rightarrow$	0.05067	0.207511	$\lvert\Delta I_3\rvert \rightarrow$	0.342480	0.207511
$\mu = 0.025$	0	1.772454	1.772453		1.284647	1.284646		0.854894	0.854894
	2	1.789069	1.693029		1.355683	1.482414		0.739884	0.657126
	4	1.711672	1.682425		1.133213	1.476250		0.412816	0.663290
	6	1.714808	1.674869		1.141655	1.468703		0.409811	0.670837
$\lvert\Delta I_1\rvert \rightarrow$		0.057646	0.0975840	$\lvert\Delta I_2\rvert \rightarrow$	0.142992	0.184057	$\lvert\Delta I_3\rvert \rightarrow$	0.445083	0.184057
$\mu = 0.01$	0	1.772454	1.772453		1.265847	1.265847		0.873694	0.873693
	2	1.825320	1.651315		1.464030	1.437490		1.304239	0.702051
	4	1.750123	1.644999		1.261045	1.439995		0.843022	0.699545
	6	1.761501	1.633634		1.294508	1.431710		0.929302	0.707830
$\lvert\Delta I_1\rvert \rightarrow$		0.010953	0.138819	$\lvert\Delta I_2\rvert \rightarrow$	0.028661	0.165863	$\lvert\Delta I_3\rvert \rightarrow$	0.055608	0.165863
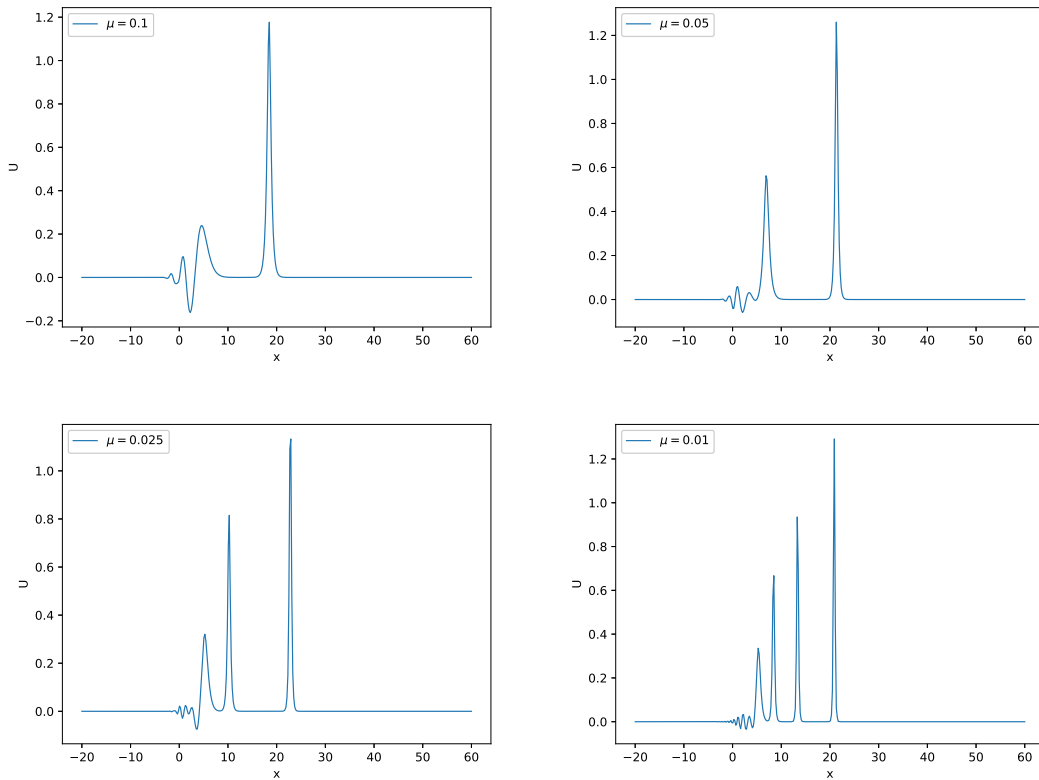
Figure 8. Numerical solution for $p = 3$, $N = 400$, $\Delta t = 0.005$ and different values of μ at $t = 6$.

by comparing calculated error norms L_2, L_∞ and invariants I_1, I_2, I_3 with exact values and with finite element, finite difference and collocation methods. It is seen that from calculations
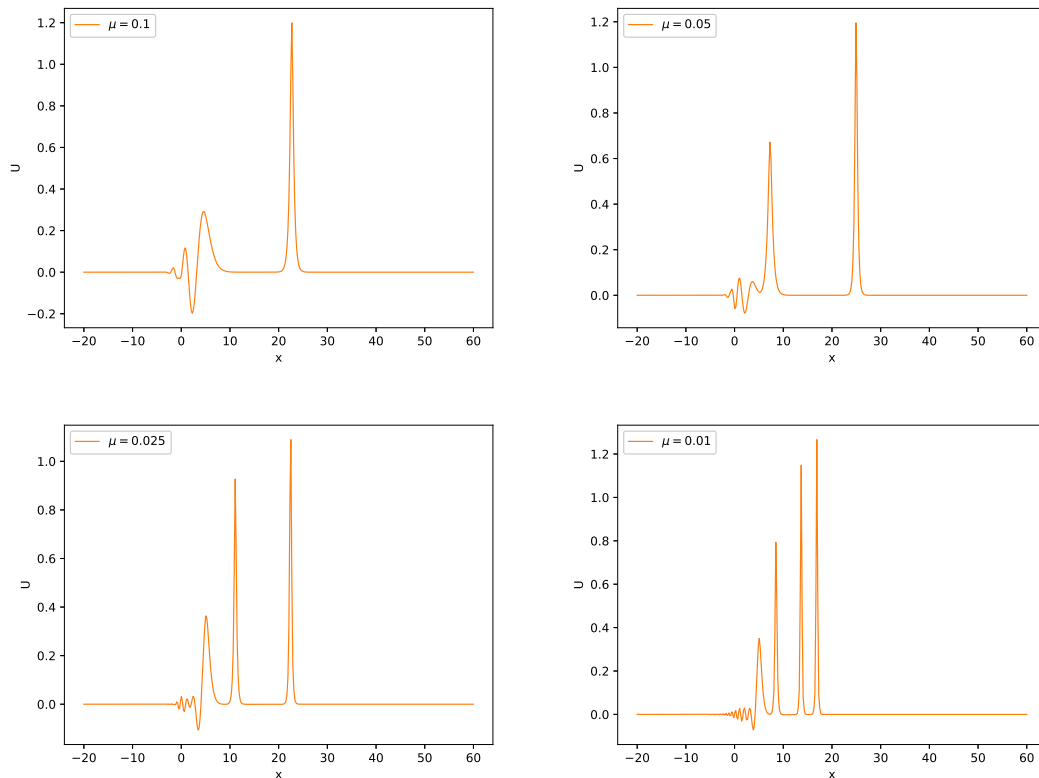
Figure 9. Numerical solution for $p = 4$, $N = 400$, $\Delta t = 0.005$ and different values of μ at $t = 6$.

the invariants are almost constant during numerical simulations and error norms are satisfactorily good even in less collocation points. The performance of the present method indicates that the present method is competitive with existing methods such as finite element method, finite difference and collocation methods. Furthermore, the performance of the present method encourages us to use the method for other nonlinear partial differential equations that have applications in various engineering and scientific fields.

Acknowledgments

References

[1] Garcia-Lopez, C.M., & Ramos, J.I.(2012). Effects of convection on a modified GRLW equation, Applied Mathematics and Computation, 219(8), 4118–4132.

[2] Peregrine, D. H.(1966). Calculations of the development of an undular bore, Journal of Fluid Mechanics, 25, 321–330.

[3] Peregrine, D. H. (1967). Long waves on a beach, Journal of Fluid Mechanics, 27(4), 815–827 .

[4] Benjamin, T. B., Bona, J. L., & Mahony, J. J. (1972). Model equations for long waves in non-linear dispersive systems, Philosophical Transactions of the Royal Society of London A, 272, 47–78.

[5] Abdulloev, Kh. O., Bogalubsky, H., & Markhankov, V.G.(1976). One more example of inelastic soliton interaction, Physics Letters A, 56, 427–428.

[6] Khalifa, A.K., Raslan, K.R., & Alzubaidi, H.M.(2008). A collocation method with cubic b-splines for solving the MRLW equation, Journal of Computational and Applied Mathematics, 212(2), 406–418

[7] Shokri, A., & Dehghan, M.(2010). A meshless method using the radial basis functions for numerical solution of the regularized long wave equation, Numerical Methods for Partial Differential Equations, 26(4), 807-825

[8] Oruç, Ö., Bulut, F., & Esen, A.(2016). Numerical Solutions of Regularized Long Wave Equation By Haar Wavelet Method, Mediterranean Journal of Mathematics, 13(5), 3235-3253.

[9] Dehghan, M., & Salehi, R.(2011). The solitary wave solution of the two-dimensional regularized long-wave equation in fluids and plasmas, Computer Physics Communications, 182, 2540-2549.

[10] Dehghan, M., Abbaszadeh, M., & Mohebbi, A.(2015). The use of interpolating element-free Galerkin technique for solving 2D generalized Benjamin-Bona-Mahony-Burgers and regularized long wave equations on non-rectangular domains with error estimate, Journal of Computational and Applied Mathematics, 286, 211-231.

[11] Dag, I., Irk, D., & Sari, M. (2013). The extended cubic b-spline algorithm for a modified regularized long wave equation, Chinese Physics B, 22(4), doi: 10.1088/ 1674-1056/22/4/040207.

[12] Karakoç, S.B.G., Yagmurlu, N.M., & Ucar, Y. (2013) Numerical approximation to a solution of the modified regularized long wave equation using quintic b-splines, Bound. Value Probl. 2013 27, doi: 10.1186/1687-2770- 2013- 27.

[13] Esen, A., & Kutluay, S.(2006). Application of a lumped Galerkin method to the regularized long wave equation, Applied Mathematics and Computation, 174, 833-845.

[14] Dogan, A.(2002). Numerical solution of RLW equation using linear finite elements within Galerkins method, Applied Mathematical Modelling, 26, 771-783.

[15] Kaya, D.(2004). A numerical simulation of solitary-wave solutions of the generalized regularized long wave equation, Applied Mathematics and Computation, 149, 833–841.

[16] Mokhtari, R., & Mohammadi, M.(2010) Numerical solution of GRLW equation using Sinc-collocation method, Computer Physics Communications, 181(7), 1266–1274.

[17] Wang, J.-F., Bai, F.-N., & Cheng, Y.-M.(2011). A meshless method for the nonlinear generalized regularized long wave equation, Chinese Physics B, 20(3), 030206.

[18] Guo, P., Zhang, L., & Liew, K.(2014). Numerical analysis of generalized regularized long wave equation using the element-free kp-Ritz method, Applied Mathematics and Computation, 240, 91–101.

[19] Kang, X., Cheng, K., & Guo, C.(2015). A second-order Fourier pseudospectral method for the generalized regularized long wave equation, Advances in Difference Equations, 2015 (1), 339, doi: 10.1186/s13662- 015- 0676- 3.

[20] Hammad, D.A., & El-Azab, M.S.(2015). A 2N order compact finite difference method for solving the generalized regularized long wave (GRLW) equation, Applied Mathematics and Computation 253, 248–261

[21] Zhang, L.(2005). A finite difference scheme for generalized regularized long-wave equation, Applied Mathematics and Computation, 168, 962–972.

[22] Roshan, T.(2012). A Petrov-Galerkin method for solving the generalized regularized long wave (GRLW) equation, Computers & Mathematics with Applications, 63, 943–956

[23] Gardner, L.R.T., Gardner, G.A., Ayoub, F.A., & Amein, N.K.(1997). Approximations of solitary waves of the MRLW equation by b-spline finite element, Arabian Journal for Science and Engineering 22, 183–193.

[24] Karakoc, S.B.G., & Zeybek, H.(2016). Solitary-wave solutions of the GRLW equation using septic B-spline collocation method, Applied Mathematics and Computation, 289, 159–171

[25] Li, Q., & Mei, L.(2018). Local momentum-preserving algorithms for the GRLW equation, Applied Mathematics and Computation 330, 77–92

[26] Reutskiy, S.Y.(2005). A boundary method of Trefftz type for PDEs with scattered data. Engineering Analysis with Boundary Elements, 29, 713–24.

[27] Tian, H.Y., Reustkiy, S., & Chen, C.S.(2007). New basis functions and their applications to PDEs. In: ICCES, vol. 3(4), 169–75.

[28] Tian, H.Y., Reustkiy, S., & Chen, C.S.(2008). A basis function for approximation and the solutions of partial differential equations, Numerical Methods for Partial Differential Equations, 24(3), 1018–36.

[29] Hon, Y.C., & Yang, Z.(2009). Meshless collocation method by Delta-shape basis functions for default barrier model. Engineering Analysis with Boundary Elements, 33, 951–958

[30] Reutskiy, S.Y.(2011). A meshless method for one-dimensional Stefan problems, Applied Mathematics and Computation, 217, 9689–9701

[31] Mokhtari, R., Isvand, D., Chegini, N.G., & Salaripanah, A.(2013). Numerical solution of the Schrödinger equations by using Delta-shaped basis functions, Nonlinear Dynamics, 74, 77–93

[32] Tian, H., & Grunewalda, A.(2017). A Delta-Shaped Basis Method for Ill-Posed Nonhomogeneous Elliptic Boundary Value Problems, Neural, Parallel, and Scientific Computations, 25, 1-18

[33] Oruç, Ö., Two meshless methods based on pseudo spectral delta-shaped basis functions

and barycentric rational interpolation for numerical solution of modified Burgers equation, International Journal of Computer Mathematics, DOI: 10.1080/00207160.2020.1755432

[34] Oliphant, T.E.(2007). Python for Scientific Computing, Computing In Science & Engineering, 9 (3), 10-20.

[35] Walt, S. van der, Colbert S. C., & Varoquaux, G. (2011) The NumPy Array: A Structure for Efficient Numerical Computation, Computing In Science & Engineering, 13 (2), 22-30.

[36] Hunter, J. D.(2007). Matplotlib: A 2D graphics environment, Computing In Science & Engineering, 9(3), 90-95.

Ömer Oruç obtained his M.Sc. degree in fuzzy differential equations from department of Mathematics, TOBB Economics and Technology University in 2011, and his Ph. D. in Haar wavelet based numerical methods from department of Mathematics, Inonu University in 2016. His current research areas include fuzzy theory, differential equations, numerical methods and scientific computing. He has over 20 papers published in SCI and SCI-Expanded indexed journals.
http://orcid.org/0000-0002-6655-3543

RESEARCH ARTICLE

A randomized adaptive trust region line search method

Saman Babaie–Kafaki[*] and Saeed Rezaee

Department of Mathematics, Faculty of Mathematics, Statistics and Computer Science, Semnan University, Semnan, Iran
sbk@semnan.ac.ir, s.rezaee@semnan.ac.ir

ARTICLE INFO	ABSTRACT
	Hybridizing the trust region, line search and simulated annealing methods, we develop a heuristic algorithm for solving unconstrained optimization problems. We make some numerical experiments on a set of CUTEr test problems to investigate efficiency of the suggested algorithm. The results show that the algorithm is practically promising.

1. Introduction

As the most basic nonlinear optimization problem with continuous variables, unconstrained optimization naturally arises in many disciplines such as regression, image and signal processing, physical systems, optimal control and so on. Even, based on penalization schemes, constrained nonlinear programming problems can be reformulated as unconstrained problems [1]. Generally, the problem can be defined as minimization of an objective function that depends on real variables without any restriction on their values.

Among the efficient tools for solving unconstrained optimization problems there are the trust region (TR) methods and the line search (LS) techniques [1]. In each iteration of a TR method, a neighborhood is defined around the available approximation of the solution, called the trust region, and then, an approximation of the objective function is minimized within the region to achieve the new estimation. The term used for the method originates from the fact that a local approximation is trusted as the predictor of the

objective function behavior. In another guideline, in each iteration of an LS method a search direction is defined at the available approximation of the solution and then, the objective function is minimized along the given direction to achieve the new estimation. As known, an LS method often requires more iterations to find a minimizer of the objective function than does a TR method, while computing the successive approximations of the solution more quickly.

To evaluate acceptability level of the local approximate model of the objective function in an arbitrary iteration of a TR method, a ratio is defined often by dividing the distance of the objective function values to the distance of their local approximations in the recent iterates. When the TR ratio is small, the approximate model is found to be a poor predictor of the objective function behavior. In such situation, the model should be resolved in a smaller region. However, when the TR ratio is large enough, the approximate model is found to be a locally suitable predictor of the

---

*Corresponding Author

objective function behavior. So, the generated estimation of the solution should be accepted and the region can be enlarged in the next iteration. It is worth noting that to decrease computational cost of the TR methods, the LS techniques can be effectively employed in the case where the TR ratio is small, as an alternative of resolving the approximate model in a reduced neighborhood. A review of the literature reveals an abundance of the studies on the TR methods; see for example [2–4] and the references therein.

Here, based on the simulated annealing strategy, we develop a randomized TR–LS method. The method is discussed in details in the next section. We provide a test bed to shed light on the advantages of our heuristic algorithm in Section 3. Finally, in Section 4 we come out with concluding remarks.

2. A randomized trust region line search algorithm

Consider the unconstrained optimization problem $\min_{x \in \mathbb{R}^n} f(x)$ in which the objective function $f : \mathbb{R}^n \to \mathbb{R}$ is assumed to be continuously differentiable. Iterative formula of the optimization algorithms is generally in the following form:

$$x_0 \in \mathbb{R}^n, \ x_{k+1} = x_k + s_k, \ k = 0, 1, ...,$$

where s_k is the step taken from x_k. In a TR method, often s_k is an approximate solution of the following subproblem, being a local quadratic approximation of the objective function:

$$\min_{s \in \mathbb{R}^n} \quad m_k(s) = f_k + g_k^T s + \frac{1}{2} s^T B_k s, \quad (1)$$
$$s.t. \quad ||s|| \leq \Delta_k,$$

where $f_k = f(x_k)$, $g_k = \nabla f(x_k)$, B_k is an approximation of the Hessian $\nabla^2 f(x_k)$, $\Delta_k > 0$ is the TR radius and $||.||$ stands for the Euclidean norm. Meanwhile, in an LS method we have $s_k = \alpha_k d_k$ where $d_k \in \mathbb{R}^n$ is a descent search direction and

$$\alpha_k \approx \arg \min_{\alpha > 0} f(x_k + \alpha d_k),$$

is called the step length.

To describe our randomization scheme, we use the framework of the TR–LS algorithm proposed in [2]. Firstly, we adopt the adaptive choice of the TR radius suggested in [5], that is

$$\Delta_k = -\frac{g_k^T q_k}{q_k^T B_k q_k} ||q_k||, \quad (2)$$

in which B_k is a positive definite quasi–Newton approximation of the Hessian and $q_k \in \mathbb{R}^n$ is a vector parameter satisfying the angle condition

[1], i.e.

$$-\frac{g_k^T q_k}{||g_k|| \ ||q_k||} \geq \tau, \quad (3)$$

for some constant $\tau \in (0, 1]$. To evaluate local consistency between the objective function and the quadratic model (1), we apply the following traditional TR ratio [1]:

$$\rho_k = \frac{f_k - f(x_k + s_k)}{m_k(0) - m_k(s_k)}. \quad (4)$$

Now, for a prespecified constant $\mu \in (0, 1)$, if ρ_k is large enough in the sense that $\rho_k > \mu$, then we set $x_{k+1} = x_k + s_k$. Otherwise, to avoid resolving the TR subproblem (1), we set $x_{k+1} = x_k + s_k$ with a specific probability which depends on the value of ρ_k, or (similar to the approach of [2]) we use the Armijo–type LS procedure proposed by Wan et al. [6] as follows:

Line search 2.1. *Let L_k be an approximation of the Lipschitz constant of the gradient and set $\beta_k = -\dfrac{g_k^T s_k}{L_k ||s_k||^2}$. The step length α_k is the largest quantity in $\{t^i \beta_k\}_{i=0}^{\infty}$ which satisfies the following inequality:*

$$f(x_k + \alpha_k s_k) \leq f_k + \sigma \alpha_k (g_k^T s_k - \frac{1}{2} \alpha_k r L_k ||s_k||^2),$$

where $t \in (0, 1)$, $\sigma \in (0, 1/2)$, and $r \in [0, +\infty)$ are real constants.

As seen, the distinct feature of our algorithm is that we may accept a trial step s_k even when $\rho_k < \mu$, despite the classical TR algorithms for which such trial steps are rejected and the subproblem (1) is resolved with a smaller radius, or an LS strategy is employed. So, we need to define a reasonable probability for the mentioned randomized part of the algorithm. In this context, we apply the probabilistic approach of the simulated annealing (SA) strategy.

Among the earliest and most popular metaheuristic techniques of optimization, there is the simulated annealing (SA) algorithm. The method origins from the successful annealing process of the materials which involves the cautious control of the cooling schedule [7]. SA is a local search algorithm capable of escaping from local optima by use of random hill–climbing moves in the search process [8,9]. It is very efficient in practice [9,10] and well–developed in theory [11,12].

To provide a detailed description of the SA method [8], note that similar to the TR technique, at the iteration t of the method a neighborhood $\mathcal{N}_t$ is defined around the iterate x_t. Then, a neighbor $y \in \mathcal{N}_t$ is randomly selected. If y is better than x_t (often in the cost function point of view, i.e. $f(y) < f(x_t)$), then we move to y in the sense

that we set $x_{t+1} = y$. However, when x_t is better than y, we move to y with the probability

$$p_t = e^{-\frac{d(x_t, y)}{T}}, \tag{5}$$

and stay in x_t otherwise, where T is a positive constant commonly called the temperature and $d(x_t, y)$ is a nonnegative function which demonstrates the measure of unfitness of the feasible solution y in contrast to x_t.

The temperature T controls the likelihood of cost increases in the sense that when T is small, cost increases are highly unlikely while when T is large, the value of $d(x_t, y)$ has an insignificant effect on the probability p_t and any particular transition. In order to guarantee the global convergence with probability one, the temperature needs to be decreased logarithmically with the iteration number t [13], making the process too slow. In practice, the temperature is usually updated by

$$T \leftarrow \lambda T, \tag{6}$$

with a prespecified constant $0 \ll \lambda < 1$ [11].

In order to allow probable moves to some inferior solutions as well as to reduce the effect of unsuccessful iterations (with $\rho_k < \mu$), we apply the SA scheme in our algorithm. In this context, when at the kth iteration of the algorithm the TR ratio is negative or a small positive number near to zero, we may accept the trial step s_k. More exactly, if $\rho_k < \mu$, then we set $x_{k+1} = x_k + s_k$ with the following probability:

$$p_{\rho_k} = e^{-\frac{\mu - \rho_k}{T}}, \tag{7}$$

and stay in x_k otherwise, where T is the temperature. Considering (4) and (5), here we set $d(x_k, y) = \mu - \rho_k$ with $y = x_k + s_k$. As seen, the given probability is small when $\rho_k \ll \mu$ or the temperature T is small.

Here, based on the above preliminaries, we are in a position to describe the algorithm in details.

Algorithm 2.1. *(A randomized trust region line search algorithm (RTRLS))*

Step 0: {*Initialization*} *Choose an initial point $x_0 \in \mathbb{R}^n$, a symmetric positive definite matrix $B_0 \in \mathbb{R}^{n \times n}$, and the constants $t \in (0, 1)$, $\sigma \in (0, 1/2)$, $r \in [0, +\infty)$, $\mu \in (0, 1]$, $L_0 > 0$, $\epsilon > 0$, and $T_0 > 0$ as the initial temperature. Compute f_0, and set $k = 0$ and $T = T_0$.*

Step 1: {*Stopping criterion*} **If** $||g_k|| < \epsilon$, **then stop.**

Step 2: *Choose q_k satisfying (3) and compute Δ_k by (2).*

Step 3: *Solve the subproblem (1) to find the trial step s_k.*

Step 4: *Compute ρ_k by (4).* **If** $\rho_k \geq \mu$, **then** *set $x_{k+1} = x_k + s_k$, and* **goto** *Step 6;* **otherwise**, *with the probability p_{ρ_k} given by (7) set $x_{k+1} = x_k + s_k$ and* **goto** *Step 6.*

Step 5: *Find the step length α_k using Line search 2.1 and set $x_{k+1} = x_k + \alpha_k s_k$.*

Step 6: *Compute the new Hessian approximation B_{k+1} by a quasi–Newton updating formula. Set $k = k + 1$, decrease the temperature T and* **goto** *Step 1.*

Note that if the temperature is decreased logarithmically, then, based on the classical convergence properties of the SA [13] and the convergence analysis conducted in [5], with probability one Algorithm 2.1 can be globally convergent.

3. Numerical experiments

Here, we present some numerical results obtained by applying MATLAB 7.14.0.739 (R2012a) implementations of RTRLS (Algorithm 2.1) and the efficient accelerated nonmonotone TR–LS algorithm proposed in [2] (in which Andrei's initial choice of the step length is employed [14]), here called AccTRLS. The runs were performed on a set of 84 unconstrained optimization test problems of the CUTEr collection [15] with the minimum dimension being equal to 50, as specified in [3], using a computer Intel(R) Core(TM)2 Duo CPU 2.00 GHz with 1.50 GB of RAM.

For both algorithms, we adopted the parameter values suggested in [2] as well as the same stopping criteria. In addition, for RTRLS we set $T_0 = ||g_0||$ and in Step 4, we decreased T by (6) with $\lambda = 0.9$, found to be appropriate. Among the wide scope of the choices of q_k satisfying (3), here we set $q_k = -B_k^{-1} g_k$. Similar to the approach of [2], to compute the Hessian approximation we used the scaled memoryless DFP formula where its inverse can be effectively determined in a memoryless form [1]. Also, we used the double Dogleg method [1] to solve the subproblem (1).

Efficiency comparisons were drawn using the Dolan–Moré performance profile [16] on the number of iterations, number of objective function evaluations, number of gradient evaluations and the running time. Performance profile gives, for every $\omega \geq 1$, the proportion $p(\omega)$ of the test problems that each considered algorithmic variant has a performance within a factor of ω of the best. Figures 1–4 illustrate the results of comparisons. As seen, generally RTRLS outperforms AccTRLS. It is worth noting that in 64% of the iterations RTRLS achieves the solution faster than AccTRLS. Thus, in general our randomized strategy

based on the SA method turns out to be practically promising. Especially, it can be employed as an alternative of the acceleration/nonmonotone schemes used in the TR–LS algorithms.
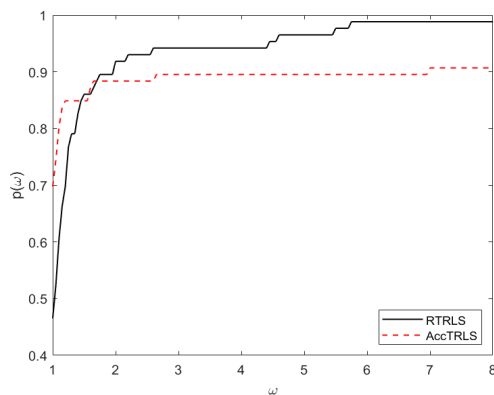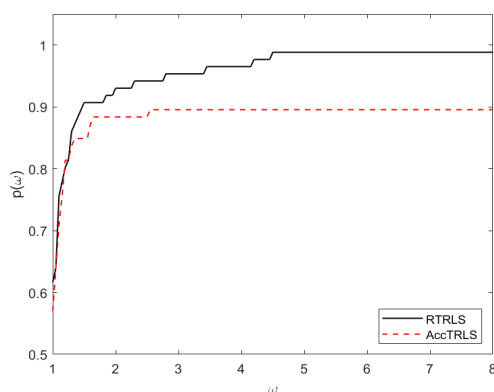

Figure 1. Number of iterations performance profiles

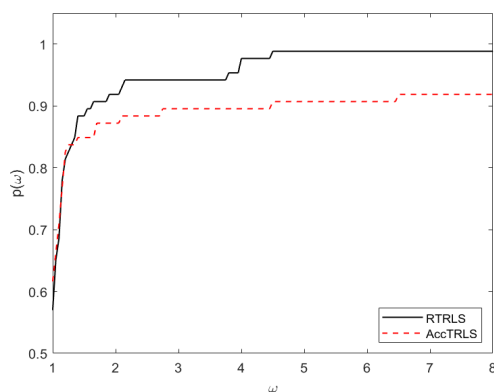**Figure 2.** Number of objective function evaluations performance profiles

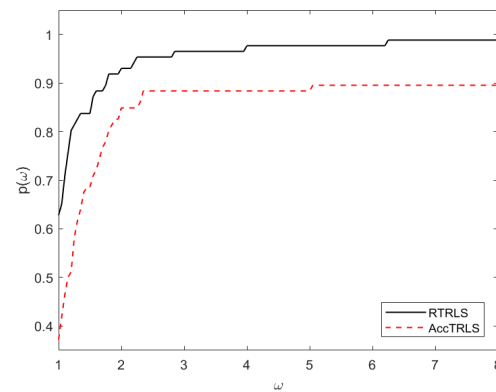**Figure 3.** Number of gradient evaluations performance profiles

Figure 4. CPU time performance profiles

4. Conclusions

Employing the simulated annealing aspects in a recent adaptive trust region line search method, a heuristic algorithm has been suggested to be used in unconstrained optimization. The method can also be considered as a randomized version of the trust region line search algorithm. Numerical experiments showed that the proposed randomization scheme can enhance efficiency of the classical trust region line search algorithms; especially, it can serve as an alternative of the acceleration/nonmonotoe approaches used in the algorithms.

As a future work, one can investigate possible employing of other metaheuristic algorithms in the trust region line search methods. In addition, effect of such randomized schemes on the backtracking line search techniques can be studied.

Acknowledgements

References

[1] Sun, W., & Yuan, Y.X. (2006). Optimization Theory and Methods: Nonlinear Programming. Springer, New York.

[2] Babaie–Kafaki, S., & Rezaee, S. (2018). Two accelerated nonmonotone adaptive trust region line search methods. *Numerical Algorithms*, 78(3), 911–928.

[3] Rezaee, S., & Babaie–Kafaki, S. (2019). An adaptive nonmonotone trust region algorithm. *Optimization Methods and Software*, 34(2), 264–277.

[4] Yuan, Y.X. (2015). Recent advances in trust region algorithms. *Mathematical Programming*, 151(1, Ser. B), 249–281.

[5] Shi, Z.J., & Guo, J.H. (2008). A new trust region method for unconstrained optimization. *Journal of Computational and Applied Mathematics*, 213(1), 509–520.

[6] Wan, W., Huang, S., & Zheng, X.D. (2012). New cautious BFGS algorithm based on modified Armijo–type line search. *Journal of Inequalities and Applications*, 2012(1), 1–10.

[7] Yang, X.S. (2014). Nature–Inspired Optimization Algorithms. Elsevier, London.

[8] Bertsimas, D., & Tsitsiklis, J.N. (1997). Introduction to Linear Optimization. Athena Scientific, Massachusetts.

[9] Henderson, D., Jacobson, S.H., & Johnson, A.W. (2003). The theory and practice of simulated annealing. In: F.W. Glover and G.A. Kochenberger, eds. *Handbook of Metaheuristics*, volume 57 of *International Series in Operations Research and Management Science*. Kluwer Academic Publishers, Boston, MA, 287–319.

[10] Reeves, C.R. (1996). Modern heuristic techniques. In: V.J. Rayward–Smith, ed. *Modern Heuristic Search Methods*. John Wiley and Sons, Chichester, 1–24.

[11] Babaie–Kafaki, S., Ghanbari, R., & Mahdavi–Amiri, N. (2012). An efficient and practically robust hybrid metaheuristic algorithm for solving fuzzy bus terminal location problems. *Asia–Pacific Journal of Operational Research*, 29(2), 1–25.

[12] Aards, E. and Korst, J., & van Laarhoren, P. (1997). Simulated annealing. In: E.H.L. Aarts and J.K. Lenstra, eds. *Local Search in Combinatorial Optimization*. John Wiley and Sons, Chichester, 91–121.

[13] Hajek, B. (1988). Cooling schedules for optimal annealing. *Mathematics of Operations Research*, 13(2), 311–329.

[14] Andrei, N. (2006). An acceleration of gradient descent algorithm with backtracking for unconstrained optimization. *Numerical Algorithms*, 42(1), 63–73.

[15] Gould, N.I.M., Orban, D., & Toint, Ph.L. (2006). CUTEr: a constrained and unconstrained testing environment, revisited. *ACM Transactions on Mathematical Software*, 29(4), 373–394.

[16] Dolan, E.D., & Moré, J.J. (2002). Benchmarking optimization software with performance profiles. *Mathematical Programming*, 91(2, Ser. A), 201–213.

[17] Hager, W.W., & Zhang, H. (2002). Algorithm 851: CG_Descent, a conjugate gradient method with guaranteed descent. *ACM Transactions on Mathematical Software*, 32(1), 113–137.

Saman Babaie–Kafaki *is a Professor in Department of Mathematics of Semnan University, Iran. He received his B.Sc. in Applied Mathematics from Mazandaran University, Iran, in 2003, and his M.Sc. and Ph.D. in Applied Mathematics from Sharif University of Technology, Iran, in 2005 and 2010, respectively, under supervision of Professor Nezam Mahdavi–Amiri. His research interests lie within numerical continuous optimization, numerical linear algebra and heuristic algorithms.*
http://orcid.org/0000-0003-0122-8384

Saeed Rezaee *received his B.Sc. in Applied Mathematics from University of Hormozgan, Iran, in 2005, his M.Sc. in Applied Mathematics from Sharif University of Technology, Iran, in 2010, and his Ph.D. in Applied Mathematics (Operational Research) from Semnan University, Semnan, Iran, in 2017. His M.Sc. supervisor was Professor Nezam Mahdavi–Amiri and his Ph.D. supervisor was Professor Saman Babaie–Kafaki. His research interests lie within nonlinear programming modelling and algorithms.*
http://orcid.org/0000-0002-2636-3868

INSTRUCTIONS FOR AUTHORS

Aims and Scope

This journal shares the research carried out through different disciplines in regards to optimization, control and their applications.

The basic fields of this journal are linear, nonlinear, stochastic, parametric, discrete and dynamic programming; heuristic algorithms in optimization, control theory, game theory and their applications. Problems such as managerial decisions, time minimization, profit maximizations and other related topics are also shared in this journal.

Besides the research articles expository papers, which are hard to express or model, conference proceedings, book reviews and announcements are also welcome.

Journal Topics

- Applied Mathematics,
- Financial Mathematics,
- Control Theory,
- Game Theory,
- Fractional Calculus,
- Fractional Control,
- Modeling of Bio-systems for Optimization and Control,
- Linear Programming,
- Nonlinear Programming,
- Stochastic Programming,
- Parametric Programming,
- Conic Programming,
- Discrete Programming,
- Dynamic Programming,
- Optimization with Artificial Intelligence,
- Operational Research in Life and Human Sciences,
- Heuristic Algorithms in Optimization,
- Applications Related to Optimization on Engineering.

Submission of Manuscripts

New Submissions

Solicited and contributed manuscripts should be submitted to IJOCTA via the journal's online submission system. You need to make registration prior to submitting a new manuscript (please click here to register and do not forget to define yourself as an "Author" in doing so). You may then click on the "New Submission" link on your User Home.

IMPORTANT: If you already have an account, please click here to login. It is likely that you will have created an account if you have reviewed or authored for the journal in the past.

On the submission page, enter data and answer questions as prompted. Click on the "Next" button on each screen to save your work and advance to the next screen. The names and contact details of at least four internationally recognized experts who can review your manuscript should be entered in the "Comments for the Editor" box.

You will be prompted to upload your files: Click on the "Browse" button and locate the file on your computer. Select the description of the file in the drop down next to the Browse button. When you have selected all files you wish to upload, click the "Upload" button. Review your submission before sending to the Editors. Click the "Submit" button when you are done reviewing. Authors are responsible for verifying all files have uploaded correctly.

You may stop a submission at any phase and save it to submit later. Acknowledgment of receipt of the manuscript by IJOCTA Online Submission System will be sent to the corresponding author, including an assigned manuscript number that should be included in all subsequent correspondence. You can also log-

on to submission web page of IJOCTA any time to check the status of your manuscript. You will receive an e-mail once a decision has been made on your manuscript.

Each manuscript must be accompanied by a statement that it has not been published elsewhere and that it has not been submitted simultaneously for publication elsewhere.

Manuscripts can be prepared using LaTeX (.tex) or MSWord (.docx). However, manuscripts with heavy mathematical content will only be accepted as LaTeX files.

Preferred first submission format (for reviewing purpose only) is Portable Document File (.pdf). Please find below the templates for first submission.

Click here to download Word template for first submission (.docx)

Click here to download LaTeX template for first submission (.tex)

Revised Manuscripts

Revised manuscripts should be submitted via IJOCTA online system to ensure that they are linked to the original submission. It is also necessary to attach a separate file in which a point-by-point explanation is given to the specific points/questions raised by the referees and the corresponding changes made in the revised version.

To upload your revised manuscript, please go to your author page and click on the related manuscript title. Navigate to the "Review" link on the top left and scroll down the page. Click on the "Choose File" button under the "Editor Decision" title, choose the revised article (in pdf format) that you want to submit, and click on the "Upload" button to upload the author version. Repeat the same steps to upload the "Responses to Reviewers/Editor" file and make sure that you click the "Upload" button again.

To avoid any delay in making the article available freely online, the authors also need to upload the source files (Word or LaTex) when submitting revised manuscripts. Files can be compressed if necessary. The two-column final submission templates are as follows:

Click here to download Word template for final submission (.docx)

Click here to download LaTeX template for final submission (.tex)

Authors are responsible for obtaining permission to reproduce copyrighted material from other sources and are required to sign an agreement for the transfer of copyright to IJOCTA.

Article Processing Charges

There are no charges for submission and/or publication.

English Editing

Papers must be in English. Both British and American spelling is acceptable, provided usage is consistent within the manuscript. Manuscripts that are written in English that is ambiguous or incomprehensible, in the opinion of the Editor, will be returned to the authors with a request to resubmit once the language issues have been improved. This policy does not imply that all papers must be written in "perfect" English, whatever that may mean. Rather, the criteria require that the intended meaning of the authors must be clearly understandable, i.e., not obscured by language problems, by referees who have agreed to review the paper.

Presentation of Papers

Manuscript style

Use a standard font of the **11-point type: Times New Roman** is preferred. It is necessary to single line space your manuscript. Normally manuscripts are expected not to exceed 25 single-spaced pages including text, tables, figures and bibliography. All illustrations, figures, and tables are placed within the text at the appropriate points, rather than at the end.

During the submission process you must enter: (1) the full title, (2) names and affiliations of all authors and (3) the full address, including email, telephone and fax of the author who is to check the proofs. Supply a brief **biography** of each author at the end of the manuscript after references.

- Include the name(s) of any **sponsor(s)** of the research contained in the paper, along with **grant number(s).**
- Enter an **abstract** of no more than 250 words for all articles.

Keywords

Authors should prepare no more than 5 keywords for their manuscript.

Maximum five **AMS Classification number** (http://www.ams.org/mathscinet/msc/msc2010.html) of the study should be specified after keywords.

Writing Abstract

An abstract is a concise summary of the whole paper, not just the conclusions. The abstract should be no more than 250 words and convey the following:

1. An introduction to the work. This should be accessible by scientists in any field and express the necessity of the experiments executed.
2. Some scientific detail regarding the background to the problem.
3. A summary of the main result.
4. The implications of the result.
5. A broader perspective of the results, once again understandable across scientific disciplines.

It is crucial that the abstract conveys the importance of the work and be understandable without reference to the rest of the manuscript to a multidisciplinary audience. Abstracts should not contain any citation to other published works.

Reference Style

Reference citations in the text should be identified by numbers in square brackets "[ ]". All references must be complete and accurate. Please ensure that every reference cited in the text is also present in the reference list (and vice versa). Online citations should include date of access. References should be listed in the following style:

Journal article

Author, A.A., & Author, B. (Year). Title of article. Title of Journal, Vol(Issue), pages.

Castles, F.G., Curtin, J.C., & Vowles, J. (2006). Public policy in Australia and New Zealand: The new global context. Australian Journal of Political Science, 41(2), 131–143.

Book

Author, A. (Year). Title of book. Publisher, Place of Publication.

Mercer, P.A., & Smith, G. (1993). Private Viewdata in the UK. 2nd ed. Longman, London.

Chapter

Author, A. (Year). Title of chapter. In: A. Editor and B. Editor, eds. Title of book. Publisher, Place of publication, pages.

Bantz, C.R. (1995). Social dimensions of software development. In: J.A. Anderson, ed. Annual review of software management and development. CA: Sage, Newbury Park, 502–510.

Internet document

Author, A. (Year). Title of document [online]. Source. Available from: URL [Accessed (date)].

Holland, M. (2004). Guide to citing Internet sources [online]. Poole, Bournemouth University. Available from: http://www.bournemouth.ac.uk/library/using/guide_to_citing_internet_sourc.html [Accessed 4 November 2004].

Newspaper article

Author, A. (or Title of Newspaper) (Year). Title of article. Title of Newspaper, day Month, page, column.

Independent (1992). Picking up the bills. Independent, 4 June, p. 28a.

Thesis

Author, A. (Year). Title of thesis. Type of thesis (degree). Name of University.

Agutter, A.J. (1995). The linguistic significance of current British slang. PhD Thesis. Edinburgh University.

Illustrations

Illustrations submitted (line drawings, halftones, photos, photomicrographs, etc.) should be clean originals or digital files. Digital files are recommended for highest quality reproduction and should follow these guidelines:

- 300 dpi or higher
- Sized to fit on journal page
- TIFF or JPEG format only
- Embedded in text files and submitted as separate files (if required)

Tables and Figures

Tables and figures (illustrations) should be embedded in the text at the appropriate points, rather than at the end. A short descriptive title should appear above each table with a clear legend and any footnotes suitably identified below.

Proofs

Page proofs are sent to the designated author using IJOCTA EProof system. They must be carefully checked and returned within 48 hours of receipt.

Offprints/Reprints

Each corresponding author of an article will receive a PDF file of the article via email. This file is for personal use only and may not be copied and disseminated in any form without prior written permission from IJOCTA.

Submission Preparation Checklist

As part of the submission process, authors are required to check off their submission's compliance with all of the following items, and submissions may be returned to authors that do not adhere to these guidelines.

1. The submission has not been previously published, nor is it before another journal for consideration (or an explanation has been provided in Comments for the Editor).
2. The submission file is in Portable Document Format (.pdf).
3. The ORCID profile numbers of "all" authors are ready to enter in the step of Article Metadata (visit https://orcid.org for more details).
4. The text is single line spaced; uses a 11-point font; employs italics, rather than underlining (except with URL addresses); and all illustrations, figures, and tables are placed within the text at the appropriate points, rather than at the end.
5. The text adheres to the stylistic and bibliographic requirements outlined in the Author Guidelines, which is found in "About the Journal".
6. Maximum five AMS Classification number (http://www.ams.org/mathscinet/msc/msc2010.html) of the study have been provided after keywords.
7. After the acceptance of manuscript (before copy editing), Word (.docx) or LaTeX (.tex) version of the paper will be presented.
8. The names and email addresses of at least four (4) possible reviewers have been indicated in "Comments for the Editor" box in Paper Submission Step 1. Please note that at least two of the recommendations should be from different countries. Avoid suggesting reviewers who are at arms-length from you or your co-authors. This includes graduate advisors, people in your current department, or any others with a conflict of interest.

Peer Review Process

All contributions, prepared according to the author guidelines and submitted via IJOCTA online submission system are evaluated according to the criteria of originality and quality of their scientific content. The corresponding author will receive a confirmation e-mail with a reference number assigned to the paper, which he/she is asked to quote in all subsequent correspondence.

All manuscripts are first checked by the Technical Editor using plagiarism detection software (iThenticate) to verify originality and ensure the quality of the written work. If the result is not satisfactory (i.e. exceeding the limit of 30% of overlapping), the submission is rejected and the author is notified.

After the plagiarism check, the manuscripts are evaluated by the Editor-in-Chief and can be rejected without reviewing if considered not of sufficient interest or novelty, too preliminary or out of the scope of the journal. If the manuscript is considered suitable for further evaluation, it is first sent to the Area Editor. Based on his/her opinion the paper is then sent to at least two independent reviewers. Each reviewer is allowed up to four weeks to return his/her feedback but this duration may be extended based on his/her availability. IJOCTA has instituted a blind peer review process where the reviewers' identities are not known to authors. When the reviews are received, the Area Editor gives a decision and lets the author know it together with the reviewer comments and any supplementary files.

Should the reviews be positive, the authors are expected to submit the revised version usually within two months the editor decision is sent (this period can be extended when the authors contact to the editor and let him/her know that they need extra time for resubmission). If a revised paper is not resubmitted within the deadline, it is considered as a new submission after all the changes requested by reviewers have been made. Authors are required to submit a new cover letter, a response to reviewers letter and the revised manuscript (which ideally shows the revisions made in a different color or highlighted). If a change in authorship (addition or removal of author) has occurred during the revision, authors are requested to clarify the reason for change, and all authors (including the removed/added ones) need to submit a written consent for the change. The revised version is evaluated by the Area editor and/or reviewers and the Editor-in-Chief brings a decision about final acceptance based on their suggestions. If necessary, further revision can be asked for to fulfil all the requirements of the reviewers.

When a manuscript is accepted for publication, an acceptance letter is sent to the corresponding author and the authors are asked to submit the source file of the manuscript conforming to the IJOCTA two-column final submission template. After that stage, changes of authors of the manuscript are not possible. The manuscript is sent to the Copyeditor and a linguistic, metrological and technical revision is made, at which stage the authors are asked to make the final corrections in no more than a week. The layout editor prepares the galleys and the authors receive the galley proof for final check before printing. The authors are expected to correct only typographical errors on the proofs and return the proofs within 48 hours. After the final check by the layout editor and the proofreader, the manuscript is assigned a DOI number, made publicly available and listed in the forthcoming journal issue. After printing the issue, the corresponding metadata and files published in this issue are sent to the databases for indexing.
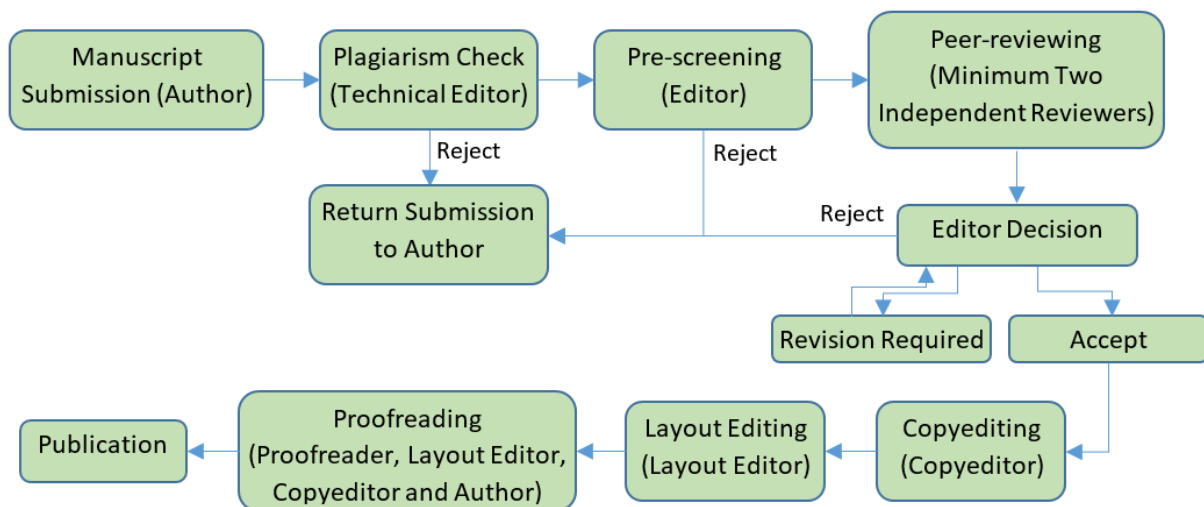
Publication Ethics and Malpractice Statement

IJOCTA is committed to ensuring ethics in publication and quality of articles. Conforming to standards of expected ethical behavior is therefore necessary for all parties (the author, the editor(s), the peer reviewer) involved in the act of publishing.

International Standards for Editors

The editors of the IJOCTA are responsible for deciding which of the articles submitted to the journal should be published considering their intellectual content without regard to race, gender, sexual orientation, religious belief, ethnic origin, citizenship, or political philosophy of the authors. The editors may be guided by the policies of the journal's editorial board and constrained by such legal requirements as shall then be in force regarding libel, copyright infringement and plagiarism. The editors may confer with other editors or reviewers in making this decision. As guardians and stewards of the research record, editors should encourage authors to strive for, and adhere themselves to, the highest standards of publication ethics. Furthermore, editors are in a unique position to indirectly foster responsible conduct of research through their policies and processes.

To achieve the maximum effect within the research community, ideally all editors should adhere to universal standards and good practices.

- Editors are accountable and should take responsibility for everything they publish.
- Editors should make fair and unbiased decisions independent from commercial consideration and ensure a fair and appropriate peer review process.
- Editors should adopt editorial policies that encourage maximum transparency and complete, honest reporting.
- Editors should guard the integrity of the published record by issuing corrections and retractions when needed and pursuing suspected or alleged research and publication misconduct.
- Editors should pursue reviewer and editorial misconduct.
- Editors should critically assess the ethical conduct of studies in humans and animals.
- Peer reviewers and authors should be told what is expected of them.
- Editors should have appropriate policies in place for handling editorial conflicts of interest.

Reference:

Kleinert S & Wager E (2011). Responsible research publication: international standards for editors. A position statement developed at the 2nd World Conference on Research Integrity, Singapore, July 22-24, 2010. Chapter 51 in: Mayer T & Steneck N (eds) Promoting Research Integrity in a Global Environment. Imperial College Press / World Scientific Publishing, Singapore (pp 317-28). (ISBN 978-981-4340-97-7) [Link].

International Standards for Authors

Publication is the final stage of research and therefore a responsibility for all researchers. Scholarly publications are expected to provide a detailed and permanent record of research. Because publications form the basis for both new research and the application of findings, they can affect not only the research community but also, indirectly, society at large. Researchers therefore have a responsibility to ensure that their publications are honest, clear, accurate, complete and balanced, and should avoid misleading, selective or ambiguous reporting. Journal editors also have responsibilities for ensuring the integrity of the research literature and these are set out in companion guidelines.

- The research being reported should have been conducted in an ethical and responsible manner and should comply with all relevant legislation.
- Researchers should present their results clearly, honestly, and without fabrication, falsification or inappropriate data manipulation.
- Researchers should strive to describe their methods clearly and unambiguously so that their findings can be confirmed by others.
- Researchers should adhere to publication requirements that submitted work is original, is not plagiarised, and has not been published elsewhere.
- Authors should take collective responsibility for submitted and published work.
- The authorship of research publications should accurately reflect individuals' contributions to the work and its reporting.

- Funding sources and relevant conflicts of interest should be disclosed.
- When an author discovers a significant error or inaccuracy in his/her own published work, it is the author's obligation to promptly notify the journal's Editor-in-Chief and cooperate with them to either retract the paper or to publish an appropriate erratum.

Reference:

Wager E & Kleinert S (2011) Responsible research publication: international standards for authors. A position statement developed at the 2nd World Conference on Research Integrity, Singapore, July 22-24, 2010. Chapter 50 in: Mayer T & Steneck N (eds) Promoting Research Integrity in a Global Environment. Imperial College Press / World Scientific Publishing, Singapore (pp 309-16). (ISBN 978-981-4340-97-7) [Link].

Basic principles to which peer reviewers should adhere

Peer review in all its forms plays an important role in ensuring the integrity of the scholarly record. The process depends to a large extent on trust and requires that everyone involved behaves responsibly and ethically. Peer reviewers play a central and critical part in the peer-review process as the peer review assists the Editors in making editorial decisions and, through the editorial communication with the author, may also assist the author in improving the manuscript.

Peer reviewers should:

- respect the confidentiality of peer review and not reveal any details of a manuscript or its review, during or after the peer-review process, beyond those that are released by the journal;
- not use information obtained during the peer-review process for their own or any other person's or organization's advantage, or to disadvantage or discredit others;
- only agree to review manuscripts for which they have the subject expertise required to carry out a proper assessment and which they can assess within a reasonable time-frame;
- declare all potential conflicting interests, seeking advice from the journal if they are unsure whether something constitutes a relevant conflict;
- not allow their reviews to be influenced by the origins of a manuscript, by the nationality, religion, political beliefs, gender or other characteristics of the authors, or by commercial considerations;
- be objective and constructive in their reviews, refraining from being hostile or inflammatory and from making libellous or derogatory personal comments;
- acknowledge that peer review is largely a reciprocal endeavour and undertake to carry out their fair share of reviewing, in a timely manner;
- provide personal and professional information that is accurate and a true representation of their expertise when creating or updating journal accounts.

Reference:

Homes I (2013). COPE Ethical Guidelines for Peer Reviewers, March 2013, v1 [Link].

Copyright Notice

Articles published in IJOCTA are made freely available online immediately upon publication, without subscription barriers to access. All articles published in this journal are licensed under the Creative Commons Attribution 4.0 International License (click here to read the full-text legal code). This broad license was developed to facilitate open access to, and free use of, original works of all types. Applying this standard license to your work will ensure your right to make your work freely and openly available.

Under the Creative Commons Attribution 4.0 International License, authors retain ownership of the copyright for their article, but authors allow anyone to download, reuse, reprint, modify, distribute, and/or copy articles in IJOCTA, so long as the original authors and source are credited.

The readers are free to:

- Share — copy and redistribute the material in any medium or format
- Adapt — remix, transform, and build upon the material

for any purpose, even commercially.

CONTENTS